REPORT DOCUMENTATION PAGE

Form Approved OMB NO. 0704-0188

1. REPORT DATE (DD-MM-YYYY)	2. REPORT TYPE	3. DATES COVERED (From - To)
20-09-2021	Final Report	21-Aug-2017 - 20-Jun-2021

4. TITLE AND SUBTITLE
Final Report: Quantum Dot Lasers with Asymmetric Barrier Layers: A Novel Type of Semiconductor Lasers

5a. CONTRACT NUMBER
W911NF-17-1-0432

5b. GRANT NUMBER

5c. PROGRAM ELEMENT NUMBER
611102

6. AUTHORS

5d. PROJECT NUMBER

5e. TASK NUMBER

5f. WORK UNIT NUMBER

7. PERFORMING ORGANIZATION NAMES AND ADDRESSES
Virginia Polytechnic Institute & State Unive
North End Center, Suite 4200
300 Turner Street, NW
Blacksburg, VA 24061 -0001

8. PERFORMING ORGANIZATION REPORT NUMBER

9. SPONSORING/MONITORING AGENCY NAME(S) AND ADDRESS (ES)
U.S. Army Research Office
P.O. Box 12211
Research Triangle Park, NC 27709-2211

10. SPONSOR/MONITOR'S ACRONYM(S)
ARO

11. SPONSOR/MONITOR'S REPORT NUMBER(S)
70668-EL.17

12. DISTRIBUTION AVAILIBILITY STATEMENT
Approved for public release; distribution is unlimited.

13. SUPPLEMENTARY NOTES
The views, opinions and/or findings contained in this report are those of the author(s) and should not contrued as an official Department of the Army position, policy or decision, unless so designated by other documentation.

14. ABSTRACT

15. SUBJECT TERMS

16. SECURITY CLASSIFICATION OF:			17. LIMITATION OF ABSTRACT	15. NUMBER OF PAGES	19a. NAME OF RESPONSIBLE PERSON
a. REPORT	b. ABSTRACT	c. THIS PAGE			Levon Asryan
UU	UU	UU	UU		19b. TELEPHONE NUMBER 540-231-7033

RPPR Final Report
as of 24-Sep-2021

Agency Code: 21XD

Proposal Number: 70668EL **Agreement Number: W911NF-17-1-0432**
INVESTIGATOR(S):

Name: Levon V. Asryan asryan@mse
Email: asryan@vt.edu
Phone Number: 5402317033
Principal: Y

Organization: **Virginia Polytechnic Institute & State University**
Address: North End Center, Suite 4200, Blacksburg, VA 240610001
Country: USA
DUNS Number: 003137015 EIN: 546001805
Report Date: 20-Sep-2021 Date Received: 20-Sep-2021
Final Report for Period Beginning 21-Aug-2017 and Ending 20-Jun-2021
Title: Quantum Dot Lasers with Asymmetric Barrier Layers: A Novel Type of Semiconductor Lasers
Begin Performance Period: 21-Aug-2017 **End Performance Period:** 20-Jun-2021
Report Term: 0-Other
Submitted By: Levon Asryan Email: asryan@vt.edu
Phone: (540) 231-7033

STEM Degrees: 1 **STEM Participants:** 2

Major Goals: The objective of this project was to explore the potential of a novel type of semiconductor lasers – quantum dot (QD) lasers with asymmetric barrier layers (ABLs) – for low-threshold, temperature-stable, high-power, and high-speed operation. To accomplish this goal, a comprehensive theory of static (threshold and power) and dynamic characteristics of ABL QD lasers has been developed and recommendations have been provided for the development of ABL QD lasers that will significantly outperform conventional QD lasers.

The following particular major goals were set for this project:

1) To calculate the threshold current density of ABL QD lasers.

2) To calculate the characteristic temperature of ABL QD lasers.

3) To calculate the internal differential quantum efficiency of ABL QD lasers.

4) To calculate the light-current characteristic (LCC) of ABL QD lasers.

5) To study dynamic properties and calculate the modulation response function of ABL QD lasers.

6) To calculate the modulation bandwidth of ABL QD lasers as a function of the dc component of the pump current density and parameters of the structure.

7) To calculate the maximum modulation bandwidth of ABL QD lasers and the optimum dc component of the pump current density at which the maximum bandwidth is attained.

8) To calculate the operating characteristics of ABL lasers considering undesirable out-tunneling leakage of charge carriers through the ABLs.

9) To study the effect of non-instantaneous capture of electrons and holes into QDs, i.e., non-instantaneous pumping of QDs, on the modulation bandwidth of ABL QD lasers.

10) To study the effect of out-tunneling leakage from QDs on the modulation bandwidth of double tunneling-injection (DTI) QD lasers.

11) To study the effects of carrier-density-dependent internal optical loss on static characteristics of semiconductor lasers with a quantum-confined active region.

12) To study the effects of varying the thickness of the optical confinement layer (OCL) on static characteristics of semiconductor lasers with a quantum-confined active region.

Accomplishments: 1) A theory of static (threshold and power) characteristics of ABL QD lasers has been developed. The use of ABLs should ideally prevent the simultaneous presence of electrons and holes (and hence parasitic electron – hole recombination) outside the QDs. It has been shown that in such a case of total suppression of parasitic recombination, the ABL QD lasers offer close-to-ideal performance: the threshold current density is below 10 A/cm^2 at any temperature, the absolute value of the characteristic temperature is above 1000 K (which manifests a virtually temperature-independent operation), the internal differential quantum efficiency is practically unity, and the LCC is linear at any pump current.

2) A search for materials suitable for implementation of 1.55 μm Al-free diode lasers based on InP with ABLs has been conducted. It has been shown that a very high (over 10^6) suppression ratio of the parasitic electron flux can be achieved using common III-V alloys for the ABLs. Hence placing such ABLs in the immediate vicinity of the active region should completely suppress the parasitic recombination in the OCL. Several optimal ABL designs have been proposed that are based on one of the following alloys: Al-free GaInPSb, ternary AlInAs, or quaternary AlGaInAs with a low Al-content. As an important and beneficial byproduct of utilization of such ABLs, an improvement of majority carrier capture into the active region has been shown to occur.

3) The local charge neutrality has been shown to be strongly violated in the active region of ABL lasers, especially at high injection currents. While violation of local neutrality has been shown to have almost no effect on the LCC of the laser (the quantum efficiency is close to 1 and the LCC is linear), it causes weakening of the temperature dependence of the threshold current and, hence, an increase in the characteristic temperature of the laser.

4) A theoretical model for ABL lasers has been proposed that includes undesirable out-tunneling leakage of charge carriers through the ABLs. By the example of an InGaAs/GaAs quantum-well laser (lasing wavelength λ = 980 nm), the effect of out-tunneling leakage of carriers through the ABLs on the device static characteristics has been studied. The ratios of out-tunneling flux suppression by the ABLs, which are required to prevent the adverse effect of parasitic recombination in the OCL, have been estimated. In the structure considered, the effect of the ABLs becomes appreciable at the suppression ratios exceeding 100. To suppress 90% of the parasitic current, the suppression ratios should be above 23000. The effect of the ABLs on the useful fluxes of carrier supply to the active region has also been studied.

5) The small-signal dynamic response of ABL QD lasers has been studied. The modulation bandwidth has been shown to have a maximum as a function of the dc component of the pump current density and parameters of the structure. This provides a clear path for optimizing the laser structure to enhance its bandwidth.

6) The effect of non-instantaneous capture of electrons and holes into QDs, i.e., non-instantaneous pumping of QDs, on the modulation bandwidth has been studied. The maximum bandwidth and the optimum dc injection current density at which it is attained have been calculated as functions of the capture cross-section.

7) It has been shown that the optimum component of the dc pump current density that maximizes the modulation bandwidth in ABL QD lasers is significantly lower than that in both conventional and double tunneling-injection (DTI) QD lasers. Hence, the maximum modulation bandwidth has been shown to be more easily attainable in ABL QD lasers as compared to both DTI and conventional QD lasers.

8) It has been shown that, even in the most dramatic situation of indirect capture of charge carriers into the lasing ground state and unlike the conventional QD lasers, the continuous-wave power of ground-state emission in ABL QD lasers does not saturate with increasing pump current – instead, it increases almost linearly with injection current. This advantage for high-power lasing of ABL QD lasers over the conventional QD lasers is due to efficient suppression of unwanted electron-hole recombination in the OCL in ABL QD lasers.

9) Using numerical simulations, a search has been carried out for designs of ABLs for a laser diode having GaAs OCL and emitting at the wavelength λ = 980 nm. Optimal designs of ABLs based on AlGaAsSb and GaInP for blocking electrons and holes, respectively, have been proposed, which make it possible to reduce the parasitic recombination current down to less than 1% of the initial value. To suppress electron transport, an alternative

structure based on three identical AlInAs barriers has also been proposed. GaAsP spacers of different thicknesses form unmatched spectra of size quantization levels between barriers thus blocking the hopping conduction channel: the parasitic electron flow is reduced by several tens of times in comparison with the case of spacers of equal thickness.

10) Effect of out-tunneling leakage of carriers from QDs on modulation bandwidth of DTI QD lasers has been studied. It has been shown that, due to zero-dimensional nature of QDs, the modulation bandwidth is practically unaffected by out-tunneling leakage from them – it depends only slightly on the out-tunneling time. Hence, concerning out-tunneling leakage, DTI QD lasers are robust — provided that tunneling-injection is fast, no significant effort should be necessary to suppress out-tunneling leakage in practical devices.

11) It has been shown that the LCC shape in QD lasers can be tailored by varying uniformity of QDs. Making the QD ensemble less uniform has been shown to result in roll-over in the LCC. The second branch in the LCC has been shown to appear with making the QD ensemble even less uniform.

12) The LCC of semiconductor lasers with a quantum-confined active region has been studied with a proper account for internal optical loss that varies with the carrier densities in the OCL. It has been shown that (i) roll-over of the LCC occurs with increasing injection current, and, (ii) depending on the parameters of laser structures, the LCC can be two-valued (can have two branches), i.e. the optical emission at two different output powers will be possible within a certain range of injection currents. While the internal differential quantum efficiency for the first (conventional) branch of the LCC is less than 1 and decreases with increasing pump current, that for the second (unconventional) branch is greater than 1 and nonmonotonous.

13) In the presence of the internal optical loss that varies with the carrier densities in the OCL, the laser characteristics have been shown to transform qualitatively with varying temperature: they are conventional, i.e., consist of one branch, at low temperatures but they have two branches, i.e., are of a binary nature, at high temperatures.

14) Operating characteristics of quantum well (QW) lasers have been studied in terms of the thickness of the OCL. The following quantities have been calculated as functions of the OCL thickness: maximum modal gain, optical confinement factor (in QW, OCL, and cladding layers), threshold current density, electron and hole densities (in QW and OCL), internal optical loss (in QW, OCL, and cladding layers), internal differential quantum efficiency, stimulated and spontaneous recombination currents, and output optical power of the laser. It has been shown that up to the pump current density 50 kA/cm^2 the output power of the considered lasers depends only slightly on the OCL thickness in the range of thicknesses 1.5-2.8 ⌣m. This result is important for designing high brightness lasers as broadened waveguides are used in such lasers to attain low beam divergence. At high pump current densities, the output power has been shown to have a maximum as a function of the OCL thickness.

Training Opportunities: 1) L. V. Asryan, Seminar at UT Dallas on “Double tunneling-injection lasers and lasers with asymmetric barrier layers: Optimizing performance by suppressing recombination outside the active region,” Oct. 19, 2018.

RPPR Final Report
as of 24-Sep-2021

Results Dissemination: Results of the work obtained during this project performance were disseminated at the following international conferences:

1) L. V. Asryan and J. L. Monk, “Excited states and optical power of ground-state emission in quantum dot lasers with asymmetric barrier layers,” All-virtual web conference, Oct. 31 – Nov. 4, 2021.

2) L. V. Asryan, Invited talk on “Internal optical loss and light-current characteristic in injection lasers,” International School and Conference "Saint Petersburg OPEN", In-person and Virtual, St. Petersburg, Russia, May 25-28, 2021.

3) L. V. Asryan, Invited talk on “Optimizing the quantum dot lasers for high-speed operation: Novel versus conventional designs,” CLEO 2021, All-virtual web conference, May 10-14, 2021.

4) L. V. Asryan, "Modulation bandwidth of quantum dot lasers with asymmetric barrier layers," International School Laser Physics, All-virtual web school, St. Petersburg, Russia, Nov. 17-18, 2020.

5) L. V. Asryan and J. L. Monk, “Small-signal dynamic response of quantum dot lasers with asymmetric barrier layers,” SPIE Photonics West, San Francisco, CA, USA, Feb. 1-6, 2020.

6) Z. N. Sokolova, N. A. Pikhtin, S. O. Slipchenko, L. V. Asryan, “Temperature-induced single-to-double branch transformation of operating characteristics in semiconductor lasers with a low-dimensional active region,” SPIE Photonics West, San Francisco, CA, USA, Feb. 1-6, 2020.

7) Z. N. Sokolova, N. A. Pikhtin, S. O. Slipchenko, and L. V. Asryan, "Effect of temperature on the quantum well laser characteristics," VII International Symp. "Coherent Optical Emission in Semiconductor Compounds and Structures", Moscow, Russia, Nov. 18-20, 2019.

8) L. V. Asryan, Invited lecture on "Novel injection lasers: Superior performance via suppression of parasitic recombination," International School Laser Physics, St. Petersburg, Russia, Oct. 22-25, 2019.

9) L. V. Asryan, Invited talk on "Tailoring the shape of the light-current characteristic in semiconductor lasers," International Conf. PhysicA.SPb, St. Petersburg, Russia, Oct. 22-24, 2019.

10) L. V. Asryan, “Light-current characteristic shape transformation in quantum-dot lasers,” SPIE Photonics West, San Francisco, CA, USA, Feb. 2-7, 2019.

11) L. V. Asryan, "Effects of carrier leakage and noninstantaneous pumping on the modulation bandwidth of a double tunneling-injection quantum dot lasers," 6th Symp. "Semiconductor Lasers: Physics and Technology", St. Petersburg, Russia, Nov. 13-16, 2018.

12) Z. N. Sokolova, N. A. Pikhtin, and L. V. Asryan, "Degenerated characteristics in semiconductor quantum well lasers," 6th Symp. "Semiconductor Lasers: Physics and Technology", St. Petersburg, Russia, Nov. 13-16, 2018.

13) F. I. Zubov, M. E. Muretova, M. V. Maximov, A. E. Zhukov, and L. V. Asryan, "Effect of tunneling transparency of asymmetric barrier layers on the characteristics of quantum well lasers," 6th Symp. "Semiconductor Lasers: Physics and Technology", St. Petersburg, Russia, Nov. 13-16, 2018.

14) L. V. Asryan, Plenary lecture on “Close-to-ideal semiconductor lasers: Optimizing performance by suppressing recombination outside the active region,” International Conf. on Microwave & THz Technologies, and Wireless Communications, Aghveran, Armenia, Sep. 19-21, 2018.

15) L. V. Asryan, Plenary lecture on “Modulation bandwidth of semiconductor lasers with a quantum-confined active region,” Young Scientists School “Advanced Electronic Devices and Materials”, Aghveran, Armenia, Sep. 19-20, 2018.

16) L. V. Asryan, Invited lecture on “Double tunneling-injection and asymmetric barrier layers: Tools for optimizing semiconductor lasers,” International Symp. "Modern Problems in Physics: 30 Year Anniversary of the Department of Theoretical Bases of Microelectronics", St. Petersburg, Russia, Sep. 17, 2018.

17) M. E. Muretova, F. I. Zubov, L. V. Asryan, E. S. Semenova, M. V. Maximov, and A. E. Zhukov, “Search for asymmetric barrier layers for 808 nm Al-free laser diode,” 26th International Symposium “Nanostructures: Physics and Technology,” Minsk, Belarus, June 18-22, 2018.

18) M. E. Muretova, F. I. Zubov, L. V. Asryan, E. S. Semenova, M. V. Maximov, and A. E. Zhukov, “Development of design of 808 nm Al-free laser heterostructures with asymmetric barrier layers,” 18th International Conference “Laser Optics 2018,” St. Petersburg, Russia, June 4–8, 2018.

19) Z. N. Sokolova, N. A. Pikhtin, and L. V. Asryan, “Two-threshold semiconductor quantum well lasers,” 18th International Conference “Laser Optics 2018,” St. Petersburg, Russia, June 4–8, 2018.

20) L. V. Asryan, “Operating characteristics of quantum dot lasers with asymmetric barrier layers,” SPIE Photonics West, San Francisco, CA, USA, Jan. 27 – Feb. 1, 2018.

21) L. V. Asryan, Keynote lecture “Recombination in waveguide, its effects on the diode laser characteristics, and methods of its suppression,” International Seminar “Current Problems in Physics and Technology of Semiconductor Nanomaterials” and SPIE Student Chapter Meeting at St. Petersburg Academic University, St. Petersburg, Russia, Nov. 10, 2017.

Honors and Awards: 1) L. V. Asryan, Feature interview with Electronics Letters, May 2019

2) L. V. Asryan, Elected to the grade of Senior Member of SPIE, June 2019

Protocol Activity Status:

Technology Transfer: Nothing to Report

PARTICIPANTS:

Participant Type: PD/PI
Participant: Levon V. Asryan
Person Months Worked: 3.00 **Funding Support:**
Project Contribution:
National Academy Member: N

Participant Type: Graduate Student (research assistant)
Participant: John Monk
Person Months Worked: 15.00 **Funding Support:**
Project Contribution:
National Academy Member: N

Participant Type: Graduate Student (research assistant)
Participant: Cody Hammack
Person Months Worked: 9.00 **Funding Support:**
Project Contribution:
National Academy Member: N

ARTICLES:

RPPR Final Report
as of 24-Sep-2021

Publication Type: Journal Article Peer Reviewed: Y **Publication Status:** 1-Published
Journal: Journal of Lightwave Technology
Publication Identifier Type: DOI Publication Identifier: 10.1109/JLT.2018.2806942
Volume: 36 Issue: 11 First Page #: 2295
Date Submitted: 8/27/18 12:00AM Date Published: 6/1/18 4:00AM
Publication Location:
Article Title: Two-Valued Characteristics in Semiconductor Quantum Well Lasers
Authors: Zinaida N. Sokolova, Nikita A. Pikhtin, Levon V. Asryan
Keywords: Quantum well laser, semiconductor laser
Abstract: Due to internal optical absorption loss, which varies with carrier density in the optical confinement region, the operating characteristics can be two valued in semiconductor quantum well lasers. Particularly, there can be two lasing thresholds and two branches in the light–current characteristic. While the internal differential quantum efficiency for the first (conventional) branch of the light–current characteristic is less than 1 and decreases with increasing pump current, that for the second (unconventional) branch is greater than 1 and nonmonotonous.
Distribution Statement: 3-Distribution authorized to U.S. Government Agencies and their contractors
Acknowledged Federal Support: **Y**

Publication Type: Journal Article Peer Reviewed: Y **Publication Status:** 1-Published
Journal: IEEE Journal of Quantum Electronics
Publication Identifier Type: DOI Publication Identifier: 10.1109/JQE.2018.2886395
Volume: 55 Issue: 01 First Page #: 2000109
Date Submitted: 1/3/19 12:00AM Date Published:
Publication Location:
Article Title: Modulation Bandwidth of Double Tunneling-Injection Quantum Dot Lasers: Effect of Out-Tunneling Leakage
Authors: Levon V. Asryan and Saurav Kar
Keywords: Quantum dot laser, semiconductor laser, tunneling injection
Abstract: The effect of out-tunneling leakage of carriers from quantum dots (QDs) on modulation bandwidth of semiconductor double tunneling-injection (DTI) QD lasers is studied. Fast tunneling-injection into QDs should be maintained to ensure high modulation bandwidth. It may also seem that out-tunneling leakage from QDs [tunneling of electrons to the hole-injecting quantum well (QW) and holes to the electron-injecting QW], which is an undesirable process, should be kept as slow as possible (or even totally suppressed) to maximize the modulation bandwidth. However, it is shown in this paper that, due to zero-dimensional nature of QDs, the modulation bandwidth is practically unaffected by out-tunneling leakage from them – it depends only slightly on the out-tunneling time. Hence, concerning out-tunneling leakage, DTI QD lasers are robust — provided that tunneling-injection is fast, no significant effort should be necessary to suppress out-tunneling leakage in practical devices.
Distribution Statement: 3-Distribution authorized to U.S. Government Agencies and their contractors
Acknowledged Federal Support: **Y**

RPPR Final Report
as of 24-Sep-2021

Publication Type: Journal Article Peer Reviewed: Y **Publication Status:** 1-Published
Journal: Semiconductors
Publication Identifier Type: DOI Publication Identifier: 10.1134/S1063782618140336
Volume: 52 Issue: 14 First Page #: 1905
Date Submitted: 1/3/19 12:00AM Date Published:
Publication Location:
Article Title: A search for asymmetric barrier layers for 1550 nm Al-free diode lasers
Authors: F. I. Zubov, M. E. Muretova, L. V. Asryan, E. S. Semenova, M. V. Maximov, V. V. Korenev, A. V. Savely
Keywords: Semiconductor lasers, Al-free diode lasers, asymmetric barrier layers
Abstract: A search for materials suitable for implementation of 1.55 um Al-free diode lasers based on InP with asymmetric barrier (AB) layers is conducted. It is shown that a very high (over 10^6) suppression ratio of the parasitic electron flux can be achieved using common III-V alloys for the ABs. Hence placing such ABs in the immediate vicinity of the active region should completely suppress the parasitic recombination in the waveguide. Several optimal AB designs are proposed that are based on one of the following alloys: Al-free GaInPSb, ternary AlInAs, or quaternary AlGaInAs with a low Al-content. As an important and beneficial byproduct of utilization of such ABs, an improvement of majority carrier capture into the active region occurs.
Distribution Statement: 3-Distribution authorized to U.S. Government Agencies and their contractors
Acknowledged Federal Support: **Y**

Publication Type: Journal Article Peer Reviewed: Y **Publication Status:** 1-Published
Journal: Semiconductors
Publication Identifier Type: DOI Publication Identifier: 10.1134/S1063782618120059
Volume: 52 Issue: 12 First Page #: 1621
Date Submitted: 1/3/19 12:00AM Date Published: 11/8/18 5:00AM
Publication Location:
Article Title: Violation of Local Electroneutrality in the Quantum Well of a Semiconductor Laser with Asymmetric Barrier Layers
Authors: L. V. Asryan, F. I. Zubov, Yu. S. Balezina (Polubavkina), E. I. Moiseev, M. E. Muretova, N. V. Kryzhanov
Keywords: Semiconductor lasers, quantum well lasers, asymmetric barrier layers
Abstract: A self-consistent model for calculating the threshold and high-power characteristics of semiconductor quantum well lasers with asymmetric barrier layers is developed. The electron and hole concentrations in the waveguide region and in the quantum well (QW) and the concentration of photons of stimulated emission are calculated. The local neutrality in the QW is shown to be strongly violated, especially at high injection currents. The violation of neutrality in a QW makes the electron and hole concentrations there dependent on the injection current under lasing conditions: in the structures under consideration, the electron concentration in the QW decreases while the hole concentration increases with increasing injection current. The violation of neutrality in the QW causes weakening of the temperature dependence of the threshold current and, hence, an increase in the characteristic temperature T_0 of the laser.
Distribution Statement: 3-Distribution authorized to U.S. Government Agencies and their contractors
Acknowledged Federal Support: **Y**

RPPR Final Report
as of 24-Sep-2021

Publication Type: Journal Article Peer Reviewed: Y **Publication Status:** 1-Published
Journal: Electronics Letters
Publication Identifier Type: DOI Publication Identifier: 10.1049/el.2019.0225
Volume: 55 Issue: 9 First Page #: 550
Date Submitted: 5/2/19 12:00AM Date Published: 5/2/19 4:00AM
Publication Location: United Kingdom
Article Title: Evolution of light-current characteristic shape in high-power semiconductor quantum well lasers
Authors: Z.N. Sokolova, N.A. Pikhtin, L.V. Asryan
Keywords: Semiconductor lasers, quantum well lasers, light-current characteristic
Abstract: The light-current characteristic (LCC) of semiconductor quantum well lasers is theoretically studied. It is discussed here that, due to internal optical absorption loss, which depends on the electron and hole densities in the optical confinement layer, (i) roll-over of the LCC occurs with increasing injection current, and, (ii) depending on the parameters of laser structures, the LCC can have two branches, i.e. the optical emission at two different output powers will be possible within a certain range of injection currents.
Distribution Statement: 3-Distribution authorized to U.S. Government Agencies and their contractors
Acknowledged Federal Support: **Y**

Publication Type: Journal Article Peer Reviewed: Y **Publication Status:** 1-Published
Journal: Quantum Electronics
Publication Identifier Type: DOI Publication Identifier: 10.1070/QEL17044
Volume: 49 Issue: 6 First Page #: 522
Date Submitted: 6/17/19 12:00AM Date Published: 6/1/19 4:00AM
Publication Location:
Article Title: Quantum dot lasers with asymmetric barrier layers: Close-to-ideal threshold and power characteristics
Authors: L V Asryan
Keywords: quantum dot lasers, semiconductor lasers
Abstract: A theory of static (threshold and power) characteristics of novel diode lasers - quantum dot (QD) lasers with asymmetric barrier layers (ABLs) - is developed. The barrier layers are asymmetric in that they have considerably different heights for the carriers of opposite signs. The use of ABLs should ideally prevent the simultaneous presence of electrons and holes (and hence parasitic electron - hole recombination) outside the QDs. It is shown in this work that in such a case of total suppression of parasitic recombination, the QD lasers with ABLs offer close-to-ideal performance: the threshold current density is below 10 A/cm^2 at any temperature, the absolute value of the characteristic temperature is above 1000 K (which manifests a virtually temperature-independent operation), the internal differential quantum efficiency is practically unity, and the light - current characteristic is linear at any pump current.
Distribution Statement: 3-Distribution authorized to U.S. Government Agencies and their contractors
Acknowledged Federal Support: **Y**

Publication Type: Journal Article Peer Reviewed: Y **Publication Status:** 1-Published
Journal: Semiconductors
Publication Identifier Type: DOI Publication Identifier: 10.1134/S1063782620030203
Volume: 54 Issue: 3 First Page #: 366
Date Submitted: 5/1/20 12:00AM Date Published: 4/1/20 4:00AM
Publication Location:
Article Title: Parasitic Recombination in a Laser with Asymmetric Barrier Layers
Authors: F. I. Zubov, M. E. Muretova, A. S. Payusov, M. V. Maximov, A. E. Zhukov, L. V. Asryan
Keywords: diode lasers, asymmetric barrier layers, parasitic waveguide recombination
Abstract: In ABL lasers, two thin barrier layers adjacent to the active region on both sides are intended to prevent bipolar population in the waveguide and, hence, to suppress parasitic recombination there. A theoretical model is proposed, which is based on rate equations and includes undesirable yet inevitable in practice carrier leakage. Solutions to equations are obtained for the steady-state case. By the example of an InGaAs/GaAs quantum-well laser (lasing wavelength ? = 980 nm), the effect of leakage through ABLs on the device characteristics is studied. The parasitic-flux suppression ratios C of ABLs which are required to prevent the adverse effect of waveguide recombination are estimated. In the case at hand, the effect of ABLs becomes appreciable at suppression ratios of C ? 10^2. To suppress 90% of the parasitic current, C should be 2.3 × 10^4. The effect of ABLs on useful carrier fluxes arriving at the active region is also studied.
Distribution Statement: 2-Distribution Limited to U.S. Government agencies only; report contains proprietary info
Acknowledged Federal Support: **Y**

CONFERENCE PAPERS:

Publication Type: Conference Paper or Presentation **Publication Status:** 1-Published
Conference Name: 18th International Conference “Laser Optics 2018”
Date Received: 27-Aug-2018 Conference Date: 05-Jun-2018 Date Published: 09-Jun-2018
Conference Location: St. Petersburg, Russia
Paper Title: Two-threshold semiconductor quantum well lasers
Authors: Z. N. Sokolova, N. A. Pikhtin, and L. V. Asryan
Acknowledged Federal Support: **Y**

Publication Type: Conference Paper or Presentation **Publication Status:** 1-Published
Conference Name: International Conference on Microwave & THz Technologies and Wireless Communications
Date Received: 03-Jan-2019 Conference Date: 19-Sep-2018 Date Published: 21-Sep-2018
Conference Location: Aghveran, Armenia
Paper Title: Close-to-ideal semiconductor lasers: Optimizing performance by suppressing recombination outside the active region
Authors: Levon V. Asryan
Acknowledged Federal Support: **Y**

Publication Type: Conference Paper or Presentation **Publication Status:** 1-Published
Conference Name: SPIE, Photonics West, Novel In-Plane Semiconductor Lasers XIX
Date Received: 01-May-2020 Conference Date: 04-Feb-2020 Date Published: 24-Feb-2020
Conference Location: San Francisco, United States
Paper Title: Temperature-induced single-to-double branch transformation of operating characteristics in semiconductor lasers with a low-dimensional active region
Authors: Z. N. Sokolova, N. A. Pikhtin, S. O. Slipchenko, and L. V. Asryan
Acknowledged Federal Support: **Y**

RPPR Final Report
as of 24-Sep-2021

Publication Type: Conference Paper or Presentation **Publication Status:** 1-Published
Conference Name: CLEO 2021
Date Received: 13-Sep-2021 Conference Date: 09-May-2021 Date Published: 01-Aug-2021
Conference Location: All-virtual, web conference format
Paper Title: Optimizing the quantum dot lasers for high-speed operation: Novel versus conventional designs
Authors: Levon V. Asryan
Acknowledged Federal Support: **Y**

Publication Type: Conference Paper or Presentation **Publication Status:** 3-Accepted
Conference Name: Frontiers in Optics + Laser Science
Date Received: 13-Sep-2021 Conference Date: 31-Oct-2021 Date Published:
Conference Location: All-virtual format
Paper Title: Excited states and optical power of ground-state emission in quantum dot lasers with asymmetric barrier layers
Authors: Levon V. Asryan, John L. Monk
Acknowledged Federal Support: **Y**

DISSERTATIONS:

Publication Type: Thesis or Dissertation
Institution: Virginia Polytechnic Institute and State University
Date Received: 28-Aug-2020 Completion Date: 4/29/20 9:13AM
Title: Theoretical Study of Semiconductor Quantum Dot Lasers with Asymmetric Barrier Layers
Authors: John L. Monk
Acknowledged Federal Support: **Y**

Partners

,

I certify that the information in the report is complete and accurate:
Signature: Levon Asryan
Signature Date: 9/20/21 12:41AM

https://doi.org/10.1070/QEL17044

Quantum dot lasers with asymmetric barrier layers: Close-to-ideal threshold and power characteristics

L.V. Asryan

Abstract. **A theory of static (threshold and power) characteristics of novel diode lasers – quantum dot (QD) lasers with asymmetric barrier layers (ABLs) – is developed. The barrier layers are asymmetric in that they have considerably different heights for the carriers of opposite signs. The ABL located on the electron- (hole-) injecting side of the structure provides a low barrier (ideally no barrier) for electrons (holes) [so that it does not prevent electrons (holes) from easily approaching the active region] and a high barrier for holes (electrons) [so that holes (electrons) injected from the opposite side of the structure do not overcome it]. The use of ABLs should thus ideally prevent the simultaneous presence of electrons and holes (and hence parasitic electron–hole recombination) outside the QDs. It is shown in this work that in such a case of total suppression of parasitic recombination, the QD lasers with ABLs offer close-to-ideal performance: the threshold current density is below 10 A cm^{-2} at any temperature, the absolute value of the characteristic temperature is above 1000 K (which manifests a virtually temperature-independent operation), the internal differential quantum efficiency is practically unity, and the light–current characteristic is linear at any pump current.**

Keywords: *quantum dot lasers, semiconductor lasers.*

1. Introduction

In conventional diode lasers, pumping the active region (i.e., creating the population inversion required for lasing) is a three-step process. It includes injection of electrons and holes to the waveguide region [optical confinement layer (OCL)] from the cladding layers located on the opposite sides of this region, transportation through this region to the active region, and capture into the latter (Fig. 1a). Only a small fraction of electrons and holes injected to the OCL is finally captured into the active region – the majority of them remains in the OCL. Besides, electrons (holes) are easily transported to that side of the OCL where holes (electrons) are coming from (right- (left-) hand side in Fig. 1a). Hence, the carrier population is bipolar throughout the OCL. While simultaneous population of electrons and holes is required in the active region, bipolar population outside the active region is undesirable. In the presence of such population, electron–hole recombination occurs there [1–21]. This recombination is parasitic as it adversely affects the laser characteristics. In particular,

L.V. Asryan Virginia Polytechnic Institute and State University, Blacksburg, Virginia 24061, USA; e-mail: asryan@vt.edu

Received 22 April 2019
Kvantovaya Elektronika **49** (6) 522–528 (2019)
Submitted in English

(i) the fraction of injection current that goes into the parasitic electron–hole recombination is considerable; hence the threshold current is increased [8, 12, 13, 15, 18];

(ii) the parasitic recombination outside the active region presents a major source for the temperature dependence of the threshold current [8, 12, 13, 15, 18]; and

(iii) the parasitic recombination rate rises superlinearly with injection current above the lasing threshold, which leads to sublinearity of the light–current characteristic (LCC) and limits the output optical power [19–21].

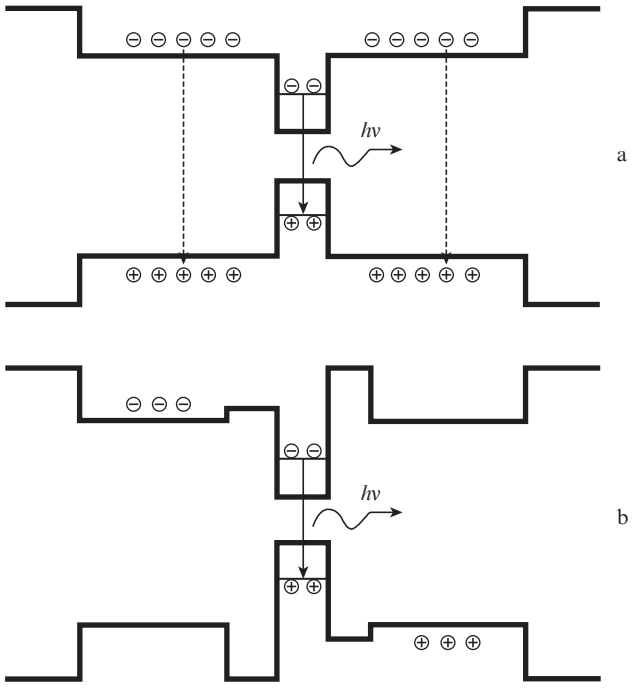

Figure 1. Energy band diagrams of (a) a conventional diode laser and (b) an ABL laser. The vertical solid arrows show the electron–hole recombination in the active region (QDs). The vertical dashed arrows show the parasitic electron–hole recombination outside the active region (in the OCL).

The use of asymmetric barrier layers (ABLs) was proposed [22, 23] as one of two approaches to suppress the recombination of electron–hole pairs outside a quantum-confined active region in semiconductor lasers. While the other approach – double tunneling-injection of charge carriers – was extensively discussed in the context of quantum dot (QD) lasers [22–31], the concept of ABLs was only applied to quantum well (QW) lasers so far [32–37]. A considerably higher tem-

perature stability of the threshold current was demonstrated in ABL QW lasers as compared to reference QW lasers without ABLs [33]. In the meantime, due to a truly discrete energy spectrum of carriers in QDs, still better characteristics are anticipated for ABL lasers, which will use a layer with QDs as the active region instead of a QW. This work explores the potential of ABL QD lasers for low-threshold, temperature-stable, and high-power operation.

In ABL QD lasers, to prevent bipolar population in the OCL and thus to suppress parasitic recombination there, the QD layer is sandwiched between two barrier layers. The layers are asymmetric – in the layer located on that side of the OCL into which electrons (holes) are injected [left- (right-) hand side in Fig. 1b], the energy barrier for electrons (holes) [i.e., the conduction (valence) band offset between the materials of the ABL and OCL] is low (ideally, zero) while that for holes (electrons) [i.e., the valence (conduction) band offset between the materials of the ABL and OCL] is high. Such asymmetry in the barrier heights for electrons and holes in each ABL will ensure that

(i) the carriers coming from that side of the structure, into which there were injected, will easily reach and be captured to the active region; and

(ii) the further transport of these carriers to the opposite side of the structure, i.e., to that side of the structure, into which the carriers of the opposite sign were injected, will be effectively blocked.

Assuming that the ABLs function ideally, there will be no bipolar population and hence parasitic electron–hole recombination in the OCL in the structure of Fig. 1b, electrons (holes) will not reach the right- (left-) hand side of the OCL. The only location in the structure, where the electrons and holes will meet together and recombine, will be the quantum-confined active region.

Asymmetric band structures and carrier blocking layers were discussed elsewhere (see, e.g., [38–46]) but for purposes other than suppression of the parasitic electron–hole recombination outside the active region.

2. Rate equations

To explore the potential of ABL QD lasers for low-threshold, temperature-stable, and high-power operation, it is assumed here that the ABLs function ideally, i.e.,

(i) the left-hand-side ABL totally blocks holes from entering the left-hand side of the OCL while not hindering at all the electron injection into QDs; and

(ii) the right-hand-side ABL totally blocks electrons from entering the right-hand side of the OCL while not hindering at all the hole injection into QDs.

The following set of rate equations is used, which includes all the main processes in the layered structure of Fig. 1b:
for free electrons in the left-hand side of the OCL,

$$b_1\frac{\partial n_{\rm L}}{\partial t}=\frac{j}{e}+\sigma_n v_n n_1 N_{\rm S} f_n-\sigma_n v_n n_{\rm L} N_{\rm S}(1-f_n) \tag{1}$$

for free holes in the right-hand side of the OCL,

$$b_2\frac{\partial p_{\rm R}}{\partial t}=\frac{j}{e}+\sigma_p v_p p_1 N_{\rm S} f_p-\sigma_p v_p p_{\rm R} N_{\rm S}(1-f_p) \tag{2}$$

for electrons and holes confined in QDs,

$$2N_{\rm S}\frac{\partial f_n}{\partial t}=\sigma_n v_n n_{\rm L} N_{\rm S}(1-f_n)-\sigma_n v_n n_1 N_{\rm S} f_n - N_{\rm S}\frac{f_n f_p}{\tau_{\rm QD}}-c_{\rm g}g^{\max}(f_n+f_p-1)n_{\rm ph}, \tag{3}$$

$$2N_{\rm S}\frac{\partial f_p}{\partial t}=\sigma_p v_p p_{\rm R} N_{\rm S}(1-f_p)-\sigma_p v_p p_1 N_{\rm S} f_p - N_{\rm S}\frac{f_n f_p}{\tau_{\rm QD}}-c_{\rm g}g^{\max}(f_n+f_p-1)n_{\rm ph} \tag{4}$$

and for photons,

$$\frac{\partial n_{\rm ph}}{\partial t}=c_{\rm g}g^{\max}(f_n+f_p-1)n_{\rm ph}-c_{\rm g}\beta n_{\rm ph.} \tag{5}$$

Here, b_1 (b_2) is the thickness of the left- (right-) hand side of the OCL [the separation between the n- (p-) cladding layer and the left- (right-) hand-side barrier (see Fig. 1b)]; $n_{\rm L}$ and $p_{\rm R}$ are the free-electron and -hole densities in the left- and right-hand sides of the OCL, respectively; j is the injection current density; e is the electron charge; $\sigma_{n,p}$ are the cross sections of electron and hole capture into a QD; $v_{n,p}$ are the electron and hole thermal velocities; $N_{\rm S}$ is the surface density of QDs; $f_{n,p}$ are the electron- and hole-level occupancies in QDs; $\tau_{\rm QD}$ is the spontaneous radiative lifetime in QDs; $c_{\rm g}$ is the group velocity of light in the cavity; $g^{\max}$ is the maximum value of the modal gain [8, 12, 15]; $\beta=(1/L)\ln(1/R)$ is the mirror loss coefficient; L is the cavity length; R is the facet reflectivity; and $n_{\rm ph}$ is the photon density (number of photons per unit area of the junction) in the lasing mode.

The quantities n_1 and p_1 in (1)–(4) characterise the intensities of electron and hole thermal escape from a QD to the OCL. They are given by

$$n_1=N_{\rm c}^{\rm 3D}\exp\left(-\frac{E_n}{T}\right),\quad p_1=N_{\rm v}^{\rm 3D}\exp\left(-\frac{E_p}{T}\right), \tag{6}$$

where $N_{\rm c,v}^{\rm 3D}=2[m_{\rm c,v}^{\rm OCL}T/(2\pi\hbar^2)]^{3/2}$ are the effective densities of states in the conduction and valence bands in the OCL; $m_{\rm c,v}^{\rm OCL}$ are the electron and hole effective masses in the OCL; $E_{n,p}$ are the electron and hole excitation energies from a QD to the OCL; and T is the temperature (in units of energy).

The first term in the right-hand side in Eqn (1) [Eqn (2)] is the electron (hole) injection flux (in units of $\rm cm^{-2}\,s^{-1}$) from the n- (p-) cladding layer to the OCL. Each of these fluxes is given by the total injection current density j divided by the electron charge: this reflects the fact that the current in the n- (p-) cladding layer (including the boundary with the OCL) is purely electron (hole) current.

The second term in the right-hand side in Eqn (1) [Eqn (2)] is the flux of thermal escape of electrons (holes) from QDs to the OCL and the third term is the flux of electron (hole) capture from the OCL into QDs.

In (3) and (4), $N_{\rm S}f_nf_p/\tau_{\rm QD}$ is the spontaneous radiative recombination flux in QDs. In (3)–(5), $c_{\rm g}g^{\max}(f_n+f_p-1)n_{\rm ph}$ is the flux of stimulated radiative recombination of electrons and holes in QDs, i.e., the flux of stimulated emission of photons. The second term in the right-hand side of (5) is the flux of photon escape from the cavity through the mirrors.

Adding up equations (1) and (3) gives

$$\frac{\partial}{\partial t}(b_1n_{\rm L}+2N_{\rm S}f_n)=\frac{j}{e}-N_{\rm S}\frac{f_nf_p}{\tau_{\rm QD}}-$$

$$- c_g g^{max}(f_n + f_p - 1)n_{ph}. \quad (7)$$

Adding up equations (2) and (4) gives

$$\frac{\partial}{\partial t}(b_2 p_R + 2N_S f_p) = \frac{j}{e} - N_S \frac{f_n f_p}{\tau_{QD}} - c_g g^{max}(f_n + f_p - 1)n_{ph}. \quad (8)$$

Subtracting Eqn (7) from Eqn (8) gives

$$\frac{\partial}{\partial t}[(b_2 p_R + 2N_S f_p) - (b_1 n_L + 2N_S f_n)] = 0. \quad (9)$$

Equation (9) is the condition of conservation of the total charge in the laser structure, which includes the charge of free electrons in the left-hand side of the OCL, free holes in the right-hand side of the OCL, and electrons and holes confined in QDs. Since the laser structure is not originally charged, the following condition of global charge neutrality is obtained from (9):

$$b_1 n_L + 2N_S f_n = b_2 p_R + 2N_S f_p. \quad (10)$$

Equality (10) simply states that the total charge of electrons in QDs and the left-hand side of the OCL is compensated for by the total charge of holes in QDs and the right-hand side of the OCL. As seen from (10), the local charge neutrality is violated in QDs, i.e., $f_n \neq f_p$ in the general case.

3. Steady-state characteristics

A GaInAsP heterostructure lasing near 1.55 μm is considered in this work [8, 12, 13, 15]. The materials of the cladding layers, OCL and QDs are InP, $Ga_{0.21}In_{0.79}As_{0.46}P_{0.54}$ and $Ga_{0.47}In_{0.53}As$, respectively, with the latter two being lattice-matched with InP. The cavity length is $L = 1.139$ mm (the mirror loss is $\beta = 10$ cm^{-1}), the width of the laser stripe is 2 μm, the surface density of the QD is $N_S = 6.11 \times 10^{10}$ cm^{-2}, and $T = 300$ K.

Continuous-wave operation is considered here and hence the rate equations (1)–(5) are solved at the steady state. At the steady state, the set of differential equations (1)–(5) reduces to the set of algebraic equations. As shown below, solving this set of algebraic equations reduces in turn to solving a single algebraic equation in one unknown [see Eqn (15)].

From Eqn (5) at the steady state, the lasing condition is obtained in the form (equality of the gain to the loss):

$$g^{max}(f_n + f_p - 1) = \beta. \quad (11)$$

From (11) and (1), f_p and n_L are expressed in terms of f_n as follows:

$$f_p(f_n) = 1 + \frac{\beta}{g^{max}} - f_n, \quad (12)$$

$$n_L(f_n) = n_1 \frac{f_n}{1 - f_n} + \frac{j}{e\sigma_n v_n N_S(1 - f_n)}. \quad (13)$$

From (2) and using (12), p_R is also expressed in terms of f_n,

$$p_R = p_1 \frac{f_p(f_n)}{1 - f_p(f_n)} + \frac{j}{e\sigma_p v_p N_S[1 - f_p(f_n)]} = p_1 \frac{1 + \beta/g^{max} - f_n}{f_n - \beta/g^{max}} + \frac{j}{e\sigma_p v_p N_S[f_n - \beta/g^{max}]}. \quad (14)$$

Substituting f_p, n_L, and p_R from (12)–(14) into (10), the following equation is obtained to find f_n:

$$b_1\left[n_1 \frac{f_n}{1 - f_n} + \frac{j}{e\sigma_n v_n N_S(1 - f_n)}\right] + 2N_S f_n = b_2\left[p_1 \frac{1 + \beta/g^{max} - f_n}{f_n - \beta/g^{max}} + \frac{j}{e\sigma_p v_p N_S(f_n - \beta/g^{max})}\right] + 2N_S\left(1 + \frac{\beta}{g^{max}} - f_n\right). \quad (15)$$

Equation (15) can be rewritten as a cubic equation in f_n. Solving (15), f_n is found and then, using (12)–(14), f_p, n_L, and p_R are calculated.

As seen from (15) and (12) and shown in Fig. 2, f_n and f_p vary with injection current density j. The fact that the electron and hole level occupancies in QDs are not pinned in the lasing regime is entirely due to violation of local neutrality in QDs, i.e., to electron–hole asymmetry. Indeed, assuming local neutrality in QDs one would immediately obtain from (11) that $f_{n,p}$ are pinned at the same (threshold) value given by

$$f_n^{neutral} = f_p^{neutral} = \frac{1}{2}\left(1 + \frac{\beta}{g^{max}}\right), \quad (16)$$

and shown by the horizontal dashed line in Fig. 2.

From Eqn (7) [or (8)] at the steady-state and using (11), the photon density is calculated,

$$n_{ph}(j) = \tau_{ph} \frac{j - j_{spon}^{QD}(j)}{e}, \quad (17)$$

where $\tau_{ph} = 1/(c_g\beta)$ is the photon lifetime in the cavity and

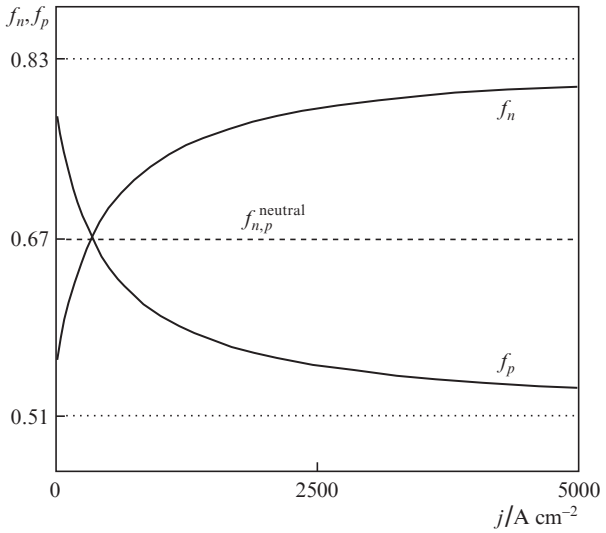

Figure 2. Electron and hole level occupancies in QDs vs. injection current density. The horizontal dashed line shows the electron and hole level occupancies calculated assuming local neutrality in QDs [Eqn (16)]. The horizontal dotted lines show the asymptotic values of the electron and hole level occupancies given by (29) and (30).

$$j_{\text{spon}}^{\text{QD}}(j) = eN_{\text{S}}\frac{f_n(j)f_p(j)}{\tau_{\text{QD}}} \tag{18}$$

is the spontaneous radiative recombination current density in QDs.

Finally, the current density of stimulated recombination, j_{stim}, and the output optical power of the laser, P, are calculated,

$$j_{\text{stim}}(j) = e\frac{n_{\text{ph}}(j)}{\tau_{\text{ph}}} = j - j_{\text{spon}}^{\text{QD}}(j), \tag{19}$$

$$P(j) = \hbar\omega\frac{n_{\text{ph}}(j)}{\tau_{\text{ph}}}S = \frac{\hbar\omega}{e}j_{\text{stim}}(j)S = \frac{\hbar\omega}{e}S[j - j_{\text{spon}}^{\text{QD}}(j)], \tag{20}$$

where $\hbar\omega$ is the photon energy, $S = WL$ is the cross section of the junction, and W is the lateral size of the device.

The output power can be written as

$$P(j) = \frac{\hbar\omega}{e}S(j - j_{\text{th}})\eta_{\text{int}}(j), \tag{21}$$

where the threshold current density j_{th} (the lowest pump current density, at which the lasing starts) is found as the root of the equation

$$j - j_{\text{spon}}^{\text{QD}}(j) = 0, \tag{22}$$

and η_{int} is the internal differential quantum efficiency (efficiency of stimulated emission), which is defined as [47]

$$\eta_{\text{int}}(j) = \frac{j_{\text{stim}}(j)}{j - j_{\text{th}}} = \frac{j - j_{\text{spon}}^{\text{QD}}(j)}{j - j_{\text{th}}}. \tag{23}$$

If QDs were neutral, the optical power would be given by

$$P^{\text{neutral}} = \frac{\hbar\omega}{e}S(j - j_{\text{th}}^{\text{neutral}}), \tag{24}$$

with

$$j_{\text{th}}^{\text{neutral}} = eN_{\text{S}}\frac{(f_n^{\text{neutral}})^2}{\tau_{\text{QD}}} \tag{25}$$

being the threshold current density in that case. As seen from (24) and (25), under the condition of local neutrality in QDs, the LCC of ABL QD lasers (the output optical power versus the injection current density) is linear.

As seen from (17), (19), and (20), the only mechanism of non-stimulated recombination in an ideally functioning ABL QD laser is the spontaneous radiative recombination in QDs. Since the level occupancies in QDs $f_n(j)$ and $f_p(j)$ cannot exceed unity, the current density consumed by spontaneous radiative recombination in QDs [see (18)] also remains limited,

$$j_{\text{spon}}^{\text{QD}}(j) \leqslant \frac{eN_{\text{S}}}{\tau_{\text{QD}}}. \tag{26}$$

For typical values of the surface density of QDs N_{S} ($< 10^{11}$ cm^{-2}) and spontaneous radiative recombination time in QDs τ_{QD} ($\approx$ 1ns), the upper limit for the spontaneous recombination current density $eN_{\text{S}}/\tau_{\text{QD}}$ is less than 20 A cm^{-2}, which is a very low value. This means that, no matter what are the particular functional dependences of f_n and f_p on j, for the pump current density $j \gg eN_{\text{S}}/\tau_{\text{QD}}$, the spontaneous recombination current density in QDs can be safely neglected compared to j in (20) thus yielding a linear LCC (Fig. 3),

$$P(j) = \frac{\hbar\omega}{e}jS. \tag{27}$$

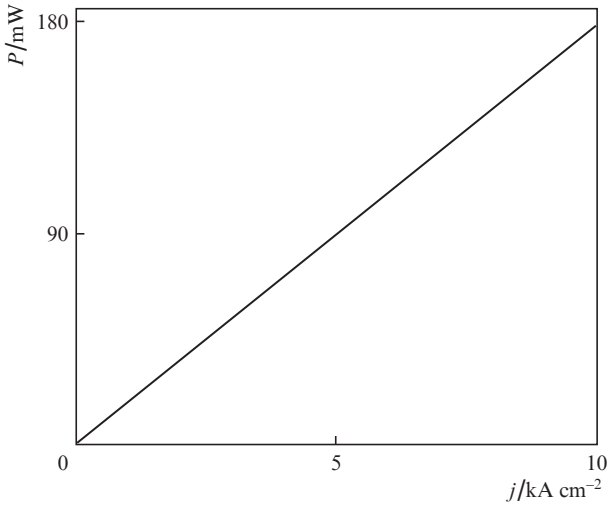

Figure 3. Light–current characteristic of an ABL QD laser: output optical power vs. injection current density; T= 300 K.

As seen from (21) and (27), the internal differential quantum efficiency η_{int} is practically equal to unity.

As it might be concluded from (20) and (18), due to violation of local neutrality in QDs and the fact that f_n and f_p are nonlinear functions of the injection current density (Fig. 2), the LCC should also be nonlinear at low j, i. e., at j slightly above j_{th}. However, even at low j, the LCC of ABL lasers is virtually linear and very close to that given by Eqn (24) for the case of neutral QDs. The physics behind this is as follows. To satisfy the lasing condition (11), the sum $f_n + f_p$ should remain constant. With (11) and (16), this sum can be written us

$$f_n + f_p = 2f_{n,p}^{\text{neutral}}. \tag{28}$$

What this means is the increase in f_n with j is compensated for by the decrease in f_p (Fig. 2). Hence, while the electron and hole level occupancies in QDs significantly vary with j, their product, which determines the spontaneous radiative recombination current density in QDs [see (18)], is almost constant and hence is not significantly affected by violation of local neutrality in QDs (Fig. 4). As a result of this, so is the LCC of the laser even at low j.

As seen from Fig. 2, f_n and f_p saturate with increasing j. From (15) and (12), the following expressions are obtained for the asymptotic values of f_n and f_p at $j \to \infty$ (the dotted horizontal lines in the figure):

$$f_{n,\text{asympt}} = \frac{\beta/g^{\max} + \tau_{p,\text{capt},0}/\tau_{n,\text{capt},0}}{1 + \tau_{p,\text{capt},0}/\tau_{n,\text{capt},0}}, \tag{29}$$

$$f_{p,\text{asympt}} = \frac{\beta/g^{\max} + \tau_{n,\text{capt},0}/\tau_{p,\text{capt},0}}{1 + \tau_{n,\text{capt},0}/\tau_{p,\text{capt},0}}, \tag{30}$$

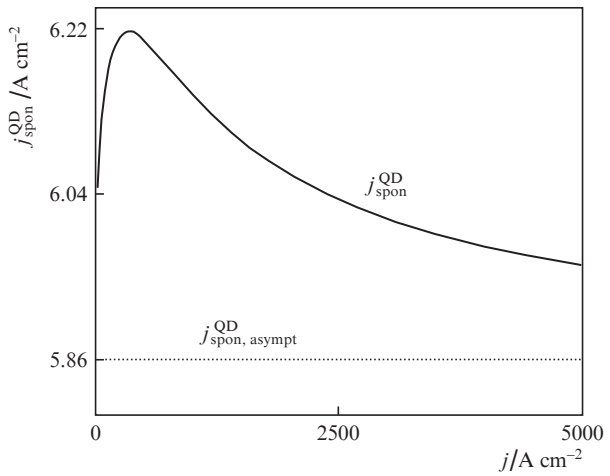

Figure 4. Spontaneous radiative recombination current density in QDs vs. injection current density. The horizontal dotted line shows the asymptotic value $j_{spon,asympt}^{QD} = (eN_S/\tau_{QD})f_{n,asympt}f_{p,asympt}$, where $f_{n,asympt}$ and $f_{p,asympt}$ are given by (29) and (30); $T = 300$ K.

where

$$\tau_{n,capt,0} = b_1/v_{n,capt,0}, \quad \tau_{p,capt,0} = b_2/v_{p,capt,0} \tag{31}$$

are the capture times of electrons and holes from the left- and right-hand sides of the OCL, respectively, into an empty QD ensemble (when $f_{n,p} = 0$). In (31), $v_{n,capt,0}$ and $v_{p,capt,0}$ are the capture velocities (in units of cm s^{-1}) into an empty QD ensemble given by [19–21]

$$v_{n,capt,0} = \sigma_n v_n N_S, \quad v_{p,capt,0} = \sigma_p v_p N_S. \tag{32}$$

While f_n and f_p differ considerably from each other, the free electron density n_L in the left-hand side of the OCL is almost the same as the free hole density p_R in the right-hand side of the OCL in the case of $b_1 = b_2$ considered here (Fig. 5). This is because each of the electron and hole charges (per unit area) confined in all QDs, $2N_S f_n$ and $2N_S f_p$, is negligible compared to the free-electron and -hole charges in the left- and right-hand sides of the OCL, $b_1 n_L$ and $b_2 p_R$.

Using (29) and (30) in (13) and (14), the following expressions are obtained for the asymptotic values of n_L and p_R at $j \to \infty$:

$$b_1 n_{L,asymp} = b_2 p_{R,asympt} = \frac{\tau_{n,capt,0} + \tau_{p,capt,0}}{1 - \beta/g^{max}} \frac{j}{e}. \tag{33}$$

While the threshold current density for the case of neutral QDs is given by a closed-form expression [see (25)], no such expression can be derived for the case of charged QDs. However, the upper limit for j_{th} can be easily found in the general case. As seen from (22), since j_{spon}^{QD} is limited [see (26)], j_{th} is limited as well and the upper limit for the latter is the same as that for j_{spon}^{QD},

$$j_{th} \leqslant eN_S/\tau_{QD}. \tag{34}$$

As with the dependence on the injection current density, violation of local neutrality in QDs leads to the temperature-dependence of f_n and f_p (see [12, 13, 15] where this has been considered in the context of conventional QD lasers). If QDs were neutral, $f_{n,p}$ [see (16)] and hence the threshold current density [see (25)] would be independent of temperature. Accordingly, the characteristic temperature (a figure of merit of a diode laser from the viewpoint of temperature-stability of j_{th}) defined as

$$T_0 = \left(\frac{\partial \ln j_{th}}{\partial T}\right)^{-1}, \tag{35}$$

would be infinitely high.

As seen from (15), primarily due to exponential [see (6)] temperature dependences of n_1 and p_1 [the T-dependence of the electron and hole thermal velocities $v_{n,p}$ also entering into (15) is much weaker compared to these], f_n should be temperature-dependent as well. Hence, so should be f_p [see (12)]. Similarly to the dependences on the injection current density (Fig. 2), since the sum $f_n + f_p$ should remain constant [see (28)], to satisfy the lasing condition (11), the increase in f_n

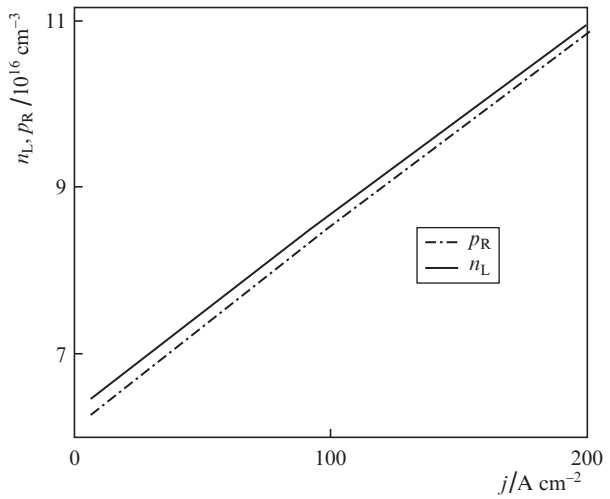

Figure 5. Free-electron density in the left hand side of the OCL and free-hole density in the right hand side of the OCL vs. injection current density; $T = 300$ K.

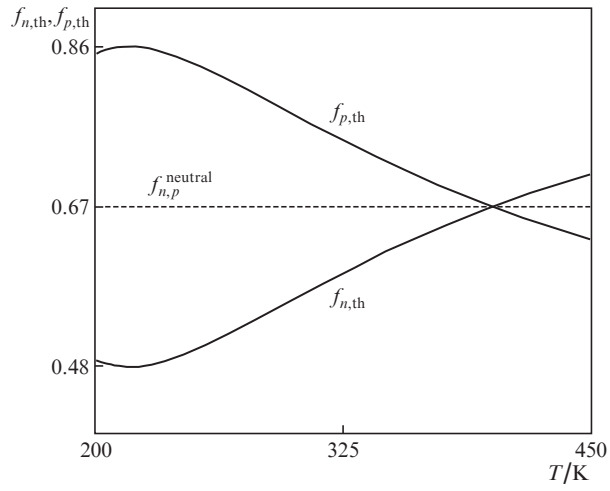

Figure 6. Electron and hole level occupancies in QDs at the lasing threshold vs. temperature. The horizontal dashed line shows the electron and hole level occupancies calculated assuming local neutrality in QDs [Eqn (16)].

with T is compensated for by the decrease in f_p (Fig. 6). As a result of this, the spontaneous recombination current density in QDs j_{th}, controlled by the product of f_n and f_p [see (18)], and hence the threshold current density j_{th} [determined from (22)], vary only slightly with temperature varying in a wide range (Fig. 7). As seen from Fig. 7, j_{th} is below 10 A cm^{-2} in the entire temperature range from 200 to 450 K. As also seen from the figure, the temperature dependence of j_{th} is nonmonotonous: with increasing temperature, j_{th} first decreases, then increases, and then decreases again. Hence the characteristic temperature T_0 twice changes its sign: it is first negative, then positive, and then negative again (Fig. 8). At the temperatures, at which j_{th} is at its minimum and maximum (217 and 401 K, respectively), the characteristic temperature is infinitely high ($T_0 = \infty$): $1/T_0 = 0$ at these temperatures in Fig. 8. As seen from Fig. 8, the absolute value of T_0 is above 1100 K in the entire temperature range. Such high values of T_0 in ABL lasers with charged QDs represent virtually temperature-independent j_{th} for any practical applications.

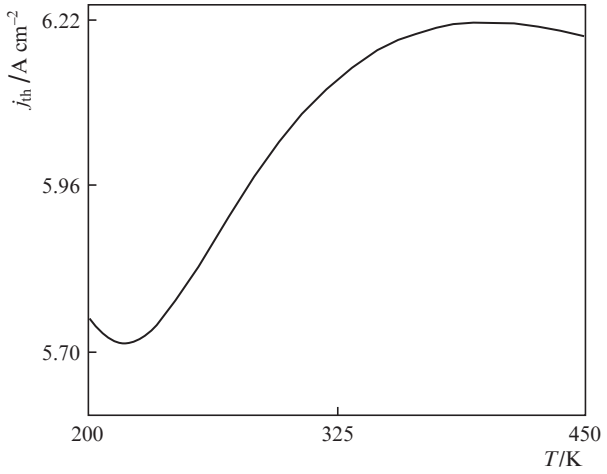

Figure 7. Threshold current density of an ABL QD laser vs. temperature.

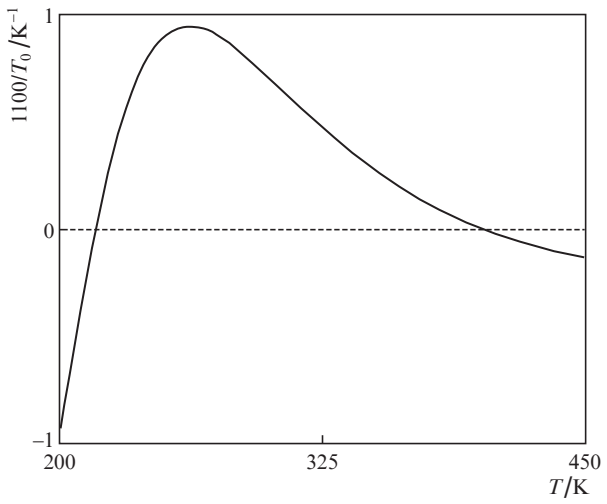

Figure 8. Reciprocal of the characteristic temperature of an ABL QD laser (multiplied by 1100) vs. temperature. The horizontal dashed line shows the reciprocal of the characteristic temperature calculated assuming local neutrality in QDs ($T_0^{neutral} = \infty$). At $T = 217$ K, $f_{n,th}$ is at its minimum and $f_{p,th}$ is at its maximum (see Fig. 6), j_{th} is at its minimum (see Fig. 7), and hence [see (35)] $1/T_0 = 0$. At $T = 401$ K, $f_{n,th} = f_{p,th} = f_{n,p}^{neutral}$ (see Fig. 6), j_{th} is now at its maximum (see Fig. 7), and hence $1/T_0$ is again equal to zero.

4. Conclusions

A theory of static characteristics of novel semiconductor lasers – QD lasers with ABLs – has been developed. Assuming that the ABLs function ideally, i. e., they completely block the simultaneous presence of electrons and holes outside the QDs, and hence the parasitic electron–hole recombination is totally suppressed there, it has been shown that the QD lasers with ABLs offer close-to-ideal performance: the threshold current density is below 10 A cm^{-2} at any temperature, the absolute value of the characteristic temperature is above 1000 K (which manifests a virtually temperature-independent operation), the internal differential quantum efficiency is practically equal to unity, and the LCC is linear at any pump current.

Acknowledgements. This work was supported by the U.S. Army Research Office (Grant No. W911NF-17-1-0432).

References

1. Garbuzov D.Z., Ovchinnikov A.V., Pikhtin N.A., Sokolova Z.N., Tarasov I.S., Khalfin V.B. *Sov. Phys. Semicond.*, **25** (5), 560 (1991) [*Fiz. Tekh. Poluprovodn.*, **25** (5), 928 (1991)].
2. Rideout W., Sharfin W.F., Koteles E.S., Vassell M.O., Elman B. *IEEE Photon. Technol. Lett.*, **3** (9), 784 (1991).
3. Tessler N., Nagar R., Eisenstein G., Chandrasekhar S., Joyner C.H., Dentai A.G., Koren U., Raybon G. *Appl. Phys. Lett.*, **61** (20), 2383 (1992).
4. Hirayama H., Yoshida J., Miyake Y., Asada M. *Appl. Phys. Lett.*, **61** (20), 2398 (1992).
5. Zory P.S. Jr. *Quantum Well Lasers* (Boston: Academic, 1993).
6. Temkin H., Coblentz D., Logan R.A., Vandenberg J.M., Yadvish R.D., Sergent A.M. *Appl. Phys. Lett.*, **63** (17), 2321 (1994).
7. Evans J.D., Simmons J.G., Thompson D.A., Puetz N., Makino T., Chik G. *IEEE J. Sel. Top. Quantum Electron.*, **1** (2), 275 (1995).
8. Asryan L.V., Suris R.A. *Semicond. Sci. Technol.*, **11** (4), 554 (1996).
9. Seki S., Oohashi H., Sugiura H., Hirono T., Yokoyama K. *IEEE J. Quantum Electron.*, **32** (8), 1478 (1996).
10. Garbuzov D., Xu L., Forrest S.R., Martinelli R., Connolly J.C. *Electron. Lett.*, **32** (18), 1717 (1996).
11. Mawst L.J., Bhattacharya A., Lopez J., Botez D., Garbuzov D.Z., DeMarco L., Connolly J.C., Jansen M., Fang F., Nabiev R.F. *Appl. Phys. Lett.*, **69** (11), 1532 (1996).
12. Asryan L.V., Suris R.A. *IEEE J. Sel. Top. Quantum Electron.*, **3** (2), 148 (1997).
13. Asryan L.V., Suris R.A. *Electron. Lett.*, **33** (22), 1871 (1997).
14. Kazarinov R.F., Shtengel G.E. *J. Lightwave Technol.*, **15** (12), 2284 (1997).
15. Asryan L.V., Suris R.A. *IEEE J. Quantum Electron.*, **34** (5), 841 (1998).
16. Kapon E. *Semiconductor Lasers: Fundamentals* (New York: Academic, 1999).
17. Asryan L.V., Suris R.A. *Appl. Phys. Lett.*, **74** (9), 1215 (1999).
18. Asryan L.V., Gun'ko N.A., Polkovnikov A.S., Zegrya G.G., Suris R.A., Lau P.-K., Makino T. *Semicond. Sci. Technol.*, **15** (12), 1131 (2000).
19. Asryan L.V., Luryi S., Suris R.A. *Appl. Phys. Lett.*, **81** (12), 2154 (2002).
20. Asryan L.V., Luryi S., Suris R.A. *IEEE J. Quantum Electron.*, **39** (3), 404 (2003).
21. Asryan L.V., Sokolova Z.N. *J. Appl. Phys.*, **115** (2), 023107 (2014).

22. Asryan L.V., Luryi S. *Solid-State Electron.*, **47** (2), 205 (2003).
23. Asryan L.V., Luryi S. U.S. Patent No. 6,870,178, Mar. 22, 2005.
24. Asryan L.V., Luryi S. *IEEE J. Quantum Electron.*, **37** (7), 905 (2001).
25. Han D.-S., Asryan L.V. *Appl. Phys. Lett.*, **92** (25), 251113 (2008).
26. Han D.-S., Asryan L.V. *Solid-State Electron.*, **52** (10), 1674 (2008).
27. Han D.-S., Asryan L.V. *J. Lightwave Technol.*, **27** (24), 5775 (2009).
28. Han D.-S., Asryan L.V. *Nanotechnology*, **21** (1), 015201 (2010).
29. Asryan L.V. *Semicond. Sci. Technol.*, **30** (3), 035022 (2015).
30. Asryan L.V. *Opt. Lett.*, **42** (1), 97 (2017).
31. Asryan L.V., Kar S. *IEEE J. Quantum Electron.*, **55** (1), 2000109 (2019).
32. Asryan L.V., Kryzhanovskaya N.V., Maximov M.V., Egorov A.Yu., Zhukov A.E. *Semicond. Sci. Technol.*, **26** (5), 055025 (2011).
33. Zhukov A.E., Kryzhanovskaya N.V., Zubov F.I., Shernyakov Y.M., Maximov M.V., Semenova E.S., Yvind K., Asryan L.V. *Appl. Phys. Lett.*, **100** (2), 021107 (2012).
34. Asryan L.V., Kryzhanovskaya N.V., Maximov M.V., Zubov F.I., Zhukov A.E. *J. Appl. Phys.*, **114** (14), 143103 (2013).
35. Zubov F.I., Zhukov A.E., Shernyakov Y.M., Maximov M.V., Semenova E.S., Asryan L.V. *J. Phys. Conf. Ser.*, **643**, 012042 (2015).
36. Asryan L.V., Zubov F.I., Kryzhanovskaya N.V., Maximov M.V., Zhukov A.E. *Semicond.*, **50** (10), 1362 (2016) [*Fiz. Tekh. Poluprovodn.*, **50** (10), 1380 (2016)].
37. Asryan L.V., Zubov F.I., Balezina (Polubavkina) Yu.S., Moiseev E.I., Muretova M.E., Kryzhanovskaya N.V., Maximov M.V., Zhukov A.E. *Semicond.*, **52** (12), 1621 (2018) [*Fiz. Tekh. Poluprovodn.*, **52** (12), 1518 (2018)].
38. Kazarinov R.F., Belenky G.L. *IEEE J. Quantum Electron.*, **31** (3), 423 (1995).
39. Mawst L.J., Botez D. *Proc. SPIE*, **3001**, 7 (1997).
40. Ishizaka S., Muro K., Fujimoto T., Yamada Y. U.S. Patent No. 5764668, June 9, 1998.
41. Tomita A. U.S. Patent No. 6014394, Jan. 11, 2000.
42. He X. U.S. Patent No. 6298077 B1, Oct. 2, 2001.
43. Wiedmann N., Schmitz J., Boucke K., Herres N., Wagner J., Mikulla M., Poprawe R., Weimann G. *IEEE J. Quantum Electron.*, **38** (1), 67 (2002).
44. Lee J.J., Mawst L.J., Botez D. *J. Cryst. Growth*, **249**, 100 (2003).
45. Pataro L.L., Deng Y., Dapkus P.D. *Proc. IEEE LEOS 17th Annual Meeting* (Puerto Rico, 2004) Vol. 2, pp 469–470.
46. Liang R., Hosoda T., Kipshidze G., Shterengas L., Belenky G. *IEEE Photon. Technol. Lett.*, **25** (10), 925 (2013).
47. Coldren L.A., Corzine S.W. *Diode Lasers and Photonic Integrated Circuits* (New York: Wiley, 1995).

ISSN 1063-7826, Semiconductors, 2018, Vol. 52, No. 12, pp. 1621–1629. © Pleiades Publishing, Ltd., 2018.
Original Russian Text © L.V. Asryan, F.I. Zubov, Yu.S. Balezina (Polubavkina), E.I. Moiseev, M.E. Muretova, N.V. Kryzhanovskaya, M.V. Maximov, A.E. Zhukov, 2018, published in Fizika i Tekhnika Poluprovodnikov, 2018, Vol. 52, No. 12, pp. 1518–1526.

PHYSICS OF SEMICONDUCTOR DEVICES

Violation of Local Electroneutrality in the Quantum Well of a Semiconductor Laser with Asymmetric Barrier Layers

L. V. Asryan[a,*], F. I. Zubov[b], Yu. S. Balezina (Polubavkina)[b], E. I. Moiseev[b], M. E. Muretova[b], N. V. Kryzhanovskaya[b], M. V. Maximov[b], and A. E. Zhukov[b]

[a] *Virginia Polytechnic Institute and State University, Blacksburg, Virginia 24061, USA*

[b] *St. Petersburg National Research Academic University, Russian Academy of Sciences, St. Petersburg, 194021 Russia*

**e-mail: asryan@vt.edu*

Submitted March 28, 2018; accepted for publication April 4, 2018

Abstract—A self-consistent model for calculating the threshold and high-power characteristics of semiconductor quantum well lasers with asymmetric barrier layers is developed. The model, which is based on a system of rate equations, uses the universal condition of global charge neutrality in the laser structure. The electron and hole concentrations in the waveguide region and in the quantum well (QW) and the concentration of photons of stimulated emission are calculated. The local neutrality in the QW is shown to be strongly violated, especially at high injection currents. The violation of neutrality in a QW makes the electron and hole concentrations there dependent on the injection current under lasing conditions: in the structures under consideration, the electron concentration in the QW decreases while the hole concentration increases with increasing injection current. In the case of the ideal functioning of asymmetric barrier layers, when electron–hole recombination in the waveguide region is completely suppressed, the violation of neutrality in the QW has almost no effect on the dependence of the output optical power on the injection current: the quantum efficiency is close to unity and the light–current characteristic is linear. Nevertheless, the violation of neutrality in the QW causes weakening of the temperature dependence of the threshold current and, hence, an increase in the characteristic temperature T_0 of the laser.

DOI: 10.1134/S1063782618120059

1. INTRODUCTION

The use of asymmetric barrier layers (ABLs) [1–4], along with the double tunneling injection of charge carriers [5–8], was previously proposed for suppressing parasitic electron–hole recombination in laser waveguides, and, thereby, for attaining a radical improvement in the characteristics of lasers with a low-dimensional active region. In both of these types of laser, recombination is suppressed by preventing the simultaneous (bipolar) presence of electrons and holes anywhere in the structure except for the active region. In lasers with ABLs (Fig. 1), the bipolar population in the waveguide region (the optical confinement layer OCL) is blocked by using two asymmetric barrier layers. One barrier layer (the left one in Fig. 1) allows electrons injected from the *n*-type emitter to enter the active region but prevents the leakage of holes from the active region to the left-hand part of the waveguide region, where there is a significant concentration of electrons. The other ABL (the right one in Fig. 1) allows holes injected from the *p*-type emitter to freely reach the active region but blocks the electron leakage from this region to the right-hand part of the waveguide region, where holes are abundant.

The operating characteristics of lasers with ABLs and a quantum-well (QW) active region were calculated in [9]. The asymmetry between the filling of electron and hole states was taken into account in these calculations, but, at the same time, it was assumed that the QW is electrically neutral, i.e., the two-dimensional concentrations of electrons and holes in the QW are the same. However, it was shown earlier [10–13] that, because of the asymmetry between the electron and hole parameters, local electroneutrality in the active region is violated even in conventional laser structures without ABLs. In lasers

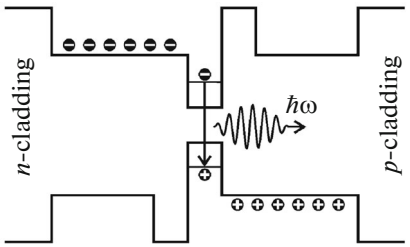

Fig. 1. Schematic energy-band diagram of a laser with asymmetric barrier layers.

with ABLs, in addition to the asymmetry between the electron and hole parameters, there is asymmetry in the spatial distribution of oppositely charged carriers in the waveguide region (in Fig. 1, electrons are present only in the left-hand part and holes only in the right-hand part of the waveguide) and, thus, the violation of local electroneutrality in the active region can be manifested to an even greater degree. In this paper, we present a self-consistent model for calculating the threshold and high-power characteristics of semiconductor QW lasers with ABLs taking into account the possible violation of electroneutrality in the active region and using the universal condition of global charge neutrality in the structure.

2. BASIC EQUATIONS

Our model is based on the following system of rate equations:

$$b_1\frac{\partial n_{\rm L}^{\rm OCL}}{\partial t}=\frac{j}{e}+\frac{n^{\rm QW}}{\tau_{n,\rm esc}}-v_{n,\rm capt,0}(1-f_n)n_{\rm L}^{\rm OCL}, \quad (1)$$

$$b_2\frac{\partial p_{\rm R}^{\rm OCL}}{\partial t}=\frac{j}{e}+\frac{p^{\rm QW}}{\tau_{p,\rm esc}}-v_{p,\rm capt,0}(1-f_p)p_{\rm R}^{\rm OCL}, \quad (2)$$

$$\frac{\partial n^{\rm QW}}{\partial t}=v_{n,\rm capt,0}(1-f_n)n_{\rm L}^{\rm OCL}-\frac{n^{\rm QW}}{\tau_{n,\rm esc}}-B_{\rm 2D}n^{\rm QW}p^{\rm QW} - c_g g^{\max}(f_n+f_p-1)n_{\rm ph}, \quad (3)$$

$$\frac{\partial p^{\rm QW}}{\partial t}=v_{p,\rm capt,0}(1-f_p)p_{\rm R}^{\rm OCL}-\frac{p^{\rm QW}}{\tau_{p,\rm esc}}-B_{\rm 2D}n^{\rm QW}p^{\rm QW} - c_g g^{\max}(f_n+f_p-1)n_{\rm ph}, \quad (4)$$

$$\frac{\partial n_{\rm ph}}{\partial t}=c_g g^{\max}(f_n+f_p-1)n_{\rm ph}-c_g\beta n_{\rm ph}. \quad (5)$$

Here, the unknowns are the three-dimensional concentration $n_{\rm L}^{\rm OCL}$ of free electrons in the left-hand part of the waveguide region, three-dimensional concentration $p_{\rm R}^{\rm OCL}$ of free holes in the right-hand part of the waveguide region, two-dimensional concentrations $n^{\rm QW}$ and $p^{\rm QW}$ of electrons and holes localized in the QW, and the concentration $n_{\rm ph}$ of stimulated-emission photons per unit contact area.

Equations (1)–(5) also feature the occupancies f_n and f_p of the states corresponding to the bottom of the electron and the top of the hole quantum-confinement subbands in the QW, respectively. However, these quantities are not independent, because they can be expressed in terms of the electron and hole concentrations in the QW [14–16]:

$$f_n=1-\exp\left(-\frac{n^{\rm QW}}{N_c^{\rm 2D}}\right),\quad f_p=1-\exp\left(-\frac{p^{\rm QW}}{N_v^{\rm 2D}}\right), \quad (6)$$

where $N_{c,v}^{\rm 2D}=m_{e,hh}^{\rm QW}T/(\pi\hbar^2)$ are the two-dimensional effective densities of states in the conduction and valence bands of the QW, $m_{e,hh}^{\rm QW}$ are the electron and hole effective masses in the QW, and T is the temperature expressed in units of energy.

The following quantities enter Eqs. (1)–(5) as parameters: b_1 and b_2 are the thicknesses of the left- and right-hand parts of the waveguide region (which are typically the same); j is the injection current density; e is the elementary charge; $\tau_{n,\rm esc}$ and $\tau_{p,\rm esc}$ are the times of thermal escape of electrons and holes from the QW to the waveguide region, respectively; $v_{n,\rm capt,0}$ and $v_{p,\rm capt,0}$ are the velocities of electron and hole capture from the waveguide region into the empty ($f_n=f_p=0$) QW, measured in cm/s; $B_{\rm 2D}$ is the coefficient of spontaneous radiative recombination in the two-dimensional region (the QW), measured in cm^2/s [17]; c_g is the group velocity of light; $g^{\max}$ is the maximum modal gain coefficient in the QW; $\beta=[1/(2L)]\ln[1/(R_1R_2)]$ represents the output loss of photons from the cavity; L is the length of the laser Fabry–Perot cavity; and R_1 and R_2 are the reflectivities of the facet mirrors of the cavity.

The times of thermal escape from the QW to the waveguide region can be expressed in terms of the velocities of capture from the waveguide to the empty QW [8, 18]. In the case of undoped waveguide and QW regions, these expressions are [8, 18]

$$\tau_{n,\rm esc}=\frac{1}{v_{n,\rm capt,0}(1-f_n)}\frac{N_c^{\rm 2D}}{n_1},$$

$$\tau_{p,\rm esc}=\frac{1}{v_{p,\rm capt,0}(1-f_p)}\frac{N_v^{\rm 2D}}{p_1}, \quad (7)$$

where

$$n_1=N_c^{\rm 3D}\exp\left(-\frac{\Delta E_c-\varepsilon_n^{\rm QW}}{T}\right),$$

$$p_1=N_v^{\rm 3D}\exp\left(-\frac{\Delta E_v-\varepsilon_p^{\rm QW}}{T}\right). \quad (8)$$

Here, $N_{c,v}^{\rm 3D}=2[m_{c,v}^{\rm OCL}T/(2\pi\hbar^2)]^{3/2}$ are the three-dimensional effective densities of states in the conduction and valence bands in the waveguide region; $m_{c,v}^{\rm OCL}$ are the electron and hole effective masses in the waveguide region; $\Delta E_{c,v}$ are the discontinuities of the conduction- and valence-band edges at the heterointerface between the QW and the waveguide region; and $\varepsilon_n^{\rm QW}$ and $\varepsilon_p^{\rm QW}$ are the energies of the bottom of the electron and the top of the hole quantum-confinement subbands in the QW, respectively.

In this study, we make the assumption, reflected in Eqs. (1)–(5), that both ABLs function perfectly: free

electrons are absent in the left-hand part and free holes in the right-hand part of the waveguide region (i.e., $n_R^{OCL} = p_L^{OCL} = 0$) and, consequently, recombination in the waveguide is completely suppressed.

Equations (1)–(5) represent a system for finding five unknowns (four charge-carrier concentrations n_L^{OCL}, p_R^{OCL}, n^{QW}, and p^{QW} and the photon concentration n_{ph}). It is shown below that four of the five unknowns in this system can be expressed via the fifth one (for definiteness, let this one be n^{QW}) thus reduce the solution of the system to the solution of an algebraic equation for this unknown (n^{QW}).

Adding Eqs. (1) and (3), we obtain

$$\frac{\partial}{\partial t}(b_1 n_L^{OCL} + n^{QW}) = \frac{j}{e} - B_{2D} n^{QW} p^{QW} - c_g g^{max}(f_n + f_p - 1) n_{ph}, \quad (9)$$

and adding Eqs. (2) and (4), we obtain

$$\frac{\partial}{\partial t}(b_2 p_R^{OCL} + p^{QW}) = \frac{j}{e} - B_{2D} n^{QW} p^{QW} - c_g g^{max}(f_n + f_p - 1) n_{ph}. \quad (10)$$

Comparing Eqs. (9) and (10), we find

$$\frac{\partial}{\partial t}[e(b_2 p_R^{OCL} + p^{QW}) - e(b_1 n_L^{OCL} + n^{QW})] = 0. \quad (11)$$

The expression in square brackets in Eq. (11) is the total charge per unit contact area in the laser structure. Therefore, this equation represents the condition for conservation of the total charge in the laser structure. Since the structure is initially neutral, we obtain from Eq. (11) the universal condition of its global electroneutrality in the form

$$b_1 n_L^{OCL} + n^{QW} = b_2 p_R^{OCL} + p^{QW}, \quad (12)$$

which presents the equality of the total charge per unit area of electrons in the QW and the left-hand part of the waveguide region to the total charge of holes in the QW and the right-hand part of the waveguide region.

We consider the continuous-wave operation of the laser and, thus, will solve the rate equations (1)–(5) for the steady-state case ($\partial/\partial t = 0$ in all equations).

From Eqs. (1) and (2), n_L^{OCL} and p_R^{OCL} can be expressed as

$$n_L^{OCL} = \frac{j}{e v_{n,capt,0}(1 - f_n)} + \frac{1}{\tau_{n,esc}} \frac{1}{v_{n,capt,0}(1 - f_n)} n^{QW}, \quad (13)$$

$$p_R^{OCL} = \frac{j}{e v_{p,capt,0}(1 - f_p)} + \frac{1}{\tau_{p,esc}} \frac{1}{v_{p,capt,0}(1 - f_p)} p^{QW}. \quad (14)$$

Taking into account Eq. (7), Eqs. (13) and (14) can be written as

$$n_L^{OCL} = \frac{j}{e v_{n,capt,0}(1 - f_n)} + n_1 \frac{n^{QW}}{N_c^{2D}}, \quad (15)$$

$$p_R^{OCL} = \frac{j}{e v_{p,capt,0}(1 - f_p)} + p_1 \frac{p^{QW}}{N_v^{2D}}. \quad (16)$$

Using Eq. (6) in Eq. (15), we ultimately express n_L^{OCL} via n^{QW}:

$$n_L^{OCL} = \frac{j}{e v_{n,capt,0}} \exp\left(\frac{n^{QW}}{N_c^{2D}}\right) + n_1 \frac{n^{QW}}{N_c^{2D}}. \quad (17)$$

In the steady-state case, Eq. (5) yields

$$f_n + f_p - 1 = \frac{\beta}{g^{max}}, \quad (18)$$

which is the lasing condition. Using Eq. (6) in Eq. (18), we obtain

$$1 - \exp\left(-\frac{n^{QW}}{N_c^{2D}}\right) - \exp\left(-\frac{p^{QW}}{N_v^{2D}}\right) = \frac{\beta}{g^{max}} \quad (19)$$

from whence p^{QW} can be expressed via n^{QW} as

$$p^{QW} = N_v^{2D} \ln \frac{1}{1 - \frac{\beta}{g^{max}} - \exp\left(-\frac{n^{QW}}{N_c^{2D}}\right)}. \quad (20)$$

From Eq. (18), we have for $(1 - f_p)$

$$1 - f_p = f_n - \frac{\beta}{g^{max}} \quad (21)$$

or, using Eq. (6),

$$1 - f_p = 1 - \frac{\beta}{g^{max}} - \exp\left(-\frac{n^{QW}}{N_c^{2D}}\right). \quad (22)$$

Using Eqs. (20) and (22) in Eq. (16), we ultimately express p_R^{OCL} via n^{QW}:

$$p_R^{OCL} = \frac{j}{e v_{p,capt,0}\left[1 - \frac{\beta}{g^{max}} - \exp\left(-\frac{n^{QW}}{N_c^{2D}}\right)\right]} + p_1 \ln \frac{1}{1 - \frac{\beta}{g^{max}} - \exp\left(-\frac{n^{QW}}{N_c^{2D}}\right)}. \quad (23)$$

Substituting expressions (17), (20), and (23) for n_L^{OCL}, p^{QW}, and p_R^{OCL} into the condition of global elec-

troneutrality represented by Eq. (12), we obtain the following transcendental algebraic equation for n^{QW}:

$$b_1\left[\frac{j}{ev_{n,\mathrm{capt},0}}\exp\left(\frac{n^{QW}}{N_c^{2D}}\right)+n_1\frac{n^{QW}}{N_c^{2D}}\right]+n^{QW}$$
$$=b_2\left\{\frac{j}{ev_{p,\mathrm{capt},0}\left[1-\frac{\beta}{g^{\max}}-\exp\left(-\frac{n^{QW}}{N_c^{2D}}\right)\right]}\right.$$
$$\left.+\,p_1\ln\frac{1}{1-\frac{\beta}{g^{\max}}-\exp\left(-\frac{n^{QW}}{N_c^{2D}}\right)}\right\} \quad (24)$$
$$+\,N_v^{2D}\ln\frac{1}{1-\frac{\beta}{g^{\max}}-\exp\left(-\frac{n^{QW}}{N_c^{2D}}\right)}.$$

The solution of this equation yields the two-dimensional concentration n^{QW} of electrons in the QW as a function of the injection current density j and the parameters of the laser structure. Having determined n^{QW}, we can then calculate n_L^{OCL}, p^{QW}, and p_R^{OCL} using Eqs. (17), (20), and (23).

The concentration of photons in the cavity can also be expressed in terms of n^{QW}. From Eqs. (9) and (10), we have for the injection current density in the steady-state case

$$j=eB_{2D}n^{QW}p^{QW}+ec_g g^{\max}(f_n+f_p-1)n_{ph}. \quad (25)$$

Using Eq. (18) and introducing the photon lifetime in the cavity

$$\tau_{ph}=\frac{1}{c_g\beta}, \quad (26)$$

we can express the injection current density as

$$j=eB_{2D}n^{QW}p^{QW}+e\frac{n_{ph}}{\tau_{ph}} \quad (27)$$

from whence the concentration of stimulated-emission photons is

$$n_{ph}=\tau_{ph}\left(\frac{j}{e}-B_{2D}n^{QW}p^{QW}\right), \quad (28)$$

where p^{QW} is expressed via n^{QW} according to Eq. (20).

The solution of Eq. (24) makes it further possible to calculate the light–current characteristic of the laser, i.e., the dependence of the output optical power on the injection current density [19, 20]:

$$P(j)=\frac{\hbar\omega}{e}Sj_{\mathrm{stim}}(j)=\hbar\omega\frac{n_{ph}}{\tau_{ph}}S$$
$$=\frac{\hbar\omega}{e}S[j-eB_{2D}n^{QW}(j)p^{QW}(j)] \quad (29)$$
$$=\frac{\hbar\omega}{e}S(j-j_{tn})\eta_{\mathrm{int}}(j),$$

where $\hbar\omega$ is the photon energy, $S=WL$ is the area of the stripe contact, W is the contact width, and j_{th} is the threshold current density.

The stimulated-recombination current density and the internal differential quantum efficiency (the efficiency of stimulated radiative recombination) appearing in Eq. (29) are given as follows [21]:

$$j_{\mathrm{stim}}=e\frac{n_{ph}}{\tau_{ph}}=j-eB_{2D}n^{QW}p^{QW}, \quad (30)$$

$$\eta_{\mathrm{int}}=\frac{j_{\mathrm{stim}}}{j-j_{th}}. \quad (31)$$

The threshold current density j_{th} is found as the root of the equation

$$n_{ph}(j)=0 \quad (32)$$

or, using Eq. (28),

$$j-eB_{2D}n^{QW}(j)p^{QW}(j)=0. \quad (33)$$

Expression (31) can be written as

$$\eta_{\mathrm{int}}(j)=\frac{j-eB_{2D}n^{QW}(j)p^{QW}(j)}{j-eB_{2D}n^{QW}(j_{th})p^{QW}(j_{th})}$$
$$=\frac{j-j_{\mathrm{spon}}^{QW}(j)}{j-j_{\mathrm{spon,th}}^{QW}}=\frac{j-j_{\mathrm{spon}}^{QW}(j)}{j-j_{th}}, \quad (34)$$

where we introduced the current density of spontaneous radiative recombination in the QW

$$j_{\mathrm{spon}}^{QW}(j)=eB_{2D}n^{QW}(j)p^{QW}(j) \quad (35)$$

and expressed the threshold current density as

$$j_{th}=j_{\mathrm{spon,th}}^{QW}=eB_{2D}n^{QW}(j_{th})p^{QW}(j_{th})$$
$$=eB_{2D}n_{th}^{QW}p_{th}^{QW}, \quad (36)$$

where

$$n_{th}^{QW}=n^{QW}(j_{th}) \quad \text{and} \quad p_{th}^{QW}=p^{QW}(j_{th}) \quad (37)$$

are the threshold concentrations of electrons and holes in the QW.

3. DISCUSSION OF THE RESULTS

In this section, we present the results of calculations performed on the basis of our model for laser structures emitting at wavelengths of λ_0 = 808 nm

(Figs. 2–7a) and 840 nm (Figs. 7b–9). In the structure emitting at 808 nm, the materials for the QW and waveguide regions are $(GaAs)_{0.9}(Ga_{0.51}In_{0.49}P)_{0.1}$ and $(GaAs)_{0.46}(Ga_{0.51}In_{0.49}P)_{0.54}$, respectively; the thickness of the QW is 7.4 nm. In the structure emitting at 840 nm, the materials for the QW and waveguide regions are GaAs and $Al_{0.2}Ga_{0.8}As$, respectively [3, 9]; the thickness of the QW is 7.5 nm. The thickness of the waveguide region in both structures is $b = 0.4$ μm. The cavity length and the width of the stripe contact are $L = 500$ μm and $W = 3$ μm, respectively.

Under the assumption of local electroneutrality in the QW [3, 9], the concentration of electrons and holes in the QW remains unchanged with increasing injection current and equal to its threshold value. As can be seen from Eq. (24), when the violation of local electroneutrality in the QW is taken into account, the electron concentration in the QW n^{QW} and, therefore, also the hole concentration p^{QW} (see Eq. (20)) become dependent on the injection current density j. According to the lasing condition (19), n^{QW} and p^{QW} cannot increase or decrease simultaneously. If n^{QW} decreases with increasing current, the fulfillment of condition (19) requires that p^{QW} increases and vice versa.

Figure 2 shows the dependences of the concentrations n^{QW} and p^{QW} on the injection current density. According to this figure, n^{QW} decreases and p^{QW} increases with increasing current in the structure under consideration. Therefore, the difference between n^{QW} and p^{QW} increases (that is, the violation of the local electroneutrality becomes stronger) with increasing pump current. Nevertheless, it can be seen that both the decrease in n^{QW} and the increase in p^{QW} level off with increasing j, so that n^{QW} and p^{QW} approach their asymptotic values (which are shown in the figure by dotted horizontal lines). The following expression for the asymptotic value of n^{QW} at $j \to \infty$ can easily be obtained from Eq. (24):

$$n^{QW}_{asympt} = N_c^{2D} \ln\left(\frac{1+\frac{\tau_{p,capt,0}}{\tau_{n,capt,0}}}{1-\frac{\beta}{g^{max}}}\right), \qquad (38)$$

where

$$\tau_{n,capt,0} = \frac{b_1}{v_{n,capt,0}} \quad \text{and} \quad \tau_{p,capt,0} = \frac{b_2}{v_{p,capt,0}} \qquad (39)$$

are the capture times of electrons from the left-hand part and holes from the right-hand part of the waveguide region into the empty QW, respectively.

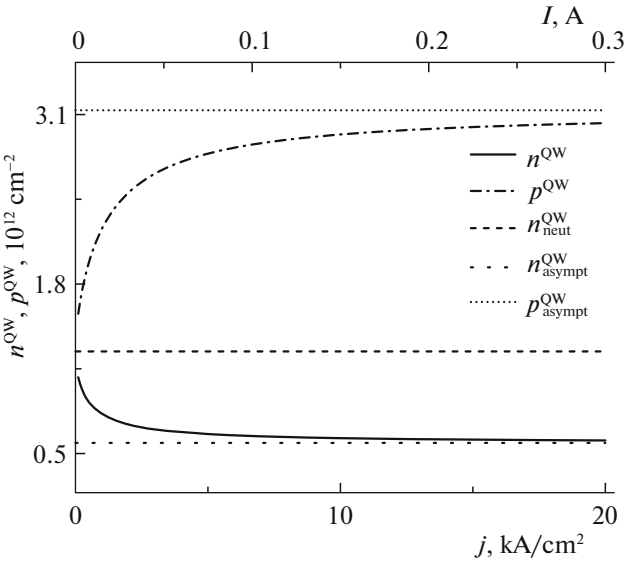

Fig. 2. Two-dimensional concentrations of electrons and holes (solid and dash-dotted curves, respectively) in the QW as functions of the injection current density (bottom axis) and injection current (top axis). The dashed horizontal line shows the concentration of electrons and holes in the QW calculated on the assumption of local electroneutrality in the QW. The dotted horizontal lines show the asymptotic values of the electron and hole concentrations in the QW, given by Eqs. (38) and (40). Figures 2–7a show the results of calculations for the structure emitting at a wavelength of $\lambda_0 = 808$ nm. In Figs. 2–9, the thickness of the waveguide region $b = 0.4$ μm, the cavity length $L = 500$ μm, and the width of the stripe contact $W = 3$ μm.

Using Eq. (38) in Eq. (20), we obtain the asymptotic value of p^{QW} at $j \to \infty$:

$$p^{QW}_{asympt} = N_v^{2D} \ln\left(\frac{1+\frac{\tau_{n,capt,0}}{\tau_{p,capt,0}}}{1-\frac{\beta}{g^{max}}}\right). \qquad (40)$$

In this paper, we use equal values for the velocities of electron and hole capture into the QW ($v_{n,capt,0} = v_{p,capt,0} = 1 \times 10^5$ cm/s) and assume that the QW is placed in the middle of the waveguide region, i.e., we use equal values for the thicknesses of the left-hand and right-hand parts of the waveguide region ($b_1 = b_2 = b/2 = 0.2$ μm). Thus, the times of electron and hole capture into the QW are the same ($\tau_{n,capt,0} = \tau_{p,capt,0} = 0.2$ ns). According to Eqs. (38) and (40), if the electron and hole capture times are equal, the maximum value of the ratio of the positive to the negative charge in the QW is

$$\frac{ep^{QW}_{asympt}}{en^{QW}_{asympt}} = \frac{N_v^{2D}}{N_c^{2D}} = \frac{m^{QW}_{hh}}{m_c^{QW}}, \qquad (41)$$

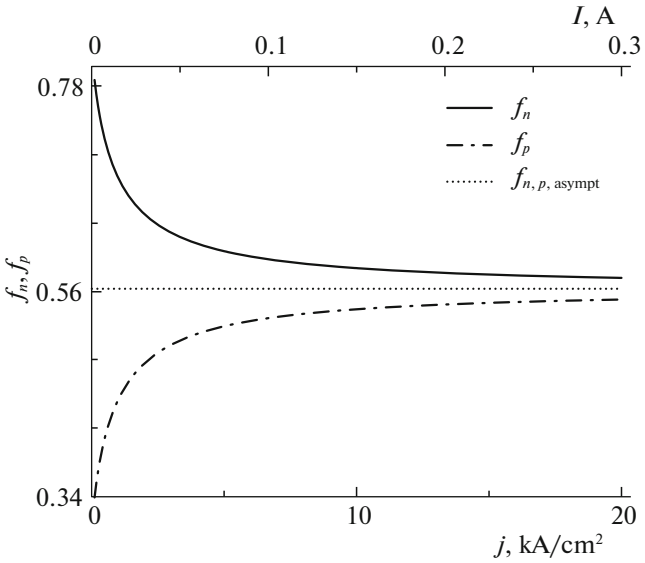

Fig. 3. Occupancies of the states corresponding to the bottom of the electron and the top of the hole quantum-confinement subbands in the QW (solid and dash-dotted curves, respectively) as functions of the injection current density (bottom axis) and injection current (top axis). The dotted horizontal line shows the asymptotic values of the occupancies, given by Eqs. (42) and (43) and coinciding with each other when the times of electron and hole capture into the QW coincide.

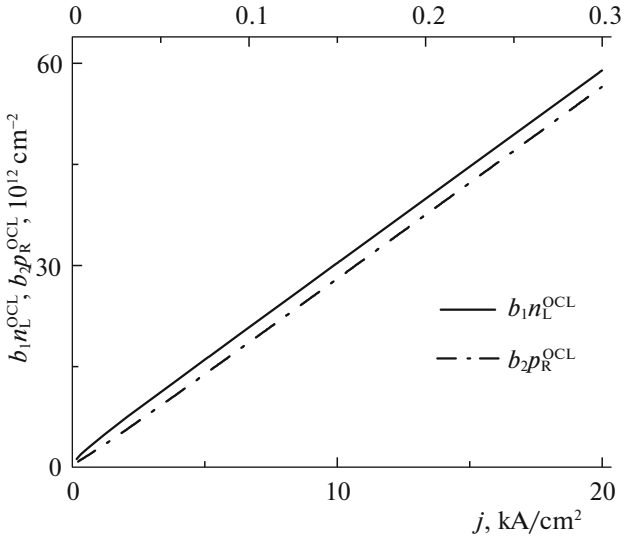

Fig. 4. Concentrations of free electrons in the left-hand part of the waveguide region and holes in its right-hand part (solid and dash-dotted curves, respectively) per unit contact area as functions of the injection current density (bottom axis) and injection current (top axis).

where we used the expressions for $N_{c,v}^{2D}$ given after Eq. (6). For the considered QW based on $(GaAs)_{0.9}(Ga_{0.51}In_{0.49}P)_{0.1}$, $p_{asympt}^{QW}/n_{asympt}^{QW} = 5.4$ (see dotted horizontal lines in Fig. 2). Thus, our calculations demonstrate that local electroneutrality in the QW is violated to a significant extent, especially at high pump currents.

Figure 3 shows the occupancies of the states corresponding to the bottom of the electron and the top of the hole quantum-confinement subbands in the QW versus the pump current density. The character of these dependences is evident from Eq. (6) and Fig. 2: f_n decreases since n^{QW} decreases, and f_p increases since p^{QW} increases. With increasing current, f_n and f_p approach the following asymptotic values:

$$f_{n,\text{asympt}} = \frac{\dfrac{\beta}{g^{\max}} + \dfrac{\tau_{p,\text{capt},0}}{\tau_{n,\text{capt},0}}}{1 + \dfrac{\tau_{p,\text{capt},0}}{\tau_{n,\text{capt},0}}}, \quad (42)$$

$$f_{p,\text{asympt}} = \frac{\dfrac{\beta}{g^{\max}} + \dfrac{\tau_{n,\text{capt},0}}{\tau_{p,\text{capt},0}}}{1 + \dfrac{\tau_{n,\text{capt},0}}{\tau_{p,\text{capt},0}}}. \quad (43)$$

When $\tau_{n,\text{capt},0} = \tau_{p,\text{capt},0}$, the asymptotic values given by Eqs. (42) and (43) coincide (see the dotted horizontal line in Fig. 3).

As far as the hole charge in the QW exceeds the electron charge (Fig. 2), the condition of global electroneutrality, given by Eq. (12), requires that the charge $eb_1 n_L^{OCL}$ of electrons in the left-hand part of the waveguide region exceeds the charge $eb_2 p_R^{OCL}$ of holes in its right-hand part. Figure 4 shows the concentrations of free electrons and holes in the left- and right-hand parts of the waveguide region, respectively, versus the injection current density. For comparison with the two-dimensional carrier concentrations in the QW (Fig. 2), the concentrations of free carriers in the waveguide shown in Fig. 4 are recalculated per unit area of the contact; i.e., we plot in Fig. 4 the values of $b_1 n_L^{OCL}$ and $b_2 p_R^{OCL}$. As can be seen from Figs. 2 and 4, the values of $b_1 n_L^{OCL}$ and $b_2 p_R^{OCL}$ are close to each other and are considerably higher than the concentrations n^{QW} and p^{QW} of electrons and holes in the QW. Thus, a small relative excess of n_L^{OCL} over p_R^{OCL} (Fig. 4) compensates for a significant excess of p^{QW} over n^{QW} (Fig. 2).

The asymptotic expression for $b_1 n_L^{OCL}$ and $b_2 p_R^{OCL}$ at $j \to \infty$ has the following form:

$$b_1 n_{L,\text{asympt}}^{OCL} = b_2 p_{R,\text{asympt}}^{OCL} = \frac{\tau_{n,\text{capt},0} + \tau_{p,\text{capt},0}}{1 - \dfrac{\beta}{g^{\max}}} \frac{j}{e}. \quad (44)$$

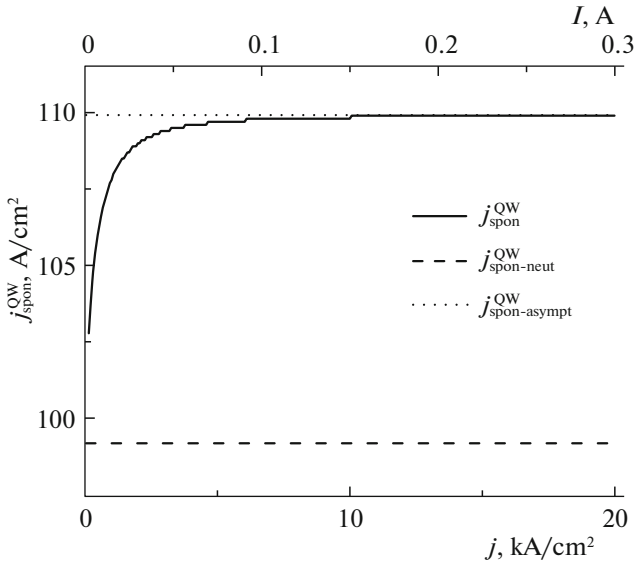

Fig. 5. Density of the spontaneous radiative-recombination current in the QW as a function of the injection current density (bottom axis) and injection current (top axis). The dashed horizontal line shows the density of the spontaneous radiative-recombination current in the QW calculated under the assumption of local electroneutrality in the QW. The dotted horizontal line shows the asymptotic value of the density of spontaneous radiative recombination current in the QW, given by Eq. (45).

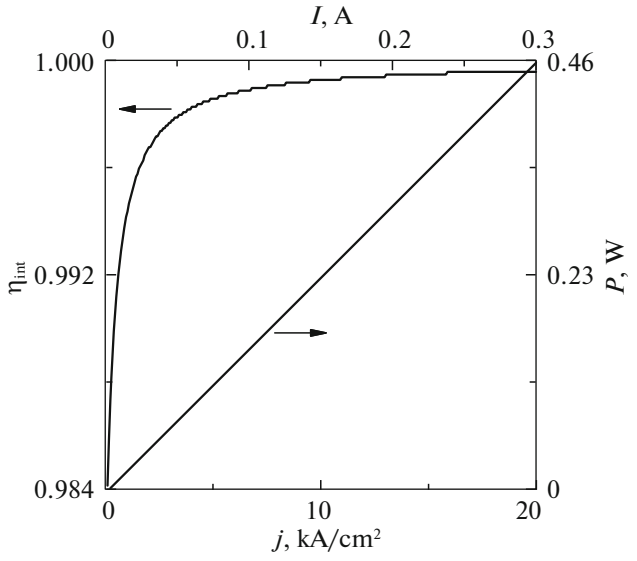

Fig. 6. Internal differential quantum efficiency (left axis) and output optical power (right axis) as functions of the injection current density (bottom axis) and injection current (top axis).

Because the electron and hole concentrations in the QW depend on the injection current density, the density of the spontaneous radiative-recombination current in the QW also depends on j: j_{spon}^{QW} increases with increasing j (see Fig. 5). However, in contrast to n^{QW} and p^{QW}, which exhibit significant variations with the injection current (Fig. 2), j_{spon}^{QW} grows insignificantly: as j varies from $j_{th} = 103$ A/cm^2 to 20 kA/cm^2, the value of j_{spon}^{QW} only changes from 103 to 110 A/cm^2. One can see from expression (35) that this behavior of j_{spon}^{QW} results from the fact that the growth in p^{QW} with the injection current is compensated to a significant degree by a reduction in n^{QW} (Fig. 2). Since both n^{QW} and p^{QW} level off with increasing current, j_{spon}^{QW} also levels off. Using Eqs. (38) and (40), we obtain the following expression for the asymptotic value of j_{spon}^{QW} at $j \to \infty$ (dotted horizontal line in Fig. 5):

$$j_{spon,asympt}^{QW} = eB_{2D}N_c^{2D}N_v^{2D} \times \ln\left(\frac{1+\frac{\tau_{p,capt,0}}{\tau_{n,capt,0}}}{1-\frac{\beta}{g^{max}}}\right)\ln\left(\frac{1+\frac{\tau_{n,capt,0}}{\tau_{p,capt,0}}}{1-\frac{\beta}{g^{max}}}\right). \quad (45)$$

Since the density of the spontaneous radiative-recombination current in the QW is low and remains bounded from above with increasing pump current (Fig. 5), it follows from Eq. (34) that the internal differential quantum efficiency should approach unity, i.e., increase with pump current, which indeed can be seen in Fig. 6 (left axis). According to this figure, η_{int} is close to unity even at the lasing threshold, and, thus, its increase is insignificant.

Figure 6 also shows the output optical power of the laser (right axis) as a function of the pump current density. One can see that the dependence is linear and is indistinguishable from the light–current characteristic calculated under the assumption of local electroneutrality in the QW [9]. The closeness of η_{int} to unity (Fig. 6) and the linearity of the light–current characteristic (similarly to the case of local neutrality in the QW) result from the assumption of the ideal functioning of ABLs, implying that recombination in the waveguide region is completely suppressed.

Figure 7 shows the characteristic temperature of the laser, defined as [11, 22]

$$T_0 = \left(\frac{\partial \ln j_{th}}{\partial T}\right)^{-1}, \quad (46)$$

as a function of the operating temperature for the structures emitting at 808 and 840 nm. For comparison, we also plot the values of T_0 calculated under the assumption of charge neutrality in the QW [3] (dashed lines). It was shown in [3] that, in the case where

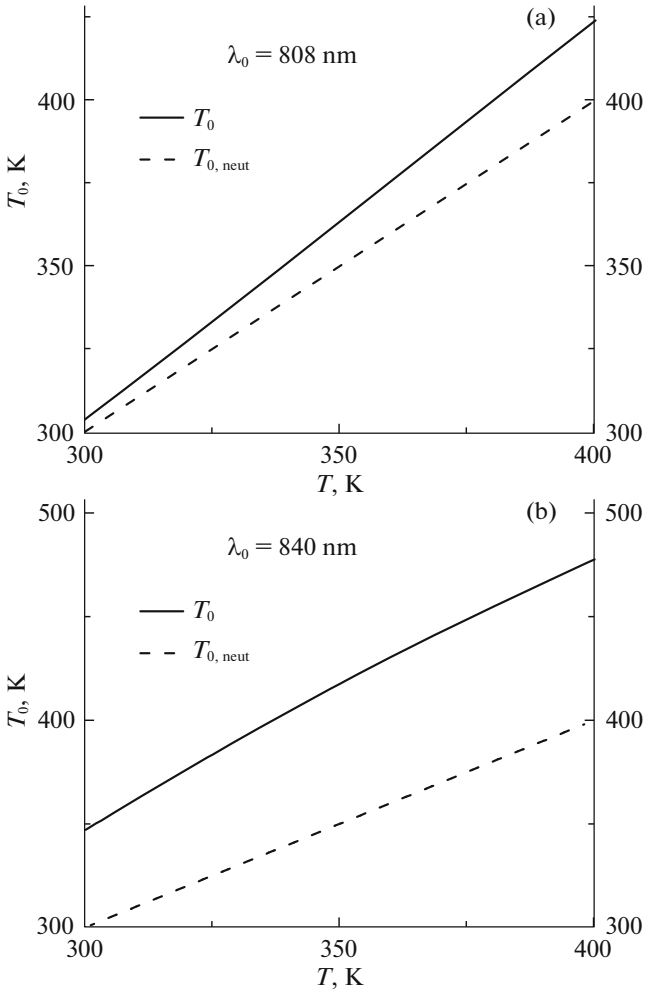

Fig. 7. Characteristic temperature of a laser with asymmetric barrier layers versus the operating temperature for the structures emitting at (a) 808 and (b) 840 nm. The dashed lines show the characteristic temperature calculated on the assumption of local electroneutrality in the QW.

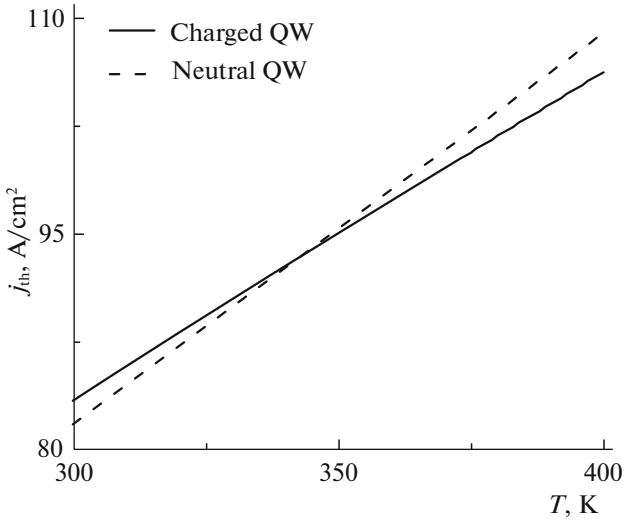

Fig. 8. Threshold current density of a laser with asymmetric barrier layers as a function of temperature. The dashed line shows the threshold current density calculated under the assumption of local electroneutrality in the QW. Figures 8 and 9 show the results of calculations for the structure emitting at a wavelength of $\lambda_0 = 840$ nm.

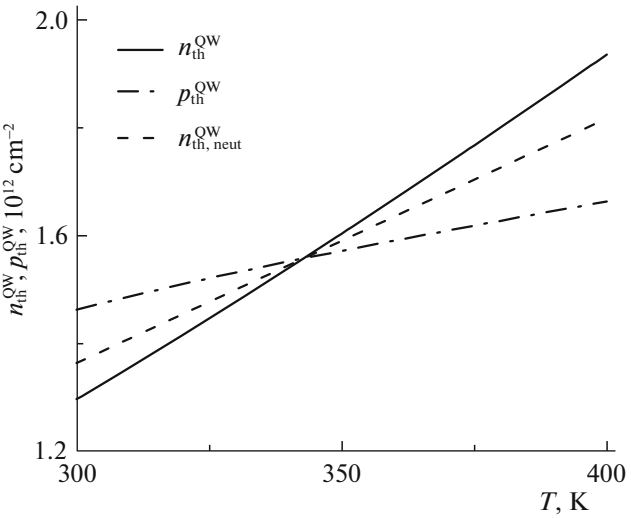

Fig. 9. Temperature dependences of the threshold concentrations of electrons and holes (solid and dash-dotted curves, respectively) in the QW. The dashed line shows the threshold concentration of electrons and holes calculated on the assumption of local electroneutrality in the QW.

recombination outside the active region is completely suppressed (the case we consider in this study)

$$T_{0,\mathrm{neut}} = T. \tag{47}$$

According to Fig. 7, the characteristic temperature T_0 calculated taking the violation of charge neutrality in the QW into account is higher than $T_{0,\,neut}$:

$$T_0 > T_{0,\mathrm{neut}}. \tag{48}$$

The value of T_0 exceeds $T_{0,\,neut}$ by a larger margin in the structure emitting at 840 nm (see Fig. 7b).

This result, which means that the violation of charge neutrality in the QW leads to weakening of the temperature dependence of the threshold current (as is shown in Fig. 8), is not self-evident. As can be seen from Eq. (36), this requires that the product of $n_{th}^{QW} p_{th}^{QW}$ grows with increasing temperature more slowly than $(n_{th,neut}^{QW})^2$, where $n_{th,neut}^{QW}$ is the concentration of electrons and holes in the case of charge neutrality in the QW. Figure 9 shows the temperature dependences of n_{th}^{QW}, p_{th}^{QW}, and $n_{th,neut}^{QW}$. One can see that, while the electron concentration n_{th}^{QW} increases with temperature faster than $n_{th,neut}^{QW}$, the hole concentration p_{th}^{QW} increases significantly more slowly than $n_{th,neut}^{QW}$,

and, thus, the product $n_{th}^{QW} p_{th}^{QW}$ indeed increases more slowly with increasing temperature than $(n_{th,neut}^{QW})^2$.

4. CONCLUSIONS

Thus, we have developed a self-consistent theoretical model for calculating the threshold and power characteristics of semiconductor QW lasers with ABLs. The model, based on a system of rate equations, makes use of the universal condition of global charge neutrality in the laser structure. The concentrations of electrons and holes in the waveguide region and in the QW and the light–current characteristics of the laser have been calculated. We have shown that local neutrality in the QW is severely violated, especially at high injection currents. The violation of charge neutrality in the QW leads to the dependence of the electron and hole concentrations there on the injection current under lasing conditions. In the structures considered here, the electron concentration in the QW decreases and the hole concentration increases with injection current. In the case of ideally functioning ABLs, when electron-hole recombination in the waveguide region is completely suppressed, the violation of neutrality in the QW has almost no effect on the internal differential quantum efficiency and the light–current characteristic of the laser: the quantum efficiency is close to unity, and the light–current characteristic is linear. However, the violation of neutrality in the QW leads to weakening of the temperature dependence of the threshold current and, thus, to an increase in the characteristic temperature T_0 of the laser.

The developed theoretical model can be used for the further optimization of laser structures with ABLs.

ACKNOWLEDGMENTS

This study was supported by the Russian Science Foundation (project no. 14-42-00006 "Novel type of semiconductor laser with characteristics improved by the use of asymmetric barriers"). L.V. Asryan also thanks the U.S. Army Research Office (grant no. W911NF-17-1-0432).

REFERENCES

1. L. V. Asryan and S. Luryi, Solid-State Electron. **47**, 205 (2003).
2. L. V. Asryan and S. Luryi, US Patent No. 6870178 (2005).
3. L. V. Asryan, N. V. Kryzhanovskaya, M. V. Maximov, A. Yu. Egorov, and A. E. Zhukov, Semicond. Sci. Technol. **26**, 055025 (2011).
4. A. E. Zhukov, N. V. Kryzhanovskaya, F. I. Zubov, Y. M. Shernyakov, M. V. Maximov, E. S. Semenova, K. Yvind, and L. V. Asryan, Appl. Phys. Lett. **100**, 021107 (2012).
5. L. V. Asryan and S. Luryi, IEEE J. Quantum Electron. **37**, 905 (2001).
6. D.-S. Han and L. V. Asryan, Appl. Phys. Lett. **92**, 251113 (2008).
7. D.-S. Han and L. V. Asryan, J. Lightwave Technol. **27**, 5775 (2009).
8. D.-S. Han and L. V. Asryan, Nanotechnology **21**, 015201 (2010).
9. L. V. Asryan, F. I. Zubov, N. V. Kryzhanovskaya, M. V. Maximov, and A. E. Zhukov, Semiconductors **50**, 1362 (2016).
10. L. V. Asryan and R. A. Suris, IEEE J. Sel. Top. Quantum Electron. **3**, 148 (1997).
11. L. V. Asryan and R. A. Suris, Electron. Lett. **33**, 1871 (1997).
12. Z. N. Sokolova, N. A. Pikhtin, I. S. Tarasov, and L. V. Asryan, Quantum Electron. **46**, 777 (2016).
13. Z. N. Sokolova, D. A. Veselov, N. A. Pikhtin, I. S. Tarasov, and L. V. Asryan, Semiconductors **51**, 959 (2017).
14. K. J. Vahala and C. E. Zah, Appl. Phys. Lett. **52**, 1945 (1988).
15. L. V. Asryan and S. Luryi, Appl. Phys. Lett. **83**, 5368 (2003).
16. L. V. Asryan and S. Luryi, IEEE J. Quantum Electron. **40**, 833 (2004).
17. L. V. Asryan, Quantum Electron. **35**, 1117 (2005).
18. L. V. Asryan and Z. N. Sokolova, J. Appl. Phys. **115**, 023107 (2014).
19. L. V. Asryan, S. Luryi, and R. A. Suris, Appl. Phys. Lett. **81**, 2154 (2002).
20. L. V. Asryan, S. Luryi, and R. A. Suris, IEEE J. Quantum Electron. **39**, 404 (2003).
21. L. A. Coldren and S. W. Corzine, *Diode Lasers and Photonic Integrated Circuits* (Wiley, New York, 1995).
22. L. V. Asryan and R. A. Suris, IEEE J. Quantum Electron. **34**, 841 (1998).

Translated by M. Skorikov

ISSN 1063-7826, Semiconductors, 2018, Vol. 52, No. 14, pp. 1905–1908. © Pleiades Publishing, Ltd., 2018.

LASERS
AND OPTOELECTRONIC DEVICES

A Search for Asymmetric Barrier Layers for 1550 nm Al-Free Diode Lasers[1]

F. I. Zubov[a,*], M. E. Muretova[a], L. V. Asryan[b], E. S. Semenova[c], M. V. Maximov[a], V. V. Korenev[a], A. V. Savelyev[a], and A. E. Zhukov[a]

[a] *St. Petersburg National Research Academic University of the Russian Academy of Sciences, St. Petersburg, Russia*
[b] *Virginia Polytechnic Institute and State University, Blacksburg, Virginia, USA*
[c] *DTU Fotonik, Department of Photonics Engineering, Technical University of Denmark, Kongens Lyngby, Denmark*
**e-mail: fedyazu@mail.ru*

Abstract—A search for materials suitable for implementation of 1.55 μm Al-free diode lasers based on InP with asymmetric barrier (AB) layers is conducted. It is shown that a very high (over 10^6) suppression ratio of the parasitic electron flux can be achieved using common III–V alloys for the ABs. Hence placing such ABs in the immediate vicinity of the active region should completely suppress the parasitic recombination in the waveguide. Several optimal AB designs are proposed that are based on one of the following alloys: Al-free GaInPSb, ternary AlInAs, or quaternary AlGaInAs with a low Al-content. As an important and beneficial byproduct of utilization of such ABs, an improvement of majority carrier capture into the active region occurs.

DOI: 10.1134/S1063782618140336

1. INTRODUCTION

Parasitic recombination of charge carriers in the waveguide layers is one of the main fundamental factors limiting the diode laser performance [1, 2]. This recombination causes an intrinsic (i.e., in the absence of self-heating) saturation of the light-current characteristic and deteriorates the temperature-stability of semiconductor lasers. To suppress the parasitic recombination, a concept of asymmetric barrier (AB) layers has been proposed [1]. The AB that adjoins the active region on the $p(n)$-emitter side blocks electrons (holes) due to the energy barrier in the conduction (valence) band while not preventing holes (electrons) from reaching the active region (see Fig. 1). Previously, the AB-concept was implemented solely for 830–850 nm AlGaAs/GaAs diode lasers, for which its effectiveness was proved experimentally [3, 4].

In this work, we discuss a need for and a possibility of application of the AB-concept to 1.55 μm Al-free lasers on InP substrates. Although there has been experimental work on the use of charge carrier blocking layers in 1.55 μm devices [5, 6], no laser heterostructures comprising two ABs, which would block charge carriers of both signs, have been realized so far. Here we perform a systematic search for AB-materials among commonly-used III–V compounds aimed to maximize the suppression of the parasitic carrier fluxes while keeping to a minimum the impact of the ABs on the useful fluxes. The optimal AB-designs are proposed and their parameters are discussed.

2. REFERENCE LASER HETEROSTRUCTURE

As a reference structure, for which we will search for ABs, we consider here a completely Al-free GaInAsP/InP laser diode having a conventional separate-confinement heterostructure design (same as in Fig. 1 but without AB layers). The elimination of Al is bene-

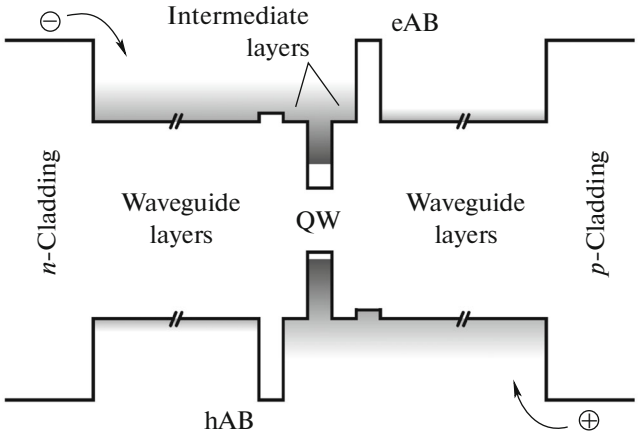

Fig. 1. Schematic energy band diagram illustrating the concept of a laser with ABs; $p(n)$-side AB [marked as eAB (hAB)] aims to suppress the electron (hole) transport.

[1] The article is published in the original.

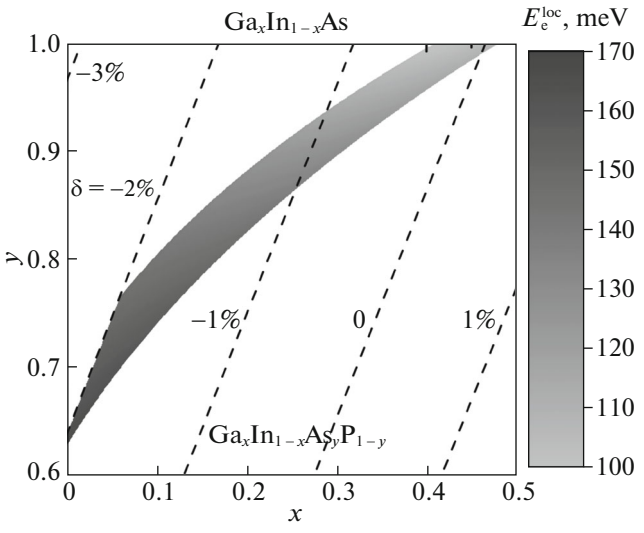

Fig. 2. Contour plot for the localization energy for electrons in the QW based on $Ga_xIn_{1-x}As_yP_{1-y}$, which can be used to achieve ground-state optical transition at 1550 nm for the case of GaInAsP barrier layers having the band-gap of 1.15 eV. The dashed lines are the contour lines for the lattice-mismatch δ.

ficial from the viewpoint of post-growth processing as GaInAsP is resistant to oxidation and characterized by a lower surface recombination velocity [7]. The waveguide we use here is a GaInAsP quaternary alloy lattice-matched to the substrate having the band gap of E_g = 1.15 eV [8]. InP is used as the material for claddings. The quantum well (QW), also made of GaInAsP, is the active region of the reference structure.

Figure 2 shows the contour plot for the localization energy of electrons in the QW for those compositions that provide the ground-state optical transition wavelength of $\lambda_0 = 1.55\ \mu m \pm 5$ nm. Here we put the following constraints on the QW design: the QW width w = 5–8 nm and the lattice-mismatch $|\delta| \le 2\%$ (see the dashed contour lines in Fig. 2). As seen from the figure, the strongest electron localization is achieved in the ternary $InAs_{0.63}P_{0.37}$ ($E_e^{loc} = 166$ meV; for holes, $E_h^{loc} = 181$ meV). However, even in this case, the electron confinement does not reach the value, which is necessary to suppress the electron escape from the QW ($7k_BT$, i.e., $E^{loc} > 175$ at room temperature [2]).

In this work, we consider a common lattice-matched ternary $Ga_{0.47}In_{0.53}As$ as the QW material instead of $InAs_{0.63}P_{0.37}$ (see Fig. 2). The advantages of using this material for the QW will be discussed below. In this QW, $E_e^{loc} = 106$ meV, $E_h^{loc} = 241$ meV; the conduction band (CB) and valence band (VB) offsets at the heterointerface with the waveguide are ΔE_C = 160 meV and $\Delta E_V = 255$ meV, respectively.

3. METHOD OF SEARCH FOR ABs

We looked for AB materials among ternary and quaternary alloys comprising commonly-used group III (Al, Ga, and In) and IV (As, P, and Sb) elements. The Al-fraction was limited to about 40%, which is dictated by the need to eliminate the non-intentional oxidation of the AB layers. A measure of effectiveness of the AB layer, which we use here, is the suppression ratio (C) of the parasitic flux by the AB with respect to the flux in the absence of AB. Correspondingly, the main goal of our search was to maximize C. When calculating the fluxes, we assumed that the ABs are incorporated in the waveguide material.

We used the following search criteria for the AB materials:

(i) the restriction on the lattice-mismatch is $|\delta| \le 2\%$;

(ii) if the AB-material forms a spurious barrier for the useful flux (in Fig. 1, such a barrier for electrons is formed by the hAB), the suppression ratio of the useful flux should not be higher than 25%;

(iii) the barrier height for the parasitic flux is limited by 300 meV, and

(iv) if the AB-material forms a spurious well (in Fig. 1, such a well for holes is formed by the eAB), the well should not be deeper than 125 meV.

Compliance with the last two criteria allows to achieve the desired wavelength $\lambda_0 = 1.55$ μm using the above selected QW-material by tuning the QW-width within the 5–8 nm range. If the AB-material forms a spurious well, we do not set any restraint [such as (ii)] on the useful flux suppression since in this case the AB can be placed immediately adjacent to the active region thus improving the capture of majority carriers into the active region.

The thickness of the AB-layer was varied from 3 nm up to the smaller of the critical thickness of dislocation formation and 15 nm. Thus the optimal thickness of the AB-layer was determined, which provides the highest parasitic flux suppression for the given material composition. A detailed description of our method of search for ABs will be presented elsewhere [9].

4. RESULTS AND DISCUSSION

Figure 3 shows the results of our search for the p-side ABs. The contour plots in the figure present the dependence of the suppression ratio of the parasitic electron flux C_e on the composition of the ABs made of GaInPSb (a) or AlGaInAs (b) alloys. The data presented satisfy the above discussed search criteria and the C_e values correspond to the optimal AB-thicknesses (only $C_e > 10^3$ and $C_e > 10^2$ are shown for GaInPSb and AlGaInAs, respectively). It is seen from the figure that these alloys allow to achieve very high

suppression ratios. The maximal values of C_e are 4.3×10^3 and 2.9×10^6 for GaInPSb and AlGaInAs, correspondingly. To compare, in the 808 nm Al-free AB-laser on the GaAs substrate, the maximal value of C_e is 160 as it follows from our calculations for the *p*-side ABs based on various III–V compounds [9]. Such a rapid (exponential) growth of the suppression ratio with increase in Al-fraction for AlGaInAs (see Fig. 3b) is due to a linear growth of the height of the barrier in the CB formed by the AB. We see that in both cases (i.e., of GaInPSb and AlGaInAs) the *p*-side ABs can be made lattice-matched (see the dashed lines in Fig. 3 that correspond to the contour lines for δ).

We should mention that the restriction on formation of a spurious well in the VB [see criterion (iv)] does not allow to use GaInPSb or AlGaInAs for the *p*-side AB. If the spurious well depth would be limited to 50 meV instead of 125 meV, there would still be no suitable composition within the AlGaInAs alloy, whereas the maximal C_e would be reduced to 200 in the case of GaInPSb. It is worth mentioning that the AlInAsP and AlInPSb quaternaries also have suitable compositions for the *p*-side AB. However, as these alloys do not provide evident advantages compared to GaInPSb or AlGaInAs, we do not present here the results for them.

Based on the above results of our search for the *p*-side AB materials, we propose three optimal designs for electron-blocking layers (eAB1, eAB2, and eAB3, labeled by the triangle, circle and cross in Fig. 3, respectively)—see Table 1 for their parameters. The advantage of the first compound ($Ga_{0.6}In_{0.4}P_{0.68}Sb_{0.32}$) is that it does not contain Al. Hence adding eAB1 to the reference structure will keep it completely Al-free. The disadvantage of the first design is the presence of Sb—the element, which utilization in epitaxy is less common. In view of this, a reasonable alternative for eAB1 is the use of either $Al_{0.42}In_{0.58}As$ (eAB2) or $Al_{0.4}Ga_{0.07}In_{0.53}As$ (eAB3) alloys, which have a moderate Al-content. $Al_{0.42}In_{0.58}As$ is a common ternary alloy providing the highest e-flux suppression ratio ($C_e = 10^5$) among our proposed ABs. As for $Al_{0.4}Ga_{0.07}In_{0.53}As$, although it is a quaternary alloy, it is lattice-matched to the substrate and common for epitaxial growth.

Note that in all three designs, a spurious potential well is formed in the VB. If the AB immediately adjoins the active QW (i.e., there is no intermediate layer), the hole capture into this QW will be mediated through the spurious well, which may increase the capture velocity into the active QW. We also note that the deviation within ±2% around the target composition of each of the proposed ABs will still keep the material in the region of suitable compounds with sufficiently high e-flux suppression ratio C_e.

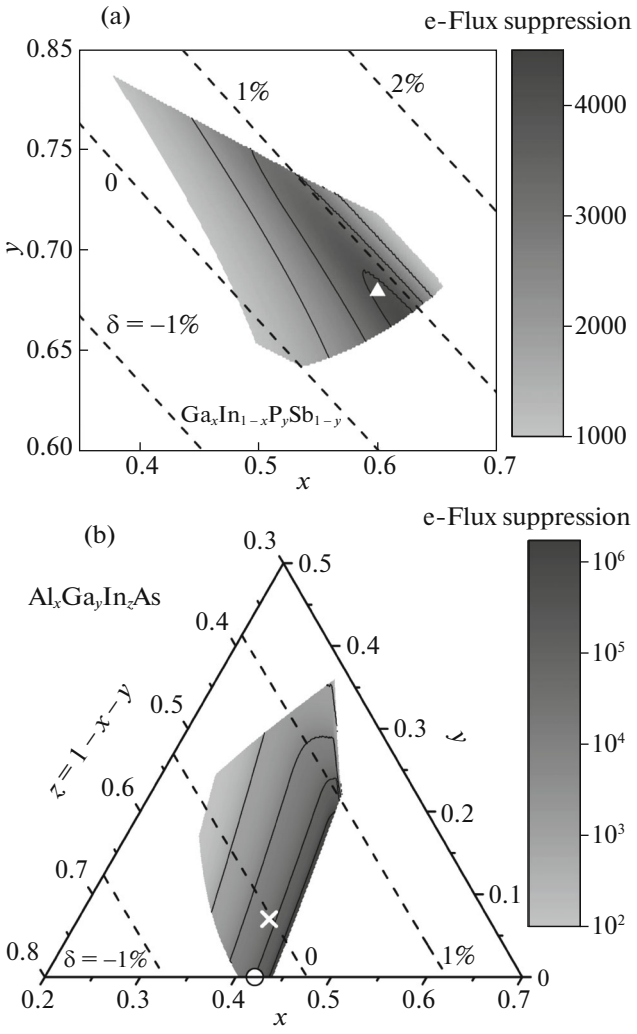

Fig. 3. Contour plots for the parasitic electron flux suppression ratio for the ABs based on $Ga_xIn_{1-x}P_ySb_{1-y}$ (a) and $Al_xGa_yIn_{1-x-y}As$ (b). Three proposed compositions for the *p*-side AB, eAB1, eAB2 and eAB3 are labeled by the triangle, circle and cross, respectively. The dashed lines are the contour lines for the lattice-mismatch δ.

As for the hole blocking AB on the *n*-side of the structure, we found no materials that satisfy all the above discussed criteria and provide a noticeable suppression of the parasitic hole flux. However, as we mentioned above, the material, which we selected for the QW in the reference structure, $Ga_{0.47}In_{0.53}As$, is characterized by high localization energy for holes, 241 meV. Hence, taking into account that this localization energy is significantly higher than the threshold energy for carrier escape ($7k_BT$), as well as a potentially improved capture of holes into the active QW in the presence of a spurious well in the structures with

Table 1. Proposed designs for the *p*-side AB and their parameters

Composition	$Ga_{0.6}In_{0.4}P_{0.68}Sb_{0.32}$	$Al_{0.42}In_{0.58}As$	$Al_{0.4}Ga_{0.07}In_{0.53}As$
Designation	eAB1	eAB2	eAB3
e-flux suppression ratio, C_e	4.1×10^3	1.0×10^5	5.7×10^4
h-flux suppression ratio, C_h	–	–	–
Mismatch, %[a)]	0.85	–0.37	–0.02
Critical thickness, nm	12.9	37.1	∞
Optimal thickness, nm	12.9	13.9	15
Barrier for e, meV	200	270	258
Well for hh, meV	47	112	78
Well for lh, meV	114	84	76

[a)] negative value—compression of the AB layer.

eAB1, eAB2, or eAB3, we can expect that the bipolar population, and hence the parasitic recombination, will be sufficiently suppressed also in the *n*-side waveguide layer in the proposed laser heterostructure.

5. CONCLUSIONS

We have identified suitable materials for the *p*-side AB for 1.55 μm Al-free InP-based diode lasers. With the use of such ABs, the bipolar population and hence parasitic recombination will be virtually suppressed on the *p*-side of the laser structure. The use of $Ga_{0.47}In_{0.53}As$ as the material for the active QW, which provides deep localization for holes, will aid in suppressing the bipolar population and parasitic recombination on the *n*-side of the structure as well.

ACKNOWLEDGMENTS

The work was supported by the Russian Foundation for Basic Research (grant no. 16-29-03123) and the Russian Ministry of Education and Science (project 3.9787.2017/8.9). L.V.A. also acknowledges the U.S. Army Research Office (Grant no. W911NF-17-1-0432). E.S.S. also acknowledges the Villum Fonden via YIP QUEENs.

REFERENCES

1. L. V. Asryan and S. Luryi, Solid-State Electron. **47**, 205 (2003).
2. C. Frevert, P. Crump, F. Bugge, S. Knigge, and G. Erbert, Semicond. Sci. Technol. **31**, 025003 (2016).
3. A. E. Zhukov, N. V. Kryzhanovskaya, F. I. Zubov, Yu. M. Shernyakov, M. V. Maximov, E. S. Semenova, K. Yvind, and L. V. Asryan, Appl. Phys. Lett. **100**, 021107 (2012).
4. F. I. Zubov, M. V. Maximov, Yu. M. Shernyakov, N. V. Kryzhanovskaya, E. S. Semenova, K. Yvind, L. V. Asryan, and A. E. Zhukov, Electron. Lett. **51**, 1106 (2015).
5. T. Garrod, D. Olson, M. Klaus, C. Zenner, C. Galstad, L. Mawst, and D. Botez, Appl. Phys. Lett. **105**, 071101 (2014).
6. J. Piprek and J. K. White, and A. J. Spring Thorpe, IEEE J. Quantum Electron. **38**, 1253 (2002).
7. M. Krakowski, M. Lecomte, N. Michel, M. Calligaro, M. Carbonnelle, M. Tran, M. Lamponi, C. Cayron, V. Ligeret, J. Bébé Manga Lobé, R. Mostallino, N. von Bandel, A. Larrue, Y. Robert, E. Vinet, O. Drisse, M. Garcia, and O. Parillaud, Proc. SPIE **9370**, 93702C (2015).
8. F. I. Zubov, E. S. Semenova, I. V. Kulkova, K. Yvind, N. V. Kryzhanovskaya, M. V. Maximov, and A. E. Zhukov, Semiconductors **51**, 1332 (2017).
9. F. I. Zubov, M. E. Muretova, L. V. Asryan, E. S. Semenova, M. V. Maximov, and A. E. Zhukov, J. Appl. Phys. **124**, 133105 (2018).

INTERNATIONAL CONFERENCE on Microwave & THz Technologies and Wireless Communications

IRPhE'2018

Dedicated to the 75th Anniversary of National Academy of Sciences of RA

Program and Abstract Book

Organized by: **Institute of Radiophysics and Electronics, National Academy of Sciences**

Sponsored by:

INSTITUTE OF RADIOPHYSICS AND ELECTRONICS

State Committee of Science of Armenia

September 19-21, 2018

Aghveran, ARMENIA

Close-to-ideal semiconductor lasers: Optimizing performance by suppressing recombination outside the active region

Levon V. Asryan

Virginia Polytechnic Institute and State University, Blacksburg, USA

In conventional diode lasers with a low-dimensional active region, the electrons and holes are first injected from the cladding layers into a bulk reservoir, which also serves as the waveguiding layer [optical confinement layer (OCL)]. The carriers are then transported to the active region and, finally, captured into the latter. Due to bipolar (i.e., both electron and hole) population in the OCL, a certain fraction of the injection current goes into electron-hole recombination there. This parasitic recombination outside the active region is a major source of the temperature dependence of the threshold current [1]. In addition, the carrier capture from the OCL into the active region is not instantaneous. For this reason, the carrier density in the OCL, and hence the parasitic recombination rate, rise, even above the lasing threshold, with injection current. This leads to sublinearity of the light-current characteristic (LCC) and limits the output power, especially at high pump currents [2–4].

To suppress the recombination outside the quantum-confined active region, two design approaches were proposed. One of the approaches [5–11] exploits double tunneling-injection (DTI), i.e., tunneling injection of both electrons and holes into the active region from two separate quantum wells (QWs). In a DTI laser, the quantum-confined active region, located in the central part of the OCL, is clad on each side by a thin barrier and a QW. Electrons and holes are injected into the active region by tunneling from the corresponding QWs. Ideally, there should be no second tunneling step, i.e. out-tunneling from the active region into the 'foreign' QWs (electron-injecting QW for holes and hole-injecting QW for electrons).

The other approach [6, 7] is based on independent tailoring of the conduction and valence bandedges by means of the use of two asymmetric barrier layers (ABLs) – one on each side of the active region. The ABL in the electron-injecting side of the structure should ideally prevent holes from entering that side while not hindering the electron-injection into the active region. The ABL in the hole-injecting side should prevent electrons from entering that side while not hindering the hole-injection into the active region. A laser utilizing ABLs was termed a bandedge-engineered laser [6, 7, 12] or an ABL laser [13–15].

In both DTI and ABL lasers, there will be no electrons (holes) in the hole- (electron-) injecting side of the structure, i.e., the bipolar population will be suppressed outside the active region.

As discussed in this presentation, the total suppression of bipolar population and, hence, of recombination outside the active region would result in close-to-ideal operating characteristics in DTI and ABL lasers, namely, virtually temperature-insensitive threshold current, close-to-one internal quantum efficiency, and linear LCC. The dynamic characteristics would also be improved in these lasers [16, 17].

This work was supported by the US Army Research Office under Grant No. W911NF-17-1-0432.

[1] L. V. Asryan and R. A. Suris, *Semicond. Sci. Technol.* **11**(4), 554 (1996).
[2] L. V. Asryan, S. Luryi, and R. A. Suris, *Appl. Phys. Lett.* **81**(12), 2154 (2002).
[3] L. V. Asryan, S. Luryi, and R. A. Suris, *IEEE J. Quantum Electron.* **39**(3), 404 (2003).
[4] L. V. Asryan and Z. N. Sokolova, *J. Appl. Phys.* **115**(2), 023107 (2014).
[5] L. V. Asryan and S. Luryi, *IEEE J. Quantum Electron.* **37**(7), 905 (2001).
[6] L. V. Asryan and S. Luryi, *Solid-State Electron.* **47**(2), 205 (2003).
[7] L. V. Asryan and S. Luryi, *U.S. Patent 6 870 178 B2*, Mar. 22, 2005.
[8] D.-S. Han and L. V. Asryan, *Appl. Phys. Lett.* **92**(25), 251113 (2008).
[9] D.-S. Han and L. V. Asryan, *Solid-State Electron.* **52**(10), 1674 (2008).
[10] D.-S. Han and L. V. Asryan, *J. Lightw. Technol.* **27**(24), 5775 (2009).
[11] D.-S. Han and L. V. Asryan, *Nanotechnology* **21**(1), Art. no. 015201 (2010).
[12] L. V. Asryan, N. V. Kryzhanovskaya, M. V. Maximov, et al., *Semicond. Sci. Technol.* **26**(5), 055025 (2011).
[13] A. E. Zhukov, N. V. Kryzhanovskaya, F. I. Zubov, Y. M. Shernyakov, M. V. Maximov, E. S. Semenova, K. Yvind, and L. V. Asryan, *Appl. Phys. Lett.* **100**(2), 021107 (2012).
[14] L. V. Asryan, N. V. Kryzhanovskaya, M. V. Maximov, et al.,, *J. Appl. Phys.* **114**(14), 143103 (2013).
[15] F. I. Zubov, A. E. Zhukov, Yu. M. Shernyakov, M. V. Maximov, E. S. Semenova, and L. V. Asryan, *J. Phys. Conf. Ser.* **643**, 012042 (2015).
[16] L. V. Asryan, *Semicond. Sci. Technol.* **30**(3), 035022 (2015).
[17] L. V. Asryan, *Opt. Lett.* **42**(1), 97 (2017).

interview

Levon Asryan

"Our work aids the understanding of the physical phenomena that control the output optical power of diode lasers with a low-dimensional active region."

Doctor Levon V. Asryan from Virginia Polytechnic Institute and State University, talks to *Electronics Letters* about the paper 'Evolution of light-current characteristic shape in high-power semiconductor quantum well lasers', page 550.

Tell us about your field of research

Diode lasers, which are also termed laser diodes, injection lasers, or semiconductor lasers, have numerous practical applications, among which are fiber-optic communication systems. In present-day diode lasers, the stimulated emission (the useful optical output) is generated in low-dimensional active regions. While reducing the dimensionality of the active region of injection lasers was proposed some time ago as an efficient tool to improve their operating characteristics, many challenges still exist for such lasers. Among them is the internal optical absorption loss, which consumes generated photons thus reducing the useful optical output of the laser. The effect of internal loss on the light output of semiconductor quantum well lasers is one of the focuses of this Letter.

Light-current characteristic (LCC) is one of the key characteristics of injection lasers. It presents the output optical power as a function of the input injection current. Ideally, this characteristic should be as steep as possible and remain linear with increasing pump current. In diode lasers with a low-dimensional active region, there are always considerable concentrations of electrons and holes in the optical confinement layer (the region wherein the emitted light is confined) in addition to those in the active region. These unwanted charge carriers outside the active region absorb the light generated in the active region. The concentrations of these carriers increase with increasing pump current. Hence more photons are absorbed with increasing pump current. As a result, the output optical power is degraded and the linearity of the LCC is adversely affected. The purpose of our study was to quantify the extent to which the LCC is impacted by the internal loss.

Can you describe the background to the work performed and the advance reported in your *Electronics Letters* paper?

We showed that, in addition to the expected decrease in linearity, roll over of the LCC occurs with increasing injection current in quantum well lasers. More surprisingly, depending on the parameters of the laser structures, the LCC can be two-valued, i.e., at high enough pump currents, there will be two possible values of the output optical power at a given current. We showed how a single-branched LCC evolves into a double-branched LCC with increasing velocity of capture of charge carriers from the optical confinement layer into the active region (quantum well).

Both the phenomena of rolling-over LCC and the existence of the second branch in the LCC present very interesting and important results. The roll-over should be inherent in any diode lasers with a quantum-confined active region. The point is that both factors contributing to rolling-over (the increase in the concentrations of charge carriers outside the quantum-confined active region that occurs with increasing injection current, and the internal absorption of generated light) are inherent in such lasers. As for the second branch in the LCC, with the parameters of a given laser structure, we can predict whether it will be present in that structure. In addition, by tuning the parameters of laser structures, we can transform a single-branched LCC into a double-branched LCC.

What is the significance of this and what challenges did you have to overcome?

Our work aids the understanding of the physical phenomena that control the output optical power of diode lasers with a low-dimensional active region, such as quantum well lasers and quantum dot lasers. In the short term, by controllably changing the parameters of laser structures, the findings of this work will help to improve the linearity of the LCC and hence to increase laser output optical power at a given pump current. In the longer term, provided that controllable transitions between the two branches of the LCC are experimentally feasible, a diode laser offering fast switching between two optical outputs will be possible.

How are you planning to develop this work and what else are you working on now?

We are planning to identify feasible approaches for experimental observation of the second branch in the LCC and for switching between the two branches. We are also currently working on other factors that control the operating characteristics of diode lasers with a low-dimensional active region, such as non-instantaneous capture into the active region and parasitic recombination outside it. Work is also planned on novel types of semiconductor lasers with a quantum-confined active region, such as double tunnelling-injection lasers and lasers with asymmetric barrier layers.

How do you think the field will develop over the next ten years?

Technological advances have allowed us to continuously improve the characteristics of the existing types of diode lasers as well as realise novel semiconductor lasers such as quantum dot lasers. Future research in the field of diode lasers, in our opinion, will be on the development of truly temperature-insensitive, high-speed, and energy-efficient laser diodes for a broad range of applications.

doi: 10.1049/el.2019.1249

Evolution of light-current characteristic shape in high-power semiconductor quantum well lasers

Z.N. Sokolova, N.A. Pikhtin and L.V. Asryan✉

The light-current characteristic (LCC) of semiconductor quantum well lasers is theoretically studied. It is discussed here that, due to internal optical absorption loss, which depends on the electron and hole densities in the optical confinement layer, (i) roll-over of the LCC occurs with increasing injection current, and, (ii) depending on the parameters of laser structures, the LCC can have two branches, i.e. the optical emission at two different output powers will be possible within a certain range of injection currents.

Introduction: We develop a theory of light-current characteristic (LCC) of semiconductor quantum well (QW) lasers (Fig. 1) in the presence of internal optical absorption loss, which depends on the carrier density in the optical confinement layer (OCL) [1]. We show that, depending on the parameters of laser structures, one of the following two situations will be realised:

(i) Roll-over of the LCC occurs with increasing injection current, i.e. the output power first increases, approaches its maximum value, and then decreases and continuously goes to zero at a certain current, which is the maximum operating current (Fig. 2, curves 1 and 2).
(ii) As in case (i), roll-over of the LCC occurs with increasing injection current. However, in contrast to case (i), the lasing quenches at a non-vanishing output power, i.e. while the output power is non-zero at the maximum operating current, there will be no lasing immediately beyond this point. In this case, in addition to the rolling-over branch of the LCC, there will be the second branch of the LCC, i.e. the second mode of lasing. The threshold for the second branch is higher than that for the first (conventional) branch and the maximum operating current is the same as that for the first branch (Fig. 2, curves 3 and 4). With increasing injection current from the second threshold to the maximum operating current, the output power of the second mode increases from zero and approaches the same value as that of the first mode, i.e. the two branches merge together (Fig. 2, curves 3 and 4). As in the first mode, there can be no lasing in the second mode beyond this merging point. Hence, in this case, above the second lasing threshold and up to the maximum operating current, there are two possible modes for lasing, i.e. the LCC is two-valued.

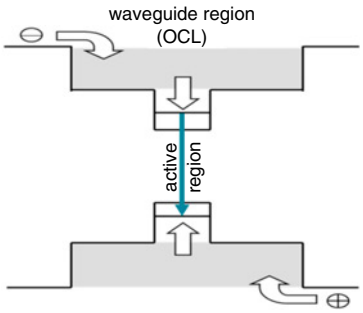

Fig. 1 *Schematic energy band diagram of a semiconductor laser with a low-dimensional active region*

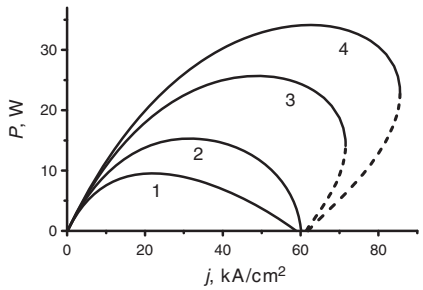

Fig. 2 *LCCs of QW laser structures or $v_{n,capt,0}$ ($\times 10^5$, cm/s): 1–5, 2–7.5, 3–10, 4–20; $v_{p,capt,0}$ ($\times 10^5$, cm/s): 1–3, 2–5, 3, 4–10*

In this work, we discuss the evolution of the LCC shape from the conventional rolled-over one [the above case (i)] to the two-valued one [case (ii)], which occurs with varying the QW laser structure parameters.

Theoretical model: Our model is based on the following set of five steady-state rate equations [2–4]:

for electrons in the OCL of thickness b $\left[b(\partial n^{\mathrm{OCL}}/\partial t)=0\right]$,

$$\frac{j}{e}+N_{\mathrm{QW}}\frac{n^{\mathrm{QW}}}{\tau_{n,\mathrm{esc}}}-N_{\mathrm{QW}}v_{n,\mathrm{capt},0}(1-f_n)\,n^{\mathrm{OCL}}-bB_{3\mathrm{D}}n^{\mathrm{OCL}}p^{\mathrm{OCL}}=0, \tag{1}$$

for holes in the OCL $\left[b(\partial p^{\mathrm{OCL}}/\partial t)=0\right]$,

$$\frac{j}{e}+N_{\mathrm{QW}}\frac{p^{\mathrm{QW}}}{\tau_{p,\mathrm{esc}}}-N_{\mathrm{QW}}v_{p,\mathrm{capt},0}(1-f_p)p^{\mathrm{OCL}}-bB_{3\mathrm{D}}n^{\mathrm{OCL}}p^{\mathrm{OCL}}=0, \tag{2}$$

for electrons in QWs $\left(\partial n^{\mathrm{QW}}/\partial t=0\right)$,

$$v_{n,\mathrm{capt},0}\,(1-f_n)\,n^{\mathrm{OCL}}-\frac{n^{\mathrm{QW}}}{\tau_{n,\mathrm{esc}}}-B_{2\mathrm{D}}n^{\mathrm{QW}}p^{\mathrm{QW}}-c_{\mathrm{g}}g^{\max}(f_n+f_p-1)\frac{N}{S}=0, \tag{3}$$

for holes in QWs $\left(\partial p^{\mathrm{QW}}/\partial t=0\right)$,

$$v_{p,\mathrm{capt},0}(1-f_p)p^{\mathrm{OCL}}-\frac{p^{\mathrm{QW}}}{\tau_{p,\mathrm{esc}}}-B_{2\mathrm{D}}n^{\mathrm{QW}}p^{\mathrm{QW}}-c_{\mathrm{g}}g^{\max}(f_n+f_p-1)\frac{N}{S}=0, \tag{4}$$

for photons in the lasing mode $\left(\partial N/\partial t=0\right)$,

$$c_{\mathrm{g}}N_{\mathrm{QW}}\,g^{\max}(f_n+f_p-1)N-c_{\mathrm{g}}(\beta+\alpha_{\mathrm{int}})N=0. \tag{5}$$

The following quantities are the five unknowns to be found from the solution of (1)–(5): n^{OCL} and p^{OCL} are the densities of electrons and holes in the OCL, n^{QW} and p^{QW} are the densities of electrons and holes in the QWs, and N is the number of photons of stimulated emission.

In (1)–(5), f_n and f_p are the occupancies of the states corresponding to the lower edge of the electron subband and to the upper edge of the hole subband in a QW. They are related to the electron and hole densities n^{QW} and p^{QW} in the QWs as follows [5–7]:

$$f_n=1-\exp\left(-n^{\mathrm{QW}}/N_{\mathrm{c}}^{2\mathrm{D}}\right),\quad f_p=1-\exp\left(-p^{\mathrm{QW}}/N_{\mathrm{v}}^{2\mathrm{D}}\right), \tag{6}$$

where $N_{\mathrm{c,v}}^{2\mathrm{D}}=m_{e,\,\mathrm{hh}}^{\mathrm{QW}}T/(\pi\hbar^2)$ are the 2D effective densities of states in the conduction and valence bands in the QWs, $m_{e,\,\mathrm{hh}}^{\mathrm{QW}}$ are the electron and hole effective masses in the QWs, and T is the temperature in units of energy.

The following parameters enter into (1)–(5): j is the injection current density, e is the electron charge, N_{QW} is the number of QWs, $v_{n,\mathrm{capt},0}$ and $v_{p,\mathrm{capt},0}$ are the capture velocities (measured in cm/s) of electrons and holes from the OCL, respectively, into an empty (at $f_n=0$ and $f_p=0$) QW, $\tau_{n,\mathrm{esc}}$ and $\tau_{p,\mathrm{esc}}$ are the thermal escape times of electrons and holes, respectively, from the QWs to the OCL which can be expressed in terms of the capture velocities – see [8, 9], $B_{3\mathrm{D}}$ and $B_{2\mathrm{D}}$ are the spontaneous radiative recombination coefficients in the bulk region (OCL) and 2D region (QWs) measured in cm^3/s and cm^2/s, respectively, (see [10, 11] for the expressions for $B_{3\mathrm{D}}$ and $B_{2\mathrm{D}}$), c_{g} is the group speed of light, $g^{\max}$ is the maximum modal gain in each QW (see [12] for the expression for $g^{\max}$), $S=WL$, where W is the stripe contact width and L is the cavity length, the mirror loss $\beta=(2L)^{-1}\,(R_1R_2)^{-1}$.

$\ln(R_1R_2)^{-1}$, R_1 and R_2 are the mirror reflectivities, and α_{int} is the internal optical absorption loss coefficient.

As seen from Fig. 1, the carriers are not directly injected into a quantum-confined active region of the laser. They are first injected from the cladding layers into the OCL and then they are captured from the OCL into the active region. A key component of our theoretical model is that we do not assume instantaneous capture of carriers from the OCL into the QWs, i.e. we do not assume that the capture velocities are infinitely high; instead, we use finite values for them. In fact, the capture velocities $v_{n,\mathrm{capt},0}$ and $v_{p,\mathrm{capt},0}$ may vary in different laser structures as they depend on the QW depth, i.e. on the compositions of the QW and OCL materials; they also depend on the QW width. In [13, 14], we evaluated the electron capture velocity for our experimental laser structures using our theoretical model.

Another key component of our theoretical model is the internal optical absorption loss, which depends on the electron and hole densities in the OCL [15]

$$\alpha_{\text{int}} = \alpha_0 + \Gamma^{\text{OCL}}\sigma_{n,\text{ int}}\, n^{\text{OCL}} + \Gamma^{\text{OCL}}\sigma_{p,\text{ int}}\, p^{\text{OCL}}, \quad (7)$$

where $\sigma_{\text{n,int}}$ and $\sigma_{p,\text{int}}$ are the cross sections of light absorption by electrons and holes in the OCL, respectively, Γ^{OCL} is the optical confinement factor in the OCL, and a_0 is the constant component of the internal loss coefficient, which is primarily due to light absorption in the cladding layers.

Owing to the fact that the carrier capture from the OCL into the QWs is not instantaneous, the densities of these carriers in the OCL are not pinned – they grow with increasing injection current in the lasing mode [16, 17]. As a result of this, as seen from (7), the internal optical loss in the OCL increases as well.

In contrast to [5, 6, 18], wherein charge neutrality was assumed to hold locally in a low-dimensional active region of the laser, we use here the condition of global charge neutrality, i.e. the condition of equality of the total charge of electrons in the OCL and QWs to the total charge of holes in these two regions [2–4]

$$e(N_{\text{QW}}n^{\text{QW}} + bn^{\text{OCL}}) = e(N_{\text{QW}}p^{\text{QW}} + bp^{\text{OCL}}). \quad (8)$$

The output optical power as a function of the injection current density (the LCC) is given as [19]

$$P(j) = \hbar\,\omega\, c_{\text{g}}\beta\, N(j), \quad (9)$$

where ω is the angular frequency of the lasing emission and $N(j)$ is the number of photons in the lasing mode, which is found from the solution of the set of rate equations (1)–(5).

In [18], under the condition of local charge neutrality in the active region, closed-form solutions of the rate equations were obtained and the following analytical criterion for the appearance of the second branch of the LCC was derived

$$\frac{\sigma_{n,\text{int}}v_{n,\text{capt},0}}{2bB_{3\text{D}}g^{\max}} > 1. \quad (10)$$

Under the condition of global charge neutrality in a QW laser structure, no closed-form solutions of the set of rate equations (1)–(5) can be obtained and, correspondingly, no analytical criterion for the appearance of the second branch of the LCC can be derived. However, the analytical criterion (10) proved to be helpful also in this case.

Discussion: We solve numerically the set of rate equations (1)–(5) for the experimental laser heterostructures emitting at 1.01 μm. A single strained QW of 50 Å width is made of indium gallium arsenide (InGaAs). The material of the OCL is GaAs, and the OCL thickness is $b = 1.7$ μm. The material of the cladding layers is $Al_{0.3}Ga_{0.7}As$. The cavity length is $L = 0.15$ cm. The cross-sections of light absorption by electrons and holes in the OCL are $\sigma_{n,\text{ int}} = 3 \times 10^{-18}$ cm^2 and $\sigma_{p,\text{int}} = 10^{-17}$ cm^2. The dopant concentrations in the n- and p-claddings are 5×10^{17} and 3.5×10^{18} cm^{-3}, respectively. The constant component of the internal loss coefficient is $\alpha_0 = 2$ cm^{-1}. The spontaneous radiative recombination coefficient in the OCL material (GaAs) is $B_{3\text{D}} = 2.044 \times 10^{-10}$ cm^3/s. The maximum modal gain is $g^{\max} = 51.89$ cm^{-1}.

Fig. 2 shows the LCCs calculated at various values of the electron and hole capture velocities from the OCL into the QW. Curve 1 corresponds to $v_{n,\text{capt},0} = 5 \times 10^5$ cm/s and $v_{p,\text{capt},0} = 3 \times 10^5$ cm/s; curve 2 corresponds to $v_{n,\text{capt},0} = 7.5 \times 10^5$ cm/s and $v_{p,\text{capt},0} = 5 \times 10^5$ cm/s; curve 3 corresponds to $v_{n,\text{capt},0} = 10^6$ cm/s and $v_{p,\text{capt},0} = 10^6$ cm/s; curve 4 corresponds to $v_{n,\text{capt},0} = 2 \times 10^6$ cm/s and $v_{p,\text{capt},0} = 10^6$ cm/s. As seen from Fig. 2, the LCC shape changes with varying the capture velocities. At relatively low capture velocities (curves 1 and 2), case (i) is realised, i.e. the output power increases, approaches its maximum value, and then decreases and continuously goes to zero. As also seen from the figure, the maximum output optical power increases with increasing capture velocities.

At high capture velocities (curves 3 and 4 in Fig. 2), case (ii) is realised, i.e. in addition to the rolling over (conventional) branch of the LCC, the second branch appears in the LCC. The threshold for the second branch is higher than that for the first branch. At the maximum operating current, the two branches merge together. Immediately beyond the merging point (at which the optical power is non-zero), there can be no lasing in the structure.

Conclusions: The LCC of semiconductor QW lasers has been theoretically studied in the presence of internal optical absorption loss, which depends on the electron and hole densities in the OCL. It has been shown that depending on the values of the electron and hole capture velocities from the OCL into the QW, two different shapes of the LCC can be realised. At low capture velocities, the LCC is single-branched and rolling over with increasing injection current. At high capture velocities, the LCC is two-branched – it has the second branch in addition to the rolling over branch. In contrast to the rolling over branch, the optical power in the second branch is continuously increasing with increasing pump current. The two branches merge together at the maximum operating current beyond which the lasing quenches in both branches.

Acknowledgments: This work was supported by the federal program of the Ioffe Institute. L.V. Asryan also thanks the U.S. Army Research Office (grant no. W911NF-17-1-0432) for support of this work.

Submitted: *16 January 2019* E-first: *25 March 2019*
doi: 10.1049/el.2019.0225
One or more of the Figures in this Letter are available in colour online.

Z.N. Sokolova and N.A. Pikhtin (*Ioffe Institute, St. Petersburg 194021, Russia*)

L.V. Asryan (*Virginia Polytechnic Institute and State University, Blacksburg, Virginia 24061, USA*)

✉ E-mail: asryan@vt.edu

References

1 Sokolova, Z.N., Pikhtin, N.A., and Asryan, L.V.: 'Two-valued characteristics in semiconductor quantum well lasers', *J. Lightwave Technol.*, 2018, **36**, (11), pp. 2295–2300
2 Sokolova, Z.N., Pikhtin, N.A., Tarasov, I.S., *et al.*: 'Theory of operating characteristics of a semiconductor quantum well laser: inclusion of global electroneutrality in the structure', *J. Phys. Conf. Ser.*, 2016, **740**, p. 012002
3 Sokolova, Z.N., Pikhtin, N.A., Tarasov, I.S., *et al.*: 'Threshold characteristics of a semiconductor quantum-well laser: inclusion of global electroneutrality in the structure', *Quantum Electron.*, 2016, **46**, (9), pp. 777–781
4 Sokolova, Z.N., Veselov, D.A., Pikhtin, N.A., *et al.*: 'Increase in the internal optical loss with increasing pump current and the output power of quantum well lasers', *Semiconductors*, 2017, **51**, (7), pp. 959–964
5 Asryan, L.V, and Luryi, S.: 'Two lasing thresholds in semiconductor lasers with a quantum-confined active region', *Appl. Phys. Lett.*, 2003, **83**, (26), pp. 5368–5370
6 Asryan, L.V, and Luryi, S.: 'Effect of internal optical loss on threshold characteristics of semiconductor lasers with a quantum-confined active region', *J. Quant. Electron.*, 2004, **40**, (7), pp. 833–843
7 Vahala, K.J., and Zah, C.E.: 'Effect of doping on the optical gain and the spontaneous noise enhancement factor in quantum well amplifiers and lasers studied by simple analytical expressions', *Appl. Phys. Lett.*, 1988, **52**, pp. 1945–1947
8 Asryan, L.V., and Sokolova, Z.N.: 'Optical power of semiconductor lasers with a low-dimensional active region', *J. Appl. Phys.*, 2014, **115**, p. 023107
9 Han, D.-S., and Asryan, L.V.: 'Output power of a double tunneling-injection quantum dot laser', *Nanotechnology*, 2010, **21**, (1), p. 015201
10 Asryan, L.V., and Suris, R.A.: 'Inhomogeneous line broadening and the threshold current density of a semiconductor quantum dot laser', *Semicond. Sci. Technol.*, 1996, **11**, (4), pp. 554–567
11 Asryan, L.V.: 'Spontaneous radiative recombination and nonradiative Auger recombination in quantum-confined heterostructures', *Quantum Electron.*, 2005, **35**, (12), pp. 1117–1120
12 Sokolova, Z.N., Tarasov, I.S., and Asryan, L.V.: 'Capture of charge carriers and output power of a quantum well laser semiconductors', *Semiconductors*, 2011, **45**, (11), pp. 1494–1500
13 Sokolova, Z.N., Bakhvalov, K.V., Lyutetskiy, A.V., *et al.*: 'Method for determination of capture velocity of charge carriers into quantum well in semiconductor laser', *Electron. Lett.*, 2015, **51**, (10), pp. 780–782
14 Sokolova, Z.N., Bakhvalov, K.V., Lyutetskiy, A.V., *et al.*: 'Dependence of the electron capture velocity on the quantum-well depth in semiconductor lasers', *Semiconductors*, 2016, **50**, (5), pp. 667–670

15 Casey, H.C., and Panish, M.B.: 'Heterostructure laser' (Academic Press, New York, 1978)
16 Asryan, L.V., Luryi, S., and Suris, R.A.: 'Intrinsic nonlinearity of the light–current characteristic of semiconductor lasers with a quantum-confined active region', *Appl. Phys. Lett.*, 2002, **81**, (12), pp. 2154–2156
17 Asryan, L.V., Luryi, S., and Suris, R.A.: 'Internal efficiency of semiconductor lasers with a quantum-confined active region', *J. Quantum Electron.*, 2003, **39**, (3), pp. 404–418
18 Asryan, L.V.: Unpublished
19 Agrawal, G.P., and Dutta, N.K.: 'Long-wavelength semiconductor lasers' (Van Nostrand, New York, 1986)

ISSN 1063-7826, Semiconductors, 2020, Vol. 54, No. 3, pp. 366–373. © Pleiades Publishing, Ltd., 2020.
Russian Text © The Author(s), 2020, published in Fizika i Tekhnika Poluprovodnikov, 2020, Vol. 54, No. 3, pp. 296–303.

PHYSICS OF SEMICONDUCTOR DEVICES

Parasitic Recombination in a Laser with Asymmetric Barrier Layers

F. I. Zubov[a,*], M. E. Muretova[a], A. S. Payusov[b], M. V. Maximov[b], A. E. Zhukov[a], and L. V. Asryan[c]

[a] *Alferov University, St. Petersburg, 194021 Russia*
[b] *Ioffe Institute, St. Petersburg, 194021 Russia*
[c] *Virginia Polytechnic Institute and State University, Blacksburg, Virginia 24061, USA*
**e-mail: fedyazu@mail.ru*

Received November 12, 2019; revised November 15, 2019; accepted November 15, 2019

Abstract—In a laser with asymmetric barrier layers (ABLs) two thin barrier layers adjacent to the active region on both sides are intended to prevent bipolar population of the waveguide layers, hence, to suppress parasitic recombination in them. A theoretical model of a laser with ABLs, based on rate equations which acknowledge undesirable carrier leakage inevitable in lasers of this type implemented in practice, is proposed. Solutions to equations are obtained for the steady-state case. By the example of an InGaAs/GaAs quantum-well laser (lasing wavelength $\lambda = 980$ nm), the effect of leakages through ABLs on the device characteristics is studied. The parasitic-flux suppression ratios C of ABLs which are required to prevent the adverse effect of waveguide recombination are estimated. In the case at hand, the effect of ABLs becomes appreciable at suppression ratios of $C \geq 10^2$. To suppress 90% of the parasitic current, C should be 2.3×10^4. The effect of ABLs on useful carrier fluxes arriving at the active region is also studied.

Keywords: diode lasers, asymmetric barrier layers, parasitic waveguide recombination
DOI: 10.1134/S1063782620030203

1. INTRODUCTION

The parasitic recombination of electrons and holes in optical-confinement layers (OCLs) is one of the major causes of degradation of the characteristics of high-power diode lasers, including the efficiency and thermal stability [1]. Previously, to suppress parasitic recombination, the use of so-called asymmetric barrier layers (ABL) adjacent to the active region was proposed [2]. In the ideal case, ABL on the *n*-emitter (*p*-emitter) side completely blocks hole (electron) entrance into the adjacent OCL but does not affect electron entrance into the active region (see Fig. 1).

Previously the concept of an ABL laser was practically implemented in AlGaAs/GaAs lasers of 830–850 nm spectral range [3, 4]. Some improvement in the temperature and power characteristics due to the use of ABLs was detected, whereas the theoretical model assuming the complete suppression of parasitic fluxes predicts a drastic increase in the characteristic temperature of the threshold current [5] and the output optical power [6].

The measure of the ABL efficiency is the ratio of suppression of parasitic carrier fluxes from one waveguide part to another with respect to the flux in the absence of ABLs. In an ideal laser with ABLs, the suppression ratios are infinitely large. However, in practice, blocking barriers have a finite height and a finite thickness, hence a finite suppression ratio.

It appears that insufficient improvement in the characteristics of practically implemented ABL lasers is associated with insufficiently high parasitic-flux suppression ratios of the used ABLs. In these lasers, as calculations show, the undesirable electron- and hole-flux suppression ratios were no more than 20 and 9×10^3, respectively.

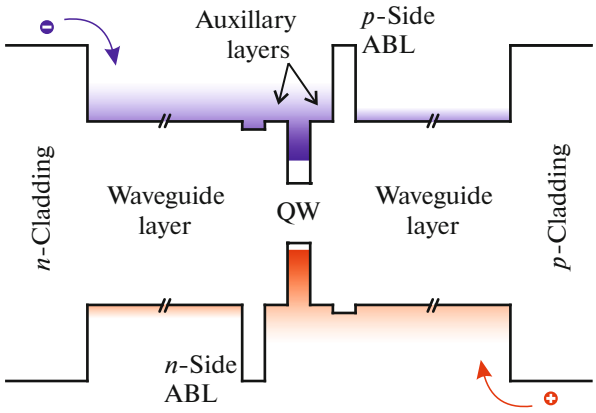

Fig. 1. Schematic energy-band diagram illustrating the ABL laser concept: the *p*-side (*n*-side) ABL is intended to suppress the parasitic electron (hole) flux from one waveguide part to another.

In view of the foregoing, two questions arise:

(i) what parasitic-flux suppression ratios are necessary to make the effect of parasitic recombination in the waveguide on lasers characteristics negligible?

(ii) Is it possible to achieve such suppression ratios in practice using semiconductor materials available for synthesizing of laser heterostructures?

In the present study, we answer the first question. To this end, a theoretical model of ABL lasers in which their "nonideality" is taken into account is developed: the system of equations describing the device is complemented by terms that correspond to carrier leakage through ABLs. The system of equations is solved for the cases of neutral active region and global neutrality of a laser heterostructure. The effect of the ratios of flux suppression by ABLs on device characteristics is studied by the example of an InGaAs/GaAs quantum-well (QW) laser (lasing wavelength is $\lambda = 980$ nm).

2. BASIC EQUATIONS

Our theoretical model of a QW ABL laser, taking into account carrier leakage through ABLs, is based on the following rate equations

$$b_L \frac{\partial n_L}{\partial t} = \frac{j}{q_0} + \frac{n}{\tau_{NE}} + v_{NT} n_R - v_{NC0}(1 - f_N) n_L - v_{NT} n_L - b_L B_{3D} n_L p_L, \quad (1)$$

$$b_R \frac{\partial n_R}{\partial t} = v_{NT} n_L - v_{NT} n_R - b_R B_{3D} n_R p_R, \quad (2)$$

$$\frac{\partial n}{\partial t} = v_{NC0}(1 - f_N) n_L - \frac{n}{\tau_{NE}} - B_{2D} np - v_g g_{max}(f_N + f_P - 1) s, \quad (3)$$

$$b_L \frac{\partial p_L}{\partial t} = v_{PT} p_R - v_{PT} p_L - b_L B_{3D} n_L p_L, \quad (4)$$

$$b_R \frac{\partial p_R}{\partial t} = \frac{j}{q_0} + \frac{p}{\tau_{PE}} + v_{PT} p_L - v_{PC0}(1 - f_P) p_R - v_{PT} p_R - b_R B_{3D} n_R p_R, \quad (5)$$

$$\frac{\partial p}{\partial t} = v_{PC0}(1 - f_P) p_R - \frac{p}{\tau_{PE}} - B_{2D} np - v_g g_{max}(f_N + f_P - 1) s, \quad (6)$$

$$\frac{\partial s}{\partial t} = v_g g_{max}(f_N + f_P - 1) s - v_g \alpha s. \quad (7)$$

Equations (1)–(3) describe the dynamics of the bulk electron concentrations in the OCL on the n-emitter side, n_L, and the OCL on the p-emitter side, n_R, as well as the two-dimensional electron concentration in the QW, n, respectively; Eqs. (4)–(6) describe the dynamics of the bulk hole concentrations in the n-side OCL, p_L, and the p-side OCL, p_R, as well as the two-dimensional hole concentration in the QW, p, respectively; Eq. (7) describes the dynamics of the two-dimensional photon density in a Fabry–Perot cavity, s. The following notations are used: b_L (b_R) is the thickness of the n-side (p-side) OCL, j is the pump current density, q_0 is the elementary charge, τ_{NE} (τ_{PE}) is the characteristic time of the thermal escape of electrons (holes) from the QW, v_{NT} (v_{PT}) is the velocity of electron (hole) tunneling through the p-side (n-side) ABL, v_{NC0} (v_{PC0}) is the velocity of electron (hole) capture into the QW completely free of carriers, f_N (f_P) is the occupancy of the QW with electrons (holes), B_{2D} (B_{3D}) is the radiative recombination constant of the QW (OCL) material [7], v_g is the group velocity of lasing-mode photons within the cavity, g_{max} is the maximum modal gain of the QW, and α is the optical loss of the laser cavity.

The right-hand sides of the rate equations contain carrier-flux densities associated with various physical processes (the plus and minus signs correspond to the carrier entrance and escape), respectively. The term j/q_0 corresponds to the carrier injection from the emitters to the OCLs, the terms containing τ_{NE} (τ_{PE}) correspond to electron (hole) escape from the QW to the OCLs, the terms containing v_{NC0} (v_{PC0}) correspond to electron (hole) capture into the QWs from the OCLs, the terms with v_{NT} (v_{PT}) correspond to electron (hole) tunneling through the ABLs on the p-emitter (n-emitter) side, the terms with B_{2D} (B_{3D}) correspond to the spontaneous radiative recombination in the QW (OCLs), the terms with g_{max} correspond to the stimulated recombination in the active region accompanied by lasing-mode photon generation, and the term with α corresponds to the lasing photon escape due to internal optical loss and mirror optical loss. The carrier concentrations entering into the flux densities on the right-hand sides of the rate equations indicate the reason for the change in the number of carriers, whose dynamics is described by this equation. For example, the term $v_{NT} n_R$ in Eq. (1) corresponds to an increase in electrons in the n-side OCL due to electron tunneling through the p-side ABL from the OCL adjacent to the p-emitter, and the term $-b_L B_{3D} n_L p_L$ describes the decrease in electrons in the n-side OCL due to the spontaneous radiative recombination of electrons and holes in it.

We note that our model assumes that the QW exchanges electrons (holes) by the capture and escape only with the n-side (p-side) OCL, and direct carrier exchange with the opposite OCL is disregarded, since it is suppressed by the ABL placed between the QW and this OCL. We also suppose that the ABL thickness is negligible.

The QW occupancies can be written in terms of carrier concentrations in the QW [8],

$$f_N = 1 - \exp\left(-\frac{n}{N_C^{2D}}\right), \quad f_P = 1 - \exp\left(-\frac{p}{N_V^{2D}}\right), \quad (8)$$

where $N_C^{2D} = m_E^{QW} k_B T/(\pi\hbar^2)$, $N_V^{2D} = m_{HH}^{QW} k_B T/(\pi\hbar^2)$ are the effective densities of states in the QW for electrons and holes, respectively, m_E^{QW} and m_{HH}^{QW} are the electron and heavy-hole effective masses in the QW, respectively, k_B is the Boltzmann constant, and T is the temperature.

The characteristic times of carrier escape from the QW can be written in terms of the capture velocities as follows [9]

$$\tau_{NE} = \frac{1}{v_{NC}}\frac{N_C^{2D}}{n_1}, \quad \tau_{PE} = \frac{1}{v_{PC}}\frac{N_V^{2D}}{p_1}, \tag{9}$$

where we introduced $v_{NC} = v_{NC0}(1 - f_N)$ and $v_{PC} = v_{PC0}(1 - f_P)$, i.e., the velocities of electron and hole capture into the active region at nonzero QW occupancies f_N and f_P, respectively; the quantities n_1 and p_1 are defined by the OCL and QW material parameters and the QW thickness,

$$n_1 = N_C^{3D}\exp\left(-\frac{\Delta E_C - \epsilon_N^{QW}}{k_B T}\right),$$
$$p_1 = N_V^{3D}\exp\left(-\frac{\Delta E_V - \epsilon_P^{QW}}{k_B T}\right). \tag{10}$$

In Eqs. (10), the effective densities of states in the OCLs for electrons and holes are given by

$$N_C^{3D} = 2\left(\frac{m_C^{OCL} k_B T}{2\pi\hbar^2}\right)^{3/2}$$
$$\text{and} \quad N_V^{3D} = 2\left(\frac{m_V^{OCL} k_B T}{2\pi\hbar^2}\right)^{3/2}, \tag{11}$$

respectively, m_C^{OCL} is the electron effective mass in the OCLs, ΔE_C (ΔE_V) is the QW depth for electrons (holes), $(m_V^{OCL})^{3/2} = (m_{HH}^{OCL})^{3/2} + (m_{LH}^{OCL})^{3/2}$, where m_{HH}^{OCL} and m_{LH}^{OCL} are the heavy- and light-hole effective masses in the OCLs, respectively, ϵ_N^{QW} (ϵ_P^{QW}) are the electron (hole) ground-state energies in the QWs, measured from the QW bottom.

The velocities of electron tunneling through the p-side ABL and hole tunneling through the n-side ABL are defined as follows

$$v_{NT} = \sqrt{\frac{k_B T}{2\pi m_C^{OCL}}}\frac{1}{C_N}, \quad v_{PT} = \sqrt{\frac{k_B T}{2\pi m_V^{OCL}}}\frac{1}{C_P}, \tag{12}$$

respectively, where C_N (C_P) is the parasitic electron (hole) flux suppression ratio by the p-side (n-side) ABL with respect to the parasitic flux in the absence of an ABL (i.e., the ratio of the flux without an ABL to the flux with an ABL). The tunneling fluxes through the ABLs in the rate equations and the corresponding tunneling velocities were determined in the Boltzmann-statistics approximation. Their derivation is given in *Appendix I*.

Let the ABL suppression ratios C_N and C_P tend to infinity (total blocking of the tunneling fluxes through the ABLs, i.e., the case of ideal ABLs), the terms containing v_{NT} and v_{PT} in the rate equations will become equal to zero, and it will follow from Eqs. (2) and (4) that the flux densities associated with the parasitic recombination in the waveguide are zero. As a result of such passage to the limit, we will obtain a system of five rate equations for an ideal ABL laser [10].

Here we are interested in the steady-state lasing. We will also suppose that the electrical neutrality condition $n = p$ in the active region is satisfied. Then Eqs. (7) and (8) yield the transcendental equation for determining n,

$$g_{max}\left[1 - \exp\left(-\frac{n}{N_C^{2D}}\right) - \exp\left(-\frac{n}{N_V^{2D}}\right)\right] - \alpha = 0. \tag{13}$$

In *Appendix II*, it is shown that all other concentrations can be expressed in terms of n.

The current densities of the parasitic spontaneous recombination in the left and right OCLs (see Fig. 1) are written as

$$j_L = q_0 b_L B_{3D} n_L p_L, \quad j_R = q_0 b_L B_{3D} n_R p_R, \tag{14}$$

respectively, and their sum j_{OCL} is the total density of the parasitic recombination current in the entire waveguide. The current density of the stimulated recombination in the QW is given by

$$j_{stim} = j - j_{QW} - j_{OCL}, \tag{15}$$

where $j_{QW} = q_0 B_{2D} np$ is the current density of the spontaneous recombination in the QW. The output power of the laser radiation is defined by the following expression

$$P_{out}(j) = \frac{\hbar\omega}{q_0} w L j_{stim}(j), \tag{16}$$

where $\hbar\omega$ is the lasing-mode photon energy, w is the stripe contact width, and L is the Fabry–Perot cavity length. The threshold current density j_{th} can be determined numerically from Eq. (15) under the condition $j_{stim} = 0$.

We note that the solution to the system of rate equations in the steady-state case can also be determined under the condition of global neutrality of the laser structure [10],

$$b_L n_L + n + b_R n_R = b_L p_L + p + b_R p_R. \tag{17}$$

The algorithm for solving this problem is as follows. The hole concentration in the QW can be written in terms of the electron concentration using Eqs. (7) and (8),

$$p = N_V^{2D}\ln\left[\frac{1}{1 - (\alpha/g_{max}) - \exp(-n/N_C^{2D})}\right]. \tag{18}$$

The concentrations p_R, n_R, and p_L can be expressed in terms of n_L (see *Appendix II*: (A.II.1), (A.II.2), and (A.II.3), respectively, and n_L can be expressed in terms of n (see *Appendix II*: (A.II.5)). Then Eq. (17) can be used to determine n.

We can see that the solution of the problem in the case of global neutrality will be slightly more laborious, than in the case of local neutrality. In what follows, we will present the results for a neutral QW. Nevertheless, the main conclusions made in this paper also take place in the case of global neutrality.

3. MODEL LASER STRUCTURE

Using the presented model, let us illustrate the effect of the nonideality of ABLs having a finite parasitic-flux suppression ratio on the characteristics of semiconductor laser. To this end, as an example, we consider a laser having GaAs OCLs and InGaAs QW laser with a lasing wavelength of 980 nm with ABLs introduced into the waveguide (see Fig. 1). We note that it is difficult to achieve efficient room-temperature lasing in the absence of ABLs in the device with such a heterostructure in view of highly pronounced parasitic recombination in the waveguide because of the low carrier-localization energy in the QW [1].

The thickness of each OCL of the model laser is taken as 400 nm, the active region material is $In_{0.18}Ga_{0.82}As$, its thickness is 7.6 nm, and the cladding layers (emitters) are made of $Al_{0.2}Ga_{0.8}As$. In this case, the electron and hole localization energies in the QW with respect to the edges of the corresponding OCL bands will be 41 and 116 meV. The waveguide under consideration supports only fundamental mode to which corresponds the Γ factor of ~1.3%.

We also suppose that one mirror is totally reflective, and the other mirror is without deposition; the cavity length is 500 nm, and the stripe width is 3 μm.

In simulating the laser, we assumed the electron and hole capture velocities into the QW to be identical and equal to 10^5 cm/s, the temperature to be 300 K, and the pump current density to be 5 kA/cm^2 (unless otherwise indicated). The internal loss was also neglected in the calculation, and the ABL flux-suppression ratios were thought to be identical and equal to C (unless otherwise indicated).

4. RESULTS AND DISCUSSION

Figure 2 shows the dependences of the electron concentrations n_L and n_R in the left and right OCLs, respectively, as functions of the parasitic-flux suppression ratio C of ABLs. We can see that the concentrations in both waveguide parts are identical when $C = 1$ (it can be said that there is no ABLs). As C increases, on reaching $C \approx 10$, the concentrations begin to change: n_L steadily increases, while n_R, on the contrary, after a small increase, begins to decrease from

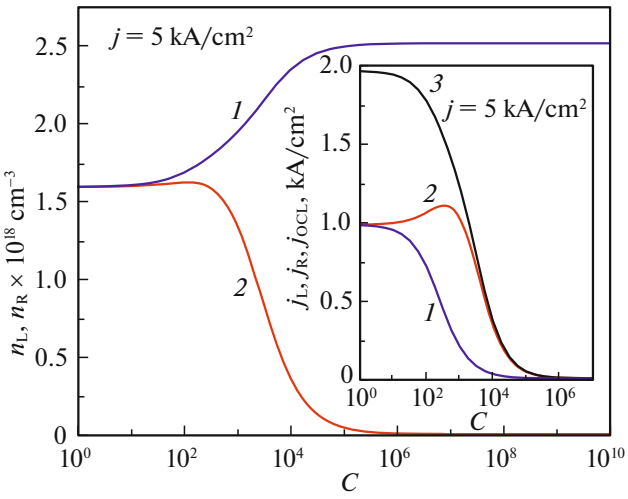

Fig. 2. Dependences of the waveguide electron concentrations in the (*1*) left OCL n_L and (*2*) right OCL n_R on the parasitic-flux suppression ratio C of ABLs. The inset shows the dependences of the recombination current densities in the waveguide on C for the (1) left OCL j_L, (*2*) right OCL j_R, and (*3*) the entire waveguide j_{OCL}. The pump current density is $j = 5$ kA/cm^2.

about $C = 150$, since electron entrance into the right OCL is blocked by the ABL on the p-emitter side (see Fig. 1). As C further increases, the increase in n_L gradually saturates, and n_R exponentially decreases to zero ($n_R = 0$ in the laser with ideal ABLs, for which $C \to \infty$). The hole concentrations in the OCLs behave similarly with increasing C with the difference being that the concentration in the left part of the waveguide on the contrary decreases to zero, and the concentration in the right part saturates after a steady increase.

The inset in Fig. 2 shows the dependences of the total parasitic recombination current density in the waveguide j_{OCL} and its components for the left and right OCLs, j_L and j_R, respectively. The total parasitic current decreases with decreasing the ABLs tunneling transparency (as C increases), which was expected. However, an appreciable drop in waveguide recombination begins only from the suppression ratios exceeding 100. Total parasitic current suppression by 90% is reached at $C \approx 2.3 \times 10^4$. We also see that a significantly lower suppression ratio is required to suppress recombination in the left part of the waveguide than in the right part: a 90% decrease in the parasitic current is achieved at $C = 2.6 \times 10^3$ and 4.3×10^4 for the left and right OCLs, respectively. This is because the hole effective mass is much greater than the electron effective mass; therefore, the tunneling velocity for holes will be lower than for electrons at identical C (see Eq. (12)).

Based on these results, we can assume that the ABL lasers previously implemented in practice [3, 4] fea-

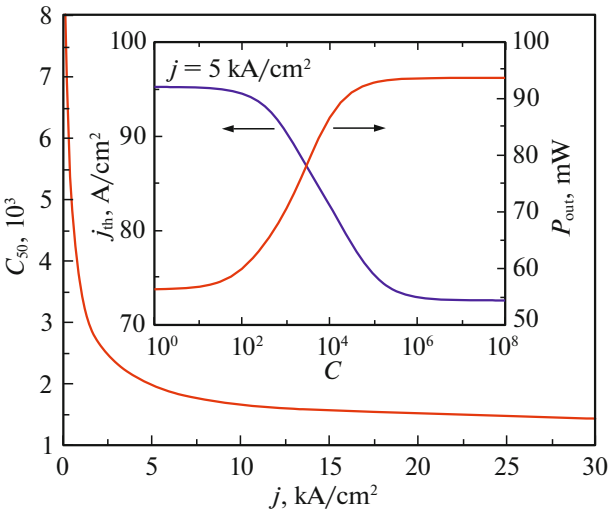

Fig. 3. ABL suppression ratio C_{50}, at which a 50% gain in the output optical power of the greatest possible one (for ideal ABLs) is attained, as a function of the pump current density j. The inset shows the threshold current density j_{th} and the output lasing power P_{out} as a function of the parasitic-flux suppression ratio C of ABLs at the pump current density of 5 kA/cm^2.

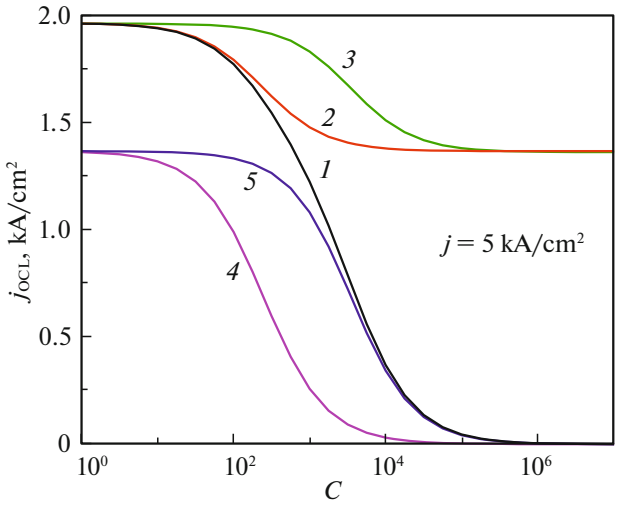

Fig. 4. Dependences of the recombination current densities in the entire waveguide, j_{OCL}, on the parasitic-flux suppression ratio C for various cases: (*1*) two ABLs with the suppression C on both sides of the QW; (*2*, *3*) only one ABL with the suppression C on the n-emitter (*2*) and p-emitter (*3*) side; (*4*, *5*) one ABL on the p-emitter (*4*) or n-emitter (*5*) side is ideal, and the other has a finite suppression ratio C.

tured rather good suppression of hole fluxes ($C_P \approx 9 \times 10^3$), hence, a low parasitic recombination current in the n-side OCL, but had a poor electron blocking (C_N no more than 20), hence, a high parasitic current in the p-side OCL. This can explain only a moderate improvement in the characteristics in those lasers due to ABLs.

We note that a slight increase in the parasitic current in the right OCL in the range $C \sim 10^2$–10^3 is probably associated with satisfying the charge neutrality condition of the active region. In the case of global neutrality, such an increment of j_R is absent: the recombination current density in the right OCL steadily decreases beginning with $C = 1$.

The inset in Fig. 3 shows the dependences of the threshold current density and output optical power on the parasitic-flux suppression ratio. For the laser under consideration the threshold current can be lowered by the ABLs insignificantly (maximum by 24%). We note that the threshold current density at $C = 1$ (in essence, there is no ABL) and high C ($C \geq 10$, i.e., suppression is close to ideal) is identical with high accuracy to the threshold currents calculated using theoretical models for an ordinary laser with a double heterostructure without ABLs and for a laser with ideal ABLs, respectively [11].

In contrast to the threshold current, the output optical power significantly increases as waveguide recombination is suppressed (up to a 66% increase at 5 kA/cm^2); therewith, the effect of the ABLs becomes stronger with increasing pumping (an optical-power increment up to 152% at 20 kA/cm^2). At 5 kA/cm^2, the ABL suppression ratio C_{50}, at which a 50% increment in the optical power of the greatest possible one is 2×10^3. This parameter steadily decreases with pumping (see Fig. 3): sharply near the threshold and gradually strarting from $j \approx 5$ kA/cm^2.

The dependences of the recombination current densities in the entire waveguide for the use of only the n-side ABL and only the p-side ABL on the suppression ratio C are shown in Fig. 4 (curves *2* and *3*, respectively). For comparison, Fig. 4 also show the dependence of j_{OCL} on C for the laser with both ABLs (curve *1*). In both cases of the use of only one ABL, the parasitic current can be ultimately suppressed by approximately the same value. For example, at 5 kA/cm^2, the ultimate reduction in the waveguide recombination current is only 30% and decreases as pumping increases further (at 20 kA/cm^2, it is already 19%).

Let us also present the simulation results for the cases when one ABL is ideal (completely blocks the corresponding undesirable transport), and another ABL features a finite parasitic flux suppression ratio C. Curves *4* and *5* in Fig. 4 show the dependences j_{OCL} on C for lasers in which the n-side and p-side ABL is nonideal, respectively. In the former case a 90% parasitic current suppression (with respect to the laser without ABL) is reached at $C \approx 1.4 \times 10^3$; in the second case, $C \approx 1.9 \times 10^4$.

In the ideal case, the ABL should totally block undesirable transport, not preventing useful carrier flux entering into the active region. However, in prac-

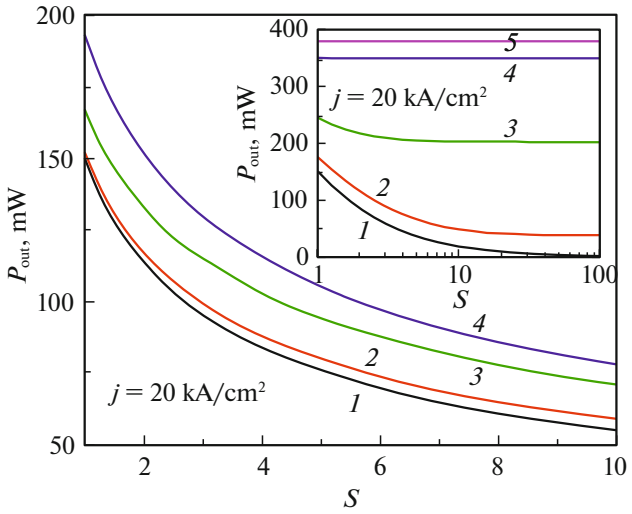

Fig. 5. Dependences of the output lasing power P_{out} on the useful flux suppression ratio S for various parasitic-flux suppression ratios $C = 1$ (*1*), 10^2 (*2*), 10^3 (*3*), and 10^6 (*4*) when using only *p*-side ABL. The inset shows the dependences $P_{out}(S)$ for $C = 1$ (*1*), 10^2 (*2*), 10^3 (*3*), 10^4 (*4*), and 10^6 (*5*) in the case of the use of both ABLs with identical parasitic-flux suppression ratios and identical useful flux suppression ratios. The pump current density is 20 kA/cm^2.

tice, it may turn out that a sufficiently high opaque main barrier for undesirable carriers can be realized only when creating of a spurious barrier (or well) suppressing the useful flux (in Fig. 1, the *n*-side ABL creates a spurious well for electrons, and the *p*-side ABL creates a spurious barrier for holes). However, we note that if the ABL forms an additional well, its placement close to the active region, on the contrary, will promote carrier capture into the QW.

The effect of spurious barriers (wells) on the laser characteristics can also be studied using the presented theoretical model and expressions derived for the steady-state conditions. Let us assume that the *n*-side (*p*-side) ABL suppresses the electron (hole) flux by a factor of S_N (S_P). Then the fluxes of carrier capture into the active region and carrier escape from it, as well as tunneling fluxes from one waveguide part to another should be decreased accordingly. To this end, the electron capture velocity, escape time, and tunneling velocity are modified as follows: $v_{NC} \to v_{NC}/S_N$, $\tau_{NE} \to \tau_{NE}S_N$, and $v_{NT} \to v_{NT}/S_N$. The corresponding hole parameters are changed in a similar way. At the same time the form of the rate equations themselves and expressions derived on their basis remain unchanged.

The dependence of the output optical power P_{out} on the spurious barrier suppression ratio S (identical for both ABLs) for various suppression ratios of the main barriers at a pump current density of 20 kA/cm^2 is shown in the inset to Fig. 5. When the main barrier suppression ratio is small ($1 \le C \lesssim 10^2$), the presence of the spurious barriers even with small S has a negative effect on the output power. For example, if $C = 10^2$, the power decreases in half in comparison with a conventional laser structure (without ABLs) even at $S \approx 4$. However, with increasing the suppression ratio of the main barriers the output power rises and the slope of $P_{out}(S)$ dependence with increasing S is slowed. As a result, if the parasitic-flux suppression ratio is sufficiently high ($C \gg 10^2$), one can achieve an appreciable power increment even in the presence of significant spurious barriers (wells). For example, if $C = 10^3$, at a twofold suppression of the useful fluxes and a pump current density of 20 kA/cm^2, the optical power will be higher by 45% than in the laser without ABLs. As C increases above 10^8, the power P saturates at the power level of the laser with ideal ABLs for the range under consideration $1 \le S \le 100$ and is almost independent of S.

It is interesting that if one of the ABLs (any) is removed, even at high parasitic-flux suppression ratios, the output power will decrease very rapidly with the suppression of the useful flux (see Fig. 5). For example, in the case of the use of only the *p*-side ABL with a very high suppression ratio, $C = 10^8$, the positive effect of the main barrier will be completely compensated even at $S \approx 2$.

5. CONCLUSIONS

Thus, by the example of an InGaAs/GaAs QW laser (λ = 980 nm), the effect of carrier leakage through ABLs on the device characteristics was studied. It was found that, to eliminate undesirable waveguide recombination, rather large parasitic-flux suppression ratios are required; therewith, the electron-flux suppression ratio should be significantly higher than the hole-flux suppression ratio, which is due to the difference in the effective mass of particles. For example, in the case at hand, a 90% parasitic current suppression in the *n*-side and *p*-side OCLs is achieved at $C = 2.6 \times 10^3$ and $C = 4.3 \times 10^4$, respectively. It was also found that, if the suppression ratios of the main ABL barriers are sufficiently large ($C \gtrsim 10^8$), even at a significant suppression ratios of the useful fluxes (S up to 10^2), the device characteristics are close to those of an ideal ABL laser. In our opinion, it is a very important result, since its consideration will make it possible to extend the class of semiconductor materials applicable to designing ABLs.

APPENDIX I

Expression for the Tunneling Flux through an Asymmetric Barrier Layer

Let us find the unidirectional carrier-tunneling flux through an ABL introduced between two OCLs (the effect of the active-region QW on tunneling is neglected). Let us use the Boltzmann statistics: in this case, the necessary expression can be obtained in an analytical form. For definiteness, we will consider electron tunneling from the left OCL to the right

OCL. It can be shown that the carrier concentration (per unit area) in the left OCL with the energy of motion E in the growth direction is written as

$$n_{\mathrm{L}}^{E} = \frac{m_{\mathrm{C}}^{\mathrm{OCL}} k_{\mathrm{B}} T}{\pi\hbar^2} \exp\left(\frac{F_{\mathrm{CL}} - E_{\mathrm{C}} - E}{k_{\mathrm{B}} T}\right), \quad \text{(A.I.1)}$$

where F_{CL} and E_{C} are the positions of the quasi-Fermi level of electrons in the left OCL and the bottom of the conduction band in the OCL, respectively. Using the Tsu–Esaki formula [12], we find the unidirectional carrier flux (from left to right) in the absence of an ABL,

$$f_{\mathrm{C0}}^{\mathrm{LR}} = \frac{1}{2\pi\hbar}\int_0^\infty n_{\mathrm{L}}^{E} dE = \frac{m_{\mathrm{C}}^{\mathrm{OCL}} (k_{\mathrm{B}} T)^2}{2\pi^2\hbar^3} \exp\left(\frac{F_{\mathrm{CL}} - E_{\mathrm{C}}}{k_{\mathrm{B}} T}\right). \quad \text{(A.I.2)}$$

Then, taking into account that the bulk electron concentration in the left OCL is

$$n_{\mathrm{L}} = \frac{1}{\sqrt{2}}\left(\frac{m_{\mathrm{C}}^{\mathrm{OCL}} k_{\mathrm{B}} T}{\pi\hbar^2}\right)^{3/2} \exp\left(\frac{F_{\mathrm{CL}} - E_{\mathrm{C}}}{k_{\mathrm{B}} T}\right),$$

the flux $f_{\mathrm{C0}}^{\mathrm{LR}}$ can be expressed in terms of the n_{L} concentration,

$$f_{\mathrm{C0}}^{\mathrm{LR}} = \sqrt{\frac{k_{\mathrm{B}} T}{2\pi m_{\mathrm{C}}^{\mathrm{OCL}}}} n_{\mathrm{L}}. \quad \text{(A.I.3)}$$

In the presence of an ABL with the electron-flux suppression ratio C_{N}, the tunneling flux from the left OCL to the right OCL will be

$$f_{\mathrm{C}}^{\mathrm{LR}} = \sqrt{\frac{k_{\mathrm{B}} T}{2\pi m_{\mathrm{C}}^{\mathrm{OCL}}}} \frac{1}{C_{\mathrm{N}}} n_{\mathrm{L}}. \quad \text{(A.I.4)}$$

The factor at n_{L} in (A.I.4) has the dimension of velocity. In the above (12), it is denoted as the electron-tunneling velocity through an ABL (v_{NT}). Finally, the desired tunneling flux takes a very simple form: $f_{\mathrm{C}}^{\mathrm{LR}} = v_{\mathrm{NT}} n_{\mathrm{L}}$. Similarly, other tunneling fluxes appearing in the rate equations of both electrons (from right to left) and holes (from left to right and vice versa) can be obtained.

APPENDIX II

Determination of the Waveguide Concentrations

Let us show that all waveguide concentrations can be determined by the electron concentration in the QW n. Subtracting Eq. (5) from (2), we obtain

$$v_{\mathrm{NC}} n_{\mathrm{L}} - \frac{n}{\tau_{\mathrm{NE}}} - v_{\mathrm{PC}} p_{\mathrm{R}} + \frac{n}{\tau_{\mathrm{PE}}} = 0.$$

From which

$$p_{\mathrm{R}} = a_1 n_{\mathrm{L}} - a_2, \quad \text{(A.II.1)}$$

where

$$a_1 = \frac{v_{\mathrm{NC}}}{v_{\mathrm{PC}}}, \quad a_2 = \frac{n}{v_{\mathrm{PC}}}\left(\frac{1}{\tau_{\mathrm{NE}}} - \frac{1}{\tau_{\mathrm{PE}}}\right).$$

Having substituted (A.II.1) into Eq. (3), we obtain n_{R},

$$n_{\mathrm{R}} = \frac{n_{\mathrm{L}}}{a_3 n_{\mathrm{L}} + a_4}, \quad \text{(A.II.2)}$$

where $a_3 = b_{\mathrm{R}} B_{\mathrm{3D}} a_1 / v_{\mathrm{NT}}$, $a_4 = 1 - b_{\mathrm{R}} B_{\mathrm{3D}} a_2 / v_{\mathrm{NT}}$. Then, using (A.II.1), from Eq. (4), we obtain

$$p_{\mathrm{L}} = \frac{a_1 n_{\mathrm{L}} - a_2}{a_5 n_{\mathrm{L}} + 1}, \quad \text{(A.II.3)}$$

where $a_5 = B_{\mathrm{L}} B_{\mathrm{3D}} / v_{\mathrm{PT}}$. One more relation can be obtained by subtracting Eq. (4) from (1),

$$\frac{j}{q_0} + \frac{n}{\tau_{\mathrm{NE}}} + v_{\mathrm{NT}} n_{\mathrm{R}} - v_{\mathrm{NC}} n_{\mathrm{L}} - v_{\mathrm{NT}} n_{\mathrm{L}} - v_{\mathrm{PT}} p_{\mathrm{R}} + v_{\mathrm{PT}} p_{\mathrm{L}} = 0. \quad \text{(A.II.4)}$$

Having substituted the expressions for p_{R}, n_{R}, and p_{L} from (A.II.1), (A.II.2), and (A.II.3), respectively, into (A.II.4), we can obtain the cubic equation for n_{L},

$$a n_{\mathrm{L}}^3 + b n_{\mathrm{L}}^2 + c n_{\mathrm{L}} + d = 0,$$

where

$$a = -a_3 a_5 (v_{\mathrm{NC}} + v_{\mathrm{NT}} + a_1 v_{\mathrm{PT}}),$$

$$b = a_3 a_5 \left(\frac{j}{q_0} + \frac{n}{\tau_{\mathrm{NE}}} + a_2 v_{\mathrm{PT}}\right) + a_5 v_{\mathrm{NT}} - (a_3 + a_4 a_5)(v_{\mathrm{NC}} + v_{\mathrm{NT}} + a_1 v_{\mathrm{PT}}) + a_1 a_3 v_{\mathrm{PT}},$$

$$c = (a_3 + a_4 a_5)\left(\frac{j}{q_0} + \frac{n}{\tau_{\mathrm{NE}}} + a_2 v_{\mathrm{PT}}\right) + v_{\mathrm{NT}} - a_4 (v_{\mathrm{NC}} + v_{\mathrm{NT}} + a_1 v_{\mathrm{PT}}) + (a_1 a_4 - a_2 a_3) v_{\mathrm{PT}},$$

$$d = a_4 \left(\frac{j}{q_0} + \frac{n}{\tau_{\mathrm{NE}}}\right).$$

These coefficients of the cubic equation depend only on the concentration (n). To find the roots, we can use Cardano's formulas. The physically meaningful root is given by

$$n_{\mathrm{L}} = \alpha_{\mathrm{C}} + \beta_{\mathrm{C}} - \frac{b}{3a}, \quad \text{(A.II.5)}$$

where

$$\alpha_{\mathrm{C}} = \sqrt[3]{-\frac{q_{\mathrm{C}}}{2} + \sqrt{Q_{\mathrm{C}}}}, \quad \beta_{\mathrm{C}} = \sqrt[3]{-\frac{q_{\mathrm{C}}}{2} - \sqrt{Q_{\mathrm{C}}}},$$

$$Q_{\mathrm{C}} = \left(\frac{p_{\mathrm{C}}}{3}\right)^3 + \left(\frac{q_{\mathrm{C}}}{2}\right)^2,$$

$$p_{\mathrm{C}} = \frac{c}{a} - \frac{b^2}{3a^2}, \quad q_{\mathrm{C}} = \frac{2b^3}{27a^3} - \frac{bc}{3a^3} + \frac{d}{a}.$$

Now, knowing n_L, we can calculate other carrier concentrations in the waveguide, using (A.II.1), (A.II.2), and (A.II.3).

FUNDING

This study was supported by the Russian Foundation for Basic Research, project no. 16-29-03123.

L.V. Asryan acknowledges the support of the U.S. Army Research Office, grant no. W911NF-17-1-0432.

CONFLICT OF INTEREST

The authors declare that they have no conflict of interest.

REFERENCES

1. C. Frevert, P. Crump, F. Bugge, S. Knigge, and G. Erbert, Semicond. Sci. Technol. **31**, 025003 (2016).
2. L. V. Asryan and S. Luryi, Solid-State Electron. **47**, 205 (2003).
3. A. E. Zhukov, N. V. Kryzhanovskaya, F. I. Zubov, Yu. M. Shernyakov, M. V. Maximov, E. S. Semenova, K. Yvind, and L. V. Asryan, Appl. Phys. Lett. **100**, 021107 (2012).
4. F. I. Zubov, M. V. Maximov, Yu. M. Shernyakov, N. V. Kryzhanovskaya, E. S. Semenova, K. Yvind, L. V. Asryan, and A. E. Zhukov, Electron. Lett. **51**, 1106 (2015).
5. L. V. Asryan, N. V. Kryzhanovskaya, M. V. Maximov, A. Yu. Egorov, and A. E. Zhukov, Semicond. Sci. Technol. **26**, 055025 (2011).
6. L. V. Asryan, N. V. Kryzhanovskaya, M. V. Maximov, F. I. Zubov, and A. E. Zhukov, J. Appl. Phys. **114**, 143103 (2013).
7. L. V. Asryan, Quant. Electron. **35**, 1117 (2005).
8. K. J. Vahala and C. E. Zah, Appl. Phys. Lett. **52**, 1945 (1988).
9. D.-S. Han and L. V. Asryan, Nanotechnology **21**, 015201 (2010).
10. L. V. Asryan, F. I. Zubov, Yu. S. Balezina (Polubavkina), E. I. Moiseev, M. E. Muretova, N. V. Kryzhanovskaya, M. V. Maximov, and A. E. Zhukov, Semiconductors **52**, 1621 (2018).
11. L. V. Asryan, F. I. Zubov, N. V. Kryzhanovskaya, M. V. Maximov, and A. E. Zhukov, Semiconductors **50**, 1362 (2016).
12. F. I. Zubov, M. E. Muretova, L. V. Asryan, E. S. Semenova, M. V. Maximov, and A. E. Zhukov, J. Appl. Phys. **124**, 133105 (2018).

Translated by A. Kazantsev

Temperature-induced single-to-double branch transformation of operating characteristics in semiconductor lasers with a low-dimensional active region

Sokolova, Zinaida, Pikhtin, Nikita, Slipchenko, Sergey, Asryan, Levon

Zinaida N. Sokolova, Nikita A. Pikhtin, Sergey O. Slipchenko, Levon V. Asryan, "Temperature-induced single-to-double branch transformation of operating characteristics in semiconductor lasers with a low-dimensional active region," Proc. SPIE 11301, Novel In-Plane Semiconductor Lasers XIX, 113010D (24 February 2020); doi: 10.1117/12.2546974

SPIE.

Event: SPIE OPTO, 2020, San Francisco, California, United States

Temperature-induced single-to-double branch transformation of operating characteristics in semiconductor lasers with a low-dimensional active region

Zinaida N. Sokolova[*a)], Nikita A. Pikhtin[**a)], Sergey O. Slipchenko[***a)], and Levon V. Asryan[****b)]

[a)] Ioffe Institute, St. Petersburg, 194021, Russia

[b)] Virginia Polytechnic Institute and State University, Blacksburg, Virginia 24061, USA

ABSTRACT

The temperature behavior of operating characteristics in semiconductor lasers with a quantum-confined active region is studied with a proper account for (i) non-instantaneous capture of charge carriers from the waveguide region into the active region and (ii) internal optical loss that depends on the carrier densities. Because of (i), the carrier densities are not pinned in the lasing mode, i.e., they are functions of the injection current. In view of (ii) and as a result of pump-current-dependence of the carrier densities, so becomes the internal loss coefficient. This in turn leads to the roll-over of the light-current characteristic at high currents (i.e., decreasing optical power with increasing injection current) and, under certain conditions, appearance of the second branch in it. The laser characteristics are shown to transform qualitatively with varying temperature: they are conventional, i.e., consist of one branch, at low temperatures but they have two branches, i.e., are of a binary nature, at high temperatures. The two branches merge together at the maximum operating current beyond which the lasing quenches. In contrast to the first (conventional) lasing threshold, the threshold for emerging the second branch decreases with increasing temperature. The pump-current-dependence of the carrier densities and internal loss coefficient is also fascinating: these quantities decrease with increasing current in their second branches.

Keywords: Internal optical loss, light-current characteristic, low-dimensional active region, semiconductor lasers

1. INTRODUCTION

Diode lasers have been extensively studied both experimentally and theoretically before (see a review article [1]). A new fascinating feature has been however predicted in [2]-[4] for semiconductor lasers with a nanosize active region: in the presence of internal optical loss that depends on the charge carrier densities [primarily in the waveguide region – optical confinement layer (OCL)], roll-over of the light-current characteristic (LCC, the dependence of the output optical power on the injection current) can occur at high pump currents. The more so, the second branch can emerge in the LCC in addition to the first 'conventional' branch; the condition for this is given by the following inequality [5]:

$$\frac{\sigma_{\text{int}} v_{\text{capt},0}}{2b\, B^{\text{OCL}} g^{\max}} > 1\,, \tag{1}$$

where σ_{int} is the cross section of internal optical loss in the OCL, $v_{\text{capt},0}$ is the velocity of carrier capture from the OCL into an empty (unoccupied) quantum-confined active region, b is the OCL thickness, B^{OCL} is the spontaneous radiative recombination constant for the OCL measured in units of cm^3/s (see [6, 7] for the expression for B^{OCL}), and $g^{\max}$ is the maximum value of the modal gain in the active region.

* zina.sokolova@mail.ioffe.ru

** nike@hpld.ioffe.ru

*** serghpl@mail.ioffe.ru

**** asryan@vt.edu

Novel In-Plane Semiconductor Lasers XIX, edited by Alexey A. Belyanin, Peter M. Smowton, Proc. of SPIE Vol. 11301, 113010D · © 2020 SPIE
CCC code: 0277-786X/20/$21 · doi: 10.1117/12.2546974

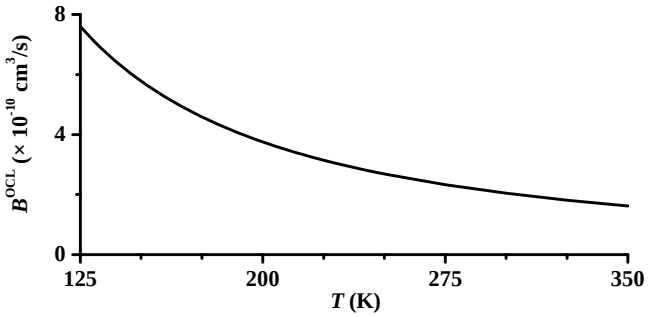

Fig. 1. Spontaneous radiative recombination constant for the OCL vs. temperature.

Varying each of the parameters entering into (1) can result in single-to-double branch transformation of the LCC. In [8], we considered a quantum well (QW) laser and theoretically demonstrated how such transformation occurs with increasing $v_{capt,0}$. Experimental methods for variation of $v_{capt,0}$ are however not straightforward. As opposed to $v_{capt,0}$, the temperature can be easily varied in laser structures. Compared to the other quantities entering into (1), the spontaneous radiative recombination constant for the OCL has the strongest temperature dependence, which is given as (see [6, 7])

$$B^{\mathrm{OCL}} \propto \frac{1}{T^{3/2}}. \tag{2}$$

As seen from (2) and shown in Fig. 1, B^{OCL} decreases with increasing temperature. Hence it follows from (1) and (2) that the condition for emergence of the second branch in the LCC should become satisfied with increasing temperature.

In this work, we study the effect of temperature on emergence of the second branch in the QW laser characteristics.

2. THEORETICAL MODEL

Our model is based on the following set of steady-state rate equations for the free electron and hole densities in the OCL, n^{OCL} and p^{OCL}, the two-dimensional (2D) densities of electrons and holes confined in the QW, n^{QW} and p^{QW}, and the number of photons in the lasing mode, N:

for free electrons in the OCL [$b(\partial n^{\mathrm{OCL}}/\partial t) = 0$],

$$\frac{j}{e} + N_{\mathrm{QW}} \frac{n^{\mathrm{QW}}}{\tau_{\mathrm{n,esc}}} - N_{\mathrm{QW}} v_{\mathrm{n,\,capt,\,0}} (1 - f_{\mathrm{n}})\, n^{\mathrm{OCL}} - bB^{\mathrm{OCL}} n^{\mathrm{OCL}} p^{\mathrm{OCL}} = 0, \tag{3}$$

for free holes in the OCL [$b(\partial p^{\mathrm{OCL}}/\partial t) = 0$],

$$\frac{j}{e} + N_{\mathrm{QW}} \frac{p^{\mathrm{QW}}}{\tau_{\mathrm{p,esc}}} - N_{\mathrm{QW}} v_{\mathrm{p,\,capt,\,0}} (1 - f_{\mathrm{p}}) p^{\mathrm{OCL}} - bB^{\mathrm{OCL}} n^{\mathrm{OCL}} p^{\mathrm{OCL}} = 0, \tag{4}$$

for electrons confined in the QWs ($\partial n^{\mathrm{QW}}/\partial t = 0$),

$$v_{\mathrm{n,\,capt,\,0}} (1 - f_{\mathrm{n}})\, n^{\mathrm{OCL}} - \frac{n^{\mathrm{QW}}}{\tau_{\mathrm{n,esc}}} - B^{\mathrm{QW}} n^{\mathrm{QW}} p^{\mathrm{QW}} - v_{\mathrm{g}} g^{\max} (f_{\mathrm{n}} + f_{\mathrm{p}} - 1) \frac{N}{S} = 0, \tag{5}$$

for holes confined in the QWs ($\partial p^{\mathrm{QW}}/\partial t = 0$),

$$v_{\mathrm{p,\,capt,\,0}} (1 - f_{\mathrm{p}}) p^{\mathrm{OCL}} - \frac{p^{\mathrm{QW}}}{\tau_{\mathrm{p,esc}}} - B^{\mathrm{QW}} n^{\mathrm{QW}} p^{\mathrm{QW}} - v_{\mathrm{g}} g^{\max} (f_{\mathrm{n}} + f_{\mathrm{p}} - 1) \frac{N}{S} = 0, \tag{6}$$

and for photons ($\partial N/\partial t = 0$),

$$v_g N_{QW} g^{max}(f_n + f_p - 1)N - v_g(\beta + \alpha_{int})N = 0 . \quad (7)$$

The occupancy of the lower (upper) edge of the electron (hole) quantum-confinement subband in the QW is denoted as f_n (f_p); f_n and f_p are expressed in terms of the 2D electron and hole densities n^{QW} and p^{QW} as follows [2, 9]:

$$f_n = 1 - \exp\left(-\frac{n^{QW}}{N_c^{2D}}\right), \qquad f_p = 1 - \exp\left(-\frac{p^{QW}}{N_v^{2D}}\right), \quad (8)$$

where $N_{c,v}^{2D} = m_{e,hh}^{QW} T/(\pi\hbar^2)$ are the 2D effective densities of states in the conduction and valence bands in the QW, $m_{e,hh}^{QW}$ are the electron and hole effective masses in the QW, and the temperature T is measured in units of energy.

The following parameters enter into eqs. (3)-(7): j is the injection current density, e is the electron charge, N_{QW} is the number of identical (of the same material composition and width) QWs, $\tau_{n,esc}$ and $\tau_{p,esc}$ are the thermal escape times of electrons and holes from a QW to the OCL, $v_{n,capt,0}$ and $v_{p,capt,0}$ are the capture velocities of electrons and holes into an empty (at $f_n = 0$ and $f_p = 0$) QW measured in units of cm/s, B^{QW} is the spontaneous radiative recombination coefficient for the 2D (QW) region measured in units of cm^2/s (see [7] for the expression for B^{QW}); v_g is the group velocity of light, g^{max} is the maximum gain in each QW, $S = WL$ is the cross-section of the junction, W is the lateral size of the device, L is the Fabry-Pérot cavity length, $\beta = (1/L)\ln(1/R)$ is the mirror loss, and R is the facet reflectivity.

A key component of our theoretical model is the internal optical loss that depends on the electron and hole densities. The expression for the internal loss coefficient α_{int} in terms of the free carrier densities in the OCL and the 2D carrier densities in the QW is

$$\alpha_{int}(j) = \alpha_0 + \Gamma^{OCL}[\sigma_n^{OCL} n^{OCL}(j) + \sigma_p^{OCL} p^{OCL}(j)] + \Gamma^{QW}[\sigma_n^{QW} n^{QW}(j) + \sigma_p^{QW} p^{QW}(j)], \quad (9)$$

where σ_n^{OCL} and σ_p^{OCL} are the cross sections of light absorption by electrons and holes in the OCL, Γ^{OCL} is the optical confinement factor in the OCL, σ_n^{QW} and σ_p^{QW} are the cross sections of light absorption by electrons and holes in the QW, Γ^{QW} is the optical confinement factor in the QWs, and α_0 is the constant component, which is primarily due to light absorption in the cladding layers.

The thermal escape times of electrons and holes from the QW into the OCL are [10, 11]:

$$\tau_{n,esc} = \frac{1}{v_{n,capt,0}(1 - f_n)} \frac{N_c^{2D}}{n_1}, \qquad \tau_{p,esc} = \frac{1}{v_{p,capt,0}(1 - f_p)} \frac{N_v^{2D}}{p_1}, \quad (10)$$

where

$$n_1 = N_c^{3D} \exp\left(-\frac{\Delta E_c - \varepsilon_n^{QW}}{T}\right), \qquad p_1 = N_v^{3D} \exp\left(-\frac{\Delta E_v - \varepsilon_p^{QW}}{T}\right), \quad (11)$$

and $N_{c,v}^{3D} = 2[m_{c,v}^{OCL} T/(2\pi\hbar^2)]^{3/2}$ are the 3D effective densities of states in the conduction and valence bands in the OCL, $m_{c,v}^{OCL}$ are the electron and hole effective masses in the OCL, $\Delta E_{c,v}$ are the conduction and valence band offsets at the heterointerface of the QW and OCL, and ε_n^{QW} (ε_p^{QW}) is the energy of the lower (upper) edge of the electron (hole) subband in the QW.

The velocities $v_{n,capt,0}$ and $v_{p,capt,0}$ of electron and hole capture from the OCL into an empty QW are the characteristics of the QW; they thus depend on the QW width and depth, i.e., on the material compositions of the QW and surrounding layers. The capture velocity can be significantly different in different laser structures. In [12], we determined the value of the electron capture velocity in the laser structure similar to the one used here as an example for our calculations (see below).

The total capture velocities $v_{n,capt}$ and $v_{p,capt}$, which take into account filling of the QW by electrons and holes, are defined as [11]

$$v_{n,\,capt} = v_{n,\,capt,\,0}(1 - f_n), \qquad v_{p,\,capt} = v_{p,\,capt,\,0}(1 - f_p). \tag{12}$$

The other key components of our model are:

(i) The capture of carriers from the OCL into the QW is non-instantaneous, which is formally accounted for by finite (i.e., not infinitely high) values of the velocities of electron and hole capture from the OCL into the QW, $v_{n,capt,0}$ and $v_{p,capt,0}$ [11-15].

(ii) We use the condition of global charge neutrality in the laser structure that is the condition of equality of the total electron charge of the OCL and QW to the total hole charge of the OCL and QW [8, 16-18],

$$e\,(N_{QW}\,n^{QW} + bn^{OCL}) = e\,(N_{QW}\,p^{QW} + bp^{OCL}). \tag{13}$$

As seen from (13), $n^{QW} \neq p^{QW}$, i.e., the local neutrality is violated in a QW in the general case. In [2-5, 19], local charge neutrality was assumed in quantum dots for the case of quantum dot lasers.

Because of (i), the free electron and hole densities in the OCL, n^{OCL} and p^{OCL}, are not pinned in the lasing mode, i.e., they are functions of the injection current [11, 13-15].

Due to (ii), i.e., violation of local neutrality in the QW, the 2D electron and hole densities in the QW, n^{QW} and p^{QW}, are also not pinned in the lasing mode [20, 21].

As a result of pump-current-dependence of the carrier densities, so becomes the internal loss coefficient α_{int}. This in turn leads to the roll-over of the light-current characteristic (LCC) at high currents (i.e., decreasing optical power with increasing injection current) and, under certain conditions, appearance of the second branch in it [2-5, 8, 16, 19].

3. DISCUSSION OF LASER CHARACTERISTICS

We consider the laser structure with a single compressive-strained InGaAs QW of width 30 Å. The QW is shifted from the centre of the OCL. The lasing wavelength is 0.9813 μm. Highly-efficient high-power diode lasers emitting at this wavelength are used for pumping fiber lasers [22]. The OCL material is GaAs and the thickness is 0.9 μm. The material of the cladding layers is AlGaAs. The cavity length is 1.5 mm and the stripe width is 100 μm. The velocities of electron and hole capture from the OCL into an empty QW are $v_{n,capt,0} = v_{p,capt,0} = 10^6$ cm/s. The cross sections of internal optical loss due to absorption of light by free electrons and holes in the OCL are $\sigma_n^{OCL} = 3 \times 10^{-18}\,\text{cm}^2$ and $\sigma_p^{OCL} = 10^{-17}\,\text{cm}^2$.

We calculate the laser characteristics as functions of the injection current density at four values of the temperature: 125, 150, 300, and 350 K. As seen from (a) in Figs. 2-6, the characteristics have only one branch at T = 125 K. The second branch emerges at the temperature slightly below 150 K. It is still hardly seen at 150 K [(b) in Figs. 2-6] but well established at considerably higher temperatures [dashed curves, (c, d) in Figs. 2-6]. The current density at which the second branch emerges is termed the second threshold current density $j_{th,\,2}$.

There is a fascinating feature in the dependences of n^{OCL}, p^{OCL}, and α_{int} on j. These quantities increase in their first branches (the increase is faster at a higher T) but they (as well as n^{QW} and p^{QW} – see Fig. 2) decrease in the second branches. The two branches merge together at the maximum operating current density j_{max} beyond which the lasing quenches.

Fig. 2 shows the 2D electron and hole densities in the QW against the injection current density. At the second threshold current density $j_{th,\,2}$, the 2D electron and hole densities in the QW in their second branches are considerably higher than those in the first branches [Fig. 2(c, d)]. This is especially strongly manifested for holes.

At a given injection current density, as we go from (a) to (d) in Fig. 2, i.e., as the temperature increases, the electron and hole densities in the QW increase.

As also seen from Fig. 2, the 2D electron and hole densities in the QW are different ($n^{QW} \neq p^{QW}$). The difference between n^{QW} and p^{QW} is actually large, i.e., local neutrality is significantly violated in the QW.

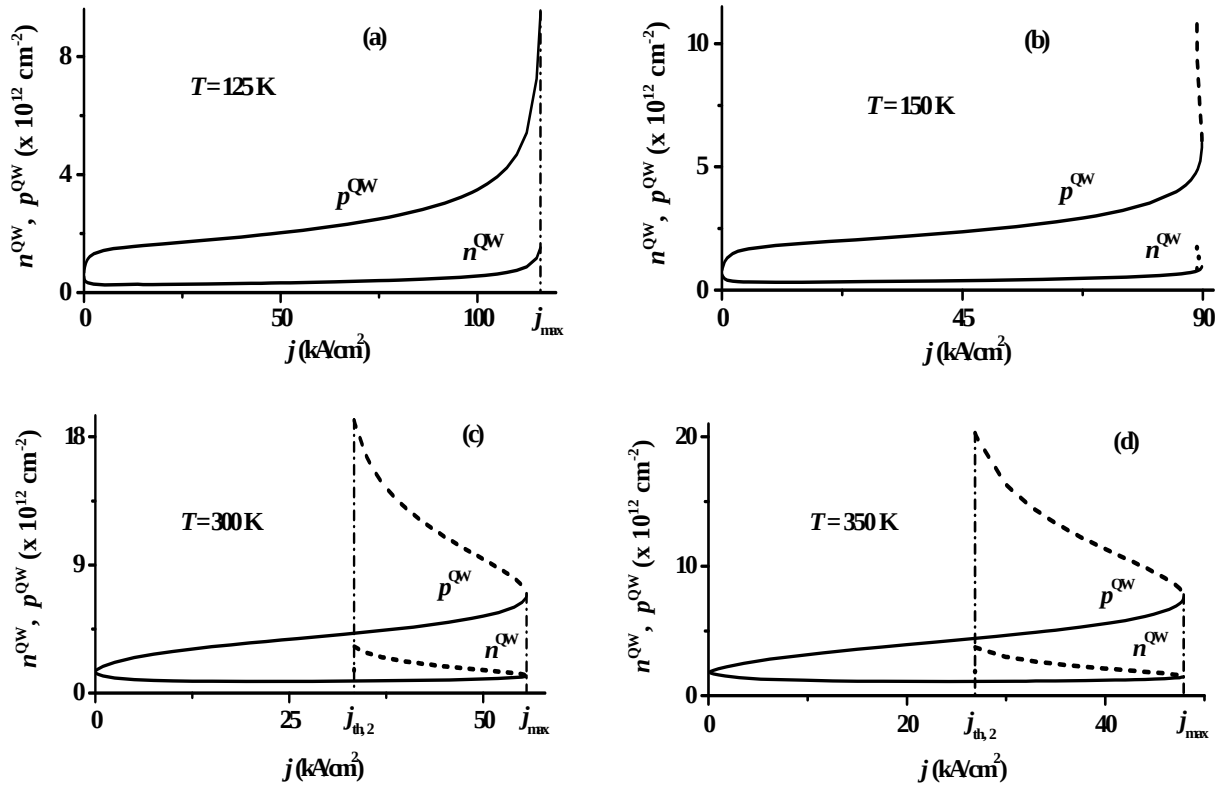

Fig. 2. 2D electron and hole densities in the QW vs. injection current density at different temperatures. The second branches are shown by the dashed curves.

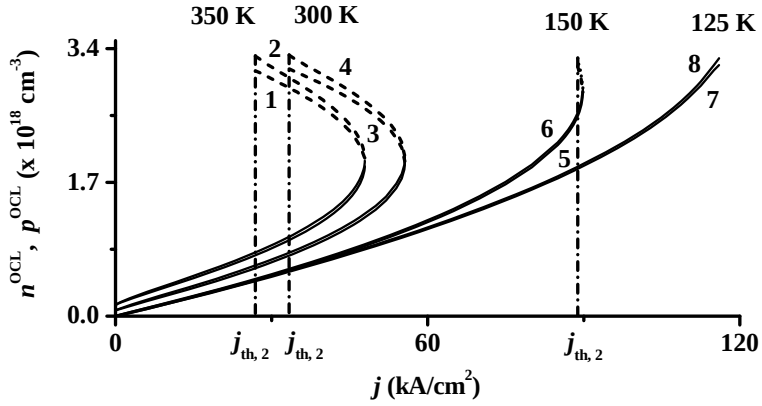

Fig. 3. Free electron and hole densities in the OCL vs. injection current density at different temperatures. The second branches are shown by the dashed curves. 1, 3, 5, 7 – holes, 2, 4, 6, 8 – electrons.

Fig. 3 shows the free electron and hole densities in the OCL against the injection current density. Similarly to n^{QW} and p^{QW}, at $j = j_{th,2}$, the free electron and hole densities in the OCL in their second branches are considerably higher than those in the first branches [Fig. 3(c, d)].

In contrast to n^{QW} and p^{QW}, the difference between the free electron and hole densities in the OCL is insignificant: n^{OCL} and p^{OCL} practically coincide in their first branches in the entire range of the current density; the differnce between n^{OCL} and p^{OCL} in the second branches becomes somewhat noticable at high temperatures only [Fig. 3(c, d)].

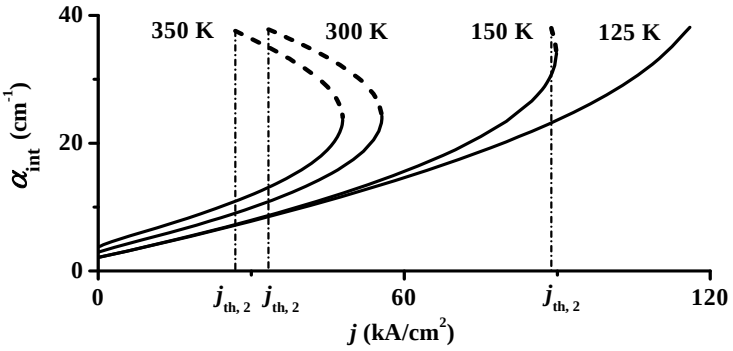

Fig. 4. Internal optical loss vs. injection current density at different temperatures. The second branches are shown by the dashed curves.

Fig. 4 shows the internal optical loss against the injection current density. As seen from (9) and Figs. 3 and 4, the dependence of α_{int} on j mainly reproduces those of the free electron and hole densities in the OCL (due to the fact that the optical confinement factor in the QW is much smaller than in the OCL, the contribution of light absorption by electrons and holes in the QW is negligible compared to that in the OCL).

As expected and shown in Figs. 3 and 4, at a given pump current, n^{OCL}, p^{OCL}, and α_{int} increase with temperature.

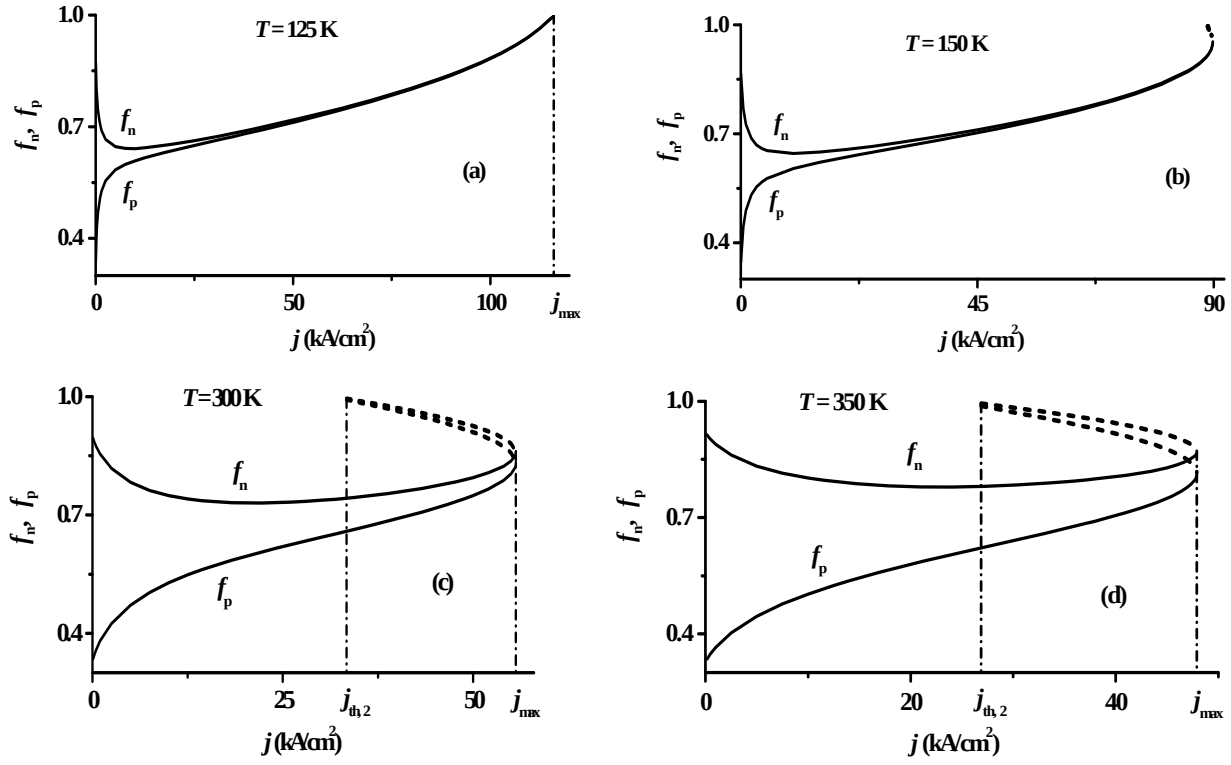

Fig. 5. Occupancies of the states corresponding to the bottom of the electron and the top of the hole quantum-confinement subbands in the QW vs. injection current density at different temperatures.

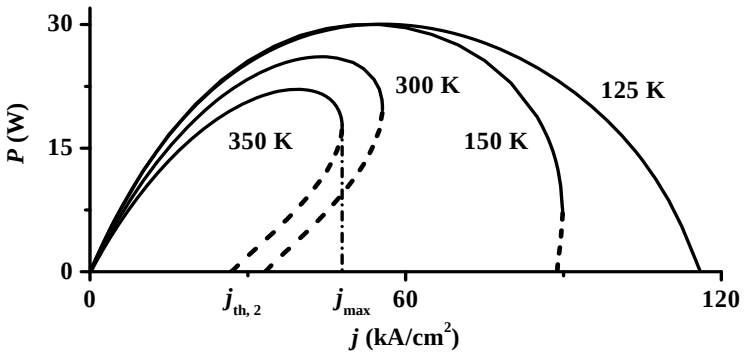

Fig. 6. Light-current characteristic at different temperatures.

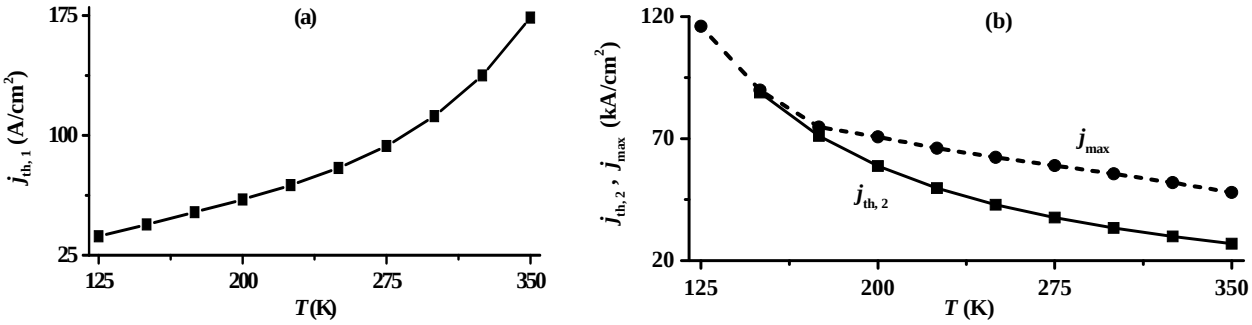

Fig. 7. First (a) and second (b) threshold current densities and maximum operating current density (b) versus temperature.

The maximum value of α_{int} [i.e., $\alpha_{int}(j_{th,2})$] is approximately the same at all temperatures (Fig. 4) and is given by

$$\alpha_{int}^{max} \approx g^{max} - \beta . \tag{14}$$

For the QW laser structure considered here, $g^{max} = 46$ cm^{-1} and $\beta = 7.6$ cm^{-1}.

Eq. (14) can be easily obtained from the lasing condition at the steady state which is the condition of equality of the modal gain to the total loss [2-5, 8, 16],

$$g^{max}(f_n + f_p - 1) = \beta + \alpha_{int} . \tag{15}$$

As the other characteristics (Figs. 2-4), the occupancies f_n and f_p of the states corresponding to the bottom of the electron and the top of the hole quantum-confinement subbands in the QW have two branches (Fig. 5). As seen from Figs. 2-4 (and also Fig. 5 that explicitly shows the second threshold current density), $j_{th,2}$ is very high in the entire temperature range. At such high $j_{th,2}$, the electron and hole subbands in the QW are almost completely filled, i.e., the occupancies f_n and f_p in their second branches are close to their maximum value: $f_{n,p} \approx 1$ (see Fig. 5). Hence the modal gain is close to its maximum value g^{max} and we obtain (14) from (15).

The occupancies f_n and f_p remain very close to each other and high in the entire second branches (i.e., for the pump current density ranging from $j_{th,2}$ to j_{max}) for temperatures up to 300 K [Fig. 5(c)]. In the first branches, the difference between f_n and f_p (being maximum at the threshold current density for the first branch $j_{th,1}$) decreases with increasing pump current; for temperatures up to 150 K and for $j > 30$ kA/cm^2, f_n and f_p almost coincide [Figs. 5(a, b)].

Fig. 6 shows the light-current characteristic (the output optical power against the injection current density). At a given pump current, the output power decreases with increasing temperature. The decrease is due to the increase of n^{OCL}, p^{OCL}, and α_{int} with increasing T.

Fig. 7 shows the first and second threshold current densities, $j_{th,1}$ and $j_{th,2,}$ and the maximum operating current density j_{max} versus temperature. In contrast to the first (conventional) lasing threshold, which increases with increasing T [Fig. 7(a)], the threshold for emerging the second branch decreases [Fig. 7(b)]. Naturally, the maximum operating current decreases with temperature [Fig. 7(b)].

4. CONCLUSION

The temperature behavior of operating characteristics in semiconductor lasers with a quantum-confined active region has been studied with a proper account for (i) non-instantaneous capture of charge carriers from the waveguide region into the active region and (ii) internal optical loss that depends on the carrier densities. Because of (i), the carrier densities are not pinned in the lasing mode, i.e., they are functions of the injection current. In view of (ii) and as a result of pump-current-dependence of the carrier densities, so becomes the internal loss coefficient. This in turn leads to the roll-over of the light-current characteristic at high currents (i.e., decreasing optical power with increasing injection current) and, under certain conditions, appearance of the second branch in it. The laser characteristics have been shown to transform qualitatively with varying temperature: they are conventional, i.e., consist of one branch, at low temperatures but they have two branches, i.e., are of a binary nature, at high temperatures. The two branches merge together at the maximum operating current beyond which the lasing quenches. In contrast to the first (conventional) lasing threshold, the threshold for emerging the second branch decreases with increasing temperature. The pump-current-dependence of the carrier densities and internal loss coefficient is also fascinating: these quantities decrease with increasing current in their second branches.

ACKNOWLEDGEMENTS

Z.N.S., N.A.P., S.O.S. acknowledge the Russian Science Foundation (Grant No. 19-79-30072) and L.V.A. acknowledges the U.S. Army Research Office (Grant No. W911NF-17-1-0432) for support of this work.

REFERENCES

[1] Zh. I. Alferov, "Nobel Lecture: The double heterostructure concept and its applications in physics, electronics, and technology," *Rev. Mod. Phys.* **73**, 767 (2001).

[2] L. V. Asryan and S. Luryi, "Two lasing thresholds in semiconductor lasers with a quantum-confined active region," *Appl. Phys. Lett.* **83**, 5368 (2003).

[3] L. V. Asryan and S. Luryi, "Effect of internal optical loss on threshold characteristics of semiconductor lasers with a quantum-confined active region," *IEEE J. Quantum Electron.* **40**, 833 (2004).

[4] L. V. Asryan, "Maximum power of quantum dot laser versus internal loss," *Appl. Phys. Lett.* **88**, Art. no. 073107 (2006).

[5] L. V. Asryan, Unpublished.

[6] L. V. Asryan and R. A. Suris, "Inhomogeneous line broadening and the threshold current density of a semiconductor quantum dot laser," *Semicond. Sci. Technol.* **11**, 554 (1996).

[7] L. V. Asryan, "Spontaneous radiative recombination and nonradiative Auger recombination in quantum-confined heterostructures," *Quantum Electron.* **35**, 1117 (2005).

[8] Z. N. Sokolova, N. A. Pikhtin, and L. V. Asryan, "Evolution of light-current characteristic shape in high-power semiconductor quantum well lasers," *Electron. Lett.* **55**, 550 (2019).

[9] K. J. Vahala and C. E. Zah, "Effect of doping on the optical gain and the spontaneous noise enhancement factor in quantum well amplifiers and lasers studied by simple analytical expressions," *Appl. Phys. Lett.* **52**, 1945 (1988).

[10] D.-S. Han and L. V. Asryan, "Output power of a double tunneling-injection quantum dot laser," *Nanotechnology* **21**, 015201 (2010).

[11] L. V. Asryan and Z. N. Sokolova, "Optical power of semiconductor lasers with a low-dimensional active region," *J. Appl. Phys.* **115**, 023107 (2014).

[12] Z. N. Sokolova, K. V. Bakhvalov, A. V. Lyutetskiy, N. A. Pikhtin, I. S. Tarasov, and L. V. Asryan, "Method for determination of capture velocity of charge carriers into a quantum well in a semiconductor laser," *Electron. Lett.* **51**, 780 (2015).

[13] L. V. Asryan, S. Luryi, and R. A. Suris, "Intrinsic nonlinearity of the light-current characteristic of semiconductor lasers with a quantum-confined active region," *Appl. Phys. Lett.* **81**, 2154 (2002).

[14] L. V. Asryan, S. Luryi, and R. A. Suris, "Internal efficiency of semiconductor lasers with a quantum-confined active region," *IEEE J. Quantum Electron.* **39**, 404 (2003).

[15] Z. N. Sokolova, I. S. Tarasov, and L. V. Asryan, "Capture of charge carriers and output power of a quantum well laser semiconductors," *Semiconductors* **45**, 1494 (2011).

[16] Z. N. Sokolova, N. A. Pikhtin, and L. V. Asryan, "Two-valued characteristics in semiconductor quantum well lasers," *J. Lightw. Technol.* **36**, 2295 (2018).

[17] Z. N. Sokolova, N. A. Pikhtin, I. S. Tarasov, and L. V. Asryan, "Theory of operating characteristics of a semiconductor quantum well laser: Inclusion of global electroneutrality in the structure," *J. Phys. Conf. Ser.* **740**, Art. no. 012002 (2016).

[18] Z. N. Sokolova, N. A. Pikhtin, I. S. Tarasov, and L. V. Asryan, "Threshold characteristics of a semiconductor quantum-well laser: Inclusion of global electroneutrality in the structure," *Quantum Electron*. **46**, 777 (2016).

[19] L. V. Asryan, "Theoretical investigation of factors controlling the operating characteristics of quantum dot lasers: A review," *J. Nanophoton*. **3**, Art. no. 031601 (2009).

[20] Z. N. Sokolova, D. A. Veselov, N. A. Pikhtin, I. S. Tarasov, and L. V. Asryan, "Increase in the internal optical loss with increasing pump current and the output power of quantum well lasers," *Semicond.* **51**, 959 (2017).

[21] L. V. Asryan, F. I. Zubov, Yu. S. Balezina (Polubavkina), E. I. Moiseev, M. E. Muretova, N. V. Kryzhanovskaya, M. V. Maximov, and A. E. Zhukov, "Violation of local electroneutrality in the quantum well of a semiconductor laser with asymmetric barrier layers," *Semicond.* **52**, 1621 (2018).

[22] V. Gapontsev, N. Moshegov, I. Berezin, A. Komissarov, P. Trubenko, D. Miftakhutdinov, I. Berishev, V. Chuyanov, O. Raisky, and A. Ovtchinnikov, "Highly-efficient high-power pumps for fiber lasers," *Proc. SPIE* **10086**, Art. no. 1008604 (2017).

Optimizing the Quantum Dot Lasers for High-Speed Operation: Novel Versus Conventional Designs

Levon V. Asryan
Virginia Polytechnic Institute and State University, Blacksburg, VA 24061, USA
asryan@vt.edu

Abstract: Direct modulation bandwidth and optimum dc current maximizing it are discussed for double tunneling-injection quantum dot (QD) lasers and QD lasers with asymmetric barrier layers and compared to those for conventional QD lasers.

The dynamic properties of novel and conventional semiconductor quantum dot (QD) lasers are reviewed. In particular, the maximum modulation bandwidth and the optimum dc current maximizing it are discussed and compared for these lasers.

In conventional semiconductor lasers, the charge carriers first appear in the optical confinement layer (OCL) on their way to the low-dimensional active region. The electrons and holes are not spatially separated in the OCL and hence can easily recombine with each other therein. This unwanted electron-hole recombination in the OCL is the main contributor to the temperature dependence of the threshold current in diode lasers [1–3]. In addition, there is a certain delay in the carrier capture from the bulk OCL into the quantum-confined active region. As a result of this delay, the electron and hole densities in the OCL, and hence the parasitic electron-hole recombination rate, do not remain fixed after the lasing starts – they grow with increasing pumping. This leads to sublinearity of the light-current characteristic (LCC) of the laser and limits its useful output optical power [4–6].

To suppress the recombination outside the quantum-confined active region, two design approaches were proposed. One of the approaches [7–13] exploits double tunneling-injection (DTI), i.e., tunneling injection of both electrons and holes into the active region from two separate quantum wells (QWs). In a DTI laser, the quantum-confined active region, located in the central part of the OCL, is clad on each side by a thin barrier and a QW. Electrons and holes are injected into the active region by tunneling from the corresponding QWs. Ideally, there should be no second tunneling step, i.e. out-tunneling from the active region into the 'foreign' QWs (electron-injecting QW for holes and hole-injecting QW for electrons).

The other approach [8, 9] is based on independent tailoring of the conduction and valence bandedges by means of the use of two asymmetric barrier layers (ABLs) – one on each side of the active region. The ABL in the electron-injecting side of the structure should ideally prevent holes from entering that side while not hindering the electron-injection into the active region. The ABL in the hole-injecting side should prevent electrons from entering that side while not hindering the hole-injection into the active region. A laser utilizing ABLs was termed a bandedge-engineered laser [8, 9, 14] or an ABL laser [15–17].

In both DTI and ABL lasers, there will ideally be no electrons (holes) in the hole- (electron-) injecting side of the structure, i.e., the bipolar population will be suppressed outside the active region.

Elimination of parasitic recombination would allow to attain close-to-ideal static operating characteristics in DTI and ABL lasers, namely, virtually temperature-insensitive threshold current, close-to-one internal quantum efficiency, and linear LCC.

The dynamic characteristics are also improved in DTI and ABL lasers as compared to conventional lasers [18–21]. Modulation bandwidth is an important parameter describing the speed with which the optical output of diode lasers is varied with altering the input injection current [18]. For the conventional, DTI, and ABL QD lasers, Fig. 1 shows the modulation bandwidth as a function of the dc component of the injection current. Except for the barriers (in the DTI and ABL structures) and injector-QWs (in the DTI structure), the structures are otherwise similar. As seen from the figure, the modulation bandwidth has a maximum at a certain optimum value of the dc component of the injection current. As also seen from the figure, the maximum bandwidth is the same in all the three structures. The point is that the maximum bandwidth is merely controlled by the photon lifetime in the cavity, which is the same in all the three structures as the cavity length is chosen to be the same. However, the optimum dc injection current is considerably different in the structures – it is highest in the conventional laser, noticeably lower in the DTI laser, and significantly lower in the ABL laser. The physics behind this is as follows: in contrast to the maximum modulation bandwidth that is not affected by the differential gain, the optimum current does depend on the differential gain – it decreases with increasing differential gain. Due to the fact that each type of carriers is only present on side of the DTI and ABL lasers, the differential gain is higher there as compared to that in the

conventional laser. Furthermore, the differential gain is higher in the ABL laser as compared to that in the DTI laser as there are no QWs and hence no extra carriers therein in the ABL laser.

In conclusion, it is discussed that the optimum dc current that maximizes the modulation bandwidth is lower in the DTI QD laser as compared to that in the conventional QD laser, and even significantly lower in the ABL QD laser. Hence, while the maximum modulation bandwidth is more easily attainable in the DTI laser as compared to the conventional laser, it is most easily attainable in the ABL laser out of the three lasers considered.

This work was supported by the US Army Research Office under Grant No. W911NF-17-1-0432.

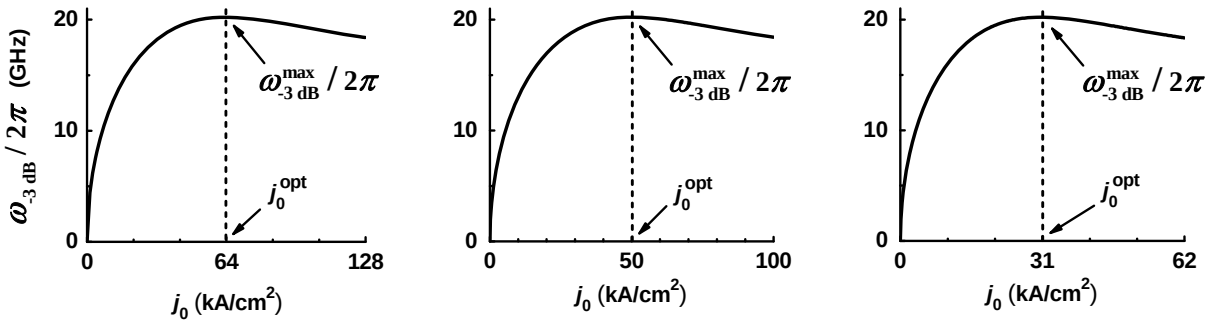

Fig. 1. Modulation bandwidth vs. dc component of injection current density in QD lasers of different designs: (a) conventional, (b) DTI, and (c) ABL.

[1] L. V. Asryan and R. A. Suris, "Inhomogeneous line broadening and the threshold current density of a semiconductor quantum dot laser," *Semicond. Sci. Technol.* **11**, 554-567 (1996).
[2] L. V. Asryan and R. A. Suris, "Spatial hole burning and multimode generation threshold in quantum-dot lasers," *Appl. Phys. Lett.* **74**, 1215-1217 (1999).
[3] L. Jiang and L. V. Asryan, "Excited-state-mediated capture of carriers into the ground state and the saturation of optical power in quantum-dot lasers," *IEEE Photon. Technol. Lett.* **18**, 2611-2613 (2006).
[4] L. V. Asryan, S. Luryi, and R. A. Suris, "Intrinsic nonlinearity of the light-current characteristic of semiconductor lasers with a quantum-confined active region," *Appl. Phys. Lett.* **81**, 2154-2156 (2002).
[5] L. V. Asryan, S. Luryi, and R. A. Suris, "Internal efficiency of semiconductor lasers with a quantum-confined active region," *IEEE J. Quantum Electron.* **39**, 404-418 (2003).
[6] L. V. Asryan and Z. N. Sokolova, "Optical power of semiconductor lasers with a low-dimensional active region," *J. Appl. Phys.* **115**, 023107 (2014).
[7] L. V. Asryan and S. Luryi, "Tunneling-injection quantum-dot laser: Ultrahigh temperature stability," *IEEE J. Quantum Electron.* **37**, 905-910 (2001).
[8] L. V. Asryan and S. Luryi, "Temperature-insensitive semiconductor quantum dot laser," *Solid-State Electron.* **47**, 205-212 (2003).
[9] L. V. Asryan and S. Luryi, "Semiconductor laser with reduced temperature sensitivity," *U.S. Patent 6 870 178 B2*, Mar. 22, 2005.
[10] D.-S. Han and L. V. Asryan, "Tunneling-injection of electrons and holes into quantum dots: A tool for high-power lasing," *Appl. Phys. Lett.* **92**, 251113 (2008).
[11] D.-S. Han and L. V. Asryan, "Characteristic temperature of a tunneling-injection quantum dot laser: Effect of out-tunneling from quantum dots," *Solid-State Electron.* **52**, 1674-1679 (2008).
[12] D.-S. Han and L. V. Asryan, "Effect of the wetting layer on the output power of a double tunneling-injection quantum-dot laser," *J. Lightw. Technol.* **27**, 5775-5782 (2009).
[13] D.-S. Han and L. V. Asryan, "Output power of a double tunneling-injection quantum dot laser," *Nanotechnology* **21**, 015201 (2010).
[14] L. V. Asryan, N. V. Kryzhanovskaya, M. V. Maximov, A. Yu. Egorov, and A. E. Zhukov, "Bandedge-engineered quantum well laser," *Semicond. Sci. Technol.* **26**, 055025 (2011).
[15] A. E. Zhukov, N. V. Kryzhanovskaya, F. I. Zubov, Y. M. Shernyakov, M. V. Maximov, E. S. Semenova, K. Yvind, and L. V. Asryan, "Improvement of temperature-stability in a quantum well laser with asymmetric barrier layers," *Appl. Phys. Lett.* **100**, 021107 (2012).
[16] L. V. Asryan, N. V. Kryzhanovskaya, M. V. Maximov, F. I. Zubov, and A. E. Zhukov, "Light-current characteristic of a quantum well laser with asymmetric barrier layers," *J. Appl. Phys.* **114**, 143103 (2013).
[17] L. V. Asryan, "Quantum dot lasers with asymmetric barrier layers: Close-to-ideal threshold and power characteristics," *Quantum Electron.* **49**, 522-528, (2019).
[18] L. V. Asryan and R. A. Suris, "Upper limit for the modulation bandwidth of a quantum dot laser," *Appl. Phys. Lett.* **96**, 221112 (2010).
[19] L. V. Asryan, "Modulation bandwidth of a double tunnelling-injection quantum dot laser," *Semicond. Sci. Technol.* **30**, 035022 (2015).
[20] L. V. Asryan, "Effect of pumping delay on the modulation bandwidth in double tunneling-injection quantum dot lasers," *Opt. Lett.* **42**, 97-100 (2017).
[21] L. V. Asryan and S. Kar, "Modulation bandwidth of double tunneling-injection quantum dot lasers: Effect of out-tunneling leakage," *IEEE J. Quantum Electron.* **55**, 2000109 (2019).

Excited states and optical power of ground-state emission in quantum dot lasers with asymmetric barrier layers

Levon V. Asryan and John L. Monk
Virginia Polytechnic Institute and State University, Blacksburg, VA 24061, USA
asryan@vt.edu

Abstract: Continuous-wave power of ground-state emission in quantum dot lasers with asymmetric barrier layers is studied. Unlike conventional lasers, the power is virtually unaffected by excited-to-ground state relaxation delay of carriers in quantum dots.

Semiconductor lasers present an important component for various applications ranging from telecommunication to medical uses. Conventional semiconductor lasers with a low-dimensional active region [Fig. 1(a)] suffer from parasitic electron-hole recombination that occurs in the optical confinement layer (OCL) [1-4]. To suppress this recombination outside the laser active region, two alternative approaches were proposed [5-12] – one based on double tunneling-injection (injection of both electrons and holes) into the quantum-confined active region and the other using asymmetric barrier layers (ABLs).

Here we discuss the optical output of quantum dot (QD) lasers with ABLs. In such lasers, the active layer with QDs is clad on each side by a thin barrier layer [Fig. 1(b)]. The barrier layers are designed in such a way that they prevent from building up bipolar carrier (i.e., both electron and hole) population in the OCL. As a result of this, the parasitic electron-hole recombination in the OCL is suppressed in ABL QD lasers.

As in conventional QD lasers [13], the QDs in ABL lasers may contain excited states in addition to the ground state. In this work, the optical power of ground-state emission in ABL QD lasers is studied in the presence of excited states in QDs. The most dramatic situation is considered in which the charge carriers injected into the OCL are not directly captured into the lasing ground state in QDs – they are first captured from the OCL into the excited state in QDs and then they relax from the excited state to the ground state [Fig. 1(b)].

The rate equations model is used for the layered structures shown in Fig. 1. The electron and hole populations in the OCL, excited-state and ground-state in QDs, and the optical power are calculated as a function of the injection current.

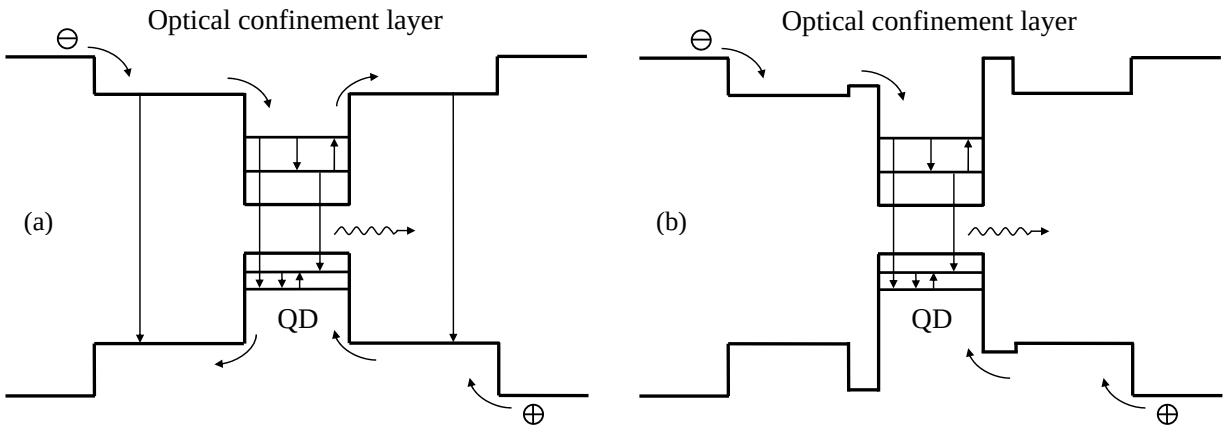

Fig. 1. Schematic energy band diagrams: (a) conventional QD laser, (b) ABL QD laser.

Fig. 2 shows the power of ground-state emission against the injection current density in (a) conventional and (b) ABL QD lasers. As seen from Fig. 2(a), the output power saturates with pumping in the conventional laser [the dashed line in (a) shows the saturation value]. The saturation is due to the combination of two effects – relaxation delay of charge carriers from the excited- to ground-state in QDs and parasitic electron-hole recombination in the OCL. As opposed to conventional QD lasers, the power of ground-state emission continues to increase with increasing injection current in the ABL laser. As the other advantages of ABL lasers, this advantage for

continuous-wave high-power lasing of ABL QD lasers over the conventional QD lasers is due to efficient suppression of unwanted electron-hole recombination in the OCL in ABL QD lasers. Indeed, in this case, even in the presence of excited-to-ground state relaxation delay in QDs, a built up of carrier population of one type only may occur in each side of the structure – electrons in the left- and holes in the right-hand side in Fig. 2(b).

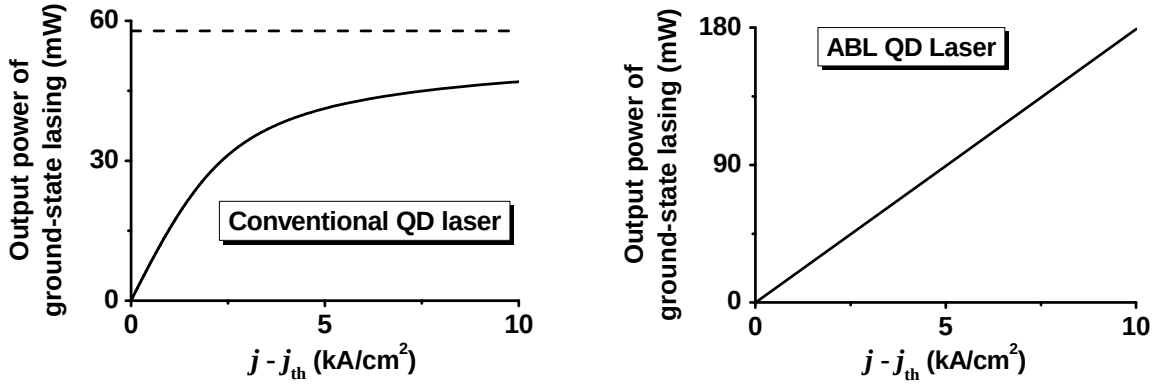

Fig. 2. Optical power of ground-state emission vs. excess of injection current density over threshold current density: (a) conventional QD laser, (b) ABL QD laser. The horizontal dashed line in (a) shows the saturation value of the power for ground-state emission in the reference conventional QD laser. The reference structure lasing near 1.55 μm is considered [13, 14].

In conclusion, it is shown that, even in the most dramatic situation of indirect capture of charge carriers into the lasing ground state and unlike the conventional QD lasers, the continuous-wave power of ground-state emission in ABL QD lasers does not saturate with increasing pump current – instead, it increases almost linearly with injection current. This advantage for high-power lasing of ABL QD lasers over the conventional QD lasers is due to efficient suppression of unwanted electron-hole recombination in the OCL in ABL QD lasers.

This work was supported by the US Army Research Office under Grant No. W911NF-17-1-0432.

[1] L. V. Asryan and R. A. Suris, "Inhomogeneous line broadening and the threshold current density of a semiconductor quantum dot laser," *Semicond. Sci. Technol.* **11**, 554-567 (1996).
[2] L. V. Asryan, S. Luryi, and R. A. Suris, "Intrinsic nonlinearity of the light-current characteristic of semiconductor lasers with a quantum-confined active region," *Appl. Phys. Lett.* **81**, 2154-2156 (2002).
[3] L. V. Asryan, S. Luryi, and R. A. Suris, "Internal efficiency of semiconductor lasers with a quantum-confined active region," *IEEE J. Quantum Electron.* **39**, 404-418 (2003).
[4] L. V. Asryan and Z. N. Sokolova, "Optical power of semiconductor lasers with a low-dimensional active region," *J. Appl. Phys.* **115**, 023107 (2014).
[5] L. V. Asryan and S. Luryi, "Tunneling-injection quantum-dot laser: Ultrahigh temperature stability," *IEEE J. Quantum Electron.* **37**, 905-910 (2001).
[6] L. V. Asryan and S. Luryi, "Temperature-insensitive semiconductor quantum dot laser," *Solid-State Electron.* **47**, 205-212 (2003).
[7] L. V. Asryan and S. Luryi, "Semiconductor laser with reduced temperature sensitivity," *U.S. Patent 6 870 178 B2*, Mar. 22, 2005.
[8] D.-S. Han and L. V. Asryan, "Tunneling-injection of electrons and holes into quantum dots: A tool for high-power lasing," *Appl. Phys. Lett.* **92**, 251113 (2008).
[9] D.-S. Han and L. V. Asryan, "Characteristic temperature of a tunneling-injection quantum dot laser: Effect of out-tunneling from quantum dots," *Solid-State Electron.* **52**, 1674-1679 (2008).
[10] D.-S. Han and L. V. Asryan, "Effect of the wetting layer on the output power of a double tunneling-injection quantum-dot laser," *J. Lightw. Technol.* **27**, 5775-5782 (2009).
[11] D.-S. Han and L. V. Asryan, "Output power of a double tunneling-injection quantum dot laser," *Nanotechnology* **21**, 015201 (2010).
[12] L. V. Asryan, "Quantum dot lasers with asymmetric barrier layers: Close-to-ideal threshold and power characteristics," *Quantum Electron.* **49**, 522-528, (2019).
[13] L. Jiang and L. V. Asryan, "Excited-state-mediated capture of carriers into the ground state and the saturation of optical power in quantum-dot lasers," *IEEE Photon. Technol. Lett.* **18**, 2611-2613 (2006).
[14] L. V. Asryan and R. A. Suris, "Spatial hole burning and multimode generation threshold in quantum-dot lasers," *Appl. Phys. Lett.* **74**, 1215-1217 (1999).

Internal optical loss and light-current characteristic in injection lasers

Zinaida N Sokolova[1], Nikita A Pikhtin[1], Sergey O Slipchenko[1] and Levon V Asryan[2]

[1] Ioffe Institute, St. Petersburg, 194021, Russia
[2] Virginia Polytechnic Institute and State University, Blacksburg, VA 24061, USA

asryan@vt.edu

Abstract. Possibility of tailoring the light-current characteristic (LCC) shape in quantum dot (QD) lasers by varying uniformity of QDs is discussed. Making the QD ensemble less uniform results in roll-over in the LCC. The second branch in the LCC appears with making the QD ensemble even less uniform.

1. Introduction

Internal optical loss that is inherent in semiconductor lasers combines different processes of unwanted photon loss as opposed to mirror loss – on purpose output of photons through the cavity mirrors. While the mirror loss presents the useful optical output from semiconductor lasers, the internal loss is undesired as it consumes the photons emitted during the laser action.

In this paper, the effect of uniformity of quantum dots (QDs) on the light-current characteristic (LCC) in QD lasers is discussed in the presence of internal optical loss. While diode lasers have been extensively studied both experimentally and theoretically before (see, e.g., a review article [1]), a new interesting feature has been however predicted in [2]-[4]: in the presence of internal optical loss that depends on the charge carrier density, roll-over of the LCC can occur. The more so, the second branch can appear in the LCC in addition to the first 'conventional' branch. Here we discuss the possibility of tailoring the LCC shape in QD lasers in the presence of internal optical loss by varying uniformity of QDs.

2. Theoretical model

Our theoretical analysis is based on rate equations that describe the dynamics of charge carries and photons in the laser. In the simplest case, we use a set of three equations – two for carriers [free carriers in the optical confinement layer (OCL) and confined carriers in QDs] and one for photons.

The equations for carriers are

$$b\frac{\partial n_{\mathrm{OCL}}}{\partial t} = \frac{j}{e} + N_{\mathrm{S}}\frac{f_{\mathrm{n}}}{\tau_{\mathrm{esc}}} - \mathrm{v}_{\mathrm{capt},0}(1-f_{\mathrm{n}})\,n_{\mathrm{OCL}} - bB_{\mathrm{3D}}n_{\mathrm{OCL}}^2, \tag{1}$$

$$N_{\mathrm{S}}\frac{\partial f_{\mathrm{n}}}{\partial t} = \mathrm{v}_{\mathrm{capt},0}(1-f_{\mathrm{n}})\,n_{\mathrm{OCL}} - N_{\mathrm{S}}\frac{f_{\mathrm{n}}}{\tau_{\mathrm{esc}}} - N_{\mathrm{S}}\frac{f_{\mathrm{n}}^2}{\tau_{\mathrm{QD}}} - c_{\mathrm{g}}\,g^{\max}(2f_{\mathrm{n}}-1)n_{\mathrm{ph}}. \tag{2}$$

Table 1. Physical quantities entering in eqs. (1)-(3).

Notation	Meaning
n_{OCL}	Free carrier density in the OCL
f_{n}	Occupancy of the energy level in a QD by a charge carrier
n_{ph}	Density of emitted photons (per unit area of the laser heterointerface)
j	Injection current density
e	Electron charge
N_{S}	Surface density of QDs
τ_{esc}	Thermal escape time of charge carriers from an individual QD to the OCL
$\mathrm{v}_{\mathrm{capt},0}$	Velocity of carrier capture into an unoccupied (at $f_{\mathrm{n}} = 0$) QD ensemble (in cm/s)
b	Thickness of the OCL
B_{3D}	Spontaneous radiative recombination constant for the bulk (OCL) region (in cm^3/s)
τ_{QD}	Spontaneous radiative lifetime in a QD
c_{g}	Group velocity of light
$g^{\max}$	Maximum modal gain (cm^{-1})
β	Mirror loss coefficient (in cm^{-1})
α_{int}	Internal optical loss coefficient (in cm^{-1})

The equation for photons is

$$\frac{\partial n_{\mathrm{ph}}}{\partial t} = c_{\mathrm{g}} g^{\max} (2 f_{\mathrm{n}} - 1) n_{\mathrm{ph}} - c_{\mathrm{g}} (\beta + \alpha_{\mathrm{int}}) n_{\mathrm{ph}} . \tag{3}$$

The parameters entering in eqs. (1)-(3) are described in table 1.

The internal optical loss coefficient in (3) is presented as

$$\alpha_{\mathrm{int}} = \alpha_0 + \sigma_{\mathrm{int}} n_{\mathrm{OCL}} , \tag{4}$$

where α_0 is its constant component and σ_{int} is its the cross-section.

Solving the set of eqs. (1)-(3) at the steady-state, we then find the emitted optical power as follows:

$$P = \hbar\omega \, c_{\mathrm{g}} \beta \, S n_{\mathrm{ph}} , \tag{5}$$

where $\hbar\omega$ is the emitted photon energy and S is the cross-section area of the laser heterointerface.

Calculations show that in the presence of internal optical loss that depends on the charge carrier density in the OCL [eq. (4)], roll-over of the LCC can occur at high pump currents and the second branch can appear in the LCC in addition to the conventional branch.

The second branch appears in the LCC if the following condition satisfies:

$$\frac{\sigma_{\mathrm{int}} \mathrm{v}_{\mathrm{capt},0}}{2 b B_{\mathrm{3D}} g^{\max}} > 1 . \tag{6}$$

Varying each of the parameters entering in (6) can result in single-to-double branch transformation of the LCC. In [4], the cross-section of internal optical loss σ_{int} was varied in QD lasers; in [5], the thickness of the OCL b was varied in quantum well (QW) lasers; in [6], the capture velocity $\mathrm{v}_{\mathrm{capt},0}$ was varied in QW lasers; and in [7], the temperature was varied in QW lasers (the spontaneous radiative

recombination constant B_{3D} entering in (6) is a function of temperature – see [8, 9]). In all these cases, the transformation of the LCC shape from single-to-double branch was shown to occur.

Here, we discuss the transformation of the LCC shape in QD lasers as the QD uniformity is changed.

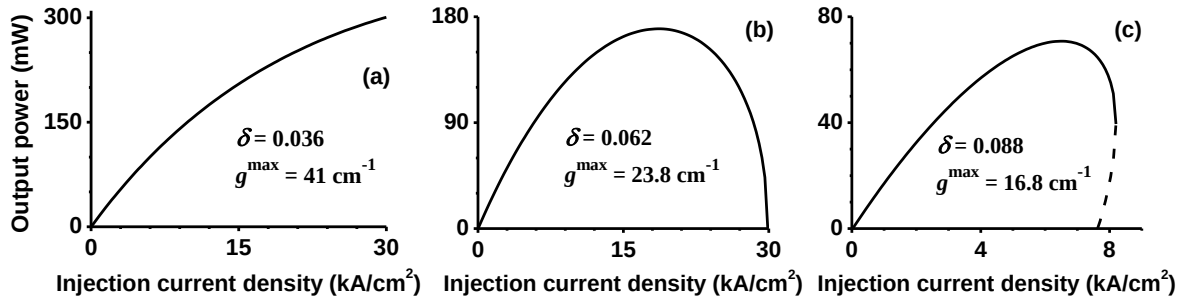

Figure 1. LCC of the QD laser for different values of the RMS of relative QD-size fluctuations δ. The corresponding values of the modal gain g^{max} are also presented. InGaAsP-based structure emitting near 1.55 μm is considered [11, 13]. The internal loss cross-section $\sigma_{int} = 2 \times 10^{-18}$ cm^2, and the constant component of the internal loss $\alpha_0 = 2$ cm^{-1}.

3. Effect of uniformity of QDs on the LCC shape

Self-assembled QDs are never identical in laser structures – they are primarily different in their sizes. The QD-size dispersion causes fluctuations in the quantized energy levels and leads to broadening in the optical transition energy (inhomogeneous line broadening [8]). Due to nonuniformity of QDs the maximum gain of the laser decreases [8], threshold current increases [8] and becomes more sensitive to temperature (the characteristic temperature decreases) [10], multimode generation threshold decreases [11], internal differential efficiency and output power both decrease [12].

Denoting δ the root mean square (RMS) of relative QD-size fluctuations, the maximum modal gain of a QD laser can be presented as follows [8]:

$$g^{max} \propto \frac{1}{\delta}. \tag{7}$$

As seen from (7), g^{max} decreases with increasing δ. Hence it follows from (6) and (7) that the condition for appearing the second branch in the LCC should become satisfied with increasing RMS of QD-size fluctuations, i.e., making the QD ensemble less uniform.

As shown in figure 1(a), at small fluctuations in QD sizes [the case of high modal gain – see (7)], the output power increases with the pump current over the entire range of interest.

At larger fluctuations in QD sizes, the slope efficiency changes from positive to negative with increasing pump current [figure 1(b)]; the output power goes continuously to zero, which marks the stop of lasing. In what follows, such a shape of the LCC is referred to as a 'conventional' roll-over to distinguish from the case of strongly nonuniform QDs.

With further increasing RMS of relative QD-size fluctuations up to a certain value, the LCC retains a conventional roll-over shape. Above that value of the RMS, the LCC transforms qualitatively [figure 1(c)]. The stop of lasing with increasing injection current occurs now at a nonvanishing output power: at the maximum operating current, the conventional branch of the LCC (solid portion of the curve) is detached from the X-axis. This upper branch of the LCC is now continued by the second, lower, branch (dashed portion of the curve); in general, with reducing the pump current the output power can follow either the upper (conventional) or lower branch. Experimental observation of the

quenching of lasing at a nonvanishing output power in diode lasers can suggest the presence of carrier-density-dependent internal loss and, in the case of QD lasers, large QD-size dispersion.

4. Conclusions

Possibility of tailoring the LCC shape in QD lasers by varying uniformity of QDs has been discussed. Making the QD ensemble less uniform has been shown to result in roll-over in the LCC. The second branch in the LCC has been shown to appear with making the QD ensemble even less uniform.

Acknowledgments

Z.N.S., N.A.P., and S.O.S. thank the federal program of the Ioffe Institute, and L.V.A. thanks the U.S. Army Research Office (Grant No. W911NF-17-1-0432) for support of this work.

References

[1] Alferov Zh I 2001 Nobel Lecture: The double heterostructure concept and its applications in physics, electronics, and technology *Rev. Mod. Phys.* **73** 767-82

[2] Asryan L V and Luryi S 2003 Two lasing thresholds in semiconductor lasers with a quantum-confined active region *Appl. Phys. Lett.* **83** 5368-70

[3] Asryan L V and Luryi S 2004 Effect of internal optical loss on threshold characteristics of semiconductor lasers with a quantum-confined active region *IEEE J. Quantum Electron.* **40** 833-43

[4] Asryan L V 2006 Maximum power of quantum dot laser versus internal loss *Appl. Phys. Lett.* **88** 073107

[5] Sokolova Z N, Pikhtin N A and Asryan L V 2018 Two-valued characteristics in semiconductor quantum well lasers *J. Lightw. Technol.* **36** 2295-300

[6] Sokolova Z N, Pikhtin N A and Asryan L V 2019 Evolution of light-current characteristic shape in high-power semiconductor quantum well lasers *Electron. Lett.* **55** 550-2

[7] Sokolova Z N, Pikhtin N A, Slipchenko S O and Asryan L V 2020 Temperature-induced single-to-double branch transformation of operating characteristics in semiconductor lasers with a low-dimensional active region *Proc. SPIE* **11301** 113010D

[8] Asryan L V and Suris R A 1996 Inhomogeneous line broadening and the threshold current density of a semiconductor quantum dot laser *Semicond. Sci. Technol.* **11** 554-67

[9] Asryan L V 2005 Spontaneous radiative recombination and nonradiative Auger recombination in quantum-confined heterostructures *Quantum Electron.* **35** 1117-20

[10] Asryan L V and Suris R A 1997 Characteristic temperature of quantum dot laser *Electron. Lett.* **33** 1871-2

[11] Asryan L V and Suris R A 1999 Spatial hole burning and multimode generation threshold in quantum-dot lasers *Appl. Phys. Lett.* **74** 1215-7

[12] Asryan L V, Luryi S and Suris R A 2002 Intrinsic nonlinearity of the light-current characteristic of semiconductor lasers with a quantum-confined active region *Appl. Phys. Lett.* **81** 2154-6

[13] Jiang L and Asryan L V 2006 Excited-state-mediated capture of carriers into the ground state and the saturation of optical power in quantum-dot lasers *IEEE Photon. Technol. Lett.* **18** 2611-3

Design of blocking layers for suppression of parasitic recombination in high-power diode lasers with GaAs waveguide

M.E. Muretova [1], *F.I. Zubov* [1, 2], *L.V. Asryan* [3], *M.V. Maximov* [1, 2], *A.E. Zhukov* [2, 1]

[1] Alferov University, 194021 St. Petersburg, Russia

[2] National Research University Higher School of Economics, 190008 St. Petersburg, Russia

[3] Virginia Polytechnic Institute and State University, Blacksburg, Virginia 24061, USA

Using numerical simulations, a search is carried out for designs of asymmetric barrier layers (ABLs) for a laser diode having GaAs waveguide and emitting at the wavelength $\lambda = 980$ nm. A pair of ABLs, adjoining the active region on both sides, blocks undesired charge carrier flows and suppresses parasitic spontaneous recombination in the waveguide layers. Optimal designs of single ABLs based on AlGaAsSb and GaInP for blocking electrons and holes, respectively, are proposed, which make it possible to reduce the parasitic recombination current down to less than 1% of the initial value. To suppress electron transport, an alternative structure based on three identical AlInAs barriers is also proposed. GaAsP spacers of different thicknesses form unmatched spectra of size quantization levels between barriers thus blocking the hopping conduction channel: the parasitic electron flow is reduced by several tens of times in comparison with the case of spacers of equal thickness.

Keywords: semiconductor lasers, asymmetric barrier layers, parasitic waveguide recombination

Operating characteristics of semiconductor quantum well lasers as functions of the waveguide region thickness

Z.N. Sokolova[1], *N.A. Pikhtin*[1], *S.O. Slipchenko*[1], *L.V. Asryan*[2]

[1] Ioffe Institute,
194021 St. Petersburg, Russia
[2] Virginia Polytechnic Institute and State University,
Blacksburg, VA 24061, USA

Abstract Operating characteristics of semiconductor quantum well (QW) lasers are theoretically studied in terms of the thickness of the waveguide region (optical confinement layer, OCL). We calculate the maximum modal gain, optical confinement factor (in QW, OCL, and cladding layers), threshold current density, electron and hole densities (in QW and OCL), internal optical loss (in QW, OCL, and cladding layers), internal differential quantum efficiency, stimulated and spontaneous recombination currents, and output optical power of the laser as functions of the OCL thickness. It is shown that up to the pump current density 50 kA/cm^2 the output power of the considered lasers depends only slightly on the OCL thickness in the range of thicknesses 1.5−2.8 μm. This result is important for designing high brightness lasers as broadened waveguides are used in such lasers to attain low beam divergence. At high pump current densities, the output power is shown to have a maximum as a function of the OCL thickness.

Two-Valued Characteristics in Semiconductor Quantum Well Lasers

Zinaida N. Sokolova, Nikita A. Pikhtin, *Member, IEEE*, and Levon V. Asryan, *Senior Member, IEEE*

***Abstract*—Due to internal optical absorption loss, which varies with carrier density in the optical confinement region, the operating characteristics can be two valued in semiconductor quantum well lasers. Particularly, there can be two lasing thresholds and two branches in the light–current characteristic. While the internal differential quantum efficiency for the first (conventional) branch of the light–current characteristic is less than 1 and decreases with increasing pump current, that for the second (unconventional) branch is greater than 1 and nonmonotonous.**

***Index Terms*—Quantum well laser, semiconductor laser.**

I. Introduction

INTERNAL optical loss is among the key factors affecting the operating characteristics of semiconductor lasers [1]–[15]. An interesting peculiarity in such lasers was theoretically studied in [16]–[20]—under certain conditions and due to internal loss, which varies with carrier density in the optical confinement layer (OCL), the second lasing threshold can exist in addition to the first (conventional) threshold. Above the second threshold, the laser characteristics become degenerated, namely, two-valued. In particular, the second, 'unconventional', branch appears in the dependence of the output optical power on the pump current (light-current characteristic—LCC) in addition to the conventional (first) branch. With increasing pump current and approaching a certain value (which is the maximum operating current), the two branches of the LCC merge together. At the merging point, the optical power is non-vanishing; immediately beyond this point, the lasing quenches. Possibility of existing of such two-valued, lobe-shape, LCC, presents considerable interest from the viewpoints of both fundamental physics and practical applications of semiconductor lasers with a quantum-confined active region.

While a general approach was developed in [16]–[20], which applies to the effects of carrier-density-dependent internal loss in semiconductor lasers with a quantum-confined active region of any dimensionality, detailed calculations were performed there for quantum dot lasers only. In this work, we study two-valued characteristics for the particular case of semiconductor quantum well (QW) lasers. In contrast to [16]–[20], wherein local charge neutrality was assumed to hold separately in the quantum-confined active region and in the OCL, we use here the condition of charge neutrality, which includes the charge of carriers both in the OCL and quantum-confined active region [21]–[23].

Manuscript received October 21, 2017; revised January 3, 2018; accepted February 12, 2018. Date of publication February 16, 2018; date of current version March 21, 2018. This work was supported in part by the Federal Program of Ioffe Institute and in part by the U.S. Army Research Office under Grant W911NF-17-1-0432. *(Corresponding author: Levon V. Asryan.)*

Z. N. Sokolova and N. A. Pikhtin are with Ioffe Institute, St. Petersburg 194021, Russia (e-mail: zina.sokolova@mail.ioffe.ru; nike@hpld.ioffe.ru).

L. V. Asryan is with the Virginia Polytechnic Institute and State University, Blacksburg, VA 24061, USA (e-mail: asryan@vt.edu).

Digital Object Identifier 10.1109/JLT.2018.2806942

II. Theoretical Model

Our theoretical model for the operating characteristics of QW lasers is based on a set of five rate equations in terms of the following unknowns: the three-dimensional (3D) densities of free electrons and holes in the OCL, n^{OCL} and p^{OCL}, the two-dimensional (2D) densities of electrons and holes confined in each QW, n^{QW} and p^{QW}, and the number of photons *N* in the lasing mode.

We use here the condition of charge neutrality in the form of equality of the total electron charge in the OCL and QWs to that of holes [21],

$$e\,(N_{\mathrm{QW}}\,n^{\mathrm{QW}} + bn^{\mathrm{OCL}}) = e\,(N_{\mathrm{QW}}\,p^{\mathrm{QW}} + bp^{\mathrm{OCL}}) \qquad (1)$$

where N_{QW} is the number of QWs, *b* is the thickness of the OCL, and *e* is the electron charge.

We use a set of rate equations presented in [21] and [24]. In [21] and [24], constant internal optical loss was assumed. A critical element of the theoretical model in this paper is the carrier-density-dependent internal loss in the OCL. We present the internal optical absorption loss coefficient as

$$\alpha_{\mathrm{int}}(j) = \alpha_0 + \sigma_{\mathrm{n,int}} n^{\mathrm{OCL}}(j) + \sigma_{\mathrm{p,int}} p^{\mathrm{OCL}}(j) \qquad (2)$$

where α_0 is the constant component, $\sigma_{\mathrm{n,int}}$ and $\sigma_{\mathrm{p,int}}$ are the cross sections of internal loss due to optical absorption by free electrons and holes in the OCL, and *j* is the injection current density. The internal optical loss in the QWs, which depends on the 2D carrier densities there, is included into the constant component α_0. This is because the 2D carrier densities in the QWs are considerably lower than the 3D carrier densities in the OCL (see below). Free carrier absorption loss in the cladding layers and intervalence band absorption loss [25] are also included into the constant component α_0.

Due to the fact that carrier capture from the OCL into the QWs is noninstantaneous, the free carrier densities in the OCL, n^{OCL} and p^{OCL}, are not pinned after the onset of lasing–they depend on the injection current density *j* [26]. Hence, as seen from (2), the internal loss coefficient α_{int} is also injection-current-dependent (see also [27]). The capture of electrons and holes from the OCL into an empty (unoccupied) QW is described

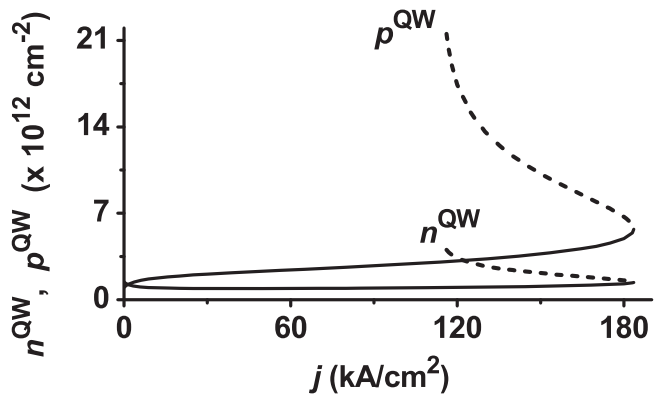

Fig. 1. 2D electron and hole densities in the QW against injection current density. In Figs. 1–8, the first (conventional) branch is shown by the solid curve and the second (unconventional) branch by the dashed curve. In Figs. 1–5, and 8, the OCL thickness $b = 0.8$ μm.

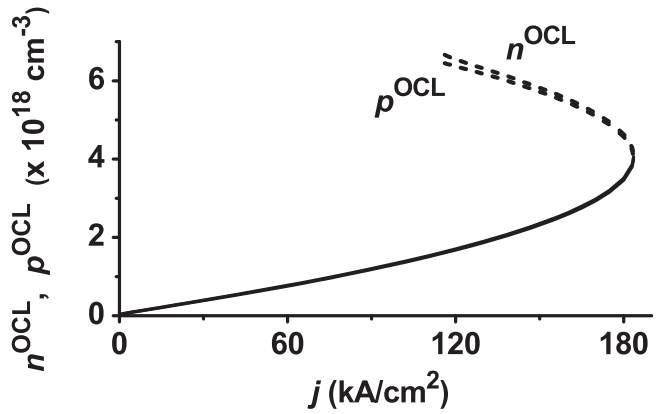

Fig. 2. 3D electron and hole densities in the OCL against injection current density.

by the capture velocities (measured in units of cm/s) $\mathrm{v_{n,capt,0}}$ and $\mathrm{v_{p,capt,0}}$. The capture velocities, being dependent on the size and material composition of the QW and surrounding layers, can considerably vary in different laser structures. In [28] and [29], a combined experimental-theoretical method for determination of the capture velocities was described and the capture velocities were determined for a specific QW laser structure emitting at 1.063 μm.

III. Discussion of Laser Characteristics

We consider here the laser structure emitting at 1.01 μm and containing a single 50 Å-wide strained InGaAs QW; the materials of the OCL and cladding layers are GaAs and AlGaAs, respectively. The following parameters are used in the calculations: the Fabry-Perot cavity length is $L = 0.15$ cm; the electron and hole capture velocities into an empty QW are $\mathrm{v_{n,capt,0}} = 2 \times 10^6$ cm/s and $\mathrm{v_{p,capt,0}} = 10^6$ cm/s, respectively; the internal loss cross sections due to optical absorption by electrons and holes in the OCL are $\sigma_{\mathrm{n,int}} = 3 \times 10^{-18}\,\mathrm{cm}^2$ and $\sigma_{\mathrm{p,int}} = 10^{-17}\,\mathrm{cm}^2$; the doping concentrations in the n- and p-cladding layers are $5 \times 10^{17}\,\mathrm{cm}^{-3}$ and $3.5 \times 10^{18}\,\mathrm{cm}^{-3}$; the constant component of the internal loss coefficient is $\alpha_0 = 2\,\mathrm{cm}^{-1}$. The OCL thickness $b = 0.8\,\mu\mathrm{m}$ is used in the calculations. The LCC and the internal differential quantum efficiency are also calculated for $b = 0.5$ and 0.2 μm.

Solving the set of rate equations at the steady-state, we obtain the electron and hole densities in the QW and OCL and the number of photons N in the lasing mode as functions of the injection current density j. We then calculate the output optical power [30], [31],

$$P(j) = \hbar\omega\, c_{\mathrm{g}} \beta\, N(j) \tag{3}$$

where ω is the angular frequency of the lasing emission, c_{g} is the group velocity of light, $\beta = (1/L)\,\ln(1/R)$ is the mirror loss coefficient, and R is the mirror reflectivity.

We find that under certain conditions and due to internal optical loss, which varies with electron and hole densities in the OCL, the second lasing threshold can exist in addition to the first (conventional) threshold. Above the second threshold, the set of rate equations has two solutions, i.e., all the laser characteristics become degenerated, namely, two-valued. In particular, the second, unconventional, branch appears in the dependence of the output optical power on the pump current (LCC) in addition to the conventional branch. With increasing pump current and approaching a certain value (which is the maximum operating current), the two branches of the LCC merge together. At the merging point, the optical power is non-vanishing; immediately beyond this point, the lasing quenches.

In [19], assuming that local charge neutrality holds separately in the quantum-confined active region and in the OCL, closed-form solutions were obtained from the steady-state rate equations and the following analytical criterion for the emergence of the second branch of the LCC was derived:

$$\frac{\sigma_{\mathrm{int}} \mathrm{v_{capt,0}}}{2b\, B^{\mathrm{OCL}} g^{\max}} > 1 \tag{4}$$

where B^{OCL} is the spontaneous radiative recombination constant for the bulk (OCL) region measured in units of cm^3/s (see [32] for the expression for B^{OCL}) and $g^{\max}$ is the maximum value of the modal gain in the active region (per single layer with quantum dots, single layer with quantum wires, or single QW). In the specific QW laser structure considered here, $g^{\max} = 89.7\ \mathrm{cm}^{-1}$ [33].

In this work, we use a more general approach, which is based on exploiting the charge neutrality condition in the form of eq. (1). With this condition, no closed-form solutions of the set of rate equations can be obtained and no analytical criterion for the emergence of the second branch of the LCC can be derived. However, the findings of [19] expressed by inequality (4) hold true also here: the internal loss cross-section and the capture velocity should be high enough and/or the OCL thickness and the maximum modal gain should be low for the second branch of the LCC to appear.

Fig. 1 shows the 2D electron and hole densities in the QW against the injection current density j. As seen from the figure, the character of the dependence of the carrier density on j in the second (unconventional) branch is opposite to that in the first (conventional) branch. While the electron and hole densities increase with j in the first branch, they decrease in the second branch. Also, as seen from the figure, the decrease of the hole density with j in the second branch is substantial. In

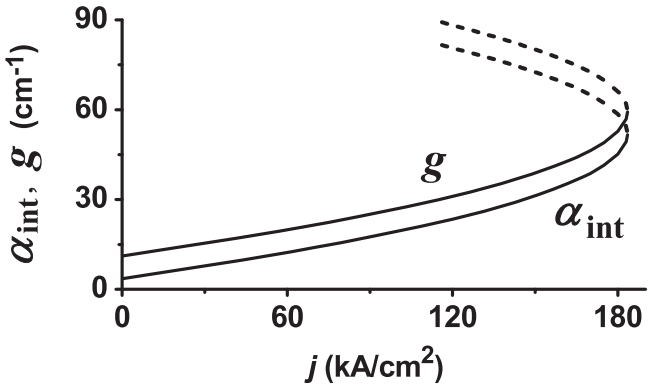

Fig. 3. Gain and internal optical absorption loss against injection current density.

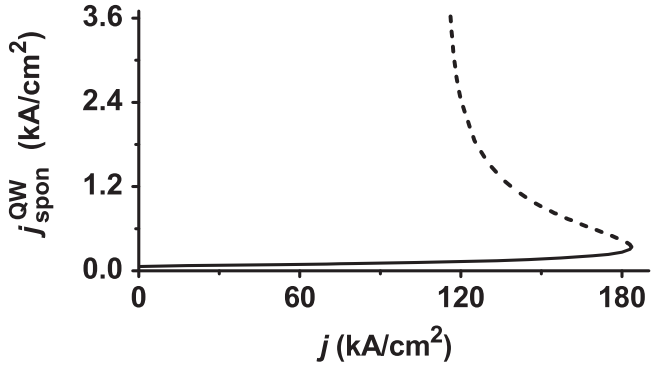

Fig. 4. Spontaneous radiative recombination current density in the QW against injection current density.

both branches (except for the initial portions in the first branch near the first lasing threshold), the hole density in the QW is considerably higher than the electron density. At the second lasing threshold, the hole-to-electron density ratio is 3.1 in the first branch and 5.3 in the second. At the maximum operating current (beyond which the lasing quenches in both branches), the hole-to-electron density ratio is 4.1. Hence, as seen from Fig. 1 and the above numbers, there is no local charge neutrality in the QW.

In contrast to the 2D electron and hole densities in the QW, the free electron and hole densities in the OCL are close to each other in both the first and second branches for the entire range of injection current values (see Fig. 2). This is because the densities of each type of carriers in the OCL are considerably higher than the densities of each type of carriers in the QWs, i.e.,

$$bn^{\mathrm{OCL}}, bp^{\mathrm{OCL}} >> N_{\mathrm{QW}} n^{\mathrm{QW}}, N_{\mathrm{QW}} p^{\mathrm{QW}}. \tag{5}$$

Hence, to maintain the charge neutrality condition (1), n^{OCL} and p^{OCL} should be close to each other. Similarly to the QW, while the carrier densities in the OCL increase with j in the first branch, they decrease in the second branch. The relative variation is, however, greater in the first branch – the carrier densities increase by a factor of 120 on going from the first lasing threshold to the lasing quenching point; the carrier densities in the second branch decrease by a factor of 1.6 only on going from the second lasing threshold to the lasing quenching point. As seen from Fig. 2, above the second lasing threshold, the free carrier densities in the OCL (especially in the second branch) are significantly high.

With the calculated dependences of the carrier densities in the OCL on j, we can easily obtain such dependences of the internal loss [see eq. (2)] and modal gain (both shown in Fig. 3). For the modal gain of a QW laser, we use [24]

$$g(j) = N_{\mathrm{QW}}\, g^{\max}[f_{\mathrm{n}}(j) + f_{\mathrm{p}}(j) - 1] \tag{6}$$

where f_{n} and f_{p} are the occupancies of the electron and hole subband edges in the QW, which are related to the 2D-carrier densities in the QW as follows [16], [17], [34]:

$$f_{\mathrm{n}} = 1 - \exp\left(-\frac{n^{\mathrm{QW}}}{N_{\mathrm{c}}^{\mathrm{2D}}}\right),\ f_{\mathrm{p}} = 1 - \exp\left(-\frac{p^{\mathrm{QW}}}{N_{\mathrm{v}}^{\mathrm{2D}}}\right) \tag{7}$$

where $N_{\mathrm{c,v}}^{\mathrm{2D}} = m_{\mathrm{c,v}}^{\mathrm{QW}} T/(\pi\hbar^2)$ are the 2D effective densities of states in the conduction and valence bands in the QW, $m_{\mathrm{c,v}}^{\mathrm{QW}}$ are the electron and hole effective masses in the QW, and the temperature T is measured in units of energy.

The modal gain and the internal loss are related to each other by the lasing condition,

$$g(j) = \alpha_{\mathrm{int}}(j) + \beta. \tag{8}$$

As seen from (8) and Fig. 3, since the mirror loss β does not depend on the injection current, the dependences of g and α_{int} reproduce each other – the curve for g is obtained from that for α_{int} by simply shifting up the latter along the vertical axis by the value equal to the mirror loss β; in the laser structure considered here, $\beta = 7.6\,\mathrm{cm}^{-1}$. Since the dependences of n^{OCL} and p^{OCL} on j have two branches, $g(j)$ and $\alpha_{\mathrm{int}}(j)$ also consist of two branches, which correspond to two solutions of the steady-state set of rate equations.

As seen from Fig. 3, both the internal loss and gain change substantially with j. In the first branch, α_{int} and g increase from 3.5 to 51.9 cm^{-1} and from 11.1 to 59.5 cm^{-1}, respectively, on going from the first lasing threshold (63 A/cm^2) to the lasing quenching point ($j_{\max} = 183.5$ kA/cm^2). In the second branch, α_{int} and g decrease from 81.6 to 51.9 cm^{-1} and from 89.2 to 59.5 cm^{-1}, respectively, on going from the second lasing threshold (116 kA/cm^2) to the lasing quenching point ($j_{\max} = 183.5$ kA/cm^2). At the lasing quenching point, both branches of α_{int} merge together (at this point, $\alpha_{\mathrm{int}} = 51.9$ cm^{-1}) and so do the two branches of g (at this point, $g = 59.5$ cm^{-1}).

Fig. 4 shows the current density of spontaneous radiative recombination in the QWs,

$$j_{\mathrm{spon}}^{\mathrm{QW}}(j) = eN_{\mathrm{QW}} B^{\mathrm{QW}} n^{\mathrm{QW}}(j) p^{\mathrm{QW}}(j) \tag{9}$$

against the injection current density. In (9), B^{QW} is the spontaneous radiative recombination constant for the 2D region (QW), which is measured in units of cm^2/s – see [32] for the expression for B^{QW}. As seen from Fig. 4, $j_{\mathrm{spon}}^{\mathrm{QW}}$ drops considerably in the second branch (from 3.6 to 0.35 kA/cm^2, i.e., by more than an order of magnitude) on going from the second lasing threshold to the lasing quenching point. However, even at the second lasing threshold, $j_{\mathrm{spon}}^{\mathrm{QW}}$ is much lower than the current density of spontaneous radiative recombination in the OCL [see eq. (10) and Fig. 5]. This is due to the fact that the carrier densities in the QW are considerably lower than those in the OCL–see (5).

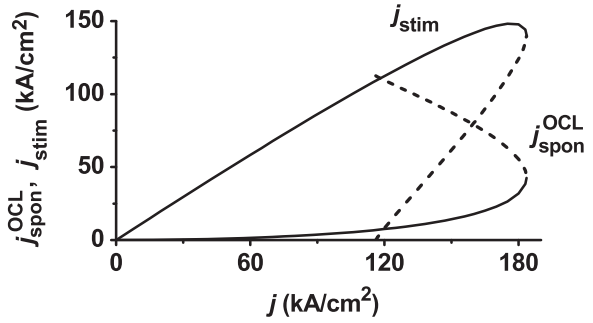

Fig. 5. Spontaneous radiative recombination current density in the OCL and stimulated radiative recombination current density in the QW against injection current density.

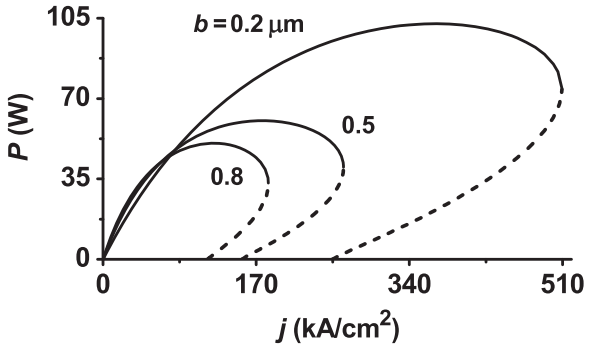

Fig. 6. Light-current characteristics for the structures with the OCL thicknesses $b = 0.2,\ 0.5$, and 0.8 μm.

The current density of spontaneous radiative recombination in the OCL,

$$j_{\rm spon}^{\rm OCL}(j) = ebB^{\rm OCL}n^{\rm OCL}(j)p^{\rm OCL}(j) \tag{10}$$

is shown in Fig. 5 against the injection current density. As seen from the figure, $j_{\rm spon}^{\rm OCL}$ is very high in the second branch – it presents a considerable fraction of the total injection current density.

Fig. 5 also shows the current density of stimulated radiative recombination in the QWs,

$$j_{\rm stim}(j) = \frac{1}{S}e\ c_{\rm g}g(j)N(j) = \frac{1}{S}e\ c_{\rm g}[\alpha_{\rm int}(j)+\beta]N(j) \tag{11}$$

against the injection current density. In (11), $S = WL$ is the cross section of the junction and W is the laser stripe width. As seen from the figure and as expected, in each of two branches, $j_{\rm stim}$ is zero at the corresponding lasing threshold. In the first branch, $j_{\rm stim}$ increases with j and approaches its maximum value; as j further increases and approaches the maximum operating current density, $j_{\rm stim}$ decreases to a non-vanishing value (140 kA/cm^2) – on further increase of j, the lasing quenches. In the second branch, $j_{\rm stim}$ increases monotonously with j. At $j = j_{\rm max}$, the two branches of $j_{\rm stim}$ merge together.

Fig. 6 shows the output optical power of the laser against the injection current density (LCC) for the OCL thicknesses $b = 0.2,\ 0.5$, and 0.8 μm; the corresponding values of the maximum modal gain $g^{\rm max}$ are 125, 115.2, and 89.7 cm^{-1}. As seen from the figure, due to the fact that the set of rate equations has two solutions in the presence of carrier-density-dependent internal loss in the OCL, the LCC has two branches; these two branches

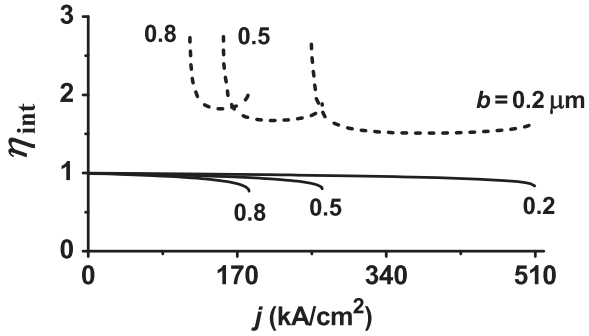

Fig. 7. Internal differential quantum efficiency against injection current density for the structures with the OCL thicknesses $b = 0.2,\ 0.5$, and 0.8 μm.

actually form a lobe-shape LCC. The first (conventional) branch of the LCC is nonmonotonous and the second (unconventional) branch is monotonous.

As seen from Fig. 6, making the OCL thinner increases the maximum optical power, the second lasing threshold, and the maximum operating current at which the lasing quenches.

Fig. 7 shows the internal differential quantum efficiency for the first and second branches of the LCC against the injection current density for three values of the OCL thickness. The internal efficiency (efficiency of stimulated recombination) is defined as [24], [26]

$$\eta_{{\rm int},1,2}(j) = \frac{j_{{\rm stim},1,2}(j)}{j - j_{{\rm th},1,2}} \tag{12}$$

where "1" and "2" in the subscripts denote the first and second branches of the LCC and $j_{{\rm th},1,2}$ are the first and second threshold current densities.

While the two branches of $j_{\rm stim}$ and of the LCC merge together at the maximum operating current density (see Figs. 5 and 6), i.e., $j_{{\rm stim},1}(j_{\rm max}) = j_{{\rm stim},2}(j_{\rm max})$, the curves for the internal efficiency for the two branches do not merge, i.e., $\eta_{{\rm int},1}(j_{\rm max}) \neq \eta_{{\rm int},2}(j_{\rm max})$ (see Fig. 7). This is because the denominators in (12) for the two branches are not the same; namely, since $j_{{\rm th},2} > j_{{\rm th},1}$, the denominator for the second branch is smaller than that for the first branch, $j - j_{{\rm th},2} < j - j_{{\rm th},1}$. Hence, at $j = j_{\rm max}$, when $j_{{\rm stim},1}(j_{\rm max}) = j_{{\rm stim},2}(j_{\rm max})$, the internal efficiency for the second branch is higher than that for the first branch, $\eta_{{\rm int},2}(j_{\rm max}) > \eta_{{\rm int},1}(j_{\rm max})$ (see Fig. 7).

Moreover, as seen from Fig. 7, while the internal efficiency for the first branch is less than 1 and decreases with increasing injection current, the internal efficiency for the second branch is greater than 1 and nonmonotonous. To explain these dependences, let us present the injection and threshold current densities as follows:

$$j = j_{\rm spon} + j_{\rm stim} = j_{\rm spon}^{\rm QW} + j_{\rm spon}^{\rm OCL} + j_{\rm stim} \tag{13}$$

$$j_{\rm th} = j_{\rm spon,th} = j_{\rm spon,th}^{\rm QW} + j_{\rm spon,th}^{\rm OCL} \tag{14}$$

With (12)–(14), we can rewrite the expressions for $\eta_{\rm int}$ for the first and second branches as follows:

$$\eta_{{\rm int},1} = \frac{j_{{\rm stim},1}}{j_{{\rm stim},1} + j_{{\rm spon},1} - j_{{\rm spon,th},1}} = \frac{1}{1 + \frac{j_{{\rm spon},1} - j_{{\rm spon,th},1}}{j_{{\rm stim},1}}} < 1 \tag{15}$$

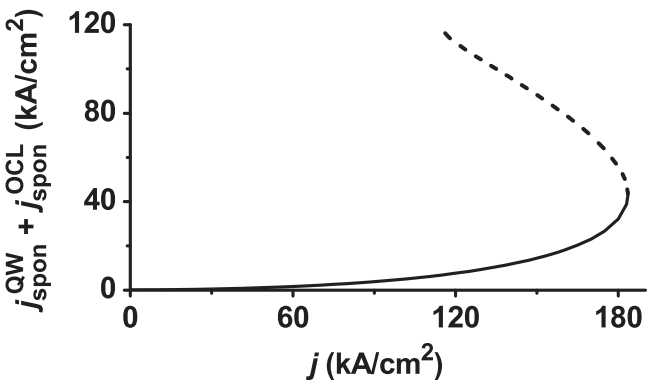

Fig. 8. Total spontaneous radiative recombination current density, $j_{\rm spon}^{\rm QW} + j_{\rm spon}^{\rm OCL}$, against injection current density. In view of (5), $j_{\rm spon}^{\rm QW} + j_{\rm spon}^{\rm OCL}$ is very close to the spontaneous radiative recombination current density in the OCL, $j_{\rm spon}^{\rm OCL}$ (shown in Fig. 5).

$$\eta_{\rm int,2} = \frac{j_{\rm stim,2}}{j_{\rm stim,2} + j_{\rm spon,2} - j_{\rm spon,th,2}} = \frac{1}{1 + \frac{j_{\rm spon,2} - j_{\rm spon,th,2}}{j_{\rm stim,2}}} = \frac{1}{1 - \frac{j_{\rm spon,th,2} - j_{\rm spon,2}}{j_{\rm stim,2}}} > 1. \tag{16}$$

As seen from Fig. 8, the total spontaneous radiative recombination current density (the sum of spontaneous radiative recombination current densities in the QWs and OCL) in the first branch (the solid curve) increases with increasing j, i.e., at any j, it is higher than at the first lasing threshold, $j_{\rm spon,1} > j_{\rm spon,1,th}$ – hence, as seen from (15), the internal efficiency for the first branch is less than 1 (see Fig. 7). The total spontaneous radiative recombination current density in the second branch (the dashed curve) decreases with increasing j, i.e., at any j, it is lower than at the second lasing threshold, $j_{\rm spon,2} < j_{\rm spon,2,th}$ – hence, as seen from (16), the internal efficiency for the second branch is greater than 1 (see Fig. 7).

Since the sum of the total spontaneous radiative recombination current density and the stimulated recombination current density is equal to the total injection current density [see (13)], the superlinearity of $j_{\rm spon,1}(j)$ (the solid curve in Fig. 8) leads to sublinearity of $j_{\rm stim,1}(j)$ (the solid curve for $j_{\rm stim}$ in Fig. 5); the sublinearity of $j_{\rm spon,2}(j)$ (the dashed curve in Fig. 8) leads to superlinearity of $j_{\rm stim,2}(j)$ (the dashed curve for $j_{\rm stim}$ in Fig. 5).

It should be noted that, in this work, to purely focus on the effects of carrier-density-dependent internal optical loss, we do not calculate self-consistently the profiles of the electrostatic field and carrier densities within the OCL. Instead, we assume that the electron and hole densities are constant within the OCL. Equation (1) does not also include the charge of ionized dopants and hence is also not self-consistent electrostatically.

With increasing operating currents (especially in short-cavity devices), the onset of lasing from higher energy states (levels in quantum dots, subbands in QWs, or bands in the bulk OCL) can occur in diode lasers simultaneously with or instead of ground-state lasing (see, e.g., [35] and the references therein). The lasing from these states will however be at a shorter wavelength than that from the ground state in the active region. In contrast to the higher-state lasing, the lasing in the second (unconventional) branch discussed in this work will occur at the same wavelength as that in the first (conventional) branch.

To verify our simulation results, we performed experiments on 100 μm-aperture diode lasers emitting at 1.06 μm. We were able to observe saturation and rollover of the conventional (first) branch of the LCC at ultra high pulse currents (> 100 kA/cm^2). As the pulse duration and repetition rate were low (50 ns /1 kHz) and hence the rollover could not be caused by temperature effects, we suppose that it was due to carrier-density-dependent internal optical loss. To observe the unconventional (second) branch of the LCC and the optical power hopping between the two branches, we plan to do more study and experiments on dynamic characteristics of diode lasers of different heterostructure designs under ultra high pulse currents exceeding the second lasing threshold (with the latter being estimated from our simulations).

IV. Conclusion

We discussed the operating characteristics of semiconductor QW lasers in the presence of internal optical absorption loss, which varies with electron and hole densities in the OCL. Due to such loss, the second lasing threshold can emerge in addition to the conventional (first) threshold. Above the second threshold, the laser characteristics are two-valued. In particular, the second, unconventional, branch appears in the dependence of the output optical power on the pump current (light-current characteristic – LCC) in addition to the conventional branch. With increasing pump current and approaching a certain value (which is the maximum operating current), the two branches of the LCC merge together. At the merging point, the optical power is nonvanishing; immediately beyond this point, the lasing quenches. The characteristics of the laser are different in two branches. Thus, while the internal differential quantum efficiency for the first branch of the LCC is less than 1 and decreases with increasing pump current, that for the second branch is greater than 1 and nonmonotonous. The dependences of other characteristics on the injection current are also different in two branches—e.g., while the electron and hole densities in the OCL increase with increasing current in the first branch, those in the second branch decrease.

The fact that the LCC can be two-valued (lobe-shaped), even though there is no experimental proof for this so far, presents considerable interest from the viewpoints of both fundamental physics and practical applications of semiconductor lasers with a quantum-confined active region. For instance, switching between the two branches of the LCC (assuming that this is feasible) would provide an opportunity for controllable change of the internal quantum efficiency of the laser.

References

[1] P. S. Zory Jr., Ed. *Quantum Well Lasers*. Boston, MA, USA: Academic, 1993.

[2] L. A. Coldren, S. W. Corzine, and M. L. Mašanović, *Diode Lasers and Photonic Integrated Circuits*, 2nd ed. Hoboken, NJ, USA: Wiley, 2012.

[3] M. Asada, A. R. Adams, K. E. Stubkjaer, Y. Suematsu, Y. Itaya, and S. Arai, "The temperature dependence of the threshold current of GaInAsPAnP DH lasers," *IEEE J. Quantum Electron.*, vol. QE-17, no. 5, pp. 611–619, May 1981.

[4] C. H. Henry, R. A. Logan, F. R. Merritt, and J. P. Luongo, "The effect of intervalence band absorption on the thermal behavior of InGaAsP lasers," *IEEE J. Quantum Electron.*, vol. QE-19, no. 6, pp. 947–952, Jun. 1983.
[5] M. Asada, A. Kameyama, and Y. Suematsu, "Gain and intervalence band absorption in quantum-well lasers," *IEEE J. Quantum Electron.*, vol. QE-20, no. 7, pp. 745–753, Jul. 1984.
[6] D. Z. Garbuzov, A. V. Ovchinnikov, N. A. Pikhtin, Z. N. Sokolova, I. S. Tarasov, and V. B. Khalfin, "Experimental and theoretical investigations of singularities of the threshold and power characteristics of InGaAsP/InP separate-confinement double-heterostructure lasers ($\lambda = 1.3$ μm)," *Sov. Phys. Semicond.*, vol. 25, no. 5, pp. 560–564, May 1991.
[7] D. A. Ackerman *et al.*, "Analysis of gain in determining T_0 in 1.3 μm semiconductor lasers," *IEEE J. Sel. Topics Quantum Electron.*, vol. 1, no. 2, pp. 250–263, Jun. 1995.
[8] E. Shtengel and D. A. Ackerman, "Internal optical loss measurements in 1.3 μm InGaAsP lasers," *Electron. Lett.*, vol. 31, no. 14, pp. 1157–1159, Jul. 1995.
[9] S. Seki, H. Oohasi, H. Sugiura, T. Hirono, and K. Yokoyama, "Dominant mechanisms for the temperature sensitivity of 1.3 μm InP-based strained-layer multiple-quantum-well lasers," *Appl. Phys. Lett.*, vol. 67, no. 8, pp. 1054–1056, Aug. 1995.
[10] S. Seki, H. Oohasi, H. Sugiura, T. Hirono, and K. Yokoyama, "Dominant mechanism for limiting the maximum operating temperature of InP-based multiple-quantum-well lasers," *J. Appl. Phys.*, vol. 79, no. 5, pp. 2192–2197, Mar. 1996.
[11] G. L. Belenky *et al.*, "Role of p-doping profile and regrowth on the static characteristics of 1.3 μm MQW InGaAsP-InP lasers: Experiment and modeling," *IEEE J. Quantum Electron.*, vol. 35, no. 10, pp. 1515–1520, Oct. 1999.
[12] A. E. Zhukov, A. R. Kovsh, V. M. Ustinov, and Z. I. Alferov, "Loss multiplication in a quantum dot laser," *Laser Phys.*, vol. 13, no. 3, pp. 319–323, Mar. 2003.
[13] J. J. Lee, L. J. Mawst, and D. Botez, "MOCVD growth of asymmetric 980 nm InGaAs/InGaAsP broad-waveguide diode lasers for high power applications," *J. Cryst. Growth*, vol. 249, nos. 1/2, pp. 100–105, Feb. 2003.
[14] A. R. Kovsh *et al.*, "InAs/InGaAs/GaAs quantum dot lasers of 1.3 μm range with enhanced optical gain," *J. Cryst. Growth*, vol. 251, nos. 1–4, pp. 729–736, Apr. 2003.
[15] N.-H. Kim, J.-H. Park, L. J. Mawst, T. F. Kuech, and M. Kanskar, "Temperature sensitivity of InGaAs quantum-dot lasers grown by MOCVD," *IEEE Photon. Technol. Lett.*, vol. 18, no. 8, pp. 989–991, Apr. 2006.
[16] L. V. Asryan and S. Luryi, "Two lasing thresholds in semiconductor lasers with a quantum-confined active region," *Appl. Phys. Lett.*, vol. 83, no. 26, pp. 5368–5370, Dec. 2003.
[17] L. V. Asryan and S. Luryi, "Effect of internal optical loss on threshold characteristics of semiconductor lasers with a quantum-confined active region," *IEEE J. Quantum Electron.*, vol. 40, no. 7, pp. 833–843, Jul. 2004.
[18] L. V. Asryan, "Maximum power of quantum dot laser versus internal loss," *Appl. Phys. Lett.*, vol. 88, no. 7, Feb. 2006, Paper no. 073107.
[19] L. V. Asryan, Unpublished.
[20] L. V. Asryan, "Theoretical investigation of factors controlling the operating characteristics of quantum dot lasers: A review," *J. Nanophoton.*, vol. 3, Jan. 2009, Paper no. 031601.
[21] Z. N. Sokolova, N. A. Pikhtin, I. S. Tarasov, and L. V. Asryan, "Theory of operating characteristics of a semiconductor quantum well laser: Inclusion of global electroneutrality in the structure," *J. Phys. Conf. Ser.*, vol. 740, Sep. 2016, Paper no. 012002.
[22] Z. N. Sokolova, N. A. Pikhtin, I. S. Tarasov, and L. V. Asryan, "Threshold characteristics of a semiconductor quantum-well laser: Inclusion of global electroneutrality in the structure," *Quantum Electron.*, vol. 46, no. 9, pp. 777–781, Sep. 2016.
[23] Z. N. Sokolova, D. A. Veselov, N. A. Pikhtin, I. S. Tarasov, and L. V. Asryan, "Increase in the internal optical loss with increasing pump current and the output power of quantum well lasers," *Semiconductors*, vol. 51, no. 7, pp. 959–964, Jul. 2017.
[24] L. V. Asryan and Z. N. Sokolova, "Optical power of semiconductor lasers with a low-dimensional active region," *J. Appl. Phys.*, vol. 115, no. 2, Jan. 2014, Paper no. 023107.
[25] N. A. Gun'ko, V. B. Khalfin, Z. N. Sokolova, and G. G. Zegrya, "Optical loss in InAs-based long-wavelength lasers," *J. Appl. Phys.*, vol. 84, no. 1, pp. 547–554, Jul. 1998.
[26] L. V. Asryan, S. Luryi, and R. A. Suris, "Intrinsic nonlinearity of the light-current characteristic of semiconductor lasers with a quantum-confined active region," *Appl. Phys. Lett.*, vol. 81, no. 12, pp. 2154–2156, Sep. 2002.
[27] E. A. Avrutin and B. S. Ryvkin, "Theory of direct and indirect effect of two-photon absorption on nonlinear optical losses in high power semiconductor lasers," *Semicond. Sci. Technol.*, vol. 32, no. 1, Dec. 2016, Paper no. 015004.
[28] Z. N. Sokolova, K. V. Bakhvalov, A. V. Lyutetskiy, N. A. Pikhtin, I. S. Tarasov, and L. V. Asryan, "Method for determination of capture velocity of charge carriers into a quantum well in a semiconductor laser," *Electron. Lett.*, vol. 51, no. 10, pp. 780–782, May 2015.
[29] Z. N. Sokolova, K. V. Bakhvalov, A. V. Lyutetskiy, N. A. Pikhtin, I. S. Tarasov, and L. V. Asryan, "Dependence of the electron capture velocity on the quantum-well depth in semiconductor lasers," *Semiconductors*, vol. 50, no. 5, pp. 667–670, May 2016.
[30] H. C. Casey and M. B. Panish, *Heterostructure Lasers*. New York, NY, USA: Academic, 1978.
[31] G. P. Agrawal and N. K. Dutta, *Long-Wavelength Semiconductor Lasers*. New York, NY, USA: Van Nostrand, 1986.
[32] L. V. Asryan, "Spontaneous radiative recombination and nonradiative Auger recombination in quantum-confined heterostructures," *Quantum Electron.*, vol. 35, no. 12, pp. 1117–1120, Dec. 2005.
[33] Z. N. Sokolova, I. S. Tarasov, and L. V. Asryan, "Capture of charge carriers and output power of a quantum well laser," *Semiconductors*, vol. 45, no. 11, pp. 1494–1500, Nov. 2011.
[34] K. J. Vahala and C. E. Zah, "Effect of doping on the optical gain and the spontaneous noise enhancement factor in quantum well amplifiers and lasers studied by simple analytical expressions," *Appl. Phys. Lett.*, vol. 52, no. 23, pp. 1945–1947, Jun. 1988.
[35] Y. Wu, L. Jiang, and L. V. Asryan, "Output power of a quantum dot laser: Effects of excited states," *J. Appl. Phys.*, vol. 118, no. 18, Nov. 2015, Paper no. 183107.

Zinaida N. Sokolova received the Ph.D. degree in physics and mathematics from Ioffe Institute, Saint Petersburg, Russia, in 1983. She is a Senior Researcher with Ioffe Institute. Her research interests include the physics of semiconductors, nano- and optoelectronics, and semiconductor lasers.

Dr. Sokolova is the Organizer of the International Biennial Symposium "Semiconductor Lasers: Physics and Technology" in Saint Petersburg since 2008.

Nikita A. Pikhtin (M'00) was born in Leningrad, Russia, on October 17, 1966. He received the M.S. degree (Hons.) in optoelectronics in 1989 and the Ph.D. degree in 2000. His dissertation was devoted to development and investigation of InP-based high power lasers and superluminescent diodes.

In 1983, he entered the Chair of Optoelectronics of V.I. Ulyanov (Lenin) Leningrad Electro-Technical Institute—an educational unit founded and headed by Prof. Zh. I. Alferov. In 1989, he joined as a member of the scientific staff the Semiconductor Luminescence and Injection Emitters Laboratory, Ioffe Institute, Russian Academy of Sciences. In 1992, within the frame of CNRS Fellowship, he spent one year in the University of Nice, France, where he was involved in solid-state lasers and fiber pumping research. He is currently the Acting Head of the Laboratory of Semiconductor Luminescence and Injection Emitters, Ioffe Institute. He is involved in the design, development, and manufacturing of high-power semiconductor laser diodes and devices on their base emitting in 650–1800 nm wavelength range. He authored more than 150 papers in technical journals and conference proceedings.

Levon V. Asryan (M'04–SM'05) received the Ph.D. and Doctor of Sciences degrees from Ioffe Institute, Saint Petersburg, Russia, in 1988 and 2003, respectively, both in physics and mathematics.

He is a Professor with Virginia Polytechnic Institute and State University (Virginia Tech). Before joining Virginia Tech, he was with Ioffe Institute of Physics and Technology, Saint Petersburg, Russia, and State University of New York at Stony Brook, USA. His research interests include the physics of semiconductors, nano- and optoelectronics, photonics, and theory of semiconductor lasers with a low-dimensional active region.

Dr. Asryan was a recipient of the Highest Award of the Russian Federation (State Prize) in Science and Technology for the year 2001 for his contributions to "fundamental investigations of heterostructures with quantum dots and development of quantum dot lasers" and the first IEEE JOURNAL OF QUANTUM ELECTRONICS Best Paper Award for his work on quantum dot lasers.

18th International Conference on Laser Optics

ICLO 2018

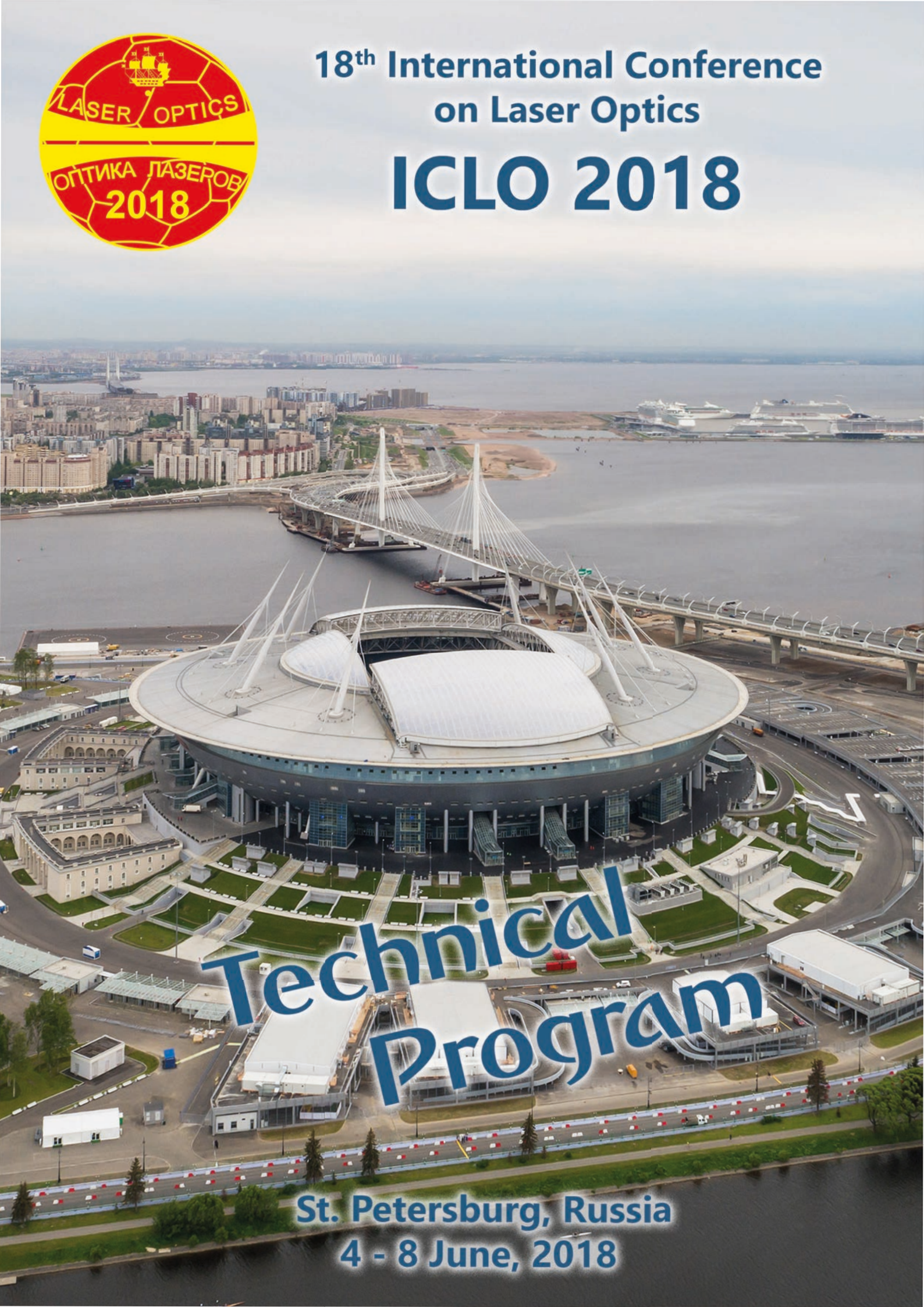

Technical Program

St. Petersburg, Russia

4 - 8 June, 2018

CONTENTS

Two-Threshold Semiconductor Quantum Well Lasers

Z.N. Sokolova [1], N.A. Pikhtin [1], and L.V. Asryan [2]

[1] Ioffe Institute, Saint Petersburg, Russia

[2] Virginia Polytechnic Institute and State University, Blacksburg, USA

e-mail: zina.sokolova@mail.ioffe.ru

***Abstract*—Threshold and power characteristics of quantum well lasers are theoretically studied in the presence of internal optical absorption loss. Due to variation of the internal loss coefficient with electron and densities in the optical confinement layer of the laser, the light-current characteristic may have two branches, each with its own threshold. The branches merge together at the maximum operating current.**

Keywords—quantum well laser, internal optical loss

I. Introduction

We study theoretically the effects of internal optical absorption loss, which depends on the electron and hole densities in the optical confinement layer (OCL), on the operating characteristics of semiconductor quantum well (QW) lasers. In contrast to [1]-[4], wherein the effects of internal loss were studied assuming that local charge neutrality holds separately in the quantum-confined active region and in the OCL, we use here the condition of charge neutrality, which includes the charge of carriers both in the OCL and QWs [5]-[7].

It is shown here that, due to carrier-density-dependent internal loss, the second lasing threshold may exist in addition to the first (conventional) threshold in semiconductor QW lasers. The second threshold is higher than the first one. Above the second threshold, the laser characteristics become two-valued. In particular, there are branches in the dependence of the output optical power on the pump current (light-current characteristic – LCC).

II. Approach

Our theoretical model for the operating characteristics of QW lasers is based on a set of five rate equations in terms of the following unknowns: the three-dimensional densities of free electrons and holes in the OCL, the two-dimensional densities of electrons and holes confined in each QW, and the number of photons in the lasing mode. A key component of our theoretical model is the dependence of the internal loss coefficient on the free electron and hole densities in the OCL. We also take into account the fact that the carriers are not directly injected into QWs. They are first injected from the cladding layers into the OCL and then they are captured from the OCL into QWs. We do not assume instantaneous capture of carriers from the OCL into the QWs, i.e., we do not assume that the capture velocities are infinitely high; instead, we use finite values for the capture velocities. Due to the fact that carrier capture from the OCL into the QWs is noninstantaneous, the free carrier densities in the OCL are not pinned after the onset of lasing – they depend on the injection current. As a result of this, the internal optical absorption loss coefficient also depends on the current.

III. Conclusion

We showed that, under certain conditions, the set of rate equations may have two solutions, i.e., the LCC of QW lasers may have two branches, each starting at its own threshold. The two branches actually form a lobe-shape LCC. The first (conventional) branch of the LCC is nonmonotonous and the second (unconventional) branch is monotonous. We also showed that, while the internal differential quantum efficiency for the first branch is less than one and decreases with increasing pump current, that for the second branch is greater than one and nonmonotonous.

IV. Acknowledgments

This work was supported by the Federal Program of the Ioffe Institute. L.V. Asryan is grateful to the U.S. Army Research Office (Grant No. W911NF-17-1-0432) for support of this work.

[1] L. V. Asryan and S. Luryi, "Two lasing thresholds in semiconductor lasers with a quantum-confined active region," *Appl. Phys. Lett.*, vol. 83, no. 26, pp. 5368-5370, Dec. 2003.

[2] L. V. Asryan and S. Luryi, "Effect of internal optical loss on threshold characteristics of semiconductor lasers with a quantum-confined active region," *IEEE J. Quant. Electron.*, vol. 40, no. 7, pp. 833-843, July 2004.

[3] L. V. Asryan, "Maximum power of quantum dot laser versus internal loss," *Appl. Phys. Lett.*, vol. 88, no. 7, pp. 073107-1–073107-3, Feb. 2006.

[4] L. V. Asryan, "Theoretical investigation of factors controlling the operating characteristics of quantum dot lasers: a review," *J. Nanophoton.*, vol. **3**, 031601-1–031601-25, Jan. 2009.

[5] Z. N. Sokolova, N. A. Pikhtin, I. S. Tarasov, and L. V. Asryan, "Theory of operating characteristics of a semiconductor quantum well laser: Inclusion of global electroneutrality in the structure," *J. Phys. Conf. Ser.*, vol. 740, 012002-1–012002-7, Sep. 2016.

[6] Z. N. Sokolova, N. A. Pikhtin, I. S. Tarasov, and L. V. Asryan, "Threshold characteristics of a semiconductor quantum-well laser: inclusion of global electroneutrality in the structure," *Quantum Electron.*, vol. 46**,** no. 9, pp. 777-781, Sept. 2016.

[7] Z. N. Sokolova, D. A. Veselov, N. A. Pikhtin, I. S. Tarasov, and L. V. Asryan, "Increase in the internal optical loss with increasing pump current and the output power of quantum well lasers," *Semiconductors*, vol. 51, no. 7, pp. 959-964, July 2017.

Modulation Bandwidth of Double Tunneling-Injection Quantum Dot Lasers: Effect of Out-Tunneling Leakage

Levon V. Asryan, *Senior Member, IEEE*, and Saurav Kar

***Abstract*— The effect of out-tunneling leakage of carriers from quantum dots (QDs) on modulation bandwidth of semiconductor double tunneling-injection (DTI) QD lasers is studied. In this type of laser, as an alternative to conventional pumping, electrons and holes are injected into QDs by tunneling from two separate quantum wells (QWs) located on the opposite sides of the QD layer and separated from the latter by thin barrier layers. Fast tunneling-injection into QDs should be maintained to ensure the high modulation bandwidth. It may also seem that out-tunneling leakage from QDs (tunneling of electrons to the hole-injecting QW and holes to the electron-injecting QW), which is an undesirable process, should be kept as slow as possible (or even totally suppressed) to maximize the modulation bandwidth. However, it is shown in this paper that, due to zero-dimensional nature of QDs, the modulation bandwidth is practically unaffected by out-tunneling leakage from them—it depends only slightly on the out-tunneling time. Hence, concerning out-tunneling leakage, DTI QD lasers are robust—provided that tunneling-injection is fast, no significant effort should be necessary to suppress out-tunneling leakage in practical devices.**

***Index Terms*— Quantum dot laser, semiconductor laser, tunneling injection.**

I. Introduction

DOUBLE tunneling-injection (DTI) quantum dot (QD) lasers, which possess several advantages over conventional semiconductor lasers, are discussed. In conventional lasers with a quantum-confined active region, there is always bipolar (i.e., both electron and hole) population and hence electron-hole recombination outside the active region [1]–[5]. This recombination negatively affects the laser operating characteristics. In particular, the threshold current is increased [3] and more temperature-sensitive (the characteristic temperature is reduced) [4]. Besides, since the rate of this recombination increases superlinearly with increasing injection current above the lasing threshold, the efficiency of stimulated recombination decreases and hence the light-current characteristic (LCC) becomes sublinear [5].

In [6]–[8], to eliminate the parasitic electron-hole recombination outside QDs, double tunneling-injection, i.e., tunneling injection of both electrons and holes, was proposed as a mechanism for pumping the QDs. In [9]–[12], the concept of DTI was applied to AlGaAs-GaAs-InGaAs-InAs QD heterostructure lasers. Other tunneling and non-tunneling approaches were also considered, such as tunneling-injection of only electrons into quantum wells (QWs) or QDs [13]–[29], injection of excitons into quantum dashes [30]–[32] or into QDs via nanobridges [33], resonant tunneling through QDs in double-barrier structures [34], and the use of extra QWs that are shallower than the active ones [35].

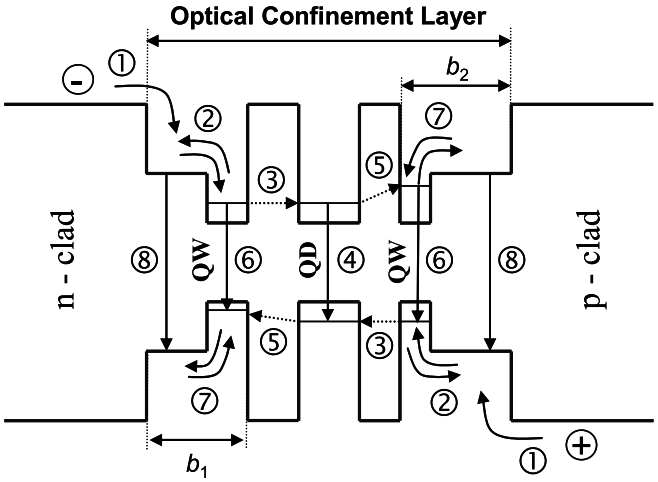

Fig. 1. Energy band diagram of a DTI QD laser and the main processes: ① injection from the cladding layers to the OCL, ② majority carrier capture from the OCL into the QW and thermal escape from the QW to the OCL, ③ tunneling-injection from the QW into a QD, ④ spontaneous and stimulated recombination in a QD, ⑤ out-tunneling from a QD into the 'foreign' QW, ⑥ spontaneous recombination in the QWs, ⑦ minority carrier thermal escape from the QW to the OCL and capture from the OCL into the QW, and ⑧ spontaneous recombination in the OCL. Reproduced from [36, Fig. 1], with the permission of AIP Publishing. The barriers between the QWs and the QD layer do not have to be necessarily implemented in the same material or, in particular, in the material of the cladding layers. The structure can be further optimized by increasing the barrier height for out-tunneling carriers while keeping it low for in-tunneling carriers (see [7, Fig. 5]).

The energy band diagram of a DTI QD laser is shown in Fig. 1. As in conventional QD lasers, electrons and holes are injected from n- and p-cladding layers, respectively, into the optical confinement layer (OCL). In contrast to conventional QD lasers, electrons and holes do not occupy the entire OCL in DTI QD lasers; each type of carriers is contained in its own part of the OCL – the one adjacent to the cladding layer injecting them. This is accomplished by means of the use of two QWs and barrier layers (one on each side of the QD layer). Each type of carriers is captured from the corresponding part

Manuscript received May 29, 2018; revised November 28, 2018; accepted December 6, 2018. Date of publication December 12, 2018; date of current version December 27, 2018. This work was supported by the U.S. Army Research Office under Grant W911NF-17-1-0432. *(Corresponding author: Levon V. Asryan.)*

The authors are with the Department of Materials Science and Engineering, Virginia Polytechnic Institute and State University, Blacksburg, VA 24061 USA (e-mail: asryan@vt.edu).

Digital Object Identifier 10.1109/JQE.2018.2886395

of the OCL into the adjacent QW. The only way for the further transport of electrons and holes is tunneling through the corresponding thin barrier layers into the QDs. Ideally, the wells and barriers should be designed so that electrons will not out-tunnel into the hole-injecting QW and holes into the electron-injecting QW [6]–[8]. In such an ideal situation, bipolar population will be maintained in QDs only. Outside the QDs, i.e., in the OCL and QWs, there will be monopolar population–electron population on the electron-injecting side of the structure and hole population on the hole-injecting side. As a result of this, there will be no electron-hole recombination outside QDs. The total suppression of parasitic recombination will result in a very low and virtually temperature-insensitive threshold current [6]–[8] and a linear LCC.

In actual structures, however, out-tunneling of carriers into the foreign QWs will not be totally suppressed. In the presence of out-tunneling, electrons injected into QDs will leak into the hole-injecting QW and further escape to the hole-injecting side of the OCL. Similarly, holes injected into QDs will leak into the electron-injecting QW and then escape to the electron-injecting side of the OCL. There will be, therefore, certain fractions of minority carriers on each side of the structure–electrons on the hole-injecting side and holes on the electron-injecting side. As a result of this, parasitic recombination will still occur outside QDs in DTI lasers. In [36]–[38], the effect of out-tunneling leakage on static characteristics of DTI QD lasers was studied.

In this work, to explore the potential of DTI QD lasers for high-frequency direct modulation of the optical output by injection current, we study the effect of out-tunneling leakage on their dynamic characteristics. The modulation bandwidth is calculated as a function of the characteristic time of out-tunneling leakage from QDs. It is shown that, due to zero-dimensional (0-D) nature of QDs, the net out-tunneling current from them remains limited with decreasing out-tunneling time. As a result of this, the modulation bandwidth is practically unaffected by out-tunneling leakage.

II. Theoretical Model

We use the following set of rate equations derived in Appendixes A and B:

$$\frac{\partial}{\partial t}\left[\left(\frac{b_1 n_1}{N_c^{2D}}+1\right)N_c^{2D}\frac{f_n}{1-f_n}+2N_S f_n\right] = \frac{j}{e}-\left[\frac{b_1 B n_1^2}{(N_c^{2D})^2}+B_{2D}\right]N_c^{2D}\frac{f_n}{1-f_n}F_{QW} - N_S\frac{f_n^2}{\tau_{QD}}-[w_{out-tunn}F_1^{QW}N_S f_n - w_{out-tunn}N_S(1-f_n)F_{QW}]-c_g g^{max}(2f_n-1)n_{ph}, \quad (1)$$

$$\frac{\partial}{\partial t}\left[\left(\frac{b_1 n_1}{N_c^{2D}}+1\right)F_{QW}\right] = [w_{out-tunn}F_1^{QW}N_S f_n - w_{out-tunn}N_S(1-f_n)F_{QW}] - \left[\frac{b_1 B n_1^2}{(N_c^{2D})^2}+B_{2D}\right]N_c^{2D}\frac{f_n}{1-f_n}F_{QW}, \quad (2)$$

TABLE I
Unknowns in Rate eqs. (1)-(3)

f_n	carrier level occupancy (occupation probability) in QDs
F_{QW}	minority carrier density in the foreign QW (i.e., electron density in the hole-injecting QW and hole density in the electron-injecting QW)
n_{ph}	two-dimensional (2-D) density of photons in the lasing mode (number of photons per unit area of the junction)

TABLE II
Parameters in Rate eqs. (1)-(3)

j	injection current density
e	electron charge
b_1	thickness of one side of the OCL (separation between the cladding layer and the barrier – Fig. 1)
B and B_{2D}	spontaneous radiative recombination constants for the bulk (OCL) and 2-D regions (QWs) measured in units of cm^3/s and cm^2/s, respectively (see [3] and [39] for the expressions for B and B_{2D})
N_S	surface density of QDs
τ_{QD}	spontaneous radiative lifetime in QDs
c_g	group velocity of light
g^{max}	maximum value of the modal gain [3]
$\beta = (1/L)\ln(1/R)$	mirror loss
L	cavity length
R	facet reflectivity

$$\frac{\partial n_{ph}}{\partial t} = c_g g^{max}(2f_n-1)n_{ph} - c_g\beta n_{ph}. \quad (3)$$

The unknowns and parameters in eqs. (1)-(3) are presented in Tables I and II, respectively.

The quantities N_c^{2D}, n_1, and F_1^{QW} in (1) and (2) are given by eqs. (A13), (A14), and (B16) in Appendixes A and B.

The parameter $w_{out-tunn}$ in (1) and (2) is the out-tunneling coefficient, i.e., the coefficient of tunneling (measured in units of cm^2/s) between QDs and the foreign QW. The out-tunneling time from a QD to the foreign QW is expressed in terms of $w_{out-tunn}$ as follows:

$$\tau_{out-tunn}^{QD\rightarrow QW} = \frac{1}{w_{out-tunn}F_1^{QW}}. \quad (4)$$

We apply the small-signal analysis to rate equations (1)-(3) and hence consider the injection current density in (1) in the form of

$$j = j_0 + (\delta j_m)\exp(i\omega t), \quad (5)$$

where ω is the modulation frequency, j_0 is the dc component and δj_m is the small amplitude of the time-harmonic ac component.

We correspondingly look for f_n, F_{QW}, and n_{ph} in (1)-(3) in the form of

$$F_{QW} = F_{QW,0} + (\delta F_{QW-m})\exp(i\omega t), \quad (6)$$

$$f_n = f_{n,0} + (\delta f_{n-m})\exp(i\omega t), \quad (7)$$

$$n_{ph} = n_{ph,0} + (\delta n_{ph-m})\exp(i\omega t), \quad (8)$$

where the dc components $f_{n,0}$, $F_{QW,0}$, and $n_{ph,0}$ are the solutions of rate equations (1)-(3) at the steady-state, which are given by

$$f_{n,0} = \frac{1}{2}\left(1+\frac{\beta}{g^{max}}\right), \quad (9)$$

$$F_{\mathrm{QW},0}=\frac{w_{\mathrm{out-tunn}}F_1^{\mathrm{QW}}N_{\mathrm{S}}f_{\mathrm{n},0}}{w_{\mathrm{out-tunn}}N_{\mathrm{S}}(1-f_{\mathrm{n},0})+\left[\frac{b_1Bn_1^2}{(N_{\mathrm{c}}^{2\mathrm{D}})^2}+B_{2\mathrm{D}}\right]N_{\mathrm{c}}^{2\mathrm{D}}\frac{f_{\mathrm{n},0}}{1-f_{\mathrm{n},0}}}, \tag{10}$$

$$n_{\mathrm{ph},0}=\tau_{\mathrm{ph}}\frac{j_0-j_{\mathrm{th}}}{e}. \tag{11}$$

In (11), the threshold current density and the photon lifetime in the cavity are given by

$$j_{\mathrm{th}}=eN_{\mathrm{S}}\frac{f_{\mathrm{n},0}^2}{\tau_{\mathrm{QD}}}+2e\left[\frac{b_1Bn_1^2}{(N_{\mathrm{c}}^{2\mathrm{D}})^2}+B_{2\mathrm{D}}\right]N_{\mathrm{c}}^{2\mathrm{D}}\frac{f_{\mathrm{n},0}}{1-f_{\mathrm{n},0}}F_{\mathrm{QW},0}, \tag{12}$$

$$\tau_{\mathrm{ph}}=\frac{1}{c_{\mathrm{g}}\beta}. \tag{13}$$

The first term in the right-hand side of (12) is the spontaneous radiative recombination current density in QDs. The second term is the parasitic recombination current density outside QDs (i.e., in the OCL and QWs); in the case of electron-hole symmetry considered here, it is twice the spontaneous radiative recombination current density in each side of the structure–hence the factor of 2 in (12).

Using (5)-(8) in (1)-(3), we obtain the following set of linear algebraic equations in the modulation frequency-dependent small amplitudes $\delta f_{\mathrm{n-m}}$, $\delta F_{\mathrm{QW-m}}$, and $\delta n_{\mathrm{ph-m}}$:

$$\begin{pmatrix} i\omega Y_1+D_1 & C_{12} & C_{13} \\ C_{21} & i\omega Y_2+D_2 & 0 \\ C_{31} & 0 & i\omega \end{pmatrix}\begin{pmatrix} \delta f_{\mathrm{n-m}} \\ \delta F_{\mathrm{QW-m}} \\ \delta n_{\mathrm{ph-m}} \end{pmatrix}=\begin{pmatrix} \delta j_{\mathrm{m}}/e \\ 0 \\ 0 \end{pmatrix}, \tag{14}$$

where the coefficients (all independent of the modulation frequency ω) are given by

$$Y_1=\left(\frac{b_1n_1}{N_{\mathrm{c}}^{2\mathrm{D}}}+1\right)N_{\mathrm{c}}^{2\mathrm{D}}\frac{1}{(1-f_{\mathrm{n},0})^2}+2N_{\mathrm{S}}, \tag{15}$$

$$Y_2=\frac{b_1n_1}{N_{\mathrm{c}}^{2\mathrm{D}}}+1, \tag{16}$$

$$D_1=\left[\frac{b_1Bn_1^2}{(N_{\mathrm{c}}^{2\mathrm{D}})^2}+B_{2\mathrm{D}}\right]N_{\mathrm{c}}^{2\mathrm{D}}\frac{1}{(1-f_{\mathrm{n},0})^2}F_{\mathrm{QW},0}+2N_{\mathrm{S}}\frac{f_{\mathrm{n},0}}{\tau_{\mathrm{QD}}}+w_{\mathrm{out-tunn}}N_{\mathrm{S}}(F_1^{\mathrm{QW}}+F_{\mathrm{QW},0})+2c_{\mathrm{g}}g^{\max}n_{\mathrm{ph},0}, \tag{17}$$

$$D_2=\left[\frac{b_1Bn_1^2}{(N_{\mathrm{c}}^{2\mathrm{D}})^2}+B_{2\mathrm{D}}\right]N_{\mathrm{c}}^{2\mathrm{D}}\frac{f_{\mathrm{n},0}}{1-f_{\mathrm{n},0}}+w_{\mathrm{out-tunn}}N_{\mathrm{S}}(1-f_{\mathrm{n},0}), \tag{18}$$

$$C_{12}=\left[\frac{b_1Bn_1^2}{(N_{\mathrm{c}}^{2\mathrm{D}})^2}+B_{2\mathrm{D}}\right]N_{\mathrm{c}}^{2\mathrm{D}}\frac{f_{\mathrm{n},0}}{1-f_{\mathrm{n},0}}-w_{\mathrm{out-tunn}}N_{\mathrm{S}}(1-f_{\mathrm{n},0}), \tag{19}$$

$$C_{13}=\frac{1}{\tau_{\mathrm{ph}}}, \tag{20}$$

$$C_{21}=\left[\frac{b_1Bn_1^2}{(N_{\mathrm{c}}^{2\mathrm{D}})^2}+B_{2\mathrm{D}}\right]N_{\mathrm{c}}^{2\mathrm{D}}\frac{1}{(1-f_{\mathrm{n},0})^2}F_{\mathrm{QW},0}-w_{\mathrm{out-tunn}}N_{\mathrm{S}}(F_1^{\mathrm{QW}}+F_{\mathrm{QW},0}), \tag{21}$$

$$C_{31}=-2c_{\mathrm{g}}g^{\max}n_{\mathrm{ph},0}. \tag{22}$$

From the solution of (14), we find the ratio $\delta n_{\mathrm{ph-m}}(\omega)/\delta n_{\mathrm{ph-m}}(0)$,

$$\frac{\delta n_{\mathrm{ph-m}}(\omega)}{\delta n_{\mathrm{ph-m}}(0)}=(C_{13}C_{31}D_2+i\omega\, Y_2C_{13}C_{31})\times\{[C_{13}C_{31}D_2+\omega^2(Y_1D_2+Y_2D_1)]+i\omega\,[(Y_2C_{13}C_{31}+C_{12}C_{21}-D_1D_2)+\omega^2\,Y_1Y_2]\}^{-1}, \tag{23}$$

and then the modulation response function $H(\omega)$,

$$H(\omega)=\left|\frac{\delta n_{\mathrm{ph-m}}(\omega)}{\delta n_{\mathrm{ph-m}}(0)}\right|^2=(C_{13}^2C_{31}^2D_2^2+\omega^2\,Y_2^2C_{13}^2C_{31}^2)\times\{[C_{13}C_{31}D_{22}+\omega^2(Y_1D_2+Y_2D_1)]^2+\omega^2\,[(Y_2C_{13}C_{31}+C_{12}C_{21}-D_1D_2)+\omega^2\,Y_1Y_2]^2\}^{-1}. \tag{24}$$

The modulation bandwidth $\omega_{-3\ \mathrm{dB}}$ is defined as the –3 dB bandwidth [40]–[42],

$$10\log_{10}H(\omega_{-3\ \mathrm{dB}})=-3. \tag{25}$$

Using (24) in (25), we obtain the following cubic equation for the square $\omega_{-3\ \mathrm{dB}}^2$ of the bandwidth:

$$\omega_{-3\ \mathrm{dB}}^6+E_4\omega_{-3\ \mathrm{dB}}^4+E_2\omega_{-3\ \mathrm{dB}}^2-E_0=0, \tag{26}$$

where the coefficients E are expressed in terms of the coefficients C, D, and Y as follows:

$$E_0=\frac{1}{Y_1^2Y_2^2}(r-1)\,C_{13}^2C_{31}^2D_2^2, \tag{27}$$

$$E_2=\frac{1}{Y_1^2Y_2^2}[(C_{12}C_{21}-D_1D_2)^2-(r-1)\,Y_2^2C_{13}^2C_{31}^2+2C_{13}C_{31}(Y_2C_{12}C_{21}+Y_1D_2^2)], \tag{28}$$

$$E_4=\frac{1}{Y_1^2Y_2^2}[Y_1^2D_2^2+Y_2^2D_1^2+2Y_1Y_2(Y_2C_{13}C_{31}+C_{12}C_{21})], \tag{29}$$

where $r=10^{0.3}\approx 1.995$.

III. Discussion

We apply the above analysis and calculate the modulation bandwidth for a GaInAsP laser structure emitting near 1.55 μm [43]–[46]. The materials of cladding layers, OCL, and QDs are InP, $Ga_{0.21}In_{0.79}As_{0.46}P_{0.54}$, and $Ga_{0.47}In_{0.53}As$, respectively, the latter two being lattice-matched to InP. The surface density of QDs $N_{\mathrm{S}}=6.11\times10^{10}$ cm^{-2}. The Fabry-Perot cavity length $L=1.139$ mm; at this cavity length and assuming as-cleaved facets (the mirror reflectivity $R=0.32$), the mirror loss $\beta=10$ cm^{-1}. Room-temperature operation is considered ($T=300$ K). In Figs. 2-5, the dc component of the injection current density $j_0=50$ kA/cm^2; at this value of j_0, the modulation bandwidth is at its maximum in an ideal DTI QD laser [45]. At $j_0=50$ kA/cm^2, $L=1.139$ mm, the laser stripe width $W=2$ μm, and the out-tunneling time $\tau_{\mathrm{out-tunn}}=1$ ps, the dc component of the output optical power is 1 W.

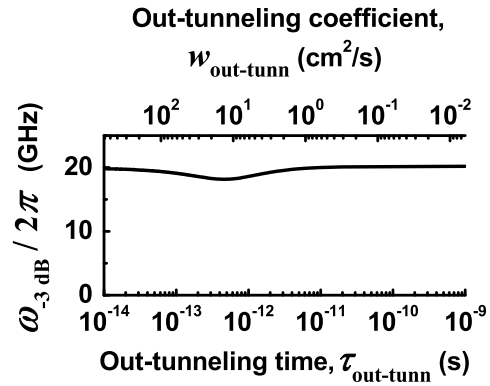

Fig. 2. Modulation bandwidth $\omega_{-3\text{ dB}}/2\pi$ vs. out-tunneling time (the bottom axis) and out-tunneling coefficient (the top axis). A GaInAsP heterostructure emitting near 1.55 μm is considered [43]–[46]. The materials of cladding layers, OCL, and QDs are InP, $Ga_{0.21}In_{0.79}As_{0.46}P_{0.54}$, and $Ga_{0.47}In_{0.53}As$, respectively, the latter two being lattice-matched to InP. In Figs. 2-5, the cavity length $L = 1.139$ mm (the mirror loss $\beta = 10$ cm^{-1}) and the surface density of QDs $N_S = 6.11 \times 10^{10}$ cm^{-2}. In Figs. 2-4, the offset energy between the carrier subband edge in the foreign QW and the level in a QD is $\Delta = T$. Room-temperature operation is considered ($T = 300$ K). In Figs. 2-5, the dc component of the injection current density $j_0 = 50$ kA/cm^2; at this value of j_0, the modulation bandwidth is at its maximum in an ideal DTI QD laser [45]. At $j_0 = 50$ kA/cm^2, $L = 1.139$ mm, the laser stripe width $W = 2$ μm, and the out-tunneling time $\tau_{\text{out-tunn}} = 1$ ps, the dc component of the output optical power is 1 W.

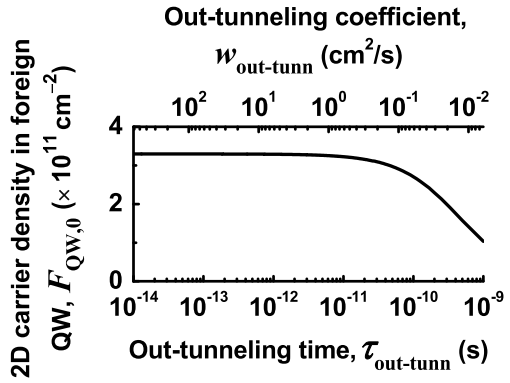

Fig. 3. 2-D carrier density in the foreign QW vs. out-tunneling time (the bottom axis) and out-tunneling coefficient (the top axis).

Figure 2 shows the modulation bandwidth $\omega_{-3\text{ dB}}$ against the out-tunneling time from a QD to the foreign QW $\tau_{\text{out-tunn}}^{\text{QD}\rightarrow\text{QW}}$ (the bottom axis). In the figure, the out-tunneling time is varied [see eq. (4)] via varying the out-tunneling coefficient $w_{\text{out-tunn}}$ (shown in the top axis). As seen from the figure, the modulation bandwidth is practically unaffected by out-tunneling from QDs – there is only a slight dip in the curve for $\omega_{-3\text{ dB}}$. In order to gain insight into this, we analyze the net out-tunneling current density, which is the difference between the current density of out-tunneling leakage from QDs to the foreign QW and the current density of backward tunneling from the foreign QW into QDs [see (2)],

$$e w_{\text{out-tunn}} F_1^{\text{QW}} N_S f_{\text{n}} - e w_{\text{out-tunn}} N_S (1 - f_{\text{n}}) F_{\text{QW}}. \quad (30)$$

At the steady-state, we have from (2),

$$e w_{\text{out-tunn}} F_1^{\text{QW}} N_S f_{\text{n},0} - e w_{\text{out-tunn}} N_S (1 - f_{\text{n},0}) F_{\text{QW},0} = e \left[\frac{b_1 B n_1^2}{(N_{\text{c}}^{\text{2D}})^2} + B_{\text{2D}} \right] N_{\text{c}}^{\text{2D}} \frac{f_{\text{n},0}}{1 - f_{\text{n},0}} F_{\text{QW},0}. \quad (31)$$

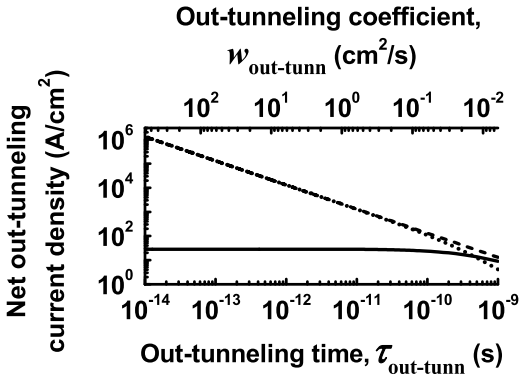

Fig. 4. Out-tunneling current density from QDs to the foreign QWs (the dashed line), current density of backward tunneling from the foreign QWs to QDs (the dotted curve), and net out-tunneling current density (the solid curve) vs. out-tunneling time (the bottom axis) and out-tunneling coefficient (the top axis).

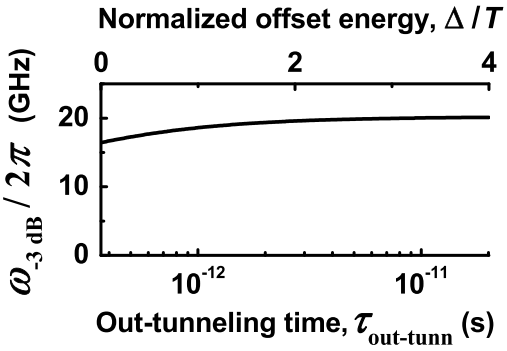

Fig. 5. Modulation bandwidth $\omega_{-3\text{ dB}}/2\pi$ vs. out-tunneling time (the bottom axis) and normalized offset energy between the carrier subband edge in the foreign QW and the level in a QD (the top axis). The out-tunneling coefficient is $w_{\text{out-tunn}} = 6.14$ cm^2/s.

For the sum of the net out-tunneling current densities of electrons and holes, we have

$$j_{\text{out-tunn},0}^{\text{net}} = 2e \left[\frac{b_1 B n_1^2}{(N_{\text{c}}^{\text{2D}})^2} + B_{\text{2D}} \right] N_{\text{c}}^{\text{2D}} \frac{f_{\text{n},0}}{1 - f_{\text{n},0}} F_{\text{QW},0}. \quad (32)$$

Naturally, $j_{\text{out-tunn},0}^{\text{net}}$ is equal to the parasitic recombination current density outside QDs [the second term in the right-hand side of (12)] since the latter is totally due to out-tunneling from QDs.

As seen from (32) and (10), $j_{\text{out-tunn},0}^{\text{net}}$ depends on $w_{\text{out-tunn}}$ via such dependence of the 2-D carrier density $F_{\text{QW},0}$ in the foreign QW. However, as seen from (10) and Fig. 3, while $F_{\text{QW},0}$ starts to increase from zero with increasing $w_{\text{out-tunn}}$, it remains saturated as $w_{\text{out-tunn}} \rightarrow \infty$, i.e., as out-tunneling becomes instantaneous ($\tau_{\text{out-tunn}}^{\text{QD}\rightarrow\text{QW}} \rightarrow 0$). For such a case of instantaneous exchange between QDs and the foreign QW, we have from (10),

$$F_{\text{QW},0}\big|_{w_{\text{out-tunn}} \rightarrow \infty} = F_1^{\text{QW}} \frac{f_{\text{n},0}}{1 - f_{\text{n},0}}, \quad (33)$$

which is the same expression as eqs. (B1) and (B2) in Appendix B relating the 2-D carrier density in the injecting QW and the level occupancy in QDs for the case of instantaneous tunneling-injection.

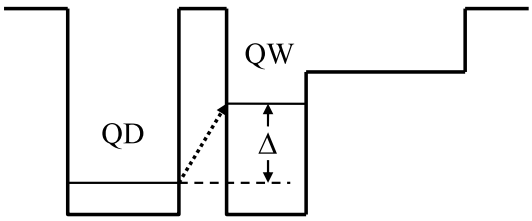

Fig. 6. Conduction band diagram in the right-hand side of the structure. Δ is the offset energy between the electron subband edge in the foreign (hole-injecting) QW and the electron level in a QD.

Due to 0-D nature of QDs, the QD population remains limited – the level occupancy $f_{\mathrm{n},0} < 1$. Hence the highest 2-D carrier density in the foreign QW, which is given by (33), is finite even in the worst case scenario of instantaneous out-tunneling from QDs. So remains the net out-tunneling current density, which is shown in Fig. 4 (the solid curve) against the out-tunneling coefficient (the top axis) and the out-tunneling time (the bottom axis). With (32) and (33), we have for the saturation value of $j^{\mathrm{net}}_{\mathrm{out-tunn},0}$,

$$j^{\mathrm{net}}_{\mathrm{out-tunn},0}\Big|_{w_{\mathrm{out-tunn}}\to\infty} = 2e\left[\frac{b_1 B n_1^2}{(N_{\mathrm{c}}^{2\mathrm{D}})^2} + B_{2\mathrm{D}}\right] \times N_{\mathrm{c}}^{2\mathrm{D}} F_1^{\mathrm{QW}} \left(\frac{f_{\mathrm{n},0}}{1-f_{\mathrm{n},0}}\right)^2. \quad (34)$$

With eq. (B16) of Appendix B for F_1^{QW}, we can rewrite (34) as follows:

$$j^{\mathrm{net}}_{\mathrm{out-tunn},0}\Big|_{w_{\mathrm{out-tunn}}\to\infty} = 2e\left[\, b_1 B n_1^2 + B_{2\mathrm{D}}(N_{\mathrm{c}}^{2\mathrm{D}})^2\right] \times \left(\frac{f_{\mathrm{n},0}}{1-f_{\mathrm{n},0}}\right)^2 \exp\left(-\frac{\Delta}{T}\right). \quad (35)$$

Hence, while the out-tunneling current density from QDs to the foreign QW [the first term in (30) and the dashed line in Fig. 4] increases with increasing $w_{\mathrm{out-tunn}}$ and becomes high, this increase is compensated for by the increase of the backward tunneling current density from the foreign QW into QDs [the second term in (30) and the dotted curve in Fig. 4] so that their difference, presenting the net out-tunneling current density (the solid curve in Fig. 4), remains saturated and low with increasing $w_{\mathrm{out-tunn}}$.

Figure 5 also shows the modulation bandwidth against the out-tunneling time. In contrast to Fig. 2, $\tau_{\mathrm{out-tunn}}^{\mathrm{QD}\to\mathrm{QW}}$ is now varied by varying the offset Δ between the energies of the subband edge in the foreign QW and the level in a QD [see eqs. (4) and (B16) and Fig. 6]. As seen from (4) and (B16), $\tau_{\mathrm{out-tunn}}^{\mathrm{QD}\to\mathrm{QW}}$ decreases (i.e., out-tunneling occurs faster) exponentially with decreasing Δ. Hence, it would be intuitive that the modulation bandwidth should decrease considerably with decreasing Δ. However, as seen from Fig. 5, the decrease in $\omega_{-3\,\mathrm{dB}}$ is actually small; $\omega_{-3\,\mathrm{dB}}$ decreases by 18% only with reducing Δ from $4T$ (high offset between the foreign QW subband edge and the QD level) to 0 (resonance between the foreign QW subband edge and the QD level), i.e., reducing $\tau_{\mathrm{out-tunn}}^{\mathrm{QD}\to\mathrm{QW}}$ by a factor of $\exp(4) \approx 55$.

Our model does not take into account possible band bending due to spatial separation of carriers (confinement of electrons and holes in the opposite sides of the structure). Such band bending may affect both the rates of tunneling-injection of carriers into QDs and out-tunneling from QDs. In such a situation, again, provided the tunneling-injection is fast enough, the out-tunneling leakage will not significantly affect the modulation bandwidth.

We do not consider non-radiative recombination of carriers. The inclusion of non-radiative recombination will affect the dc components of the carrier densities in the OCL and QWs. However, the main derivation of this work (independence of modulation bandwidth of out-tunneling leakage from QDs) will remain unchanged – due to zero-dimensional nature of QDs, the net out-tunneling current from them will still remain limited.

IV. Conclusion

We studied the effect of out-tunneling leakage of carriers from QDs on dynamic characteristics of DTI QD lasers. We calculated the modulation bandwidth as a function of the characteristic time of out-tunneling leakage from QDs. The out-tunneling time is varied by varying the out-tunneling coefficient and the offset energy between the subband edge in the foreign QW and the level in a QD. We showed that, due to 0-D nature of QDs, the 2-D carrier densities in the foreign QWs and the net out-tunneling current from QDs to the foreign QWs remain limited with decreasing out-tunneling time, i.e., making out-tunneling faster. As a result of this, the modulation bandwidth depends only slightly on the out-tunneling time. This is in contrast to tunneling-injection of carriers into QDs, which strongly limits the modulation bandwidth and should be made fast [46] to increase the bandwidth. Hence, concerning out-tunneling leakage, DTI QD lasers are robust — provided that tunneling-injection is fast, no significant effort should be necessary to suppress out-tunneling leakage in practical devices.

Appendix A
General Rate Equations

In the general case, the operating characteristics of DTI QD lasers (see Fig. 1 for the energy band diagram) are described by the following set of rate equations:

for electrons and holes in the left-hand side of the OCL,

$$b_1\frac{\partial n_L}{\partial t} = \frac{j}{e} + \frac{n_{\mathrm{QW}}^L}{\tau_{\mathrm{n,esc}}^L} - \mathrm{v}_{\mathrm{n,capt}}^L n_L - b_1 B n_L p_L, \quad (A1)$$

$$b_1\frac{\partial p_L}{\partial t} = \frac{p_{\mathrm{QW}}^L}{\tau_{\mathrm{p,esc}}^L} - \mathrm{v}_{\mathrm{p,capt}}^L p_L - b_1 B n_L p_L, \quad (A2)$$

for holes and electrons in the right-hand side of the OCL,

$$b_2\frac{\partial p_R}{\partial t} = \frac{j}{e} + \frac{p_{\mathrm{QW}}^R}{\tau_{\mathrm{p,esc}}^R} - \mathrm{v}_{\mathrm{p,capt}}^R p_R - b_2 B n_R p_R, \quad (A3)$$

$$b_2\frac{\partial n_R}{\partial t} = \frac{n_{\mathrm{QW}}^R}{\tau_{\mathrm{n,esc}}^R} - \mathrm{v}_{\mathrm{n,capt}}^R n_R - b_2 B n_R p_R, \quad (A4)$$

TABLE III
QUANTITIES IN RATE EQS. (A1)-(A11)

b_1 (b_2)	thickness of the left- (right-) hand side of the OCL [separation between the n- (p-) cladding layer and the left- (right-) hand-side barrier – see Fig. 1]
n_L (n_R) and p_L (p_R)	free-electron and -hole densities in the left- (right-) hand side of the OCL
$n^L_{\rm QW}$ ($n^R_{\rm QW}$) and $p^L_{\rm QW}$ ($p^R_{\rm QW}$)	2-D electron and hole densities in the left- (right-) hand-side QW (Fig. 1)
$f_{\rm n,p}$	electron- and hole-level occupancies in QDs
$w^{L,R}_{\rm n,p,\,tunn}$	coefficients of electron and hole tunneling between the QD ensemble and the QWs (measured in units of cm^2/s)

for electrons and holes in the electron-injecting (left-hand-side) QW,

$$\frac{\partial n^L_{\rm QW}}{\partial t} = {\rm v}^L_{\rm n,capt} n_L - \frac{n^L_{\rm QW}}{\tau^L_{\rm n,esc}} - w^L_{\rm n,\,tunn} N_S (1-f_{\rm n}) n^L_{\rm QW} + w^L_{\rm n,tunn} n_1^{L,{\rm QW}} N_S f_{\rm n} - B_{\rm 2D} n^L_{\rm QW} p^L_{\rm QW}, \quad \text{(A5)}$$

$$\frac{\partial p^L_{\rm QW}}{\partial t} = {\rm v}^L_{\rm p,capt} p_L - \frac{p^L_{\rm QW}}{\tau^L_{\rm p,esc}} - w^L_{\rm p,tunn} N_S (1-f_{\rm p}) p^L_{\rm QW} + w^L_{\rm p,tunn} p_1^{L,\,{\rm QW}} N_S f_{\rm p} - B_{\rm 2D} n^L_{\rm QW} p^L_{\rm QW}, \quad \text{(A6)}$$

for holes and electrons in the hole-injecting (right-hand-side) QW,

$$\frac{\partial p^R_{\rm QW}}{\partial t} = {\rm v}^R_{\rm p,capt} p_R - \frac{p^R_{\rm QW}}{\tau^R_{\rm p,esc}} - w^R_{\rm p,tunn} N_S (1-f_{\rm p}) p^R_{\rm QW} + w^R_{\rm p,tunn} p_1^{R,\,{\rm QW}} N_S f_{\rm p} - B_{\rm 2D} n^R_{\rm QW} p^R_{\rm QW}, \quad \text{(A7)}$$

$$\frac{\partial n^R_{\rm QW}}{\partial t} = {\rm v}^R_{\rm n,capt} n_R - \frac{n^R_{\rm QW}}{\tau^R_{\rm n,esc}} - w^R_{\rm n,tunn} N_S (1-f_{\rm n}) n^R_{\rm QW} + w^R_{\rm n,tunn} n_1^{R,\,{\rm QW}} N_S f_{\rm n} - B_{\rm 2D} n^R_{\rm QW} p^R_{\rm QW}, \quad \text{(A8)}$$

for electrons and holes confined in QDs,

$$2N_S \frac{\partial f_{\rm n}}{\partial t} = w^L_{\rm n,tunn} N_S (1-f_{\rm n}) n^L_{\rm QW} - w^L_{\rm n,tunn} n_1^{L,{\rm QW}} N_S f_{\rm n} + w^R_{\rm n,tunn} N_S (1-f_{\rm n}) n^R_{\rm QW} - w^R_{\rm n,tunn} n_1^{R,\,{\rm QW}} N_S f_{\rm n} - N_S \frac{f_{\rm n} f_{\rm p}}{\tau_{\rm QD}} - c_{\rm g} g^{\max} (f_{\rm n} + f_{\rm p} - 1) n_{\rm ph}, \quad \text{(A9)}$$

$$2N_S \frac{\partial f_{\rm p}}{\partial t} = w^R_{\rm p,tunn} N_S (1-f_{\rm p}) p^R_{\rm QW} - w^R_{\rm p,tunn} p_1^{R,\,{\rm QW}} N_S f_{\rm p} + w^L_{\rm p,tunn} N_S (1-f_{\rm p}) p^L_{\rm QW} - w^L_{\rm p,tunn} p_1^{L,\,{\rm QW}} N_S f_{\rm p} - N_S \frac{f_{\rm n} f_{\rm p}}{\tau_{\rm QD}} - c_{\rm g} g^{\max} (f_{\rm n} + f_{\rm p} - 1) n_{\rm ph}, \quad \text{(A10)}$$

and for photons,

$$\frac{\partial n_{\rm ph}}{\partial t} = c_{\rm g} g^{\max} (f_{\rm n} + f_{\rm p} - 1) n_{\rm ph} - c_{\rm g} \beta n_{\rm ph}. \quad \text{(A11)}$$

The quantities entering into eqs. (A1)–(A11), which were not introduced earlier, are presented in Table III.

The thermal escape times of electrons and holes from the QWs to the OCL, $\tau^{L,R}_{\rm n,p,esc}$, and the capture velocities from the OCL to the QWs, ${\rm v}^{L,R}_{\rm n,p,\,capt}$, are related to each other [37]. For undoped OCL and QW, the relation is

$$\tau_{\rm n,\,esc} = \frac{1}{{\rm v}_{\rm n,\,capt}} \frac{N^{\rm 2D}_{\rm c}}{n_1}, \quad \tau_{\rm p,\,esc} = \frac{1}{{\rm v}_{\rm p,\,capt}} \frac{N^{\rm 2D}_{\rm v}}{p_1}, \quad \text{(A12)}$$

where

$$N^{\rm 2D}_{\rm c,v} = \frac{m^{\rm QW}_{\rm c,v} T}{\pi \hbar^2} \quad \text{(A13)}$$

are the 2-D effective densities of states in the conduction and valence bands in the QWs, $m^{\rm QW}_{\rm c,v}$ are the electron and hole effective masses in the QWs, and the temperature T is measured in units of energy.

The quantities n_1 and p_1 are

$$n_1 = N^{\rm 3D}_{\rm c} \exp\left(-\frac{\Delta E_{\rm c} - \varepsilon^{\rm QW}_{\rm n}}{T}\right), \quad p_1 = N^{\rm 3D}_{\rm v} \exp\left(-\frac{\Delta E_{\rm v} - \varepsilon^{\rm QW}_{\rm p}}{T}\right), \quad \text{(A14)}$$

where

$$N^{\rm 3D}_{\rm c,v} = 2\left(\frac{m^{\rm OCL}_{\rm c,v} T}{2\pi \hbar^2}\right)^{3/2} \quad \text{(A15)}$$

are the three-dimensional (3-D) effective densities of states in the conduction and valence bands in the OCL, $m^{\rm OCL}_{\rm c,v}$ are the electron and hole effective masses in the OCL, $\Delta E_{\rm c,v}$ are the conduction and valence band offsets between the OCL and the QW, and $\varepsilon^{\rm QW}_{\rm n,p}$ are the energies of the electron- and hole-subband edges in the QW.

The quantities $n_1^{L,R,\,{\rm QW}}$ and $p_1^{L,\,R,\,{\rm QW}}$ entering into the electron and hole tunneling fluxes from the QD ensemble to the QWs [see (A5)–(A10)] are measured in units of cm^{-2}. In the general case, they are given by [37, eq. (B3)]. In the case of undoped QW and if $\varepsilon^{\rm QW}_{\rm n} \geq \varepsilon^{\rm QD}_{\rm n}$ and $\varepsilon^{\rm QW}_{\rm p} \geq \varepsilon^{\rm QD}_{\rm p}$, where $\varepsilon^{\rm QD}_{\rm n,p}$ are energies of the electron and hole levels in a QD, the expressions for $n_1^{\rm QW}$ and $p_1^{\rm QW}$ are

$$n_1^{\rm QW} = N^{\rm 2D}_{\rm c} \exp\left(-\frac{\varepsilon^{\rm QW}_{\rm n} - \varepsilon^{\rm QD}_{\rm n}}{T}\right), \quad p_1^{\rm QW} = N^{\rm 2D}_{\rm v} \exp\left(-\frac{\varepsilon^{\rm QW}_{\rm p} - \varepsilon^{\rm QD}_{\rm p}}{T}\right). \quad \text{(A16)}$$

The flux of electron (and similarly hole) tunneling from a QD ensemble to a QW can be written as

$$w_{\rm n,tunn} n_1^{\rm QW} N_S f_{\rm n} = N_S \frac{f_{\rm n}}{\tau^{\rm QD\to QW}_{\rm n,tunn}}, \quad \text{(A17)}$$

where

$$\tau^{\rm QD\to QW}_{\rm n,tunn} = \frac{1}{w_{\rm n,tunn} n_1^{\rm QW}} \quad \text{(A18)}$$

can be viewed as the tunneling time from a QD to a QW.

The flux of electron tunneling from a QW to a QD ensemble can be written as

$$w_{\rm n,tunn} N_S (1-f_{\rm n})\, n_{\rm QW} = \frac{n_{\rm QW}}{\tau^{\rm QW\to QDs}_{\rm n,tunn}}, \quad \text{(A19)}$$

where

$$\tau_{\mathrm{n,tunn}}^{\mathrm{QW}\to\mathrm{QDs}}=\frac{\tau_{\mathrm{n,tunn,0}}^{\mathrm{QW}\to\mathrm{QDs}}}{1-f_{\mathrm{n}}} \tag{A20}$$

can be considered as the tunneling time from a QW to a QD ensemble, and

$$\tau_{\mathrm{n,tunn,0}}^{\mathrm{QW}\to\mathrm{QDs}}=\frac{1}{w_{\mathrm{n,tunn}}N_S} \tag{A21}$$

can be correspondingly considered as the tunneling time into an unoccupied QD ensemble (when $f_{\mathrm{n}}=0$).

Adding up eqs. (A1), (A5), and (A9), we obtain

$$\begin{aligned}\frac{\partial}{\partial t}&(b_1n_L+n_{\mathrm{QW}}^L+2N_Sf_{\mathrm{n}})\\&=\frac{j}{e}-b_1Bn_Lp_L-B_{2\mathrm{D}}n_{\mathrm{QW}}^Lp_{\mathrm{QW}}^L\\&\quad-N_S\frac{f_{\mathrm{n}}f_{\mathrm{p}}}{\tau_{\mathrm{QD}}}-c_{\mathrm{g}}g^{\max}(f_{\mathrm{n}}+f_{\mathrm{p}}-1)n_{\mathrm{ph}}\\&\quad-[w_{\mathrm{n,tunn}}^Rn_1^{R,\,\mathrm{QW}}N_Sf_{\mathrm{n}}-w_{\mathrm{n,tunn}}^RN_S(1-f_{\mathrm{n}})n_{\mathrm{QW}}^R].\end{aligned} \tag{A22}$$

Adding up eqs. (A2) and (A6), we obtain

$$\begin{aligned}\frac{\partial}{\partial t}&(b_1p_L+p_{\mathrm{QW}}^L)\\&=[w_{\mathrm{p,tunn}}^Lp_1^{L,\,\mathrm{QW}}N_Sf_{\mathrm{p}}-w_{\mathrm{p,tunn}}^LN_S(1-f_{\mathrm{p}})p_{\mathrm{QW}}^L]\\&\quad-b_1Bn_Lp_L-B_{2\mathrm{D}}n_{\mathrm{QW}}^Lp_{\mathrm{QW}}^L.\end{aligned} \tag{A23}$$

Adding up eqs. (A3), (A7), and (A10), we obtain

$$\begin{aligned}\frac{\partial}{\partial t}&(b_2p_R+p_{\mathrm{QW}}^R+2N_Sf_{\mathrm{p}})\\&=\frac{j}{e}-b_2Bn_Rp_R-B_{2\mathrm{D}}n_{\mathrm{QW}}^Rp_{\mathrm{QW}}^R\\&\quad-N_S\frac{f_{\mathrm{n}}f_{\mathrm{p}}}{\tau_{\mathrm{QD}}}-c_{\mathrm{g}}g^{\max}(f_{\mathrm{n}}+f_{\mathrm{p}}-1)n_{\mathrm{ph}}\\&\quad-[w_{\mathrm{p,tunn}}^Lp_1^{L,\,\mathrm{QW}}N_Sf_{\mathrm{p}}-w_{\mathrm{p,tunn}}^LN_S(1-f_{\mathrm{p}})p_{\mathrm{QW}}^L].\end{aligned} \tag{A24}$$

Adding up eqs. (A4) and (A8), we obtain

$$\begin{aligned}\frac{\partial}{\partial t}&(b_2n_R+n_{\mathrm{QW}}^R)\\&=[w_{\mathrm{n,tunn}}^Rn_1^{R,\,\mathrm{QW}}N_Sf_{\mathrm{n}}-w_{\mathrm{n,tunn}}^RN_S(1-f_{\mathrm{n}})n_{\mathrm{QW}}^R]\\&\quad-b_2Bn_Rp_R-B_{2\mathrm{D}}n_{\mathrm{QW}}^Rp_{\mathrm{QW}}^R.\end{aligned} \tag{A25}$$

Adding up eqs. (A1), (A4), (A5), (A8), and (A9), we obtain

$$\begin{aligned}\frac{\partial}{\partial t}&(b_1n_L+n_{\mathrm{QW}}^L+2N_Sf_{\mathrm{n}}+b_2n_R+n_{\mathrm{QW}}^R)\\&=\frac{j}{e}-b_1Bn_Lp_L\\&\quad-B_{2\mathrm{D}}n_{\mathrm{QW}}^Lp_{\mathrm{QW}}^L-b_2Bn_Rp_R-B_{2\mathrm{D}}n_{\mathrm{QW}}^Rp_{\mathrm{QW}}^R\\&\quad-N_S\frac{f_{\mathrm{n}}f_{\mathrm{p}}}{\tau_{\mathrm{QD}}}-c_{\mathrm{g}}g^{\max}(f_{\mathrm{n}}+f_{\mathrm{p}}-1)n_{\mathrm{ph}}.\end{aligned} \tag{A26}$$

Adding up eqs. (A2), (A3), (A6), (A7), and (A10), we obtain

$$\begin{aligned}\frac{\partial}{\partial t}&(b_2p_R+p_{\mathrm{QW}}^R+2N_Sf_{\mathrm{p}}+b_1p_L+p_{\mathrm{QW}}^L)\\&=\frac{j}{e}-b_1Bn_Lp_L\\&\quad-B_{2\mathrm{D}}n_{\mathrm{QW}}^Lp_{\mathrm{QW}}^L-b_2Bn_Rp_R-B_{2\mathrm{D}}n_{\mathrm{QW}}^Rp_{\mathrm{QW}}^R\\&\quad-N_S\frac{f_{\mathrm{n}}f_{\mathrm{p}}}{\tau_{\mathrm{QD}}}-c_{\mathrm{g}}g^{\max}(f_{\mathrm{n}}+f_{\mathrm{p}}-1)n_{\mathrm{ph}}.\end{aligned} \tag{A27}$$

As seen from (A26) and (A27),

$$\begin{aligned}\frac{\partial}{\partial t}&(b_1n_L+n_{\mathrm{QW}}^L+2N_Sf_{\mathrm{n}}+b_2n_R+n_{\mathrm{QW}}^R)\\&=\frac{\partial}{\partial t}(b_2p_R+p_{\mathrm{QW}}^R+2N_Sf_{\mathrm{p}}+b_1p_L+p_{\mathrm{QW}}^L),\end{aligned} \tag{A28}$$

which gives

$$\begin{aligned}b_1n_L&+n_{\mathrm{QW}}^L+2N_Sf_{\mathrm{n}}+b_2n_R+n_{\mathrm{QW}}^R\\&=b_2p_R+p_{\mathrm{QW}}^R+2N_Sf_{\mathrm{p}}+b_1p_L+p_{\mathrm{QW}}^L.\end{aligned} \tag{A29}$$

Eq. (A29) is the condition of global charge neutrality in the structure.

Appendix B
Derivation of Rate Equations (1)-(3)

In this work, to focus on the effect of out-tunneling leakage from QDs, we make the following assumptions:

1) Carrier exchange between the OCL and QW on each side of the structure (processes ② and ⑦ in Fig. 1) is instantaneous ($v_{\mathrm{n,p,\,capt}}^{L,\,R}\to\infty$ and hence $\tau_{\mathrm{n,p,\,esc}}^{L,\,R}\to 0$). As shown in [46], for the capture into the QW to be considered a fast process in the specific structure considered here, the capture time should be shorter than 1 ps.

2) Tunneling-injection into QDs (processes ③ in Fig. 1) is instantaneous ($w_{\mathrm{n,\,tunn}}^L\to\infty$ and hence $\tau_{\mathrm{n,tunn,0}}^{L,\,\mathrm{QW}\to\mathrm{QDs}}\to 0$; similarly, $w_{\mathrm{p,\,tunn}}^R\to\infty$ and hence $\tau_{\mathrm{p,tunn,0}}^{R,\,\mathrm{QW}\to\mathrm{QDs}}\to 0$). As shown in [46], for the tunneling into the QD ensemble to be considered a fast process in the structure considered here, the tunneling time should be shorter than 0.1 ps.

Out-tunneling leakage from QDs (processes ⑤ in Fig. 1) is characterized by the coefficients $w_{\mathrm{n,\,tunn}}^R$ and $w_{\mathrm{p,\,tunn}}^L$, or, equivalently, the out-tunneling times $\tau_{\mathrm{n,tunn}}^{\mathrm{QD}\to R,\,\mathrm{QW}}$ and $\tau_{\mathrm{p,tunn}}^{\mathrm{QD}\to L,\,\mathrm{QW}}$ to the "foreign" QWs, i.e., the tunneling times of electrons from a QD to the hole-injecting QW [see eq. (A18)] and holes from a QD to the electron-injecting QW. We will calculate the modulation bandwidth as a function of these parameters.

With the assumption of instantaneous tunneling-injection into QDs, we have from (A5) and (A7),

$$n_{\mathrm{QW}}^L=n_1^{L,\,\mathrm{QW}}\frac{f_{\mathrm{n}}}{1-f_{\mathrm{n}}}=N_{\mathrm{c}}^{2\mathrm{D}}\frac{f_{\mathrm{n}}}{1-f_{\mathrm{n}}}, \tag{B1}$$

$$p_{\mathrm{QW}}^R=p_1^{R,\,\mathrm{QW}}\frac{f_{\mathrm{p}}}{1-f_{\mathrm{p}}}=N_{\mathrm{v}}^{2\mathrm{D}}\frac{f_{\mathrm{p}}}{1-f_{\mathrm{p}}}. \tag{B2}$$

In (B1) and (B2), eqs. (A16) were used assuming $\varepsilon_{\mathrm{n}}^{L,\,\mathrm{QW}}=\varepsilon_{\mathrm{n}}^{\mathrm{QD}}$ and $\varepsilon_{\mathrm{p}}^{R,\,\mathrm{QW}}=\varepsilon_{\mathrm{p}}^{\mathrm{QD}}$.

With the assumption of instantaneous carrier exchange between the OCL and QW on each side of the structure and using (A12), we have from (A1)-(A4),

$$n_L=\frac{n_1}{N_{\mathrm{c}}^{2\mathrm{D}}}n_{\mathrm{QW}}^L=n_1\frac{f_{\mathrm{n}}}{1-f_{\mathrm{n}}}, \tag{B3}$$

$$p_L=\frac{p_1}{N_{\mathrm{v}}^{2\mathrm{D}}}p_{\mathrm{QW}}^L, \tag{B4}$$

$$p_R = \frac{p_1}{N_{\rm v}^{\rm 2D}} p_{\rm QW}^R = p_1 \frac{f_{\rm p}}{1-f_{\rm p}}, \tag{B5}$$

$$n_R = \frac{n_1}{N_{\rm c}^{\rm 2D}} n_{\rm QW}^R. \tag{B6}$$

We used eq. (B1) in (B3) and eq. (B2) in (B5).

Using (B1)-(B6) in (A22), (A23), (A25), and (A29), we obtain

$$\begin{aligned}\frac{\partial}{\partial t}&\left[\left(\frac{b_1 n_1}{N_{\rm c}^{\rm 2D}}+1\right) N_{\rm c}^{\rm 2D}\frac{f_{\rm n}}{1-f_{\rm n}} + 2N_S f_{\rm n}\right] = \frac{j}{e} \\ &- \left(\frac{b_1 B n_1 p_1}{N_{\rm c}^{\rm 2D} N_{\rm v}^{\rm 2D}} + B_{\rm 2D}\right) N_{\rm c}^{\rm 2D}\frac{f_{\rm n}}{1-f_{\rm n}} p_{\rm QW}^L - N_S \frac{f_{\rm n} f_{\rm p}}{\tau_{\rm QD}} \\ &- c_{\rm g} g^{\max}(f_{\rm n}+f_{\rm p}-1) n_{\rm ph} \\ &- [w_{\rm n,tunn}^R n_1^{R,\,\rm QW} N_S f_{\rm n} - w_{\rm n,tunn}^R N_S (1-f_{\rm n}) n_{\rm QW}^R],\end{aligned} \tag{B7}$$

$$\begin{aligned}\frac{\partial}{\partial t}&\left[\left(\frac{b_1 p_1}{N_{\rm v}^{\rm 2D}}+1\right) p_{\rm QW}^L\right] \\ &= [w_{\rm p,tunn}^L p_1^{L,\,\rm QW} N_S f_{\rm p} - w_{\rm p,tunn}^L N_S (1-f_{\rm p}) p_{\rm QW}^L] \\ &- \left(\frac{b_1 B n_1 p_1}{N_{\rm c}^{\rm 2D} N_{\rm v}^{\rm 2D}} + B_{\rm 2D}\right) N_{\rm c}^{\rm 2D}\frac{f_{\rm n}}{1-f_{\rm n}} p_{\rm QW}^L,\end{aligned} \tag{B8}$$

$$\begin{aligned}\frac{\partial}{\partial t}&\left[\left(\frac{b_2 n_1}{N_{\rm c}^{\rm 2D}}+1\right) n_{\rm QW}^R\right] \\ &= [w_{\rm n,tunn}^R n_1^{R,\,\rm QW} N_S f_{\rm n} - w_{\rm n,tunn}^R N_S (1-f_{\rm n}) n_{\rm QW}^R] \\ &- \left(\frac{b_2 B n_1 p_1}{N_{\rm c}^{\rm 2D} N_{\rm v}^{\rm 2D}} + B_{\rm 2D}\right) N_{\rm v}^{\rm 2D}\frac{f_{\rm p}}{1-f_{\rm p}} n_{\rm QW}^R,\end{aligned} \tag{B9}$$

$$\begin{aligned}&\left(\frac{b_1 n_1}{N_{\rm c}^{\rm 2D}}+1\right) N_{\rm c}^{\rm 2D}\frac{f_{\rm n}}{1-f_{\rm n}} + 2N_S f_{\rm n} + \left(\frac{b_2 n_1}{N_{\rm c}^{\rm 2D}}+1\right) n_{\rm QW}^R \\ &= \left(\frac{b_2 p_1}{N_{\rm v}^{\rm 2D}}+1\right) N_{\rm v}^{\rm 2D}\frac{f_{\rm p}}{1-f_{\rm p}} + 2N_S f_{\rm p} + \left(\frac{b_1 p_1}{N_{\rm v}^{\rm 2D}}+1\right) p_{\rm QW}^L.\end{aligned} \tag{B10}$$

Using eq. (B10), we can express $n_{\rm QW}^R$ in terms of $p_{\rm QW}^L$, $f_{\rm p}$, and $f_{\rm n}$ as follows:

$$\begin{aligned}n_{\rm QW}^R = \frac{1}{\frac{b_2 n_1}{N_{\rm c}^{\rm 2D}}+1}&\left\{\left(\frac{b_1 p_1}{N_{\rm v}^{\rm 2D}}+1\right) p_{\rm QW}^L \right. \\ &+ \left[\left(\frac{b_2 p_1}{N_{\rm v}^{\rm 2D}}+1\right) N_{\rm v}^{\rm 2D}\frac{f_{\rm p}}{1-f_{\rm p}} + 2N_S f_{\rm p}\right] \\ &\left. - \left[\left(\frac{b_1 n_1}{N_{\rm c}^{\rm 2D}}+1\right) N_{\rm c}^{\rm 2D}\frac{f_{\rm n}}{1-f_{\rm n}} + 2N_S f_{\rm n}\right]\right\}.\end{aligned} \tag{B11}$$

Eqs. (B7)-(B9) [wherein $n_{\rm QW}^R$ is given by (B11)] and eq. (A11) present four equations for finding four unknowns $p_{\rm QW}^L$, $f_{\rm p}$, $f_{\rm n}$, and $n_{\rm ph}$.

We can still further simplify our consideration assuming electron-hole symmetry. In such a case, in particular,

$$w_{\rm n,\,tunn}^R = w_{\rm p,\,tunn}^L, \tag{B12}$$

$$n_1^{R,\,\rm QW} = p_1^{L,\,\rm QW}, \tag{B13}$$

$$f_{\rm n} = f_{\rm p}, \tag{B14}$$

$$n_{\rm QW}^R = p_{\rm QW}^L. \tag{B15}$$

Let us denote the out-tunneling coefficients $w_{\rm n,\,tunn}^R = w_{\rm p,\,tunn}^L$ by $w_{\text{out-tunn}}$, the minority carrier densities $n_{\rm QW}^R = p_{\rm QW}^L$ in the foreign QWs by $F_{\rm QW}$, and the parameters $n_1^{R,\,\rm QW} = p_1^{L,\,\rm QW}$ by $F_1^{\rm QW}$. The parameter $F_1^{\rm QW}$ can be written as [see (A16)]

$$F_1^{\rm QW} = N_{\rm c}^{\rm 2D} \exp\left(-\frac{\Delta}{T}\right), \tag{B16}$$

where $\Delta = \varepsilon_{\rm n}^{\rm QW} - \varepsilon_{\rm n}^{\rm QD}$ is the offset energy between the subband edge in the foreign QW and the level in a QD (Fig. 6).

Equations (B8) and (B9) will now coincide and we will have from (B7), (B8), and (A11) the set (1)-(3) of three rate equations for finding $f_{\rm n}$, $F_{\rm QW}$, and $n_{\rm ph}$.

REFERENCES

[1] P. S. Zory, Jr., *Quantum Well Lasers*. Boston, MA, USA: Academic, 1993.

[2] E. Kapon, *Semiconductor Lasers: Fundamentals*. New York, NY, USA: Academic, 1999.

[3] L. V. Asryan and R. A. Suris, "Inhomogeneous line broadening and the threshold current density of a semiconductor quantum dot laser," *Semicond. Sci. Technol.*, vol. 11, no. 4, pp. 554–567, Apr. 1996.

[4] L. V. Asryan and R. A. Suris, "Characteristic temperature of quantum dot laser," *Electron. Lett.*, vol. 33, no. 22, pp. 1871–1872, Oct. 1997.

[5] L. V. Asryan, S. Luryi, and R. A. Suris, "Intrinsic nonlinearity of the light–current characteristic of semiconductor lasers with a quantum-confined active region," *Appl. Phys. Lett.*, vol. 81, no. 12, pp. 2154–2156, Sep. 2002.

[6] L. V. Asryan and S. Luryi, "Tunneling-injection quantum-dot laser: Ultrahigh temperature stability," *IEEE J. Quantum Electron.*, vol. 37, no. 7, pp. 905–910, Jul. 2001.

[7] L. V. Asryan and S. Luryi, "Temperature-insensitive semiconductor quantum dot laser," *Solid-State Electron.*, vol. 47, no. 2, pp. 205–212, Feb. 2003.

[8] L. V. Asryan and S. Luryi, "Semiconductor laser with reduced temperature sensitivity," U.S. Patent 6 870 178 B2, Mar. 22, 2005.

[9] T. Chung, G. Walter, and N. Holonyak, Jr., "Coupled strained-layer InGaAs quantum-well improvement of an InAs quantum dot AlGaAs–GaAs–InGaAs–InAs heterostructure laser," *Appl. Phys. Lett.*, vol. 79, no. 27, pp. 4500–4502, Dec. 2001.

[10] G. Walter, T. Chung, and N. Holonyak, Jr., "High-gain coupled InGaAs quantum well InAs quantum dot AlGaAs–GaAs–InGaAs–InAs heterostructure diode laser operation," *Appl. Phys. Lett.*, vol. 80, no. 7, pp. 1126–1128, Feb. 2002.

[11] G. Walter, T. Chung, and N. Holonyak, Jr., "Coupled-stripe quantum-well-assisted AlGaAs–GaAs–InGaAs–InAs quantum-dot laser," *Appl. Phys. Lett.*, vol. 80, no. 17, pp. 3045–3047, Apr. 2002.

[12] P. K. Kondratko, S.-L. Chuang, G. Walter, T. Chung, and N. Holonyak, Jr., "Observations of near-zero linewidth enhancement factor in a quantum-well coupled quantum-dot laser," *Appl. Phys. Lett.*, vol. 83, no. 23, pp. 4818–4820, Dec. 2003.

[13] Y. Arakawa, "Fabrication of quantum wires and dots by MOCVD selective growth," *Solid-State Electron.*, vol. 37, nos. 4–6, pp. 523–528, 1994.

[14] K. Kamath, D. Klotzkin, and P. Bhattacharya, "Small-signal modulation characteristics of self-organized quantum dot separate confinement heterostructure and tunneling injection lasers," in *Proc. IEEE LEOS 10th Annu. Meeting*, vol. 2, Nov. 1997, pp. 498–499.

[15] P. Bhattacharya *et al.*, "High-speed tunnel-injection quantum well and quantum dot lasers," *Proc. SPIE*, vol. 3283, pp. 702–709, Jul. 1998.

[16] P. Bhattacharya and S. Ghosh, "Tunnel injection $In_{0.4}Ga_{0.6}As$/GaAs quantum dot lasers with 15 GHz modulation bandwidth at room temperature," *Appl. Phys. Lett.*, vol. 80, no. 19, pp. 3482–3484, May 2002.

[17] Y. Qiu, D. Uhl, R. Chacon, and R. Q. Yang, "Lasing characteristics of InAs quantum-dot lasers on (001) InP substrate," *Appl. Phys. Lett.*, vol. 83, no. 9, pp. 1704–1706, Apr. 2003.

[18] V. Tokranov, M. Yakimov, J. van Eisden, and S. Oktyabrsky, "Tunnel quantum well-on-dots InGaAs-InAs high-gain medium for laser diodes," *Proc. SPIE*, vol. 6129, Feb. 2006, Art. no. 612908.

[19] A. A. George, P. M. Smowton, Z. Mi, and P. Bhattacharya, "Long wavelength quantum-dot lasers selectively populated using tunnel injection," *Semicond. Sci. Technol.*, vol. 22, no. 5, pp. 557–560, May 2007.

[20] W. Rudno-Rudziński *et al.*, "Room temperature free carrier tunneling in dilute nitride based quantum well-quantum dot tunnel injection system for 1.3 μm," *Appl. Phys. Lett.*, vol. 94, no. 17, 2009, Art. no. 171906.

[21] E.-M. Pavelescu, C. Gilfert, J. P. Reithmaier, A. Martin-Minguez, and I. Esquivias, "High-power tunnel-injection 1060-nm InGaAs–(Al)GaAs quantum-dot lasers," *IEEE Photon. Technol. Lett.*, vol. 21, no. 14, pp. 999–1001, Jul. 15, 2009.
[22] D. Gready and G. Eisenstein, "Carrier dynamics in tunneling injection quantum dot lasers," *IEEE J. Quantum Electron.*, vol. 46, no. 11, pp. 1611–1618, Nov. 2010.
[23] D. Gready and G. Eisenstein, "Effects of homogeneous and inhomogeneous broadening on the dynamics of tunneling injection quantum dot lasers," *IEEE J. Quantum Electron.*, vol. 47, no. 7, pp. 944–949, Jul. 2011.
[24] W. Rudno-Rudziński *et al.*, "Carrier wavefunction control in a dilute nitride-based quantum well—A quantum dot tunnel injection system for 1.3 μm emission," *Semicond. Sci. Technol.*, vol. 26, no. 8, 2011, Art. no. 085004.
[25] W. Rudno-Rudziński, G. Sęk, J. Andrzejewski, J. Misiewicz, F. Lelarge, and B. Rousseau, "Electronic structure and optical properties of 1.55 μm emitting InAs/InGaAsP quantum dash tunnel injection structures," *Semicond. Sci. Technol.*, vol. 27, no. 10, 2012, Art. no. 105015.
[26] M. T. Crowley, N. A. Naderi, H. Su, F. Grillot, and L. F. Lester, "GaAs-based quantum dot lasers," in *Advances in Semiconductor Lasers* (Semiconductors and Semimetals), vol. 86. San Diego, CA, USA: Elsevier, 2012, pp. 371–417, ch. 10, doi: 10.1016/B978-0-12-391066-0.00010-1.
[27] S. Bhowmick, M. Z. Baten, T. Frost, B. S. Ooi, and P. Bhattacharya, "High performance InAs/$In_{0.53}Ga_{0.23}Al_{0.24}As$/InP quantum dot 1.55$\mu$m tunnel injection laser," *IEEE J. Quantum Electron.*, vol. 50, no. 1, pp. 7–14, Jan. 2014.
[28] A. Mielnik-Pyszczorski, K. Gawarecki, and P. Machnikowski, "Phonon-assisted tunneling of electrons in a quantum well/quantum dot injection structure," *Phys. Rev. B, Condens. Matter*, vol. 91, no. 19, 2015, Art. no. 195421.
[29] J. Andrzejewski, "Electronic structure calculations of InP-based coupled quantum dot-quantum well structures," *Acta Phys. Polonica A*, vol. 129, no. 1-A, pp. A-97–A-99, 2016.
[30] P. Podemski, R. Kudrawiec, J. Misiewicz, A. Somers, J. P. Reithmaier, and A. Forchel, "On the tunnel injection of excitons and free carriers from In0.53Ga0.47As/In0.53Ga0.23Al0.24As quantum well to InAs/In0.53Ga0.23Al0.24As quantum dashes," *Appl. Phys. Lett.*, vol. 89, no. 6, Art. no. 061902, 2006.
[31] G. Sęk *et al.*, "Experimental evidence on quantum well–quantum dash energy transfer in tunnel injection structures for 1.55μm emission," *Appl. Phys. Lett.*, vol. 90, no. 8, 2007, Art. no. 081915.
[32] W. Rudno-Rudziński *et al.*, "Carrier delocalization in InAs/InGaAlAs/InP quantum-dash-based tunnel injection system for 1.55 μm emission," *AIP Adv.*, vol. 7, no. 1, Jan. 2017, Art. no. 015117.
[33] V. G. Talalaev *et al.*, "Light-emitting tunneling nanostructures based on quantum dots in a Si and GaAs matrix," *Semiconductors*, vol. 46, no. 11, pp. 1460–1470, Nov. 2012.
[34] K. Lüdge and E. Schöll, "Current instabilities in resonant tunneling quantum dot structures," *AIP Conf. Proc.*, vol. 893, no. 1, p. 835, May 2007.
[35] A. R. Adams *et al.*, "Semiconductor quantum well lasers with a temperature-insensitive threshold current," *IEEE J. Sel. Topics Quantum Electron.*, vol. 21, no. 6, Nov./Dec. 2015, Art. no. 1500806.
[36] D.-S. Han and L. V. Asryan, "Tunneling-injection of electrons and holes into quantum dots: A tool for high-power lasing," *Appl. Phys. Lett.*, vol. 92, no. 25, Jun. 2008, Art. no. 251113.
[37] D.-S. Han and L. V. Asryan, "Output power of a double tunneling-injection quantum dot laser," *Nanotechnology*, vol. 21, no. 1, Jan. 2010, Art. no. 015201.
[38] D.-S. Han and L. V. Asryan, "Characteristic temperature of a tunneling-injection quantum dot laser: Effect of out-tunneling from quantum dots," *Solid-State Electron.*, vol. 52, no. 10, pp. 1674–1679, Oct. 2008.
[39] L. V. Asryan, "Spontaneous radiative recombination and nonradiative Auger recombination in quantum-confined heterostructures," *Quantum Electron.*, vol. 35, no. 12, pp. 1117–1120, Dec. 2005.
[40] G. P. Agrawal, *Long-Wavelength Semiconductor Lasers*. New York, NY, USA: Van Nostrand Reinhold Company, 1986, p. 474.
[41] L. A. Coldren, S. W. Corzine, and M. L. Mashanovitch, *Diode Lasers and Photonic Integrated Circuits*. New York, NY, USA: Wiley, 1995, p. 594.
[42] S. L. Chuang, *Physics of Photonic Devices*, 2nd ed. New York, NY, USA: Wiley, 2009.
[43] L. V. Asryan and R. A. Suris, "Spatial hole burning and multimode generation threshold in quantum-dot lasers," *Appl. Phys. Lett.*, vol. 74, no. 9, pp. 1215–1217, Mar. 1999.
[44] L. V. Asryan and R. A. Suris, "Upper limit for the modulation bandwidth of a quantum dot laser," *Appl. Phys. Lett.*, vol. 96, no. 22, May 2010, Art. no. 221112.
[45] L. V. Asryan, "Modulation bandwidth of a double tunnelling-injection quantum dot laser," *Semicond. Sci. Technol.*, vol. 30, no. 3, Mar. 2015, Art. no. 035022.
[46] L. V. Asryan, "Effect of pumping delay on the modulation bandwidth in double tunneling-injection quantum dot lasers," *Opt. Lett.*, vol. 42, no. 1, pp. 97–100, Jan. 2017.

Levon V. Asryan (M'04–SM'05) received the Ph.D. and D.Sc. degrees in physics and mathematics from the Ioffe Institute of Physics and Technology, Saint Petersburg, Russia.

He was with the Ioffe Institute of Physics and Technology and the State University of New York at Stony Brook, USA. He is currently a Professor with the Virginia Polytechnic Institute and State University. His research interests include the physics of semiconductors, nano- and optoelectronics, photonics, and the theory of semiconductor lasers with a low-dimensional active region.

Dr. Asryan was a recipient of the Highest Award of the Russian Federation (State Prize) in Science and Technology for the year 2001 for his contributions to fundamental investigations of heterostructures with quantum dots and development of quantum dot lasers and the first IEEE JOURNAL OF QUANTUM ELECTRONICS Best Paper Award for his work on quantum dot lasers.

Saurav Kar received the B.S. degree from the National Institute of Technology, Durgapur, India, in 2015. He is currently a Graduate Student at the Virginia Polytechnic Institute and State University.

Theoretical Study of Semiconductor Quantum Dot Lasers with Asymmetric Barrier Layers

John L. Monk III

Thesis submitted to the faculty of the

Virginia Polytechnic Institute and State University

in partial fulfillment of the requirements for the degree of

Master of Science

In

Materials Science and Engineering

Levon V. Asryan, Chair

Giti A. Khodaparast

William T. Reynolds

April 29th, 2020

Blacksburg, Virginia

Keywords: quantum dot lasers, semiconductor lasers

Theoretical Study of Semiconductor Quantum Dot Lasers with Asymmetric Barrier Layers

Jack Monk

ABSTRACT

Small-signal dynamic response of semiconductor quantum dot (QD) lasers with asymmetric barrier layers was studied. Semiconductor lasers are used in many communication systems. Fiber optic communication systems use semiconductor lasers in order to transmit information. DVD and Blu-ray disk players feature semiconductor lasers as their readout source. Barcode readers and laser pointers also use semiconductor lasers. A medical application of semiconductor lasers is for minor soft tissue procedures. Semiconductor lasers are also used to pump solid-state and fiber lasers. Semiconductor lasers are able to transmit telephone, internet, and television signals through fiber optic cables over long distances. The amount of information able to be transferred is directly related to the bandwidth of the laser. By introducing asymmetric barrier layers, the modulation bandwidth of the laser will improve, allowing for more information to be transferred. Also, by introducing asymmetric barrier layers, the output power will be unrestricted, meaning as more current is applied to the system, the laser will get more powerful. An optimum pumping current was found which maximized modulation bandwidth at -3dB, and is lower in QD lasers with asymmetric barrier layers (ABL) as opposed to conventional QD lasers. Modulation bandwidth was found to increase with cross section of carrier capture before reaching an asymptote. Both surface density of QDs and cavity length had optimum values which

maximized modulation bandwidth. Relative QD size fluctuation was considered in order to see how variation in QD sizes effects the modulation bandwidth of the semiconductor QD laser with ABLs. These calculations give a good starting point for fabricating semiconductor QD lasers with ABLs featuring the largest modulation bandwidth possible for fiber optic communication systems.

In semiconductor QD lasers, the electrons and holes may be captured into excited states within the QDs, rather than the ground state. The particles may also jump from the ground state up to an excited state, or drop from the excited state to the ground state. Recombination of electron-hole pairs can occur from the ground state to the ground state or from an excited state to an excited state. In the situation if the capture of charge carriers into the ground state in QDs takes place via the excited-state, then this two-step capture process makes the output power from ground-state lasing to saturate in conventional QD lasers. By using ABLs in the QD laser, it is predicted that the output power of ground-state lasing will continue to rise with applied current, as the ABLs will stop the electrons and holes from recombining in the optical confinement layer. Thus, ABL QD lasers will be able to be used in applications that require large energy outputs.

Theoretical Study of Semiconductor Quantum Dot Lasers with Asymmetric Barrier Layers

Jack Monk

GENERAL AUDIENCE ABSTRACT

Semiconductor lasers (also known as diode lasers) have been used in numerous applications ranging from communication to medical applications. Among all applications of diode lasers, of particular importance is their use for high speed transmission of information and data in fiber optic communication systems. This is accomplished by direct conversion of the diode laser input (electrical current) to its output (optical power). Direct modulation of the laser optical output through varying electrical current helps cut costs by not requiring other expensive equipment in order to perform modulation.

The performance of conventional semiconductor lasers suffers from parasitic recombination outside of the active region – an unwanted process that consumes a considerable fraction of the laser input (injection current) while not contributing to the useful output and thus damaging its performance.

Asymmetric barrier layers were proposed as a way to suppress parasitic recombination in semiconductor lasers. In this study, the optimal conditions for semiconductor quantum dot lasers with asymmetric barrier layers were calculated in order to maximize their modulation bandwidth – the parameter that determines the highest speed of efficient information transmission. This

includes finding the optimal values of the dc component of the pump current, quantum dot surface density and size fluctuations, and cavity length. As compared to conventional quantum dot lasers, the optimal dc current maximizing the modulation bandwidth is shown to be considerably lower in quantum dot lasers with asymmetric barrier layers thus proving their outperforming efficiency.

In the presence of extra states in quantum dots in conventional lasers, the optical output of needed ground-state lasing may be heavily impacted – it may remain almost unchanged with increasing the laser input current. As opposed to conventional lasers, the output power of ground-state lasing in devices with asymmetric barrier layers will continue growing as more input current is applied to the system.

Acknowledgments

I would like to give a sincere thank you to the following individuals for their support and encouragement throughout my Ph.D. course:

- My wonderful advisor, Dr. Levon Asryan, for all his guidance and support throughout my time working with him. No words would adequately describe his influence both professionally and personally, so I will simply say thank you.
- Dr. Giti Khodaparast and Dr. William Reynolds for taking the time to be on my committee. Their courses and guidance have proven instrumental in extending my knowledge in both physics and materials science.

I would like to thank the United States Army Research Office (Grant No. W911NF-17-1-0432) for funding this work.

I would also like to thank all the members of the MSE Department and my friends that I have made during my time at Virginia Tech. None of this would have happened without you all.

I would of course like to thank my fiancé, Samantha Drewry, for her love, patience, encouragement, and understanding. I look forward to many more adventures with you.

I would be amiss to not thank my wonderful mother, grandmother, and sister; whose love, support, encouragement and belief have never failed.

I would finally like to thank my grandfather, John L Monk Sr., and my father John L. Monk Jr. I have looked up to you both all my life, and would not be the man I am today without you both. I am proud to be the third.

Table of Contents

List of Figures

Chapter 1. Introduction

Semiconductor lasers, also known as laser diodes or diode lasers, are used for a variety of applications, such as laser printers, bar-code readers, and laser pointers. Semiconductor lasers use p-n junctions, commonly used in semiconductor devices, to achieve lasing. Semiconductor lasers feature direct modulation through a varying electrical current, helping cut costs by not requiring other expensive equipment in order to perform modulation. Because of this, these lasers are also used in high-speed fiber optic communication systems as transmitters that are able to convert input electrical signal to output optical signal.

The ability to control the semiconductor material conductivity through doping with various impurities and the carrier injection opened the doors to semiconductor electronics development.

Heterostructure development allowed the control of fundamental parameters within semiconductor devices and crystals, including band gaps and refractive indices. Semiconductor heterostructure based devices include laser-based communication systems and light-emitting diodes (LED's).

Semiconductor lasers operate using stimulated emission, where one incoming photon stimulates the emission of a second photon through recombination of an electron-hole pair. Figure 1 shows a schematic of the interaction between light and matter. When an incident photon enters a semiconductor, it may be absorbed by an electron in the valence band, and excite the electron. This excited electron will then jump up into the conduction band, leaving behind a positively charged hole in its stead. Thus, the electron-hole pair is generated [Fig. 1 (a)].

Electron-hole pairs may recombine with no external influence, in a process called spontaneous emission, as shown in Fig. 1 (b). The emitted photons from spontaneous emission are at different phases with random direction. When recombination is stimulated by an incident photon [Fig 1 (c)], the emitted photon from the electron-hole recombination has the same wavelength, phase, and direction of propagation as the incident photon. This process is called stimulated emission, and emits coherent photons.

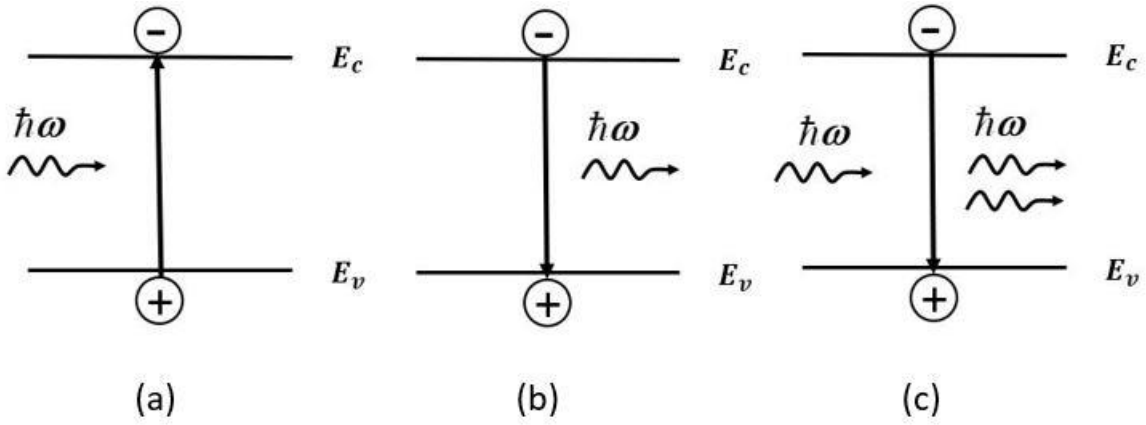

Fig. 1. Schematic illustration of (a) excitation of an electron from the valence band to the conduction band through absorption of a photon, (b) spontaneous emission of a photon, and (c) stimulated emission by an incident photon.

In semiconductors under thermal equilibrium, the electron distribution follows the Fermi-Dirac statistics and the lower energy levels are more populated than the higher energy levels of the semiconductor. Thusly, the photon absorption process is dominant and no coherent light is emitted. In order for lasing to occur, the stimulated emission of photons must overtake the photon absorption process of the semiconductor. Therefore, pumping is required to make the

upper energy level of the semiconductor more populated than the lower one, creating a population inversion. This allows the optical gain and amplification of electro-magnetic radiation to be established. Thus, a laser is created (Light Amplification by Stimulated Emission of Radiation).

The first studies on semiconductor lasers were performed in the early 1960s [1-3]. In 1964, the first electrically operated semiconductor laser was created by Hall [4]. Hall's design operated at 77K, and was based upon a GaAs p-n junction. Also in 1964, other groups managed to obtain lasing in semiconductor in both visible and infrared light ranges [5,6]. These homojunction structures were created using p-n junctions composing of the same semiconductor material, and featured poor lasing efficiencies and suffered additionally from high threshold current density. They also suffered from high optical and electrical loss. These early homojunction lasers were unable to achieve lasing outside of cryogenic temperatures.

In 1963, the first double-heterostructure (DHS) laser was conceptualized [7, 8]. By 1970, the first double heterostructure laser was demonstrated [9-11]. These double heterostructure lasers were shown to operate continuously at room temperature and had a lower threshold current density than previously designed homojunction lasers. Due to the separate confinement of carriers and photons in DHS lasers, the lasing threshold was lowered significantly and continuous wave operation at room temperature became possible [12]. The double heterostructures lasers also allowed the emitted surface to be enlarged and new materials to be used.

In conventional diode lasers, lasing is achieved through recombination of electrons and holes in the active region located in the center of the optical confinement layer (OCL). The OCL

confines photons emitted in the active region: due to the fact that the OCL refractive index is higher than that of the cladding layers, a waveguide is created, and confines the emitted photons within the OCL effectively.

The electrons and holes are injected into the OCL from cladding layers on opposite sides of the OCL. They are then transported into the active region, and recombine there. The electron-hole pairs that recombine in the active region output photons of a desired energy. The active region bandgap dictates the energy of the output photon.

In quantum well (QW), quantum wire (QWR), and QD lasers, the quantum-confined region is embedded into the OCL. The electrons first enter the OCL, then get captured into the active region. By using low dimensional active region, the laser performance is improved, compared with bulk laser performance. Emitted photon wavelength is tunable by changing the thickness of the low-dimensional active layer, in addition to changing the composition and material used in the active layer.

Bulk material was used in the active region of early heterostructure lasers, which allowed the carriers freedom to wander in three dimensions. This limited the operation of the laser. By shrinking the active region to a size comparable to the de Broglie wavelength of the carrier, the carrier becomes quantum confined in the active region and has a discrete energy spectrum. The classification of the laser is based on the number of degrees of freedom of the carrier in the active region: 2 (quantum well), 1 (quantum wire), or 0 (quantum dot).

Thermal spreading of carriers over multiple energy states causes the threshold current temperature dependence in bulk lasers. In QW lasers, the density of states is a step-function, shown in Fig. 3. (b) [13]. This limits thermal spreading, as opposed to bulk lasers (Fig. 3. (a)). QWR

lasers further suppress the temperature effect of thermal spreading due to the density of states taking the form of a decreasing function of energy (Fig. 3. (c)). QDs ideally cause thermal spreading of carriers to disappear, since the density of states in QDs is a delta-function, and there are no additional available states for carriers to move to through thermal spreading, as shown in Fig. 3. (d).

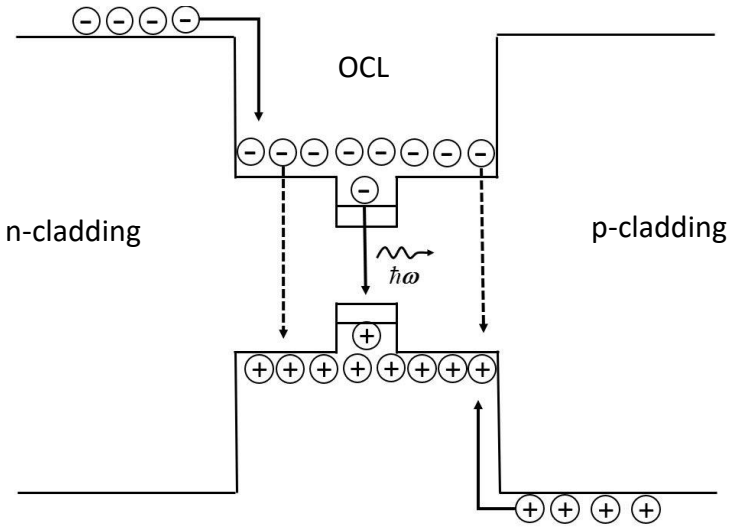

Fig. 2. A conventional quantum dot laser. Solid arrow shows recombination in the active region. Dashed arrows show recombination in the OCL (parasitic recombination).

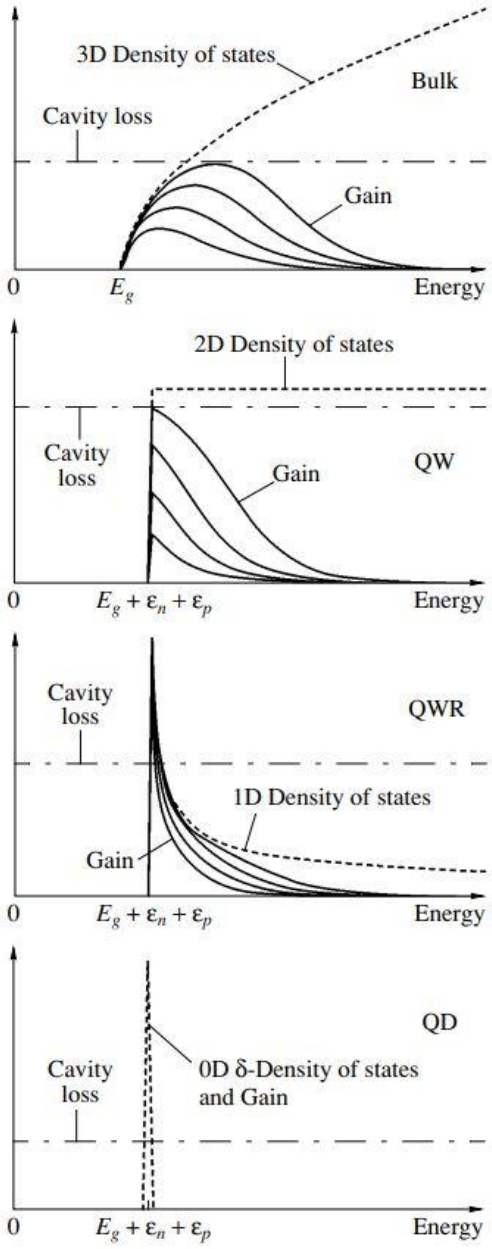

Fig. 3. Modification of the density of states and the shape of the gain spectrum with decreasing dimensionality of the active region. [13] (Reprinted by permission from Springer Nature) Springer Semiconductors L.V. Asryan and R.A. Suris, "Theory of threshold characteristics of semiconductor quantum dot lasers," Semicond., vol. 38, no. 1, pp. 1-22, Jan. 2004.

Because of the compact size and direct modulation of the emitted power through alternating electric current capabilities, semiconductor lasers are commonly used in high-speed communication systems. The semiconductor laser acts as a transmitter, converting electrical signal to optical, as shown in Figure 4. The directly-modulating bias current input signal causes the following changes in laser optical output power, and transmits information through this process. In light wave communication systems, the modulation bandwidth is the highest frequency at which the modulation continues to be efficient, which directly determines the amount of information that can be transmitted per unit time. Thus, the response of semiconductor lasers to alternating pumping current is critical for successful application in high-speed communication systems.

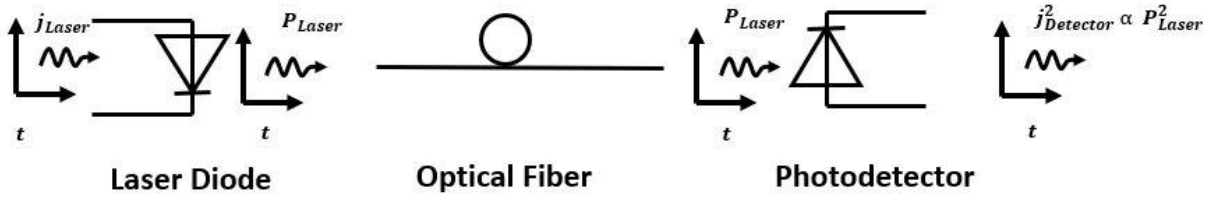

Fig. 4. Schematic diagram of a basic optical fiber communication system.

Several factors may limit the modulation bandwidth of the semiconductor QD laser. In an ideal QD laser, all the QDs would be identical in shape and size, and the density of states would appear as a delta-function. However, when fabricating QDs, there are inherent size and shape fluctuations, which can alter the QDs behaviors [14]. The size fluctuations lead to varying energies of electrons and holes, which leads to inhomogeneous broadening of the gain spectrum and to

the maximum modal gain decrease [15]. At a certain maximum inhomogeneous broadening, the lasing is no longer achievable in QD lasers [15]; the modulation bandwidth is zero at this point.

While carrier capture into the quantum-confined active region should be ideally instantaneous, in reality it is not instantaneous [15-17]. Because stimulated emission is produced by the carriers confined in QDs, the carrier capture cross-section applies a massive effect on the QD laser dynamics. In conventional semiconductor QD lasers, the carrier capture delay from the OCL into the QDs largely reduces the laser modulation bandwidth.

In conventional lasers, electrons can easily go beyond the active region and end up in the OCL on the side where the holes entered the system. Holes mirror the electrons, and will also escape the active region into the OCL on the opposite side of the active region. Electron-hole pairs that recombine in the OCL outside the active region also output a photon, but of an undesired wavelength. This is called parasitic electron-hole recombination, and is detrimental to the laser characteristics of the system, sapping power and introducing noise in the optical output signal. This is shown as the dashed arrows in Fig 2.

Asymmetric barrier layers (ABLs) were proposed [18,19] as a way to suppress parasitic recombination in semiconductor lasers, and are shown in figure 5. Asymmetric barrier layers feature a shorter wall before electrons (holes) enter the active region, and a much taller wall after the active region. This assures that the electrons, and thusly the holes, will be unable to escape the active region and cause parasitic recombination in the OCL to occur. In [20], a theoretical model for the threshold and power characteristics of ABL QD lasers was developed.

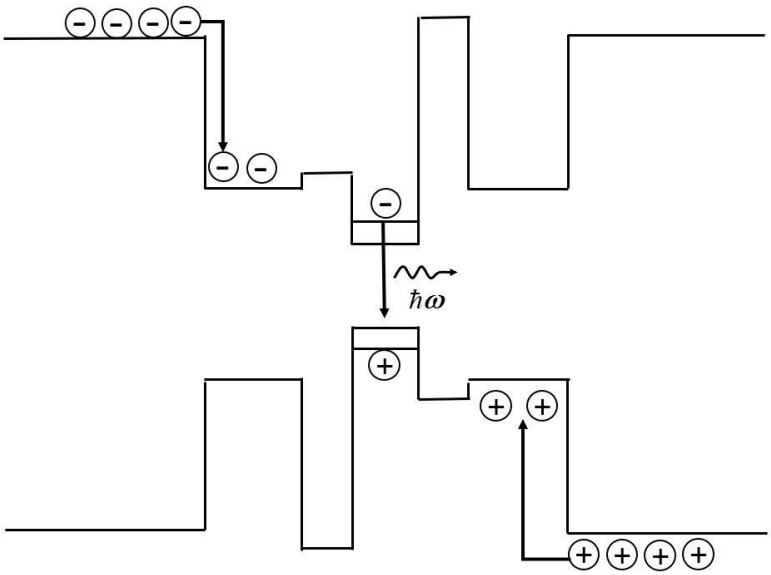

Fig. 5. Quantum dot laser with asymmetric barrier layers.

In this work, a semiconductor QD laser with ABLs was modeled, and the effects of applied current, carrier capture cross section, and the parameters of the laser structure were investigated with regards to modulation bandwidth. The effects of relative QD size fluctuation on modulation bandwidth was also investigated.

Ideally, only one electron (and hole) energy level should exist in a QD. In actual QDs containing excited states in addition to the ground state, it is possible for a carrier to be captured into an excited state, rather than the ground state. Should the carrier capture into the QD ground-state be excited-state-mediated, the ground-state lasing power will eventually reach an asymptotic value rather than continues to increase with increasing pump current in a conventional QD lasers. In this study, QD lasers with ABLs were modeled to investigate how ABLs effect the output power of ground-state lasing in the case of the carrier capture into the QD ground-state again being excited-state-mediated.

While there has been no experimental work on QD lasers with ABLs so far, there is an ongoing experimental and theoretical activity on QW lasers with ABLs.

In [21, 22], a QW laser with ABLs was fabricated for the first time. The QW material was GaAs and the OCL material was $Al_{0.2}Ga_{0.8}As$. The lasing wavelength was 835.6 nm. The material of the ABL on the n-side of the structure was $Ga_{0.55}In_{0.45}P$ and that on the p-side – $Al_{0.42}Ga_{0.36}In_{0.22}As$. Already in this first experimental ABL QW laser, a reduced and less temperature-sensitive threshold current was achieved as compared to a reference QW laser (a laser without ABLs that was otherwise similar to the laser with the ABLs).

In [23, 24], for the ABL QW laser of the same material composition as in [21, 22, 25], improved power characteristics were observed as compared to a reference structure: the light-current characteristic was more linear, the slope and wall-plug efficiencies were higher, and the maximum output optical power was obtained at a lower pump current.

In [26], using the method of scanning near-field optical microscopy, it was directly observed that the luminescence associated with the parasitic recombination in the OCL was less intense in the ABL QW laser as compared to the reference laser.

It is assumed in this study that the ABLs function ideally, i.e., the ABL on the n-side of the OCL completely blocks the hole transport (both by tunneling and over the barrier) to that side of the structure while not affecting the electron injection into the QDs. Similarly, the ABL on the p-side of the OCL is assumed to completely block the electron transport (both by tunneling and over the barrier) to that side of the structure while not affecting the hole injection into the QDs. It should be noted here that a rigorous study of the candidate materials for the ABLs will be needed for a proper design of experimental QD lasers with ABLs blocking the transport of foreign

carriers to an extent that will be sufficient for a considerable suppression of the parasitic recombination in the OCL. That study should particularly focus on the search for the materials compositions providing a low conduction band offset and a high valence band offset on the n-side of the structure and a low valence band offset and a high conduction band offset on the p-side. That study is beyond the scope of this work. For QW lasers with the ABLs, such a study has been performed in [27]–[30].

The present-day commercial diode lasers use QWs as their active region. Despite the fact that there has been a remarkable progress in fabricating QD lasers (the progress was largely made possible with the use of the self-assembly technique (the Stranski-Krastanov growth mode) for forming QDs [14, 31, 32]), the conventional QD lasers have not yet superseded the QW lasers in large-scale commercial applications. The QD lasers with properly designed ABLs (so that the parasitic recombination in their OCL is significantly suppressed) possess major advantages both over the conventional QD and QW lasers and hence are a viable candidate for their replacement.

Manuscript in Preparation

[1] J. L. Monk and L. V. Asryan, "Small-signal modulation bandwidth of quantum-dot lasers with asymmetric barrier layers."

Presentation at Conferences

[1] L. V. Asryan and J. L. Monk, "Small-signal dynamic response of quantum-dot lasers with asymmetric barrier layers," International Conf. "SPIE Photonics West", San Francisco, USA, Feb. 4, 2020. Paper no. 11274-25.

Presentation at the seminars at the Department of Materials Science and Engineering at Virginia Polytechnic Institute and State University

[1] J. L. Monk and L. V. Asryan, "Semiconductor quantum dot lasers with asymmetric barrier layers," Oct. 18, 2019.

Chapter 1 Bibliography

[1] N. G. Basov, B. M. Vul and Y. M. Popov, "Quantum-mechanical semiconductor generators and amplifiers of electromagnetic oscillations," Sov. Phys. JETP, vol. 10, pp. 416, 1960.

[2] W. S. Boyle and D. G. Tomas, "Optical maser," U.S. Patent 3 059 117, Oct. 16, 1962.

[3] N. G. Basov, O. N. Krokhin and Y. M. Popov, "Production of negative-temperature states in p-n junctions of degenerate semiconductors," Sov. Phys. JETP, vol. 13, pp. 1320-1321, 1961.

[4] R. N. Hall, G. E. Fenner, J. D. Kingsley, T. J. Soltys and R. O. Carlson, "Coherent Light Emission From GaAs Junctions," Phys. Rev. Lett., vol. 9, no. 9, pp. 366-368, Nov. 1962.

[5] J. N. Holonyak and S. F. Bevacqua, "Coherent (visible) light emission from Ga(As1-xPx) junctions," Appl. Phys. Lett., vol. 1, no. 4, pp. 82-83, Dec. 1962.

[6] M. I. Nathan, W. P. Dumke, G. Burns, J. F. H. Dill and G. Lasher, "Stimulated emission of radiation from GaAs p-n junctions," Appl. Phys. Lett., vol. 1, no. 3, pp. 62-64, Nov. 1962.

[7] Zh. I. Alferov and R. F. Kazarinov, "Semiconductor laser with electric pumping," USSR Patent 181737, Mar. 30, 1963.

[8] H. Kroemer, "Solid state radiation emitters," U.S. Patent 3 309 553, Aug. 16, 1963.

[9] Zh. I. Alferov, V. M. Andreev, D. Z. Garbuzov, Yu. V. Zhilyaev, E. P. Morozov, E. L. Portnoi and V. G. Trofim, "Investigation of influence of AlAs-GaAs heterostructure parameters on laser

threshold current and realization of continuous emission at room temperature," Fiz. Tekh. Poluprovodn., vol. 4, no. 9, pp. 1826-1829, 1970.

[10] I. Hayashi, M. B. Panish, P. W. Foy and S. Sumski, "Junction lasers which operate continuously at room temperature," Appl. Phys. Lett., vol. 17, no. 3, pp. 109-111, Aug. 1970.

[11] M. B. Panish, I. Hayashi and S. Sumski, "Double-heterostructure injection lasers with roomtemperature thresholds as low as 2300 A/cm2," Appl. Phys. Lett., vol. 16, no. 8, pp. 326-327, Apr. 1970.

[12] Zh. I. Alferov, "Nobel Lecture: The double heterostructure concept and its applications in physics, electronics, and technology," Reviews of Modern Physics, vol. 73, no. 3, pp. 767-782, July 2001.

[13] L.V. Asryan and R.A. Suris, "Theory of threshold characteristics of semiconductor quantum dot lasers," Semicond., vol. 38, no. 1, pp. 1-22, Jan. 2004.

[14] D. Leonard, S. Fafard, K. Pond, Y. H. Zhang, J. L. Merz and P. M. Petroff, "Structural and Optical-Properties of Self-Assembled InGaAs Quantum Dots," J Vac Sci Technol B, vol. 12, no. 4, pp. 2516-2520, Jul./Aug. 1994.

[15] L. V. Asryan and R. A. Suris, "Inhomogeneous line broadening and the threshold current density of a semiconductor quantum dot laser," Semicond. Sci. Technol., vol. 11, no. 4, pp. 554-567, Apr. 1996.

[16] L. V. Asryan, S. Luryi and R. A. Suris, "Intrinsic nonlinearity of the light-current characteristic of semiconductor lasers with a quantum-confined active region," Appl. Phys. Lett., vol. 81, no. 12, pp. 2154-2156, Sept. 2002.

[17] L. V. Asryan, S. Luryi and R. A. Suris, "Internal efficiency of semiconductor lasers with a quantum-confined active region," IEEE J. Quantum. Electron., vol. 39, no. 3, pp. 404-418, Mar. 2003.

[18] L.V. Asryan and S. Luryi, "Temperature-insensitive semiconductor quantum dot laser," Solid-State Electron., vol. 47, no. 2, pp. 205-212, Feb. 2003.

[19] L.V. Asryan and S. Luryi, "Semiconductor laser with reduced temperature sensitivity," U.S. Patent No. 6,870,178, Mar. 22, 2005

[20] L. V. Asryan, "Quantum dot lasers with asymmetric barrier layers: Close-to-ideal threshold and power characteristics," Quantum Electron., vol. 49, no. 6, pp. 522-528, June 2019.

[21] A.E. Zhukov, N.V. Kryzhanovskaya, F.I. Zubov, Y.M. Shernyakov, M.V. Maximov, E.S. Semenova, K. Yvind, and L.V. Asryan, “Improvement of temperature-stability in a quantum well laser with asymmetric barrier layers,” Appl. Phys. Lett., vol. 100, no. 2, Art. no. 021107, Jan. 2012.

[22] A.E. Zhukov, L.V. Asryan, Yu.M. Shernyakov, M.V. Maximov, F.I. Zubov, N.V. Kryzhanovskaya, K. Yvind, and E.S. Semenova, “Effect of asymmetric barrier layers in the waveguide region on the temperature characteristics of quantum-well lasers,” Semicond., vol. 46, no. 8, pp. 1027-1031, Aug. 2012.

[23] F.I. Zubov, A.E. Zhukov, Yu.M. Shernyakov, M.V. Maximov, N.V. Kryzhanovskaya, K. Yvind, E.S. Semenova, and L.V. Asryan, “The effect of asymmetric barrier layers in the waveguide region on power characteristics of QW lasers,” Technical Phys. Lett., vol. 41, no. 5, pp. 439-442, May 2015.

[24] F.I. Zubov, M.V. Maximov, Yu.M. Shernyakov, N.V. Kryzhanovskaya, E.S. Semenova, K. Yvind,

L.V. Asryan, and A.E. Zhukov, “Suppression of sublinearity of light–current curve in 850 nm quantum well laser with asymmetric barrier layers,” Electron. Lett., vol. 51, no. 14, pp. 1106-1108, July 2015.

[25] F.I. Zubov, A.E. Zhukov, Yu.M. Shernyakov, M.V. Maximov, E.S. Semenova, and L.V. Asryan, “Diode lasers with asymmetric barriers for 850 nm spectral range: experimental studies of power characteristics,” J. Phys. Conf. Ser., vol. 643, Art. no. 012042, Nov. 2015.

[26] Yu.S. Polubavkina, F.I. Zubov, E.I. Moiseev, N.V. Kryzhanovskaya, M.V. Maximov, E.S. Semenova, K. Yvind, L.V. Asryan, and A.E. Zhukov, “Specific features of waveguide recombination in laser structures with asymmetric barrier layers,” Semicond., vol. 51, no. 2, pp. 254-259, Feb. 2017.

[27] L.V. Asryan, N.V. Kryzhanovskaya, M.V. Maximov, A.Yu. Egorov, and A.E. Zhukov, "Bandedge-engineered quantum well laser," Semicond. Sci. Technol., vol. 26, no. 5, Art. no. 055025, 8 pages, May 2011.

[28] F.I. Zubov, M.E. Muretova, L.V. Asryan, E.S. Semenova, M.V. Maximov, and A.E. Zhukov, “Feasibility study for Al-free 808 nm lasers with asymmetric barriers suppressing waveguide recombination,” J. Appl. Phys., vol. 124, no. 13, Art. no. 133105, 8 pages, Oct. 2018.

[29] F.I. Zubov, M.E. Muretova, L.V. Asryan, E.S. Semenova, M.V. Maximov, V.V. Korenev, A.V. Savelyev, and A.E. Zhukov, “A search for asymmetric barrier layers for 1550 nm Al-free diode lasers,” Semicond., vol. 52, no. 14, pp. 1905-1908, Dec. 2018.

[30] F.I. Zubov, M.E. Muretova, A.S. Payusov, M.V. Maximov, A.E. Zhukov, and L.V. Asryan, “Parasitic recombination in a laser with asymmetric barrier layers,” Semicond., vol. 54, no. 3, pp. 296-303, Mar. 2020.

[31] A.Yu. Egorov, A. E. Zhukov, P. S. Kop'ev, N. N. Ledentsov, M. V. Maksimov, and V. M. Ustinov, "Effect of deposition conditions on the formation of (In,Ga)As quantum clusters in a GaAs matrix," Semicond., vol. 28, no. 8, pp. 809-811, Aug. 1994.

[32] G. T. Liu, A. Stintz, H. Li, K. J. Malloy, and L. F. Lester, "Extremely low room-temperature threshold current density diode lasers using InAs dots in $In_{0.15}Ga_{0.85}As$ quantum well," Electron. Lett., vol. 35, no. 14, pp. 1163–1165, Jul. 1999.

Chapter 2. Modulation Bandwidth of Semiconductor Quantum Dot Lasers with Asymmetric Barrier Lasers.

By modifying the conduction and valence bandedges of the semiconductor QD laser, asymmetric barrier layers can be created on each side of the active region (Fig.5). These will prevent electrons and holes from escaping the active region and entering the wrong side of the OCL. We assume that the asymmetric barrier layers are ideal, such that the left-hand ABL denies holes from entering the left-hand side of the OCL and the right-hand side ABL denies electrons from entering the right-hand side of the OCL. This is all done while not hindering the injection of electrons and holes into the QDs.

2.1. Theoretical Model: Rate Equations

The theoretical model is based on the following rate equations:

for electrons in the left hand side of the OCL,

$$b_1 \frac{\partial n_{\mathrm{L}}}{\partial t} = \frac{j}{e} + \sigma_{\mathrm{n}} \mathrm{v}_{\mathrm{n}} n_1 N_{\mathrm{S}} f_{\mathrm{n}} - \sigma_{\mathrm{n}} \mathrm{v}_{\mathrm{n}} n_{\mathrm{L}} N_{\mathrm{S}} (1 - f_{\mathrm{n}}), \tag{1}$$

for holes in the right hand side of the OCL,

$$b_2 \frac{\partial p_{\mathrm{R}}}{\partial t} = \frac{j}{e} + \sigma_{\mathrm{p}} \mathrm{v}_{\mathrm{p}} p_1 N_{\mathrm{S}} f_{\mathrm{p}} - \sigma_{\mathrm{p}} \mathrm{v}_{\mathrm{p}} p_{\mathrm{R}} N_{\mathrm{S}} (1 - f_{\mathrm{p}}), \tag{2}$$

for electrons and holes confined in the QDs,

$$2N_{\mathrm{S}} \frac{\partial f_{\mathrm{n}}}{\partial t} = \sigma_{\mathrm{n}} \mathrm{v}_{\mathrm{n}} n_{\mathrm{L}} N_{\mathrm{S}} (1 - f_{\mathrm{n}}) - \sigma_{\mathrm{n}} \mathrm{v}_{\mathrm{n}} n_1 N_{\mathrm{S}} f_{\mathrm{n}} - N_{\mathrm{S}} \frac{f_{\mathrm{n}} f_{\mathrm{p}}}{\tau_{\mathrm{QD}}} - c_{\mathrm{g}} g^{\max} (f_{\mathrm{n}} + f_{\mathrm{p}} - 1) n_{\mathrm{ph}}, \tag{3}$$

$$2N_{\mathrm{S}} \frac{\partial f_{\mathrm{p}}}{\partial t} = \sigma_{\mathrm{p}} \mathrm{v}_{\mathrm{p}} p_{\mathrm{R}} N_{\mathrm{S}} (1 - f_{\mathrm{p}}) - \sigma_{\mathrm{p}} \mathrm{v}_{\mathrm{p}} p_1 N_{\mathrm{S}} f_{\mathrm{p}} - N_{\mathrm{S}} \frac{f_{\mathrm{n}} f_{\mathrm{p}}}{\tau_{\mathrm{QD}}} - c_{\mathrm{g}} g^{\max} (f_{\mathrm{n}} + f_{\mathrm{p}} - 1) n_{\mathrm{ph}}, \tag{4}$$

and for output photons,

$$\frac{\partial n_{\mathrm{ph}}}{\partial t} = c_{\mathrm{g}} g^{\max}(f_{\mathrm{n}} + f_{\mathrm{p}} - 1) n_{\mathrm{ph}} - c_{\mathrm{g}} \beta n_{\mathrm{ph}} . \tag{5}$$

For equations (1)-(5), b_1 (b_2) is the thickness of the left (right) hand side of the OCL [the separation between the n- (p-) cladding layer and the left (right) hand side barrier]. n_L and p_R are the free-electron and -hole densities. j is the injection current density, e is the electron charge, and $\sigma_{\mathrm{n,p}}$ are the cross-sections of electron and hole capture into a QD. $v_{\mathrm{n,p}}$ are the electron and hole thermal velocities, N_{S} is the surface density of QDs, $f_{\mathrm{n,p}}$ are the electron- and hole-level occupancies in QDs, τ_{QD} is the spontaneous radiative lifetime in QDs, while c_{g} is the group velocity of light in the cavity. $g^{\max}$ is the maximum value of the modal gain [15].

$$\beta = (1/L)\ln(1/R) \tag{6}$$

β is the mirror loss coefficient, L is the cavity length, R is the facet reflectivity, and n_{ph} is the photon density (number of photons per unit area of the junction).

The maximum value of the modal gain in a QD laser is [15]

$$g^{\max} = \frac{\xi}{4}\left(\frac{\lambda_0}{\sqrt{\epsilon_g}}\right)^2 \frac{1}{\tau_{\mathrm{QD}}} \frac{\hbar}{(\Delta\varepsilon)_{\mathrm{inhom}}} \frac{\Gamma}{a} N_{\mathrm{S}} , \tag{7}$$

where $\xi = 1/\pi$ and $\xi = 1/\sqrt{2\pi}$ for the Lorentzian and Gaussian QD-size distributions, respectively, λ_0 is the lasing wavelength, $\sqrt{\epsilon_g}$ is the group index of the dispersive OCL material, a is the mean size of QDs, and Γ is the optical confinement factor in a QD layer.

Inhomogeneous line broadening caused by fluctuations in QD size is as follows:

$$(\Delta\varepsilon)_{\mathrm{inhom}} = (q_{\mathrm{n}}\varepsilon_{\mathrm{n}} + q_{\mathrm{p}}\varepsilon_{\mathrm{p}})\,\delta , \tag{8}$$

where $\varepsilon_{n,p}$ are the energy levels of an electron and a hole in a mean-sized QD, $q_{n,p} = -(\partial \ln \varepsilon_{n,p} / \partial \ln a)$, and δ is the root mean square of relative QD-size fluctuations.

n_1 and p_1 in (1)–(4) characterize the intensities of electron and hole thermal escape from a QD to the OCL, and are given by

$$n_1 = N_c^{3D} \exp\left(-\frac{E_n}{T}\right), \qquad p_1 = N_v^{3D} \exp\left(-\frac{E_p}{T}\right), \tag{9}$$

where

$$N_{c,v}^{3D} = 2\left(\frac{m_{c,v}^{OCL} T}{2\pi\hbar^2}\right)^{3/2} \tag{10}$$

are the densities of states in the valence and conduction bands in the OCL, $m_{c,v}^{OCL}$ are the electron and hole effective masses in the OCL, $E_{n,p}$ are electron and hole excitation energies from a QD to the OCL, and T is the temperature (in energy units).

The first term in the right-hand side of eqn. (1) is the electron injection flux from the n-cladding layer in the OCL in units of $cm^{-2}s^{-1}$. The following term is the flux of thermal escape of electrons from the QDs to the OCL. The third and final term on the right-hand side of eqn (1) is the flux of electron capture from the OCL into the QDs.

The first term in the right-hand side of eqn. (2) is the hole injection flux from the p-cladding layer into the OCL. The following term is the flux of thermal escape of holes from QDs to the OCL. The third and final term on the right-hand of eqn. (2) is the flux of electron capture from the OCL into the QDs.

In (3) and (4), $N_S f_n f_p / \tau_{QD}$ is the spontaneous radiative recombination flux in QDs and $c_g g^{max} (f_n + f_p - 1) n_{ph}$ is the stimulated radiative recombination flux in QDs.

The first term in the right-hand side of eqn. (5) is the rate of stimulated emission of photons in units of s^{-1}. The second term is the rate of escape of photons from the cavity through the mirrors.

2.2. Electron-Hole Symmetry

In this research, electron-hole symmetry was assumed. Thus, the following three rate equations are followed, instead of eqs. (1)-(5):

for free carriers in one side of the OCL (for definiteness, for electrons in the left-hand side of the OCL),

$$b_1 \frac{\partial n_{\mathrm{L}}}{\partial t} = \frac{j}{e} + \sigma_{\mathrm{n}} \mathrm{v}_{\mathrm{n}} n_1 N_{\mathrm{S}} f_{\mathrm{n}} - \sigma_{\mathrm{n}} \mathrm{v}_{\mathrm{n}} n_{\mathrm{L}} N_{\mathrm{S}} (1 - f_{\mathrm{n}}) , \tag{11}$$

for carriers confined in QDs,

$$2N_{\mathrm{S}} \frac{\partial f_{\mathrm{n}}}{\partial t} = \sigma_{\mathrm{n}} \mathrm{v}_{\mathrm{n}} n_{\mathrm{L}} N_{\mathrm{S}} (1 - f_{\mathrm{n}}) - \sigma_{\mathrm{n}} \mathrm{v}_{\mathrm{n}} n_1 N_{\mathrm{S}} f_{\mathrm{n}} - N_{\mathrm{S}} \frac{f_{\mathrm{n}}^2}{\tau_{\mathrm{QD}}} - c_{\mathrm{g}} g^{\max} (2 f_{\mathrm{n}} - 1) n_{\mathrm{ph}} , \tag{12}$$

and for photons,

$$\frac{\partial n_{\mathrm{ph}}}{\partial t} = c_{\mathrm{g}} g^{\max} (2 f_{\mathrm{n}} - 1) n_{\mathrm{ph}} - c_{\mathrm{g}} \beta n_{\mathrm{ph}} . \tag{13}$$

2.2.1. Steady-State Solutions of (11)-(13)

Adding up eqs. (11) and (12), we will obtain

$$\frac{\partial}{\partial t} (b_1 n_{\mathrm{L}} + 2N_{\mathrm{S}} f_{\mathrm{n}}) = \frac{j}{e} - N_{\mathrm{S}} \frac{f_{\mathrm{n}}^2}{\tau_{\mathrm{QD}}} - c_{\mathrm{g}} g^{\max} (2 f_{\mathrm{n}} - 1) n_{\mathrm{ph}} . \tag{14}$$

From (14), we have

$$n_{\mathrm{L}} = n_1 \frac{f_{\mathrm{n}}}{1-f_{\mathrm{n}}} + \frac{1}{\sigma_{\mathrm{n}} \mathrm{v}_{\mathrm{n}} N_{\mathrm{S}} (1-f_{\mathrm{n}})} \left(\frac{j}{e} - b_1 \frac{\partial n_{\mathrm{L}}}{\partial t} \right). \quad (15)$$

By putting $\frac{\partial}{\partial t}$ to 0 in equations (11)-(13), the dc (steady state) quantities of $n_{L,0}$ $f_{n,0}$ and $n_{ph,0}$ were found from the following steady-state equations:

$$0 = \frac{j_0}{e} + \sigma_n v_n n_1 N_s f_{n,0} - \sigma_n v_n n_{L,0} N_s (1 - f_{n,0}) \quad (16)$$

$$0 = \sigma_n v_n n_{L,0} N_s \left(1 - f_{n,0}\right) - \sigma_n v_n n_1 N_s f_{n,0} - N_s \frac{f_{n0}^2}{\tau_{QD}} - c_g g^{max} \left(2 f_{n,0} - 1\right) n_{ph,0} \quad (17)$$

$$0 = c_g g^{max} \left(2 f_{n,0} - 1\right) n_{ph,0} - c_g \beta n_{ph,0.} \quad (18)$$

Because $n_{ph,0}$ cannot be zero, (or there would be no lasing) we obtained from (18) the following steady-state lasing condition:

$$g^{max} \left(2 f_{n,0} - 1\right) = \beta \quad (19)$$

From (19), we found:

$$f_{n,0} = \frac{1}{2} \left(1 + \frac{\beta}{g^{max}}\right) \quad (20)$$

From (16), we were able to express $n_{L,0}$ in terms of $f_{n,0}$ as follows:

$$n_{L,0} = n_1 \frac{f_{n,0}}{1 - f_{n,0}} + \frac{j_0}{e \sigma_n v_n N_s (1 - f_{n,0})} \quad (21)$$

By combining equations (16) and (17), we got

$$0 = \frac{j_0}{e} - N_s \frac{f_{n,0}^2}{\tau_{QD}} - c_g g^{max} \left(2 f_{n,0} - 1\right) n_{ph,0} \quad (22)$$

By using (19) and (22), we found

$$j_0 = e N_s \frac{f_{n,0}^2}{\tau_{QD}} + e c_g \beta n_{ph,0} \quad (23)$$

Introducing the photon lifetime in the cavity

$$\tau_{ph} = \frac{1}{c_g \beta} \tag{24}$$

Rewriting (23), we have

$$j_0 = eN_s \frac{f_{n,0}^2}{\tau_{QD}} + e\frac{n_{ph,0}}{\tau_{ph}} \tag{25}$$

Rearranging (25), we found for $n_{ph,0}$

$$n_{ph,0} = \tau_{ph}\left(\frac{j_0}{e} - N_s \frac{f_{n,0}^2}{\tau_{QD}}\right) \tag{26}$$

Equations (20), (21), and (26) give the steady-state (dc) values of the electron density in the left-handed side of the OCL, the electron level occupancy in QDs, and photon density respectively.

2.3. Small Signal Analysis of Rate Equations

In order to study the modulation response of ABL QD lasers, the small-signal analysis was applied to eqs. (11)-(13). The injection current density was

$$j = j_0 + (\delta j_{\mathrm{m}})\exp(i\omega t), \tag{27}$$

where j_0 is the dc component and the amplitude δj_{m} of the time-harmonic ac component is small. n_{L}, f_{n}, and n_{ph} in the rate equations (11) – (13) were in the form of

$$n_{\mathrm{L}} = n_{\mathrm{L},0} + (\delta n_{\mathrm{L-m}})\exp(i\omega t), \tag{28}$$

$$f_{\mathrm{n}} = f_{\mathrm{n},0} + (\delta f_{\mathrm{n-m}})\exp(i\omega t), \tag{29}$$

$$n_{\mathrm{ph}} = n_{\mathrm{ph},0} + (\delta n_{\mathrm{ph-m}})\exp(i\omega t), \tag{30}$$

where the dc components $n_{L,0}$, $f_{n,0}$, and $n_{ph,0}$ are the solutions of the rate equations (11)–(13) at the steady-state ($\partial/\partial t = 0$ in the left-hand side of these equations), which correspond to the dc component j_0 of the injection current density.

Using (28)-(30) in (11)-(13) a set of algebraic equations in the frequency-dependent small amplitudes δn_{L-m}, δf_{n-m}, and δn_{ph-m} was obtained. The solution yielded the modulation response function

$$H(\omega) = \left| \frac{\delta n_{\mathrm{ph-m}}(\omega)}{\delta n_{\mathrm{ph-m}}(0)} \right|^2 . \tag{31}$$

For the case of electron hole symmetry, using the expression for $H(\omega)$, the modulation bandwidth was calculated, defined as the -3dB bandwidth, where the response function has fallen to half of its dc ($\omega = 0$) value,

$$10 \log_{10} H(\omega_{-3\,\mathrm{dB}}) = -3 . \tag{32}$$

Using eqns. (28), (29), and (30) in (11)-(13), we obtained the following set of three algebraic equations in three small amplitudes δn_{L-m}, δf_{n-m}, and δn_{ph-m}:

$$\begin{pmatrix} C_{11} & C_{12} & C_{13} \\ C_{21} & C_{22} & C_{23} \\ C_{31} & C_{32} & C_{33} \end{pmatrix} \begin{pmatrix} \delta n_{\mathrm{L-m}} \\ \delta f_{\mathrm{n-m}} \\ \delta n_{\mathrm{ph-m}} \end{pmatrix} = \begin{pmatrix} \delta j_{\mathrm{m}}/e \\ 0 \\ 0 \end{pmatrix}. \tag{33}$$

In order to solve for C_{ij} eqns (11) and (12) were rewritten as

$$\frac{\partial n_L}{\partial t} = \frac{j}{e b_1} + \sigma_n v_n n_1 \frac{N_s}{b_1} f_n - \sigma_n v_n n_L \frac{N_s}{b_1}(1 - f_n), \tag{34}$$

$$\frac{\partial f_n}{\partial t} = \frac{1}{2}\sigma_n v_n n_L (1 - f_n) - \frac{1}{2}\sigma_n v_n n_1 f_n - \frac{1}{2}\frac{f_n^2}{\tau_{QD}} - \frac{1}{2} c_g \frac{g^{max}}{N_s}(2 f_n - 1) n_{ph} \tag{35}$$

respectively. By linearizing eqn. (14), using eqns. (27), (28), (29) and (11), we have

$$i\omega\delta n_{L-m} = \frac{\partial j_m}{eb_1} + \sigma_n v_n n_1 \frac{N_s}{b_1} f_{n-m} - \sigma_n v_n n_1 \frac{N_s}{b_1}(1 - f_{n,0})\delta n_{L-m} + \sigma_n v_n n_{L,0} \frac{N_s}{b_1} f_{n-m} \quad (36)$$

Eqn. (24) can be rewritten as

$$[\sigma_n v_n \frac{N_s}{b_1}(1 - f_{n,0}) + i\omega]\delta n_{L-m} - \sigma_n v_n \big(n_1 + n_{L,0}\big) \frac{N_s}{b_1} \delta f_{n-m} = \frac{\partial j_m}{eb_1} \quad (37)$$

Linearizing eqn. (35), with equations (30) and (12), we find

$$i\omega\delta f_{n-m} = \frac{1}{2}\sigma_n v_n (1 - f_{n,0})\delta n_{L-m} - \frac{1}{2}\sigma_n v_n \big(n_1 + n_{L,0}\big)\delta f_{n-m} - \frac{f_{n,0}}{\tau_{QD}}\delta f_{n-m} \quad (38)$$

$$- c_g \frac{g^{max}}{N_s} n_{ph,0}\delta f_{n-m} - \frac{1}{2} c_g \frac{g^{max}}{N_s}\big(2f_{n,0} - 1\big)\delta n_{ph-m}$$

Equation (38) can be then rewritten as

$$-\frac{1}{2}\sigma_n v_n (1 - f_{n,0})\delta n_{L-m} + \left(\frac{1}{2}\sigma_n v_n \big(n_1 + n_{L,0}\big) + \frac{f_{n,0}}{\tau_{QD}} + c_g \frac{g^{max}}{N_s} n_{ph,0} + i\omega\right)\delta f_{n-m} \quad (39)$$

$$+ \frac{1}{2} c_g \frac{g^{max}}{N_s}\big(2f_{n,0} - 1\big)\delta n_{ph-m} = 0$$

Linearizing (26) with (29) and (30), we have

$$i\omega\delta n_{ph-m} = 2c_g g^{max} n_{ph,0}\delta f_{n-m} + c_g g^{max}\big(2f_{n,0} - 1\big)\delta n_{ph-m} - c_g \beta \delta n_{ph-m} \quad (40)$$

$$-2c_g g^{max} n_{ph,0}\delta f_{n-m} + \big[c_g\{\beta - g^{max}\big(2f_{n,0} - 1\big)\} + i\omega\big]\delta n_{ph-m} = 0 \quad (41)$$

Returning to the linearization of the rate equations, we used (19) and (24) in the last term in the left-handed side of equation (39) to rewrite (39) as

$$-\frac{1}{2}\sigma_n v_n (1 - f_{n,0})\delta n_{L-m} + \left\{\frac{1}{2}\sigma_n v_n \big(n_1 + n_{L,0}\big) + \frac{f_{n,0}}{\tau_{QD}} + c_g \frac{g^{max}}{N_s} n_{ph,0} + i\omega\right\}\delta f_{n-m} \quad (42)$$

$$+ \frac{1}{2}\frac{1}{\tau_{ph}}\frac{1}{N_s}\delta n_{ph-m} = 0$$

Using equation (19) in (41), we found

$$-2c_g g^{max} n_{ph,0} \delta f_{n-m} + i\omega \delta n_{ph-m} = 0 \tag{43}$$

Equations (37), (42), and (43) fill out the set in (33). Thus, we found the coefficients $C_{i,j}$ (*i,j* = 1,2,3)

$$C_{11} = \sigma_n v_n \frac{N_s}{b_1}\left(1 - f_{n,0}\right) + i\omega \tag{44}$$

$$C_{12} = -\sigma_n v_n (n_1 + n_{L,0}) \frac{N_s}{b_1} \tag{45}$$

$$C_{13} = 0 \tag{46}$$

$$C_{21} = -\frac{1}{2}\sigma_n v_n \left(1 - f_{n,0}\right) \tag{47}$$

$$C_{22} = \frac{1}{2}\sigma_n v_n \left(n_1 + n_{L,0}\right) + \frac{f_{n,0}}{\tau_{QD}} + c_g \frac{g^{max}}{N_s} n_{ph,0} + i\omega \tag{48}$$

$$C_{23} = \frac{1}{2}\frac{1}{\tau_{ph}}\frac{1}{N_s} \tag{49}$$

$$C_{31} = 0 \tag{50}$$

$$C_{32} = -2c_g g^{max} n_{ph,0} \tag{51}$$

$$C_{33} = i\omega \tag{52}$$

Using these coefficients, we can solve for $\delta n_{ph-m}(\omega)$

$$\delta n_{ph-m}(\omega) = \frac{\begin{vmatrix} C_{11}(i\omega) & C_{12} & \frac{\delta jm}{e} \\ C_{21} & C_{22}(i\omega) & 0 \\ 0 & C_{32} & 0 \end{vmatrix}}{\begin{vmatrix} C_{11}(i\omega) & C_{12} & 0 \\ C_{21} & C_{22}(i\omega) & C_{23} \\ 0 & C_{32} & i\omega \end{vmatrix}} \tag{53}$$

Dividing $\delta n_{ph-m}(\omega)$ by $\delta n_{ph-m}(0)$, we found

$$\frac{\delta n_{ph-m}(\omega)}{\delta n_{ph-m}(0)} = \frac{\begin{vmatrix} C_{11}(i\omega) & C_{12} & \frac{\delta j_m}{e} \\ C_{21} & C_{22}(i\omega) & 0 \\ 0 & C_{32} & 0 \end{vmatrix}}{\begin{vmatrix} C_{11}(0) & C_{12} & \frac{\delta j_m}{e} \\ C_{21} & C_{22}(0) & 0 \\ 0 & C_{32} & 0 \end{vmatrix}} \frac{\begin{vmatrix} C_{11}(0) & C_{12} & 0 \\ C_{21} & C_{22}(0) & C_{23} \\ 0 & C_{32} & 0 \end{vmatrix}}{\begin{vmatrix} C_{11}(i\omega) & C_{12} & 0 \\ C_{21} & C_{22}(i\omega) & C_{23} \\ 0 & C_{32} & i\omega \end{vmatrix}} \tag{54}$$

Breaking this into 2 parts, we began with the first part of the right hand side of equation (54),

$$\frac{\begin{vmatrix} C_{11}(i\omega) & C_{12} & \frac{\delta j_m}{e} \\ C_{21} & C_{22}(i\omega) & 0 \\ 0 & C_{32} & 0 \end{vmatrix}}{\begin{vmatrix} C_{11}(0) & C_{12} & \frac{\delta j_m}{e} \\ C_{21} & C_{22}(0) & 0 \\ 0 & C_{32} & 0 \end{vmatrix}} = \frac{-C_{32}\begin{vmatrix} C_{11}(i\omega) & \frac{\delta j_m}{e} \\ C_{21} & 0 \end{vmatrix}}{-C_{32}\begin{vmatrix} C_{11}(0) & \frac{\delta j_m}{e} \\ C_{21} & 0 \end{vmatrix}} \tag{55}$$

Which simplifies into

$$\frac{C_{21}\frac{\delta j_m}{e}}{C_{21}\frac{\delta j_m}{e}} = 1 \tag{56}$$

Because the first part of equation (54) simplifies into 1, we are able to only focus on the second half of the right hand side of the equation. Thus, (54) simplifies into

$$\frac{\delta n_{ph-m}(\omega)}{\delta n_{ph-m}(0)} = \frac{\begin{vmatrix} C_{11}(0) & C_{12} & 0 \\ C_{21} & C_{22}(0) & C_{23} \\ 0 & C_{32} & 0 \end{vmatrix}}{\begin{vmatrix} C_{11}(i\omega) & C_{12} & 0 \\ C_{21} & C_{22}(i\omega) & C_{23} \\ 0 & C_{32} & i\omega \end{vmatrix}} \tag{57}$$

Splitting (57) into real and imaginary parts, we found

$$\frac{-C_{32}\begin{vmatrix} C_{11}(0) & 0 \\ C_{21} & C_{23} \end{vmatrix}}{-C_{32}\begin{vmatrix} C_{11}(i\omega) & 0 \\ C_{21} & C_{23} \end{vmatrix} + i\omega \begin{vmatrix} C_{11}(i\omega) & C_{12} \\ C_{21} & C_{22}(i\omega) \end{vmatrix}} \tag{58}$$

Which further simplifies to

$$\frac{C_{32}C_{23}C_{11}(0)}{C_{32}C_{23}C_{11}(i\omega) - i\omega[C_{11}(i\omega)C_{22}(i\omega) - C_{12}C_{21}]} \tag{59}$$

Remembering equation (31)

$$H(\omega)=\left|\frac{\delta n_{\text{ph-m}}(\omega)}{\delta n_{\text{ph-m}}(0)}\right|^2 . \tag{31}$$

ω_{-3dB} was found from the equation:

$$10log_{10}H(\omega_{-3dB})=-3 \tag{60}$$

$$H(\omega_{-3dB})=10^{-0.3} \tag{61}$$

Denoting

$$r=10^3\approx 1.995 \tag{62}$$

We have

$$H(\omega_{-3dB})=\frac{1}{r} \tag{63}$$

Equation (63) was then rewritten as

$$rH(\omega_{-3dB})=1 \tag{64}$$

$C_{11}(i\omega)$ and $C_{22}(i\omega)$ were also rewritten as

$$C_{11}(i\omega)=C_{11}(0)+i\omega \tag{65}$$

$$C_{22}(i\omega)=C_{22}(0)+i\omega \tag{66}$$

We then have

$$\frac{\delta n_{ph-m}(\omega)}{\delta n_{ph-m}(0)}=\frac{C_{32}C_{23}C_{11}(0)}{C_{32}C_{23}[C_{11}(0)+i\omega]-i\omega[[C_{11}(0)+i\omega][C_{22}(0)+i\omega]-C_{12}C_{21}]} \tag{67}$$

The denominator of (67) was rewritten as

$$C_{32}C_{23}C_{11}(0)+i\omega C_{32}C_{23}\text{-}\, i\omega\{C_{11}(0)C_{22}(0)+i\omega[C_{11}(0)+C_{22}(0)]+(i\omega)^2-C_{12}C_{21}\} \tag{68}$$

Which simplifies to

$$C_{32}C_{23}C_{11}(0) + i\omega[C_{32}C_{23} + C_{12}C_{21} - C_{11}(0)C_{22}(0)] - (i\omega)^2[C_{11}(0) + C_{22}(0)] - (i\omega)^3 \quad (69)$$

Breaking this into real and imaginary parts, we found

$$\{C_{32}C_{23}C_{11}(0) + [C_{11}(0) + C_{22}(0)]\omega^2\} + i\omega\{[C_{32}C_{23} + C_{12}C_{21} - C_{11}(0)C_{22}(0)] + \omega^2\} \quad (70)$$

Hence, we had for $\frac{\delta n_{ph-m}(\omega)}{\delta n_{ph-m}(0)}$,

$$\frac{\delta n_{ph-m}(\omega)}{\delta n_{ph-m}(0)} = \quad (71)$$

$$\frac{C_{32}C_{23}C_{11}(0)}{\{C_{32}C_{23}C_{11}(0)+[C_{11}(0)+C_{22}(0)]\omega^2\}+ i\omega\{[C_{32}C_{23}+C_{12}C_{21}-C_{11}(0)C_{22}(0)]+\omega^2\}}$$

Using (71), we found the modulation response function

$$H(\omega) = \left|\frac{\delta n_{ph-m}(\omega)}{\delta n_{ph-m}(0)}\right|^2 = \quad (72)$$

$$\frac{C_{32}^2C_{23}^2C_{11}^2(0)}{\{C_{32}C_{23}C_{11}(0)+[C_{11}(0)+C_{22}(0)]\omega^2\}^2+\omega^2\{[C_{32}C_{23}+C_{12}C_{21}-C_{11}(0)C_{22}(0)]+\omega^2\}^2}$$

With (72), we had from (64) for the modulation bandwidth ω_{-3dB}

$$\{C_{32}C_{23}C_{11}(0) + [C_{11}(0) + C_{22}(0)]\omega_{-3dB}^2\}^2 + \omega_{-3dB}^2\{[C_{32}C_{23} + C_{12}C_{21} - C_{11}(0)C_{22}(0)] + \omega_{-3dB}^2\}^2 = rC_{32}^2C_{23}^2C_{11}^2(0) \quad (73)$$

By rearranging (73), we derived the following cubic equation in terms of ω_{-3dB}^2

$$\omega_{-3dB}^6 + \{[C_{11}(0) + C_{22}(0)]^2 + 2[C_{32}C_{23} + C_{12}C_{21} - C_{11}(0)C_{22}(0)]\omega_{-3dB}^4 + \{[C_{32}C_{23} + C_{12}C_{21} - C_{11}(0)C_{22}(0)]^2 + 2C_{32}C_{23}C_{11}(0)[C_{11}(0) + C_{22}(0)]\}\omega_{-3dB}^2 - (r-1)C_{32}^2C_{23}^2C_{11}^2(0) = 0 \quad (74)$$

Equation (74) was rewritten in the form

$$\omega_{-3dB}^{6} + E_4\omega_{-3dB}^{4} + E_2\omega_{-3dB}^{2} - E_0 = 0 \tag{75}$$

where

$$E_4 = C_{11}^2(0) + C_{22}^2(0) + 2[C_{32}C_{23} + C_{12}C_{21}] \tag{76}$$

$$E_2 = [C_{32}C_{23} + C_{12}C_{21} - C_{11}(0)C_{22}(0)]^2 + 2C_{32}C_{23}C_{11}(0)[C_{11}(0) + C_{22}(0)] \tag{77}$$

$$E_0 = (r-1)C_{32}^2C_{23}^2C_{11}^2(0) \tag{78}$$

We then introduced all positive coefficients A_0, A_1, and A_2 as follows

$$A_0 = -C_{32}C_{23}C_{11}(0) \tag{79}$$

$$A_1 = C_{11}(0)C_{22}(0) - C_{32}C_{23} - C_{12}C_{21} \tag{80}$$

$$A_2 = C_{11}(0) + C_{22}(0) \tag{81}$$

Hence, we had from (79) - (81) and (44) – (52) the coefficients A_0, A_1, and A_2

$$A_0 = C_g g^{max} \frac{1}{b_1} \frac{n_{ph,0}}{\tau_{ph}} \sigma_n v_n (1 - f_{n,0}) \tag{82}$$

$$A_1 = \sigma_n v_n \frac{N_s}{b_1}\left(1 - f_{n,0}\right)\left[\frac{f_{n,0}}{\tau_{QD}} + \frac{1}{N_s}C_g g^{max} n_{ph,0}\right] + \frac{1}{N_s}C_g g^{max}\frac{n_{ph,0}}{\tau_{ph}} \tag{83}$$

$$A_2 = \sigma_n v_n \frac{N_s}{b_1}\left(1 - f_{n,0}\right) + \frac{1}{2}\sigma_n v_n\left(n_1 + n_{L,0}\right) + \frac{f_{n,0}}{\tau_{QD}} + c_g \frac{g^{max}}{N_s} n_{ph,0} \tag{84}$$

Using (82)-(84), equation (31) was rewritten as

$$H(\omega) = \frac{A_0^2}{(A_2\omega^2 - A_0)^2 + (\omega^3 - A_1\omega)^2} \tag{85}$$

With (85), we have from (64),

$$\frac{rA_0^2}{(A_2\omega_{-3dB}^2 - A_0)^2 + (\omega_{-3dB}^3 - A_1\omega_{-3dB})^2} = 1 \tag{86}$$

From (86), we have

$$\omega_{-3dB}^{6} + (A_2^2 - 2A_1)\omega_{-3dB}^{4} + (A_1^2 - 2A_0A_2)\omega_{-3dB}^{2} - (r-1)A_0^2 = 0 \quad (87)$$

Hence, for the coefficients E_4, E_2 and E_0, we have

$$E_4 = A_2^2 - 2A_1 \quad (88)$$

$$E_2 = A_1^2 - 2A_0A_2 \quad (89)$$

$$E_0 = (r-1)A_0^2 \quad (90)$$

Using A_0, A_1, and A_2 we wrote the expression (67) as follows:

$$\frac{\delta n_{ph-m}(\omega)}{\delta n_{ph-m}(0)} = \frac{A_0}{(A_0 - A_2\omega^2) + i\omega(A_1 - \omega^2)} \quad (91)$$

or

$$\frac{\delta n_{ph-m}(\omega)}{\delta n_{ph-m}(0)} = \frac{A_0}{(A_0 - A_2\omega^2) + i(A_1\omega - \omega^3)} \quad (92)$$

Chapter 2.4. Discussion of Results

Equation (75) (or, equivalently, eq. (87)) is a cubic equation in terms of ω_{-3dB}^{2}. Solving this equation, we modeled the behavior of ABL QD lasers at varying currents, and with different laser parameters, such as QD surface density, QD size fluctuation, and cavity length. The optimum conditions were classified as those which gave the maximum modulation bandwidth of the laser system.

2.4.1. Modulation Bandwidth vs DC Pump Current

The first parameter varied was the dc component of the pump current. Using eq. (75) [(87)], wherein j was varied, Figure 6 was found.

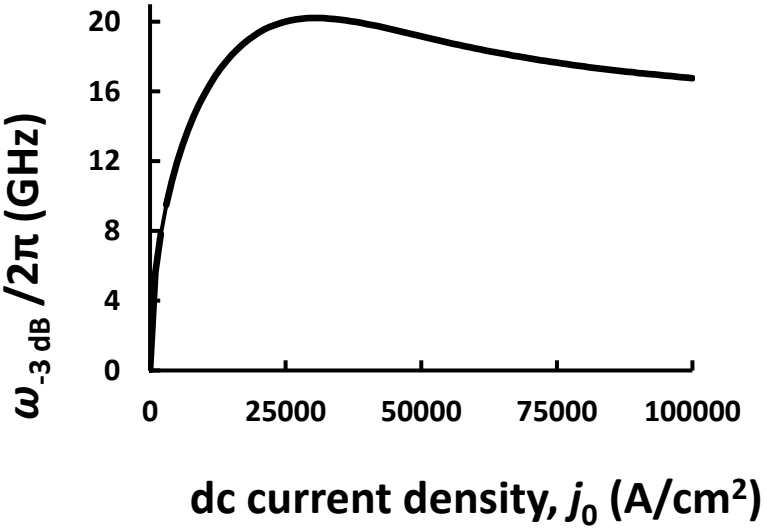

Fig. 6. $\omega_{-3dB}/2\pi$ (GHz) vs dc current density (A/cm^2).

Figure 6 clearly shows that modulation bandwidth reaches an optimum value, before falling and approaching an asymptote. The maximum value of the modulation bandwidth is 20 GHz. The optimum pump current is approximately 30 kA/cm^2. This data allows us to know the optimal pump current to operate the ABL QDL at for the largest modulation bandwidth possible. If the DC applied current is below the threshold current, lasing will not be achieved. However, if the applied current is too high, the modulation bandwidth of the ABL QDL will suffer.

Compared to optimum dc injection current of conventional QD lasers [33,34], the optimum dc injection current for ABL QD lasers is lower. Thus, the maximum bandwidth is easier to obtain in ABL QD lasers.

2.4.2. Modulation Bandwidth vs Carrier Capture Cross Section

The next parameter tested was the cross section of carrier capture. Figure 7 below shows modulation bandwidth versus current density, with varying cross sections of carrier capture.

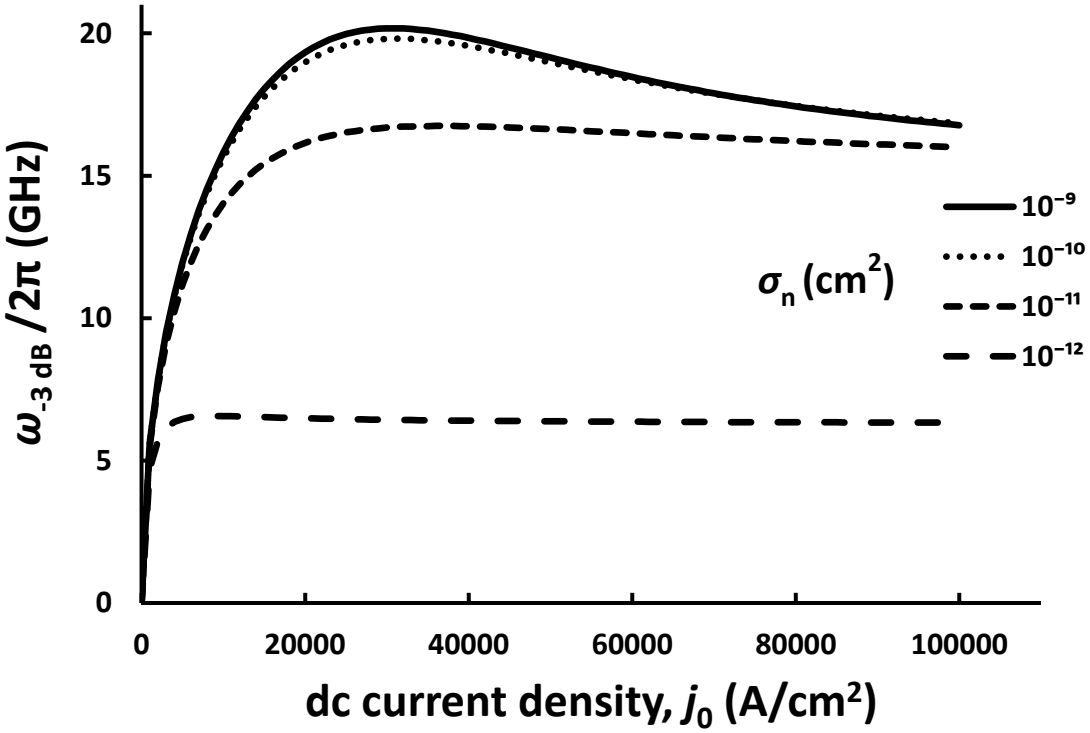

Fig. 7. Modulation bandwidth (GHz) vs dc current density (A/cm^2) with varying cross section of carrier capture (cm^2).

As shown in figure 7, at a specific current density, the bandwidth increases and finally asymptotically approaches its value corresponding to the case of instantaneous capture into QDs [33].

In order to explore how maximum modulation bandwidth increases with increasing cross section of carrier capture, the following graph was created, as shown in Figure 8.

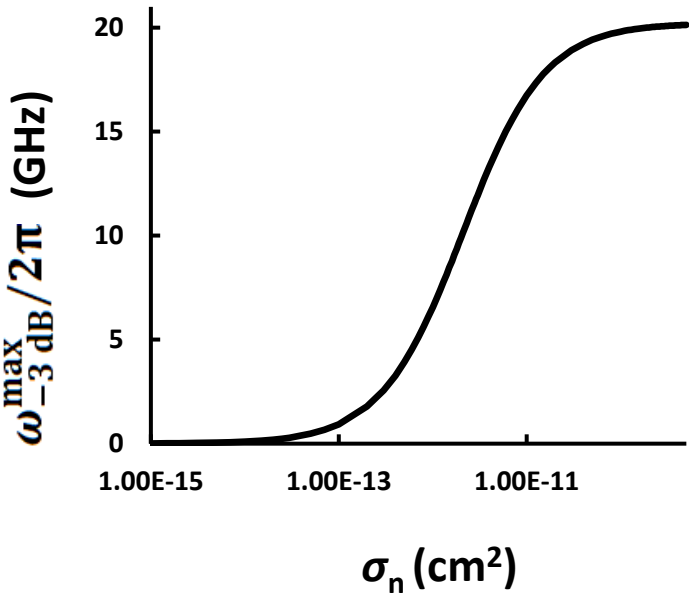

Fig. 8. Maximum modulation bandwidth (GHz) vs cross section of carrier capture (cm^2).

As shown in figure 8, as the cross section of carrier capture gets larger, the maximum modulation bandwidth increases to an asymptotic value of 20 GHz. Thus, when fabricating ABL QDLs, one should strive to have the largest cross section of carrier capture possible. However, once your cross section of carrier capture gets too large, there is no longer any benefit to the larger carrier capture. The modulation bandwidth begins at zero because if no electrons are

captured, lasing does not occur. Once carrier capture hits a certain point, the modulation bandwidth does not change considerably because all the electrons are properly being captured by the QDs, and the laser is operating optimally.

In figure 9, modulation bandwidth was plotted with varying cross section of carrier capture, and with different injection currents.

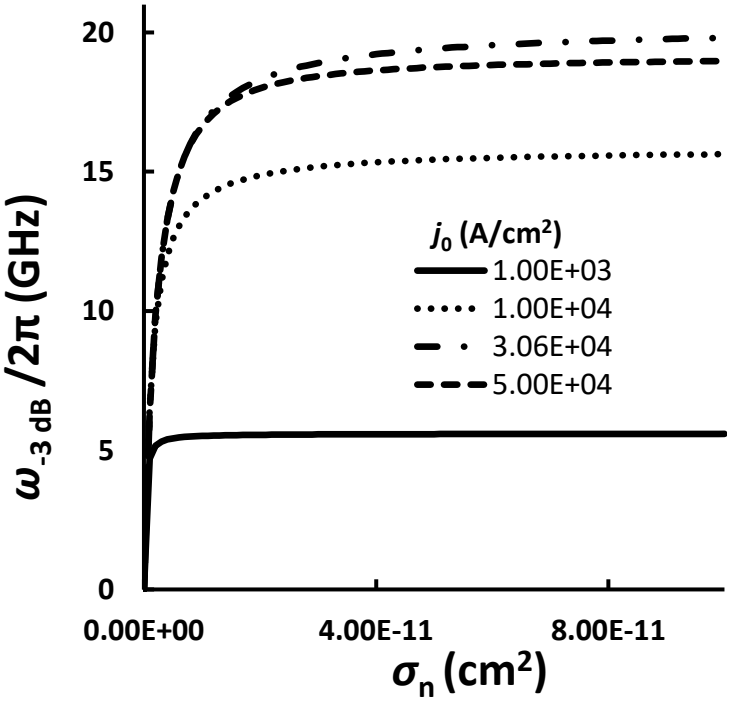

Fig. 9. Modulation bandwidth vs cross section of carrier capture, with varying injection current.

As shown in figure 9, the optimal injection current to maximize modulation bandwidth is 30.61 kA/cm^2. At injection currents lower than the optimal value, the modulation bandwidth achievable is much lower than the value at the optimum value. The modulation bandwidth

increases as the optimum injection current is approached, and drops lower again once the optimum injection current is passed.

2.4.3. Modulation Bandwidth vs Surface Density of QDs

Another parameter tested for was surface density of QDs. This was defined as the amount of QDs per centimeter squared. Figure 10 shows our findings.

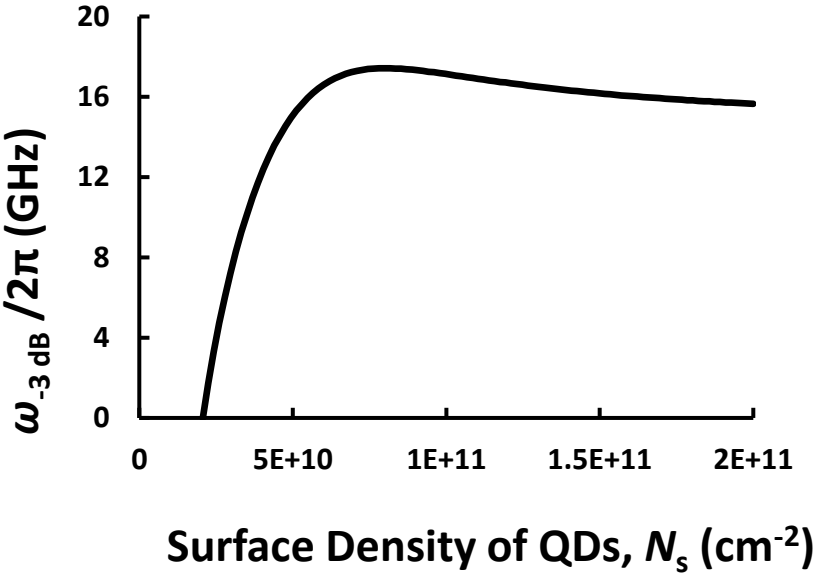

Fig. 10. Modulation bandwidth (GHz) vs surface density of QDs (cm^{-2}).

As shown in Fig 10, modulation bandwidth increases with surface density of QDs, until reaching a maximum value and lowering towards an asymptotic value. Thus, the optimal density of QDs exists.

2.4.4. Modulation Bandwidth vs Cavity Length

The dependence of the modulation bandwidth on the cavity length of the laser was investigated and plotted in Figure 11.

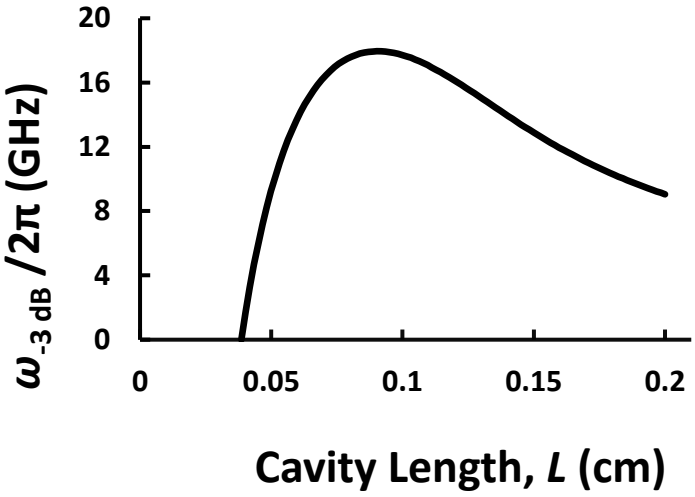

Fig. 11. Modulation bandwidth (GHz) vs cavity length (cm).

As shown in figure 11, modulation bandwidth does not exist until the cavity length is at least 386 μm. Once the cavity is long enough to achieve lasing, the modulation bandwidth increases to a maximum, before dropping to a lower value as the cavity length continues to increase. This mirrors [35], where a minimum cavity length also existed. An optimum cavity length also existed in [35], where the effect of the internal optical loss on the modulation bandwidth was studied.

2.4.5. Modulation Bandwidth vs Root Means Square (RMS) of QD-Size Fluctuations.

While QDs are only a few nanometers in diameter, size variation is inevitable when fabricated. Thus, QD size fluctuation was accounted for in this research. Figure 12 below shows us the modulation bandwidth of the ABL QDL versus RMS of relative QD size fluctuations.

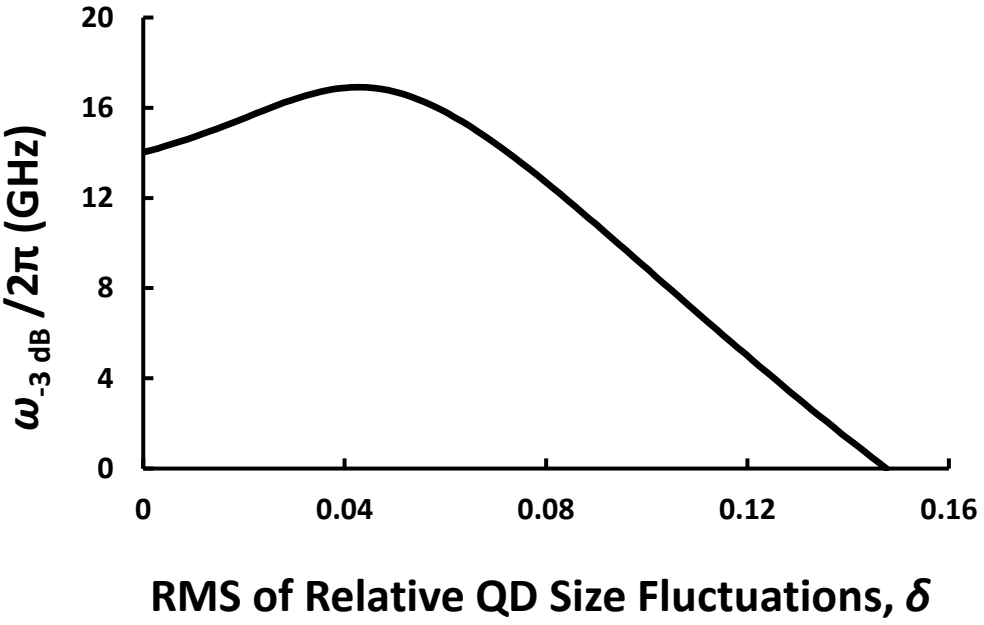

Fig. 12. Modulation bandwidth (GHz) vs RMS of relative QD size fluctuations.

As shown in Fig 12, a slight increase in the size fluctuations of QDs is actually beneficial to the maximum modulation bandwidth of the ABL QDLs, as with a RMS of 0.05, the maximum modulation bandwidth of the system increases by roughly 2.5 GHz. However, if the QD size fluctuations get too large, the modulation bandwidth drops to zero. This is due to the fact that if the size fluctuations of the QD increases and approaches a critical value, the maximum value of

the modal gain of a QD laser [see equations (7) and (8)] will become lower than the mirror loss β [see equation 6] and the lasing condition (19) will not be satisfied.

2.5. Summary

In chapter 2, a theoretical model for QD lasers with ABLs was created. These ABLs were positioned to deny carrier escape from the active region into the OCL. By blocking carrier escape from the active region to the OCL, parasitic recombination of carriers outside the active region is eliminated. This design does not hinder the injection of electrons and holes into the QDs, where recombination occurs. In our model, electron-hole symmetry was assumed. The rate equations for the system were then solved for the steady state case. Small signal analysis of the rate equations was then undertaken, in order to study the modulation response of the ABL QD lasers. The resulting cubic equation in terms of ω_{-3dB}^{2} was then solved to model the behavior of ABL QD lasers at varying currents and different laser parameters, including QD surface density, QD size fluctuation, and cavity length. The cross section of carrier capture was also modeled. An optimum value of dc current density, surface density of QDs, cavity length, and QD size fluctuations were all found, which maximized the modulation bandwidth of the QD lasers with ABLs.

Chapter 2 Bibliography

[33] L. V. Asryan and R. A. Suris, “Upper limit for the modulation bandwidth of a quantum dot laser”, Appl. Phys. Lett. 96, 221112 (2010); https://doi.org/10.1063/1.3446968

[34] L.V. Asryan, Yu. Wu and R. A. Suris, “Carrier capture delay and modulation bandwidth in an edge-emitting quantum dot laser”, Appl. Phys. Lett. 98, 131108 (2011); https://doi.org/10.1063/1.3571295

[35] Yu. Wu, R. A. Suris, and L.V. Asryan, “Effect of internal optical loss on the modulation bandwidth of a quantum dot laser”, Appl. Phys. Lett. 100, 131106 (2012); http://dx.doi.org/10.1063/1.3697683

Chapter 3. Excited States in Quantum Dots

When a carrier is injected into the QD, there is a possibility for the carrier to be captured into an excited state, rather than the ground state. It would be desirable if QDs would contain only one electron and only one hole energy state. However, large and/or deep enough QDs contain excited states as well. Multiple excited states can exist in each of the conduction and valence bands, and can each hold a charge carrier [36-39]. Carriers can recombine through excited states in addition to recombination through the ground state, as shown in figure 13.

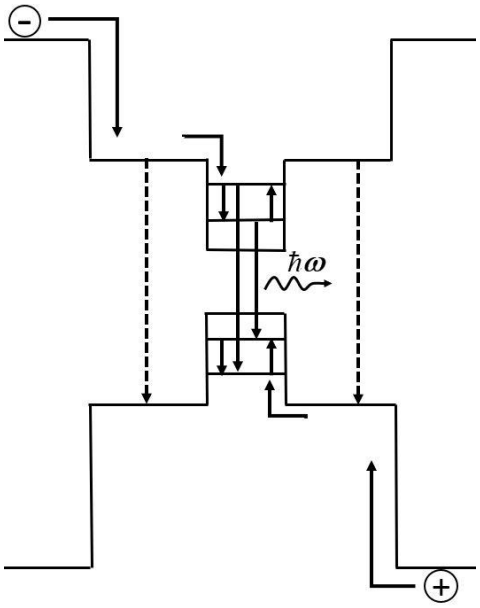

Fig. 13. Energy band diagram of a conventional QD laser.

These excited states can affect the carrier capture from the OCL into the lasing ground state in a QD. If the carrier capture into the QD ground-state takes places via the excited-states,

the emitted power of ground-state lasing eventually reaches an asymptotic value rather than continues to increase with increasing pump current in a conventional QD lasers [36].

By introducing ABLs as before, the electrons and holes will not be able to escape from the active region into the OCL. In figure 14, the energy band diagram and the main processes in an ABL QD laser are shown.

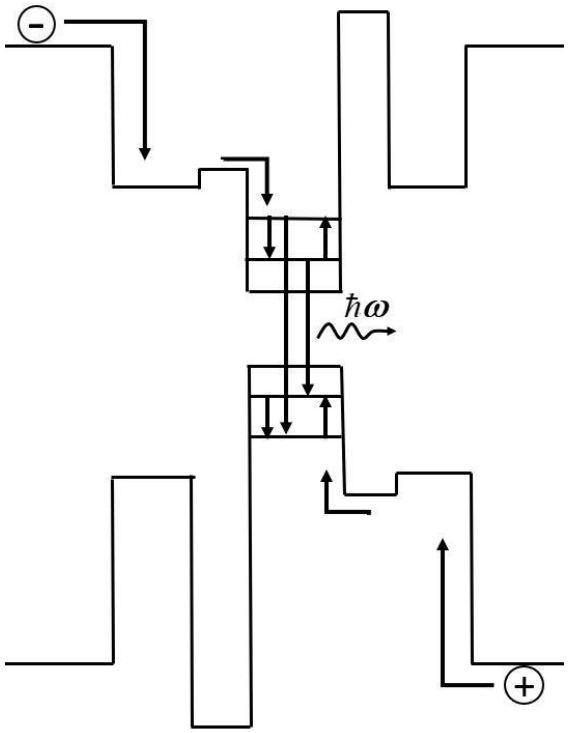

Fig. 14. Energy band diagram of ABL QD lasers.

3.1. Excited-State-Mediated Capture into Ground State in ABL QD Lasers

By assuming electron-hole symmetry, we can use the following set of four rate equations:

for free carriers (electrons) in the left-hand side of the OCL,

$$b_1 \frac{\partial n_{\mathrm{L}}}{\partial t} = \frac{j}{e} + \sigma_{\mathrm{n2}} \mathrm{v}_{\mathrm{n}} n_1 N_{\mathrm{S}} f_{\mathrm{n2}} - \sigma_{\mathrm{n2}} \mathrm{v}_{\mathrm{n}} n_{\mathrm{L}} N_{\mathrm{S}} (1 - f_{\mathrm{n2}}), \quad (93)$$

for carriers confined in the excited states of the QDs:

$$2N_{\mathrm{S}} \frac{\partial f_{\mathrm{n2}}}{\partial t} = \sigma_{\mathrm{n2}} \mathrm{v}_{\mathrm{n}} n_{\mathrm{L}} N_{\mathrm{S}} (1 - f_{\mathrm{n2}}) - \sigma_{\mathrm{n2}} \mathrm{v}_{\mathrm{n}} n_1 N_{\mathrm{S}} f_{\mathrm{n2}} + N_{\mathrm{S}} \frac{f_{\mathrm{n1}}(1 - f_{\mathrm{n2}})}{\tau_{12}} - N_{\mathrm{S}} \frac{f_{\mathrm{n2}}(1 - f_{\mathrm{n1}})}{\tau_{21}} - N_{\mathrm{S}} \frac{f_{\mathrm{n2}}^2}{\tau_{\mathrm{QD2}}} \quad (94)$$

for carriers confined in the ground state in QDs:

$$2N_{\mathrm{S}} \frac{\partial f_{\mathrm{n1}}}{\partial t} = N_{\mathrm{S}} \frac{f_{\mathrm{n2}}(1 - f_{\mathrm{n1}})}{\tau_{21}} - N_{\mathrm{S}} \frac{f_{\mathrm{n1}}(1 - f_{\mathrm{n2}})}{\tau_{12}} - N_{\mathrm{S}} \frac{f_{\mathrm{n1}}^2}{\tau_{\mathrm{QD1}}} - c_{\mathrm{g}} g_1^{\max} (2 f_{\mathrm{n1}} - 1) n_{\mathrm{ph1}}, \quad (95)$$

and for stimulated photons emitted via the ground-state transitions in QDs,

$$\frac{\partial n_{\mathrm{ph1}}}{\partial t} = c_{\mathrm{g}} g_1^{\max} (2 f_{\mathrm{n1}} - 1) n_{\mathrm{ph1}} - c_{\mathrm{g}} \beta_1 n_{\mathrm{ph1}}. \quad (96)$$

At steady-state, eqs. (93)-(96) become

$$0 = \frac{j}{e} + \sigma_{\mathrm{n2}} \mathrm{v}_{\mathrm{n}} n_1 N_{\mathrm{S}} f_{\mathrm{n2}} - \sigma_{\mathrm{n2}} \mathrm{v}_{\mathrm{n}} n_{\mathrm{L}} N_{\mathrm{S}} (1 - f_{\mathrm{n2}}), \quad (97)$$

$$0 = \sigma_{\mathrm{n2}} \mathrm{v}_{\mathrm{n}} n_{\mathrm{L}} N_{\mathrm{S}} (1 - f_{\mathrm{n2}}) - \sigma_{\mathrm{n2}} \mathrm{v}_{\mathrm{n}} n_1 N_{\mathrm{S}} f_{\mathrm{n2}} + N_{\mathrm{S}} \frac{f_{\mathrm{n1}}(1 - f_{\mathrm{n2}})}{\tau_{12}} - N_{\mathrm{S}} \frac{f_{\mathrm{n2}}(1 - f_{\mathrm{n1}})}{\tau_{21}} - N_{\mathrm{S}} \frac{f_{\mathrm{n2}}^2}{\tau_{\mathrm{QD2}}}, \quad (98)$$

$$0 = N_{\mathrm{S}} \frac{f_{\mathrm{n2}}(1 - f_{\mathrm{n1}})}{\tau_{21}} - N_{\mathrm{S}} \frac{f_{\mathrm{n1}}(1 - f_{\mathrm{n2}})}{\tau_{12}} - N_{\mathrm{S}} \frac{f_{\mathrm{n1}}^2}{\tau_{\mathrm{QD1}}} - c_{\mathrm{g}} g_1^{\max} (2 f_{\mathrm{n1}} - 1) n_{\mathrm{ph1}}, \quad (99)$$

$$0 = c_{\mathrm{g}} g_1^{\max} (2 f_{\mathrm{n1}} - 1) n_{\mathrm{ph1}} - c_{\mathrm{g}} \beta_1 n_{\mathrm{ph1}}. \quad (100)$$

In order to have $n_{\mathrm{ph1}} \neq 0$, the following lasing condition was found from (100):

$$g_1^{\max} (2 f_{\mathrm{n1}} - 1) = \beta_1. \quad (101)$$

From (101), the ground-state level occupancy is found:

$$f_{\mathrm{n1}} = \frac{1}{2}\left(1 + \frac{\beta_1}{g_1^{\max}}\right). \tag{102}$$

The output optical power produced by stimulated emission via the ground-state transitions in QDs is

$$P_1 = \hbar\omega_1 c_{\mathrm{g}} \beta_1 n_{\mathrm{ph1}} S = \hbar\omega_1 \frac{n_{\mathrm{ph1}}}{\tau_{\mathrm{ph1}}} S\,, \tag{103}$$

where the photon lifetime in cavity is introduced as

$$\tau_{\mathrm{ph1}} = \frac{1}{c_{\mathrm{g}} \beta_1}\,. \tag{104}$$

Adding up (97) and (98), we found

$$0 = \frac{j}{e} + N_s \frac{f_{n1}(1-f_{n2})}{\tau_{12}} - N_s \frac{f_{n2}(1-f_{n1})}{\tau_{21}} - N_s \frac{f_{n2}^2}{\tau_{QD2}} \tag{105}$$

Rewriting, we get

$$\frac{f_{n2}^2}{\tau_{QD2}} + \frac{f_{n2}(1-f_{n1})}{\tau_{21}} - \frac{f_{n1}(1-f_{n2})}{\tau_{12}} - \frac{j}{eN_s} = 0 \tag{106}$$

which can once again be rewritten to

$$\frac{f_{n2}^2}{\tau_{QD2}} + \left[\frac{(1-f_{n1})}{\tau_{21}} + \frac{f_{n1}}{\tau_{12}}\right] f_{n2} - \left(\frac{f_{n1}}{\tau_{12}} + \frac{j}{eN_s}\right) = 0 \tag{107}$$

Substituting in the following variables, we see

$$a f_{n2}^2 + b f_{n2} + c = 0 \tag{108}$$

$$f_{n2} = \frac{-b \pm \sqrt{b^2 - 4ac}}{2a} \tag{109}$$

$$a = \frac{1}{\tau_{QD2}} \tag{110}$$

$$b = \frac{(1 - f_{n1})}{\tau_{21}} + \frac{f_{n1}}{\tau_{12}} \tag{111}$$

$$c = -\left(\frac{f_{n1}}{\tau_{12}} + \frac{j}{eN_s}\right) \tag{112}$$

Solving the quadratic equation (108) using equations (109)-(112), we begin with

$$b^2 - 4ac = \left(\frac{(1 - f_{n1})}{\tau_{21}} + \frac{f_{n1}}{\tau_{12}}\right)^2 + \frac{4}{\tau_{QD2}}\left(\frac{f_{n1}}{\tau_{12}} + \frac{j}{eN_s}\right) \tag{113}$$

Because b > 0 (eq. 111), the negative solution of the quadratic equation (eq. 109) is a negative value, and thus is dropped (as negative f_{n2} is impossible). Hence, we have

$$f_{n2}(j) = \frac{\tau_{QD2}}{2}\left[\sqrt{\left(\frac{(1 - f_{n1})}{\tau_{21}} + \frac{f_{n1}}{\tau_{12}}\right)^2 + \frac{4}{\tau_{QD2}}\left(\frac{f_{n1}}{\tau_{12}} + \frac{j}{eN_s}\right)} - \left(\frac{(1 - f_{n1})}{\tau_{21}} + \frac{f_{n1}}{\tau_{12}}\right)\right] \tag{114}$$

As shown in (114), f_{n2} increases with increasing *j*. However, f_{n2} cannot exceed one. Hence, (114) applies for the currents

$$j_{th1} \leq j \leq j_2 \tag{115}$$

where j_{th1} is the threshold current density for lasing through the ground state, and j_2 follows the condition

$$f_{n2}(j_2) = 1 \tag{116}$$

Using (114) or (107) (where f_{n2} is set equal to 1), we obtain

$$\frac{1}{\tau_{QD2}} + \frac{(1-f_{n1})}{\tau_{21}} + \frac{f_{n1}}{\tau_{12}} = \frac{f_{n1}}{\tau_{12}} + \frac{j_2}{eN_s} \tag{117}$$

From this, we have

$$j_2 = eN_s\left(\frac{1}{\tau_{QD2}} + \frac{(1-f_{n1})}{\tau_{21}}\right) \tag{118}$$

Hence, for $j_{th1} \le j \le j_2$, f_{n2} is given by (114); for $j \ge j_2$,

$$f_{n2} = 1 \tag{119}$$

From eq. (100) we have

$$\sigma_{n2} v_n n_L N_s (1-f_{n2}) = \frac{j}{e} + \sigma_{n2} v_n n_1 N_s f_{n2} \tag{120}$$

Thus, for n_L, we have

$$n_L(j) = n_1 \frac{f_{n2}(j)}{1-f_{n2}(j)} + \frac{j}{e\sigma_{n2} v_n N_s (1-f_{n2}(j))}. \tag{121}$$

Adding up equations (97), (98), and (99), we have

$$\frac{j}{e} = N_s \frac{f_{n2}^2(j)}{\tau_{QD2}} + N_s \frac{f_{n1}^2}{\tau_{QD1}} + c_g \beta_1 n_{ph1}. \tag{122}$$

In the last term in the right-hand side of (122), we used equation (101).

Using equation (104) for τ_{ph1}, we have

$$\frac{j}{e} = N_s \frac{f_{n2}^2(j)}{\tau_{QD2}} + N_s \frac{f_{n1}^2}{\tau_{QD1}} + \frac{n_{ph1}}{\tau_{ph1}} \tag{123}$$

Rearranging (123), we have

$$n_{ph1}(j) = \tau_{ph1}\left[\frac{j}{e} - \frac{N_s f_{n2}^2(j)}{\tau_{QD2}} - N_s \frac{f_{n1}^2}{\tau_{QD1}}\right] \tag{124}$$

for $j < j_2$. However, when $j > j_2, f_{n2} = 1$ and we have

$$n_{ph1}(j) = \tau_{ph1}\left[\frac{j}{e} - \frac{N_s}{\tau_{QD2}} - N_s\frac{f_{n1}^2}{\tau_{QD1}}\right] \tag{125}$$

For the output power of lasing in the ground-state transitions when $j < j_2$, we have

$$P_1 = \hbar\omega_1 c_g \beta_1 n_{ph1} S = \hbar\omega_1 \frac{n_{ph1}}{\tau_{ph1}} S = \hbar\omega_1 \left[\frac{j}{e} - \frac{N_s f_{n2}^2(j)}{\tau_{QD2}} - N_s\frac{f_{n1}^2}{\tau_{QD1}}\right] S. \tag{126}$$

When $j > j_2$,

$$P_1 = \hbar\omega_1 c_g \beta_1 n_{ph1} S = \hbar\omega_1 \frac{n_{ph1}}{\tau_{ph1}} S = \hbar\omega_1 \left[\frac{j}{e} - \frac{N_s}{\tau_{QD2}} - N_s\frac{f_{n1}^2}{\tau_{QD1}}\right] S. \tag{127}$$

We then found the threshold current density for ground-state lasing by setting $n_{ph1} = 0$ in equation (123) and using the f_{n2} value given by equation (114) [where $j = j_{th1}$]. We arrived at the following equation:

$$j_{th1} = eN_s\frac{f_{n2}^2(j_{th1})}{\tau_{QD2}} + eN_s\frac{f_{n1}^2}{\tau_{QD1}} \tag{128}$$

Equation (128) could then be solved for j_{th1}. However, it is much simpler to find j_{th1} a different way. Setting $n_{ph1} = 0$ in equation (99), we found

$$0 = N_s\frac{f_{n2}(j_{th1})(1 - f_{n1})}{\tau_{21}} - N_s\frac{f_{n1}\left(1 - f_{n2}(j_{th1})\right)}{\tau_{12}} - N_s\frac{f_{n1}^2}{\tau_{QD1}} \tag{129}$$

From this equation, we found

$$\left[\frac{(1 - f_{n1})}{\tau_{21}} + \frac{f_{n1}}{\tau_{12}}\right] f_{n2}(j_{th1}) = \frac{f_{n1}}{\tau_{12}} + \frac{f_{n1}^2}{\tau_{QD1}} \tag{130}$$

Hence, we have

$$f_{n2}(j_{th1}) = \frac{\frac{f_{n1}}{\tau_{12}} + \frac{f_{n1}^2}{\tau_{QD1}}}{\frac{(1-f_{n1})}{\tau_{21}} + \frac{f_{n1}}{\tau_{12}}} \tag{131}$$

Using (131) in (128), we had

$$j_{th1} = \frac{eN_s}{\tau_{QD2}} \left(\frac{\frac{f_{n1}}{\tau_{12}} + \frac{f_{n1}^2}{\tau_{QD1}}}{\frac{(1-f_{n1})}{\tau_{21}} + \frac{f_{n1}}{\tau_{12}}} \right)^2 + \frac{eN_s}{\tau_{QD1}} f_{n1}^2 \tag{132}$$

As seen from (121), for $j \geq j_2$, when $f_{n2} = 1$,

$$n_L = \infty \tag{133}$$

The model used here does not consider the fact that at some current density j_{th2}, stimulated recombination via the excited-states will turn on and for $j > j_{th2}$ there will be both ground-state and excited-state lasing. When this is taken into account, f_{n2} will not increase to 1 with increasing *j.* Instead, it will increase up to

$$f_{n2}(j_{th2}) \equiv f_{n2,th2} < 1 \tag{134}$$

and then will remain pinned with increasing *j*. Hence, n_L will not be infinitely high. We however did not include this into our model.

3.2. Ground-state-lasing power against pump current

The output power versus excess injection current density in conventional QD lasers is shown below in figure 15.

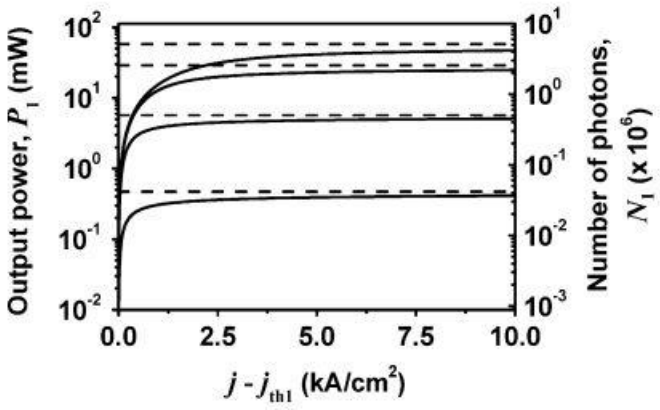

Fig. 15. Output power P_1 (left axis) and number of photons N_1 (right axis) of ground-state lasing versus excess injection current density in conventional QD lasers. The horizontal dashed line shows P_1^{max} and N_1^{max}. Each solid line has a different transition time between excited and ground states. From top to bottom, 1, 2, 10, and 100 ps respectively. [36] © [2006] IEEE

At the lasing threshold ($j = j_{th1}$), the output power is zero (Fig. 15). The output power asymptotically approaches a maximum as current density increases. This is due to the fact that the parasitic recombination in the OCL continuously increases with increasing pump current.

Figure 16 below shows the ground-state-lasing power against excess pump current in QD lasers with ABLs.

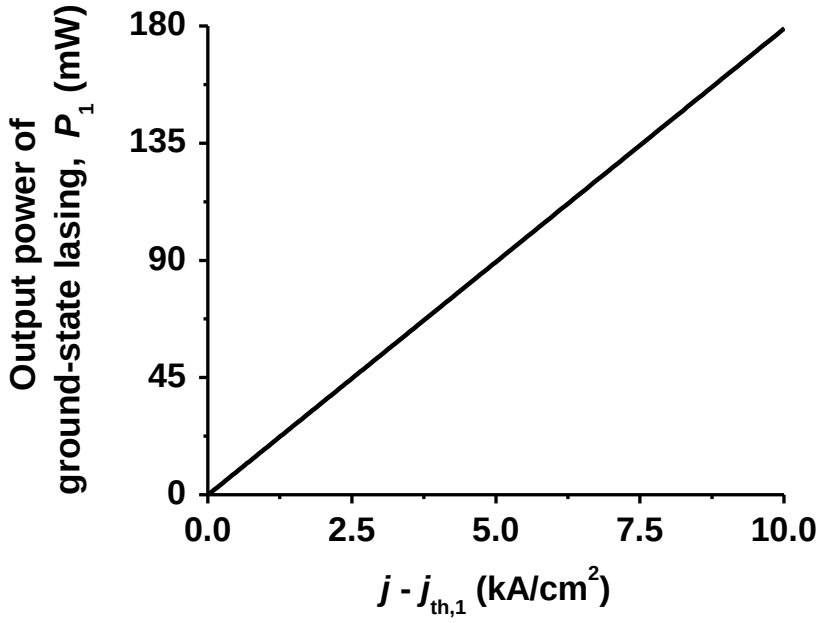

Fig. 16. Output power of ground-state lasing vs excess injection current in ABL QD lasers.

As shown in figure 16, when ABL QD lasers are used, the ground-state lasing power continues to grow as more injection current is applied to the system. This is due to the fact that the ABLs suppress parasitic recombination in the OCL. Thusly, output power will not reach a maximum value as current is applied, and semiconductor QD lasers with ABLs will be able to be applied in systems that required greater output powers.

3.4. Summary

In chapter 3, the output power of ground-state lasing of ABL QD lasers was examined in the presence of excited states in QDs. In ABL QD lasers, by preventing carriers from escaping into

the OCL, parasitic recombination was eliminated from the system. In conventional QD lasers, the output power of ground-state lasing reaches an asymptotic value as pump current increases.

A theoretical model for QD lasers with ABLs was created, which considered excited state mediated capture of carriers into the QD ground state.

It was found that in ABL QD lasers, the output power of ground-state lasing will not reach an asymptotic value with increasing pump current. Rather, the output-power of ground state lasing will continue to increase linearly. This allows QD lasers with ABLs to be used in applications which require high output power.

Chapter 3 Bibliography

[36] L. Jiang and L.V. Asryan, “Excited-state-mediated capture of carriers into the ground state and the saturation of optical power in quantum-dot lasers’, IEEE Photonics Technology Letters, vol. 18, no. 24, pp. 2611-2613, Dec. 2006.

[37] T. Kitamura, R. Ohtsubo, M. Murayama, T. Kuroda, K. Yamaguchi, and A. Tackeuchi, “Direct observation of phonon relaxation bottleneck in InAs quantum dots of high-uniformity,” Phys. Stat. Sol. C, vol. 0, no. 4, pp. 1165–1168, June 2003.

[38] Y. Wu and L.V. Asryan, “Direct and indirect capture of carriers into the lasing ground state and the light-current characteristic of quantum dot lasers,” J. Appl. Phys., vol. 115, no. 10, Art. no. 103105, 5 pages, March 2014.

[39] Y. Wu, L. Jiang, and L.V. Asryan, “Output power of a quantum dot laser: Effects of excited states,” J. Appl. Phys., vol. 118, no. 18, Art. no. 183107, 14 pages, Nov. 2015.

Chapter 4: Conclusion

In this research on semiconductor QD lasers, ABLs were designed in order to stop parasitic recombination of carriers outside of the active region. The optimum pump current was found which maximized modulation bandwidth at -3dB, which was lower than that in conventional QD lasers. Optimal values for surface density of QDs and cavity length were found as well. Relative QD size fluctuation was also investigated, and an optimal value was found. This data gives strong parameters for fabricating semiconductor QD lasers with ABLs with the largest possible modulation bandwidth.

Output power of semiconductor QD lasers with ABLs was also investigated. By including ABLs and suppressing parasitic recombination, the output power of ground state lasing will continue to rise with increasing injection current, as opposed to reaching an asymptotic value as occurs in conventional QD lasers. This allows QD lasers with ABLs to be used in systems that require higher power applications.